Offshore Oil Spill Modelling Report

Results from Simulations of Oil Spills at the Hebron Well Site

Prepared in support of the:

Hebron Project
Comprehensive Study Report

For:



Suite 701, Atlantic Place
215 Water Street
St. John's, NL, A1C 6C9

Prepared by:

Applied Science Associates, Inc.
55 Village Square Dr
South Kingstown, RI
02879

July 2011

Prepared for:
Stantec Consulting Ltd.

Offshore Oil Spill Modelling Report
Results from Simulations of Oil Spills at the Hebron Well Site

ASA Project 2010–261 **July 18, 2011**

Prepared by:

Chris Galagan
Nicholas Cohn
Matthew Horn
Rachel Shmookler



Applied Science Associates, Inc.
55 Village Square Drive
South Kingstown, RI02879

Executive Summary

The SIMAP oil spill model was used to simulate spills of crude and fuel oil at the Hebron offshore site southeast of St. Johns, Newfoundland and Labrador. The model scenarios utilize wind data obtained from model hindcasts, current data from a hydrodynamic model and ice data from the Canadian Ice Service. The SIMAP model was used in stochastic and deterministic modes to predict the range of water surface, subsurface and shoreline oiling possible due to spills occurring over a range of seasonal conditions. This report describes the wind, current and ice data used in the modeling. It also describes the models applied to simulate the hydrodynamics and the oil spills, and presents and discusses the model results.

Possible spills considered at the site of the Hebron platform include well blowouts of crude oil, with oil released either at the seafloor or from the top of the drilling platform, with durations ranging from 30 to 120 days. Short-duration (24 hours or less) small volume batch transfer spills of crude oil and marine diesel fuel were also modeled. All spill scenarios were simulated without any spill countermeasures applied. Additional extended duration spill simulations were completed for platform blowouts. These spills were run for an additional 200 days beyond the termination of the blowout release in order to track oil remaining on the sea surface within the model domain. The results of the extended duration spills are included in an addendum to this report.

Wind data for the oil spill simulations were obtained from two sources. One source is the MSC50 Wind Hindcast, a model reanalysis product that provides hindcast winds for the North Atlantic for the period 1954 through 2008. The data were supplied as hourly speed and direction values by Environment Canada, MSC Atlantic Operations, for the 30-year period 1978-2008. Additional wind data were obtained from the National Centers for Environmental Prediction (NCEP) at multiple locations across the North Atlantic for the same 30-year period. Oil spill simulations were run using winds from all times of the year in order to capture seasonal differences in possible spill trajectories.

Currents for the North Atlantic region were acquired from the HYCOM (HYbrid Coordinate Ocean Model) circulation model. Hindcast currents from HYCOM consisting of daily mean speed and direction were obtained for the period November 2003 through September 2010 for the North Atlantic region and used in the SIMAP oil spill model to simulate spills originating at the Hebron platform and from the seafloor blowout.

Ice data used in the oil spill model simulations were obtained from the National Snow and Ice Data Center (http://nsidc.org/index.html) for the months of February and March. Data from the 1989-1990 winter were selected because they show the greatest extent of ice coverage over the past several decades.

The SIMAP stochastic model was used to determine the probability of oiling the water surface and the shoreline based on specified thickness thresholds, and of oiling the water column using a concentration threshold. The following thresholds were applied:

- Surface oil average thickness > 0.01 mm (10 µm)
- Shoreline oil average thickness > 0.01 mm (10 µm)
- Subsurface oil (entrained in water) average concentration > 10 ppb

The majority of spills at the site are predicted to travel eastward. The distance traveled is generally controlled by the blowout duration and the season. The typically higher velocity winter winds result in greater oil transport. The summer and winter blowout spill simulations greater than 30 days duration are predicted to have a less than 10% probability of reaching the Newfoundland shoreline.

Marine diesel and crude oil released in small volume batch transfer spills is predicted to travel primarily toward the east away from Newfoundland. The marine diesel fuel is more easily dispersed into the water column than the crude oil and modeling predicts slightly higher entrained oil fractions for these spills. The marine diesel is capable of reaching a smaller minimum thickness than the crude oil, resulting in a relatively higher sea surface area exposed to oil. None of the batch transfer spills are predicted to reach the Newfoundland shoreline. The mass balance summary table lists the volume of oil on the water surface, dispersed in the water column, evaporated or decayed, as a percent of the total spill at the end of the deterministic model simulations.

Mass Balance Summary - percentage of total spill volume remaining at the end of the simulation

Spill	% Water Surface	% Evaporated	% Decayed	% Water Column
Platform Blowout	51 – 79%	8 – 12%	12 – 37%	0.2 – 0.3%
Seafloor Blowout	29 – 35%	29 – 32%	26 – 30%	9 – 10%
Marine Diesel Batch Transfer	0%	6 – 45%	15 – 24%	40 – 70%
Crude Batch Transfer	64%	12 – 13%	22 – 23%	0.4 – 0.5%

Table of Contents

Executive Summary ii
Table of Contents iv
List of Figures v
List of Tables vii
1. Introduction 1
2. Model Inputs and Spill Scenarios 3
2.1 Study Area 3
2.2 Model Scenarios 4
2.3 Oil Characterization 6
2.4 Wind Data 6
2.5 Current Data 17
2.6 Ice Data 20
2.7 Shoreline Type Data 24
3. Modeling Description 26
3.1 Overall Modeling Approach 26
3.2 Blowout Releases of Crude Oil 31
Blowouts 31
Blowout Plume Dynamics 32
3.3 Batch Transfer Spills 33
3.4 Oil Weathering 33
4. Model Results 39
4.1 Stochastic Model Results 39
4.2 Deterministic Model Results 42
4.3 Newfoundland Shoreline Oiling 44
5. References 46
Appendix A: SIMAP Model Description 1
Appendix B: Blowout Model Description 1
Appendix C: Stochastic Model Results 1
Appendix D: Deterministic Model Results 1

List of Figures

Figure 2.1-1. Map showing the Newfoundland region. 4

Figure 2.4-1. Map showing the locations of MSC50 and NCEP wind data stations for the offshore modeling. 8

Figure 2.4-2. Location and identity of MSC50 wind data stations in the vicinity of the Hebron well site. 8

Figure 2.4-3. Wind rose and wind speed frequency distribution of the MSC50 wind data from site M6010632 near the Hebron platform location for all months of the year. The plot indicates the direction from which the wind is coming for the 30 years 1978 through 2008. 10

Figure 2.4-4. Wind rose and wind speed frequency distribution of the MSC50 wind data from site M6010632 near the Hebron platform location for the spring months. The plot indicates the direction from which the wind is coming for the 30 years 1978 through 2008. 11

Figure 2.4-5. Wind rose and wind speed frequency distribution of the MSC50 wind data from site M6010632 near the Hebron platform location for the summer months. The plot indicates the direction from which the wind is coming for the 30 years 1978 through 2008. 12

Figure 2.4-6. Wind rose and wind speed frequency distribution of the MSC50 wind data from site M6010632 near the Hebron platform location for the fall months. The plot indicates the direction from which the wind is coming for the 30 years 1978 through 2008. 13

Figure 2.4-7. Wind rose and wind speed frequency distribution of the MSC50 wind data from site M6010632 near the Hebron platform location for the winter months. The plot indicates the direction from which the wind is coming for the 30 years 1978 through 2008. 14

Figure 2.4-8. Comparison of wind speed and direction data collected at the Hibernia well site (top plot) with data from the MSC50 model hindcast site M6010632 (bottom plot) for the first 15 days in February, 1981. 16

Figure 2.4-9. Comparison of wind speed and direction data collected at the Hibernia well site (top plot) with data from the MSC50 model hindcast site M6010632 (bottom plot) for the last 13 days in February, 1981. 17

Figure2.5-1.Map of the large scale ocean currents in the Newfoundland region. (Source: U.S. Coast Guard, International Ice Patrol). 18

Figure 2.6-1. Total accumulated ice coverage for the period of record from the Canadian Ice Service. 21

Figure 2.6-2.Ice concentration chart from the Canadian Ice Service for the week of 12March, 1990. 22

Figure 2.6-3. Sea ice coverage used in the oil spill model simulations for the month of February. 23

Figure 2.6-4. Sea ice coverage used in the oil spill model simulations for the month of March.. 24

Figure 3.1-1. Time coverage for blowout simulations. 27

Figure 3.1-2. Comparison between the 30-year MSC50 wind data occurring at site M6010632 (left rose plots) and the wind data from the same source that was used by the SIMAP model to simulate spills (right rose plot) for the 30 day platform blowout. The top pair of plots is from the summer season, the bottom pair compares winter data. 28

Figure 3.1-3. Comparison between the 30-year MSC50 wind data occurring at site M6010632 (left rose plots) and the wind data from the same source that was used by the SIMAP model to simulate spills (right rose plot) for the 100 day platform blowout. The top pair of plots is from the summer season, the bottom pair compares fall data. 29

Figure 3.1-4. Comparison between the 30-year MSC50 wind data occurring at site M6010632 (left rose plots) and the wind data from the same source that was used by the SIMAP model to simulate spills (right rose plot) for the 120 day platform blowout. The top pair of plots is from the winter season, the bottom pair compares spring data. 30

Figure 3.2-1. Perspective view of example oil/gas plume reaching termination depth. 32

Figure 3.4-1. Change in residue viscosity with time for 4 types of oil according to the IKU Oil Weathering Model with 5 m/s wind and water temperature of 15°C (Nordiv, 1995)..... 34

Figure 3.4-2. Change in emulsion viscosity with time for 4 types of oil according to the IKU Oil Weathering Model with 5 m/s wind and water temperature of 15°C (Nordiv, 1995)..... 34

Figure 3.4-3. Evaporative loss with time for 6 types of oil according to the IKU Oil Weathering Model with 5 m/s wind and water temperature of 15°C (Nordiv, 1995). 35

Figure 3.4-4. Conceptual model oil weathering over time (Hume, et al., 1983). 36

Figure 3.4-5. A prediction of swept spill area with time (Hume, et al., 1983) 37

Figure 3.4-6. Mass balance from a representative instantaneous spill of Hebron D-94 oil..... 38

List of Tables

Table 2.2-1.Oil spill scenarios modeled at the Hebron Platform location. 5

Table 2.3-1. Characteristics of oil used in the spill simulations.....6

Table 2.7-1Shorelinecharacteristics for the shore type used in the spill simulations (based on Gundlach, 1987).....24

Table 3.2-1.Blowout model inputs defining the seafloor blowout.....33

Table 3.2-2.Oil droplet size distribution for the subsea blowout at the Hebron platform.....33

Table 4.1-1. Summary of the stochastic simulations of the platform and seafloor blowouts at the Hebron well site. The 50th and 95th percentile values are determined by ranking all 100 spills in each scenario according to the area of sea surface exposed to oil, the length of shoreline exposed to oil and the volume of entrained (naturally dispersed) oil above the stated thresholds.....40

Table 4.1-2. Summary of stochastic simulations of the batch transfer spills modeled at the Hebron well site. The 95th percentile values are determined by ranking all 100 spills in each scenario according to the area of sea surface exposed to oil, the length of shoreline exposed to oil and the volume of entrained (naturally dispersed) oil above the stated thresholds.....41

Table A-1. Definition of four distillation cuts and the eight pseudo-components in the model (monoaromatic hydrocarbons, MAHs; benzene + toluene + ethybenzene + xylene, BTEX; polynuclear aromatic hydrocarbons, PAHs).....3

Table A-2: Typical beach widths by shore type (CERC, 1984; French et al, 1996).....7

Table A-3: Summary of oil-in-ice advection and weathering effects accounted for in the SIMAP model. 10

1. Introduction

ExxonMobil Canada Properties (EMCP) contracted ASA for oil spill modeling services to simulate spills at locations off the coast of Newfoundland. The SIMAP model was used to simulate spills of crude and fuel oil at the Hebron offshore site, located approximately 340 km southeast of St. Johns. The model scenarios utilize wind data obtained from model hindcasts and current data from a hydrodynamic model. The SIMAP model was used in stochastic and deterministic modes to predict the range of water surface, subsurface and shoreline oiling possible from well blowouts at the site and small batch transfer spills near the site.

This report presents the model input data, describes the models applied to simulate the hydrodynamics and the oil spills, and presents and discusses the results of simulations performed at the Hebron well site. An addendum contains the results from extended period model simulations performed at the Hebron site. A companion report provides the same information for spill simulations performed at the Nalcor Energy Bull Arm Fabrication Site (Bull Arm Site).

A previous oil spill modeling study was completed for the Hebron project in 2010 (AMEC, 2010). In this study, spill model simulations were run to determine the trajectory of the surface release of fuel oil spills at the Hebron well site. A model simulation was commenced on each day of the year for a thirty-year period. Simulations were allowed to run until the spill terminated on a coastline, reached an external model boundary (edge of the model grid) or for a maximum of thirty days. The results from the fuel spill simulations for each month of the year were overlain on a grid of the region and the number of times surface oil passed through each grid cell was counted to determine the probability that oil released during the month would reach any place within the gridded water surface. This approach is deemed deterministic in that the model is forced using a prescribed set of wind data to generate a set of model trajectories that can be reproduced at any time by using the same input data set. Results from these model simulations are presented in the AMEC (2010) report as maps of surface oil probability for each month of the year.

In the AMEC study, spill model simulations were also run to determine the trajectory of the surface release of crude oil spills at the Hebron well site. These simulations were deterministic in that they used winds and currents for a given time period to generate a single, reproducible spill trajectory. The results from three batch spills and three blowouts were presented on maps showing the presence of oil on the sea surface at discrete points in time during the spill, as well as the sea surface area swept by the surface oil over the entire spill duration. Simulations for summer and winter environmental conditions were presented on individual maps.

In contrast to the deterministic approach employed in the previous study, the present study utilized a stochastic approach to determine the potential fate of spills from the Hebron well site. In this approach, a spill trajectory model is run repeatedly but with a randomly selected start date that falls within the desired season. Using wind speed and direction data from a model hindcast and currents generated by a hydrodynamic model, each oil spill simulation was run starting on the randomly selected date. In this approach, a sufficient number of model runs will

adequately sample all of the variability in the wind speed and direction in the region of interest and will result in a prediction of the probability of oil pathways for a spill at the prescribed location. Running multiple spill simulations during a single season will provide a reliable prediction of the oiling probability for a spill occurring during that season.

The SIMAP model has been applied to predictions of multiple spill events using the stochastic approach and has been validated against actual spills. Reports describing these applications of the model and validation against actual spills are listed in a special section of Appendix A titled '*References – SIMAP Example Applications and Validations*'. Copies of these papers can be provided by sending a request to asa@asascience.com and requesting one or more specific papers.

2. Model Inputs and Spill Scenarios

The spill scenarios modeled were defined in consultation with ExxonMobil Canada Properties and ExxonMobil Biomedical Sciences to represent the spills that may occur at the offshore Hebron production site. Possible spills at the offshore site include crude oil from a well blowout, either at the seafloor or from the drilling platform, and small volume batch spills of crude or diesel fuel on the sea surface.

ExxonMobil's well control philosophy is focused on prevention using safety / risk management systems, management of change procedures, and global standards. ExxonMobil has a mature Operations Integrity Management System (OIMS) that emphasizes relentless attention to Safety, Well Control, and Environmental Protection. This includes proper preparation for wells (well control equipment inspections / tests), detecting the influx early, closing-in the well efficiently (personnel training / drills), and circulating out the kick with kill weight mud in a controlled manner.

In the event of a blow-out, ExxonMobil's primary objective would be to stop the flow as quickly as possible. For both surface and subsea wells, this would involve shutting in at the wellhead and killing the well through the wellhead. Relief well drilling, and the subsequent dynamic kill, is considered a back-up strategy in the event shut-in and/or killing through the wellhead is not possible or is unsuccessful.

Two model systems were used to simulate the spills. The first model, the ASA blowout model, simulates the near-field dynamics of the plume of a gas/oil mixture discharged from the subsea well blowout, and the second model, SIMAP, simulates the far-field transport and weathering of oil released into the water column or at the sea surface. This section describes the spill scenarios considered, and the wind, current and ice data defining the environment.

2.1 Study Area

Newfoundland comprises a series of islands off the east coast of Canada, and along with Labrador forms the easternmost Canadian province. The relatively shallow waters of the continental shelf extend eastward up to 500 km from the Newfoundland coast. Known as the Grand Banks, this area contains significant petroleum resources. The Hebron well is located near the edge of the Grand Banks approximately 340 km southeast of St John's (map in Figure 2.1-1). The model domain is defined as the rectangle from 60° to 30°W longitude and from 40°to 56°N latitude.



Figure 2.1-1. Map showing the Newfoundland region.

2.2 Model Scenarios

The spills simulated originate at two locations: the proposed Hebron platform and at the seafloor. The scenarios presented are based on an oil release rate determined for a blowout at the Hebron field. This rate was derived based on existing knowledge of Hebron crude properties, known reservoir properties for the Hebron field and assumptions made for specific well conditions at the time of the blowout. Reservoirs differ greatly from one to another and their properties (pressure, volume, oil/gas ratio, etc.) are unique to each reservoir. Therefore, historical flow rates from other spill events are not predictive of what would happen in other reservoirs, although they can be used to put specific events into perspective.

Flow rates for Hebron platform wells were estimated at 5,600 m^3/day (approximately 35,000 bbl/day) based on the reservoir properties, assuming a blowout to the atmosphere (e.g. ~70 m above mean sea level) and accounting for the viscous (thick, resistant to flow) nature of the oil from this reservoir.

Flow rates for MODU wells were estimated at 3,200 m^3/day (approximately 20,000 bbl/day) based upon the properties of its reservoir, a subsea blowout (~90m below sea level) and lighter, less viscous oil.

Multiple spill scenarios were modeled to assess the fate of oil spilled from the offshore Hebron well location. These spills were simulated using the SIMAP 3D fates model. All spill scenarios were simulated without the application of any spill countermeasures applied.

Two kinds of blowouts were simulated at the Hebron well site: a platform blowout that originates 70 meters above the sea surface, and a seafloor blowout that originates at a wellhead in approximately 98 meters water depth. The platform blowout introduces Hebron D-94 crude oil directly onto the sea surface during a long-term, continuous release. To reproduce the dynamic and complex processes of a seabed blowout release, a near-field analysis using ASA's blowout plume model was performed prior to simulating the far-field movement of the Ben Nevis crude oil in SIMAP.

Six small volume batch spills were also modeled at the Hebron site. The batch spills include diesel fuel released instantaneously onto the sea surface and crude oil spills released onto the sea surface over a 24-hour period.

Table 2.2-1 lists the specifics for the spill scenarios. The characteristics of the spilled oils are discussed in more detail in Section 2.3.

Table 2.2-1.Oil spill scenarios modeled at the Hebron Platform location.

Scenario	Total Spill Volume	Spill Duration	Simulation Duration	Season
Offshore - Hebron Platform Site (46.5440573° N, 48.49803617° W)				
Platform Blowout (D-94 crude)	1,050,000 bbl (166,936.6 m^3)	30 days	30 days 60 days	Summer
	1,050,000 bbl (166,936.6 m^3)	30 days	30 days 60 days	Winter
	1,050,000 bbl (166,936.6 m^3)	30 days	30 days 60 days	Winter (ice present)
	3,500,000 bbl (556,455.4 m^3)	100 days	100 days	Summer
	4,200,000 bbl (667,746.5 m^3)	120 days	120 days	Winter
	4,200,000 bbl (667,746.5 m^3)	120 days	120 days	Winter (ice present)
Offshore - Hebron Subsea Site (46.5754111° N, 48.3956028° W)				
Seafloor Blowout (Ben Nevis crude)	2,000,000 bbl (317,975 m^3)	100 days	100 days	Summer
	2,400,000 bbl (381,569 m^3)	120 days	100 days	Winter
	2,400,000 bbl (381,569 m^3)	120 days	100 days	Winter (ice present)
Offshore Batch Spill Site(46.5440573° N, 48.49803617° W)				
Batch Transfer (marine diesel)	5,031 bbl (800 m^3)	Instantaneous	30 days	Summer
	5,031 bbl (800 m^3)	Instantaneous	30 days	Winter
	5,031 bbl (800 m^3)	Instantaneous	30 days	Winter (ice present)

Scenario	Total Spill Volume	Spill Duration	Simulation Duration	Season
Batch OLS Transfer (crude oil)	31,449 bbl (5000 m^3)	24 hours	30 days	Summer
	31,449 bbl (5000 m^3)	24 hours	30 days	Winter
	31,449 bbl (5000 m^3)	24 hours	30 days	Winter (ice present)
Offshore - Hebron Platform Site (46.5440573° N, 48.49803617° W) **Extended Period Runs**				
Platform Blowout (D-94 crude)	1,050,000 bbl (166,936.6m^3)	30 days	230 days	Winter
	3,500,000 bbl (556,455.4 m^3)	100 days	300 days	Summer
	4,200,000 bbl (667,746.5 m^3)	120 days	320 days	Winter

As indicated in Table 2.2-1, spill simulations were stopped once flow from the well ceased except for the 30-day duration blowout scenarios which were also run for 60 days in order to track the oil for an additional 30 days, and the extended run simulations which were run for an additional 200 days. The three extended run simulations listed at the bottom of Table 2.2-1 use the same blowout duration, rate of release and total release volume as their shorter duration counterparts, however, the model run time is extended by 200 days. The results from the extended run scenarios are presented in an addendum to this report.

2.3 Oil Characterization

Selected characteristics of the oil types used in the spill simulations are listed in Table 2.3-1. The data used to characterize the crude oils are taken from the Environment Canada Oil Properties database (http://www.etc-cte.ec.gc.ca/databases/oilproperties/). The SIMAP model uses these characteristics to calculate oil weathering simultaneously with oil transport in the environment.

Table 2.3-1. Characteristics of oil used in the spill simulations.

Oil	Spill	API Gravity	Density (g/cm^3)	Viscosity (cP)
Hebron D-94 Crude	Platform blowout Batch OLS Transfer	20.1	0.92691 @ 25° C	265.374 @ 25° C
Ben Nevis L55 Well	Subsea blowout	30.8	0.8711 @ 15° C	15.556 @ 25° C
Marine Diesel Fuel	Batch Transfer Spills	37.6	0.82910 @ 25° C	4.0 @ 25° C

2.4 Wind Data

Wind over the Grand Banks blows predominantly from the southwest, west and northwest throughout the year. Winter season winds are most frequently from the west and northwest with higher velocity than summer season winds, which typically come from the southwest. Spring

and fall months are transition periods between the more consistent summer and winter wind regimes. Low pressure systems, tropical and extra-tropical storms pass through the Grand Banks on a regular basis generating significant wind speeds for short periods of time.

A multi-year, or preferably multi-decade, long wind speed and direction dataset is required to conduct an oil spill modeling study in order to capture the variability that occurs from year-to-year. Oil spill trajectories run using long-term wind datasets are representative of possible wind conditions at the site. Wind datasets of 10 years or longer provide the best results.

Oil released during long term events such as well blowouts has the potential to travel long distances, and the wind speed and direction data must cover a large geographic area in order to cover the area of potential oil transport and capture any spatial variability that may occur. The temporal and spatial requirements for wind datasets suitable for use in oil spill modeling studies at offshore sites limit the possible sources of data to models capable of simulating wind fields over large continuous regions using past meteorological data. These models are used to perform hindcasts of wind and other environmental conditions over decades that are suitable for oil spill modeling studies. A wind model hindcast is performed by using wind records, atmospheric pressure fields and storm track data as input to an established model to produce a wind field over a large area that is continuous in space and time.

For this study, wind data for oil spill model simulations were obtained from two sources. One source is the MSC50 Wind Hindcast(Swail et al., 2006), a model reanalysis product that provides winds for the North Atlantic for the period 1954 through 2008. The data are supplied as hourly wind speed and direction values for surface wind 10 meters above the sea surface at evenly spaced points (0.1° east-west, north-south) for the area surrounding the Hebron well site. The data were provided by Environment Canada, MSC Atlantic Operations. Additional wind data were obtained from the National Centers for Environmental Prediction (NCEP) for multiple point locations across the North Atlantic for the same 30 year time period. The NCEP data are provided as speed and direction on a 6-hour interval at evenly spaced 2° intervals. Figure 2.4-1 is a map showing the locations of the MSC50 (sites clustered around the Hebron well site) and NCEP (more widely spaced points) wind data. The map in Figure 2.4-1 also shows the extent of the oil spill model domain (gray box). Figure 2.4-2 is a map of the area around the Hebron well site with the MSC50 wind data locations identified.

The MSC50 Wind and Wave reanalysis project has its roots in three previous oceanographic modeling studies in the North Atlantic, the most recent of which is the AES40 study (Swail, et al., 2006). In AES40, winds for the period 1954 through 2004 were hindcast and supplemented with measured winds from buoys, platforms and C-MAN stations. The wind hindcast was evaluated against satellite altimeter and in-situ wind speed measurements (Swail, et al., 2006). The MSC50 project was intended to improve on the AES40 model by increasing the resolution within the Canadian east coast region and increasing overall model accuracy in order to reduce uncertainties in the hindcast predictions.

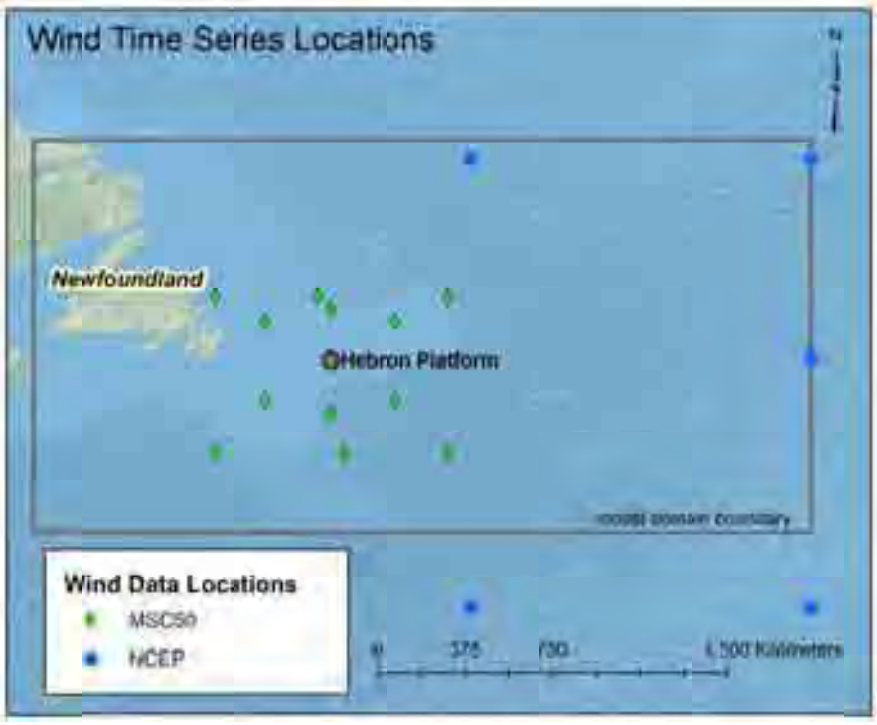


Figure 2.4-1. Map showing the locations of MSC50 and NCEP wind data stations for the offshore modeling.

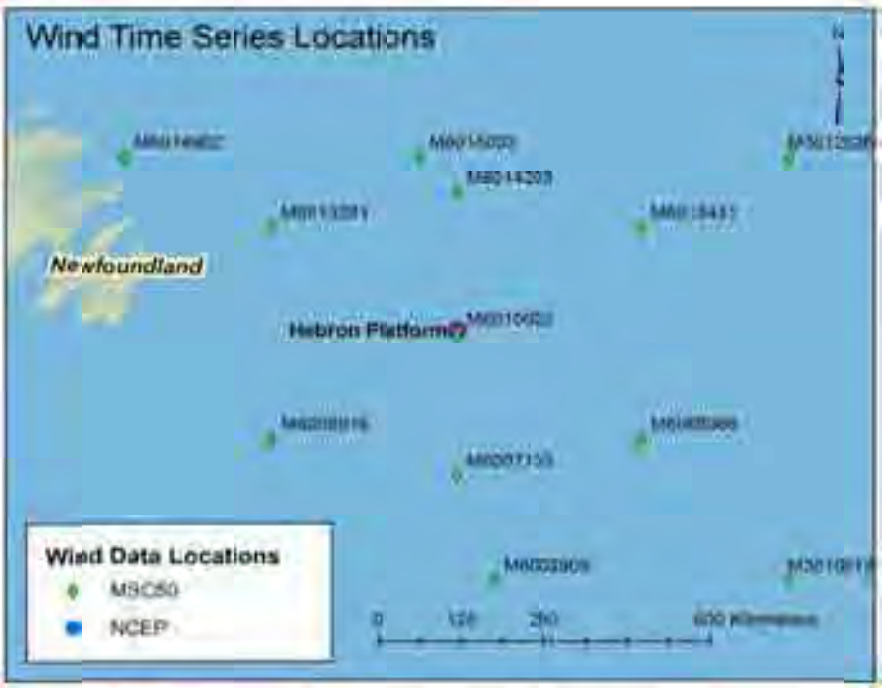


Figure 2.4-2. Location and identity of MSC50 wind data stations in the vicinity of the Hebron well site.

The MSC50 wind model hindcast incorporates the passage of storm systems, particularly those that originate along the New England coast in winter and move into Canadian waters. Sea ice was also incorporated into the MSC50 model with the ice edge changing on a weekly basis, sufficient to capture changes in sea ice during transition seasons.

Comparison of the in-situ data from the period 1954-2005 with the MSC50 model hindcast show consistent agreement (Swail et al., 2006). Swail et al. state:

> *"The wind and wave data are considered to be of sufficiently high quality to be used in the analysis of long return period statistics, and other engineering applications."*

The NCEP wind data are output from a numerical atmospheric model maintained by the National Center for Environmental Predictions Environmental Modeling Center Regional Spectral Model, part of the U.S. National Oceanic and Atmospheric Administration – Cooperative Institute for Research in Environmental Studies (NOAA – CIRES) Climate Diagnostics Center (CDC) in Boulder, Colorado (Kalnay et al., 1996). NCEP Reanalysis data were provided by the NOAA/OAR/ESRL PSD, Boulder, Colorado, USA, from their Web site at http://www.esrl.noaa.gov/psd/data/gridded/data.ncep.reanalysis.surfaceflux.html. The wind data from NCEP consist of wind speed and direction on a 6-hour time increment (four times daily) at 10 meters above the sea surface from a set of points spaced 2° apart (see Figure 2.4-1).

Figure 2.4-3 is a wind rose showing the distribution of annual wind directions and speeds from the MSC50 model hindcast data obtained for location M6010632adjacent to the Hebron well site. The wind comes from all directions at this site but it comes most frequently from the northwest, west and southwest. There is seasonality in the wind at this location that differentiates the summer and winter seasons. The summer (June-July-August) and winter (December-January-February) wind regimes are periods where winds show a pattern of predominant wind direction, while the spring (March-April-May) and fall (September-October-November) wind regimes represent periods of transition between them. Figures 2.4-4 through 2.4-7 are wind roses (top plot) showing the speed and direction of the wind and frequency distributions of wind speeds (bottom plot) at MSC50 site M6010632 for the four seasons. As can be seen in these plots, summer season winds are predominantly from the southwest with speeds less than 10 m/s approximately 90% of the time. Wind speeds greater than 15 m/s occur less than 1% of the time during the summer months. Winter season winds at this site are predominantly from the west with speeds greater than 10 m/s occurring 54% of the time. Wind speeds greater than 20 m/s occur at this site approximately 3% of the time during the winter. Spring season wind direction is highly variable as is typical for transition seasons at these latitudes. Fall wind direction is somewhat less variable than spring wind with a slightly higher frequency of wind coming from the west.

All oil spill simulations performed with the SIMAP system utilized a 30-year wind time series that was spatially interpolated from among the wind stations shown in Figure 2.4-1.

Annual

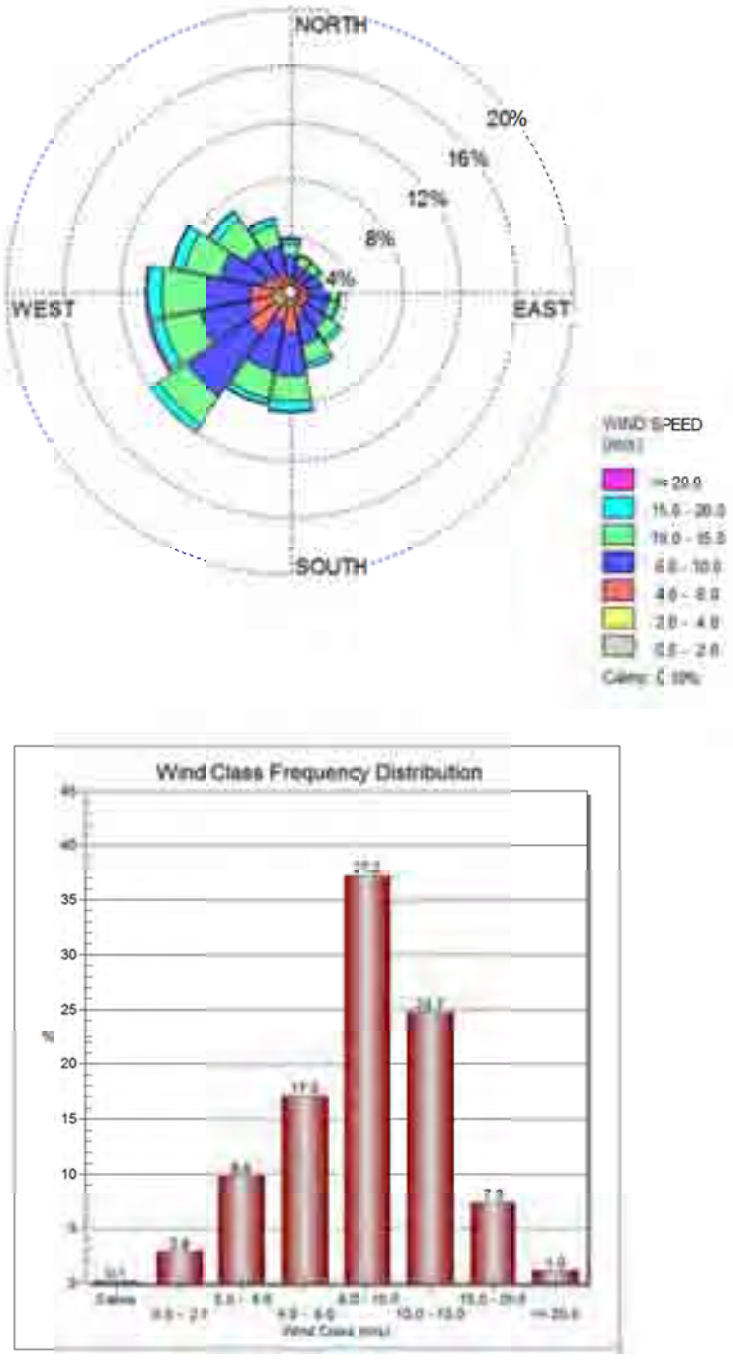
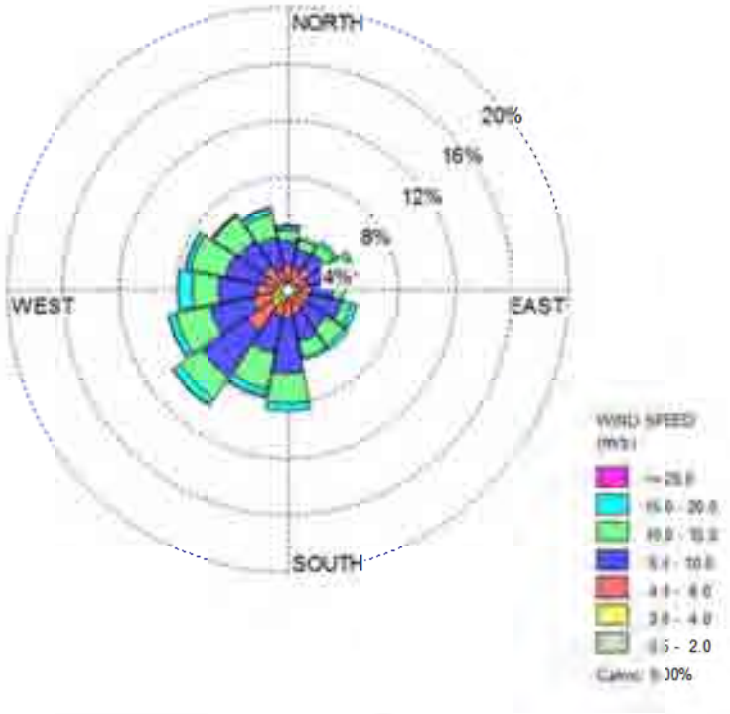


Figure 2.4-3. Wind rose and wind speed frequency distribution of the MSC50 wind data from site M6010632 near the Hebron platform location for all months of the year. The plot indicates the direction from which the wind is coming for the 30 years 1978 through 2008.

Spring



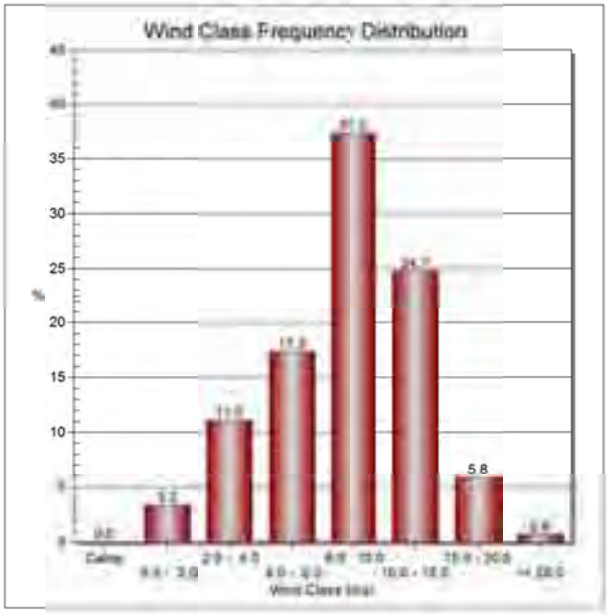
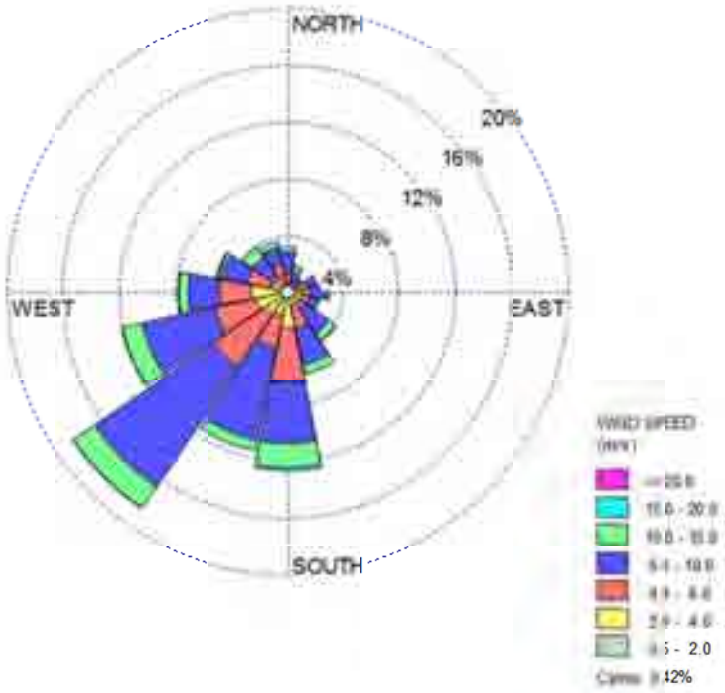


Figure 2.4-4. Wind rose and wind speed frequency distribution of the MSC50 wind data from site M6010632 near the Hebron platform location for the spring months. The plot indicates the direction from which the wind is coming for the 30 years 1978 through 2008.

Summer



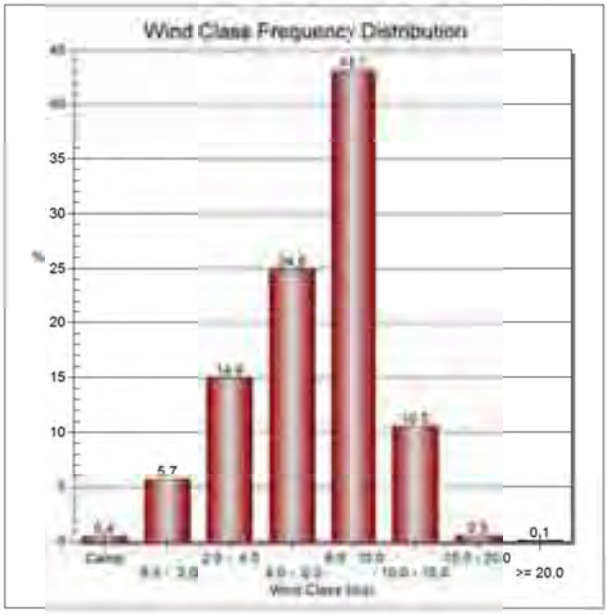
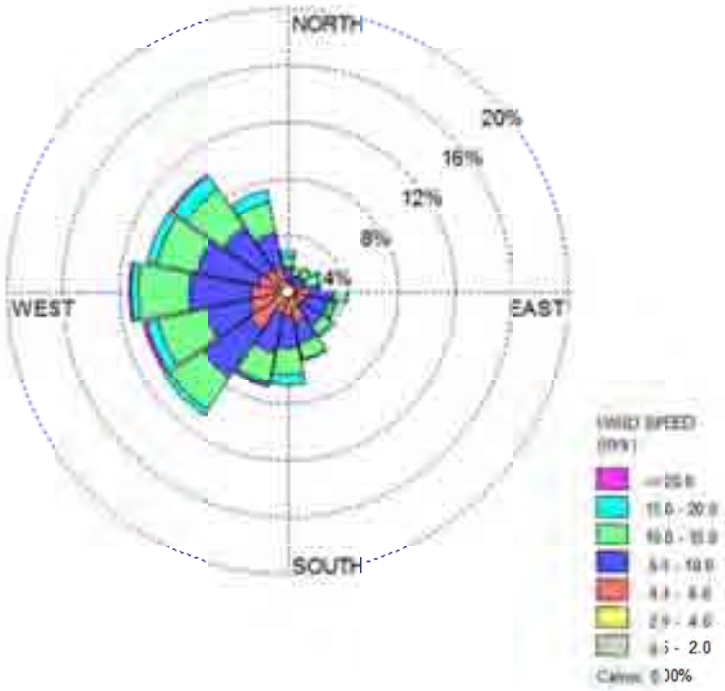


Figure 2.4-5. Wind rose and wind speed frequency distribution of the MSC50 wind data from site M6010632 near the Hebron platform location for the summer months. The plot indicates the direction from which the wind is coming for the 30 years 1978 through 2008.

Fall



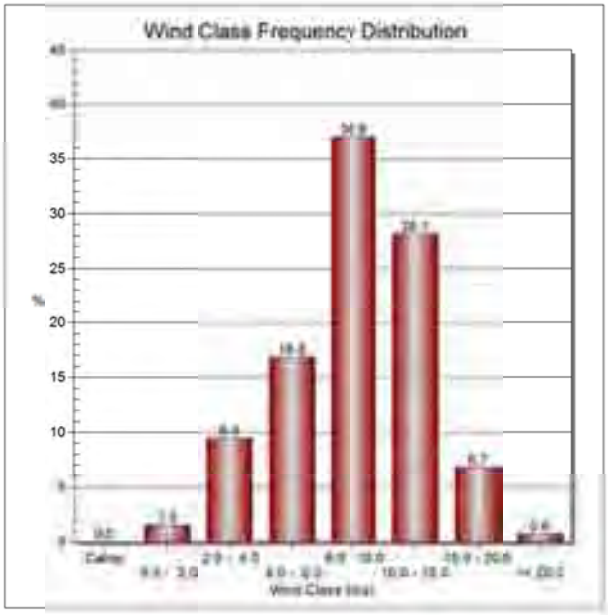
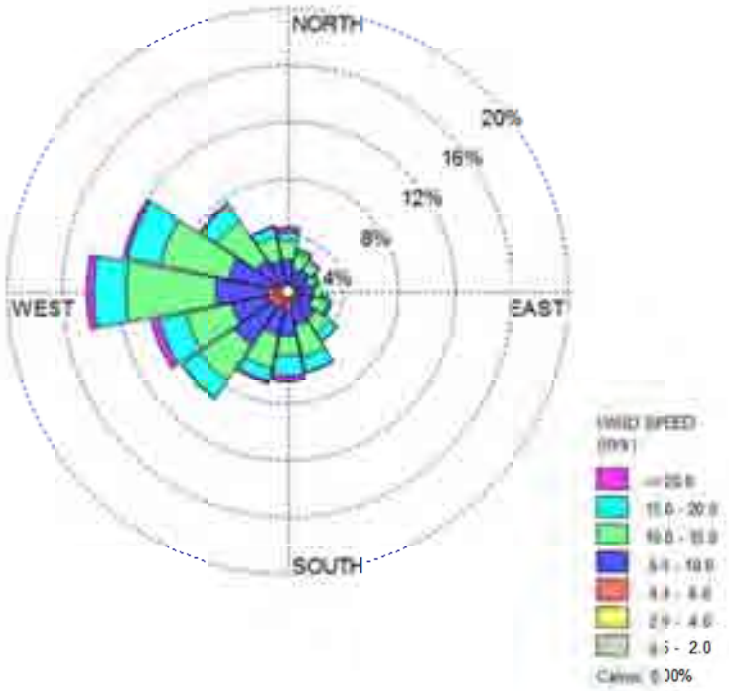


Figure 2.4-6. Wind rose and wind speed frequency distribution of the MSC50 wind data from site M6010632 near the Hebron platform location for the fall months. The plot indicates the direction from which the wind is coming for the 30 years 1978 through 2008.

Winter



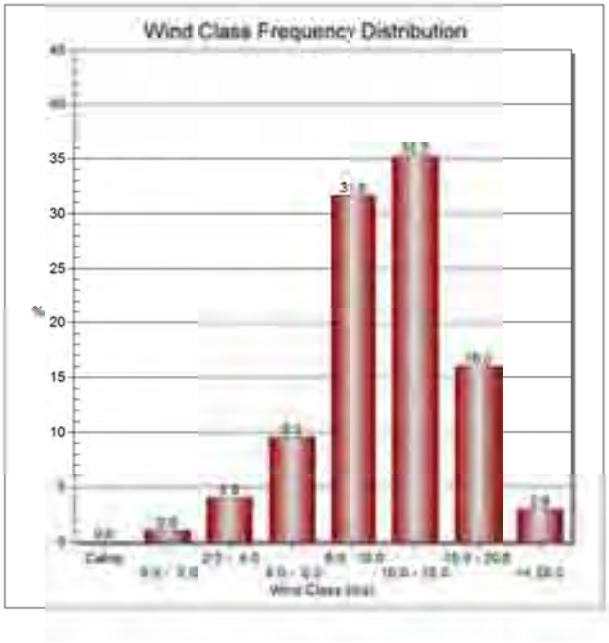


Figure 2.4-7. Wind rose and wind speed frequency distribution of the MSC50 wind data from site M6010632 near the Hebron platform location for the winter months. The plot indicates the direction from which the wind is coming for the 30 years 1978 through 2008.

A comparison of wind speed and direction data from the MSC50 site M6010632 and wind data measured at the site of the Hibernia platform approximately 35 km to the northwest (48.7859° W, 46.7514° N) in February 1981 are shown in Figures 2.4-7 and 2.4-8. The MSC50 wind data correspond to a height of 10 meters above the sea surface while the wind observations from the Hibernia site were made at 80 meters height, so the MSC50 wind speeds were scaled up using a $1/7^{th}$ power law method as follows:

$$U/U_r = (Z/Z_r)^m$$

Where:

U_r = wind speed at the reference height

Z_r = reference height (10m)

U = estimated wind speed

Z = height at estimate

m = assumed to be 1/7 (sea surface roughness)

It can be seen that there is reasonably good agreement between the MSC50 model hindcast data used in the spill modeling and the measured wind data from the Hibernia platform for this particular period, with both datasets showing the same patterns of wind direction and speed.

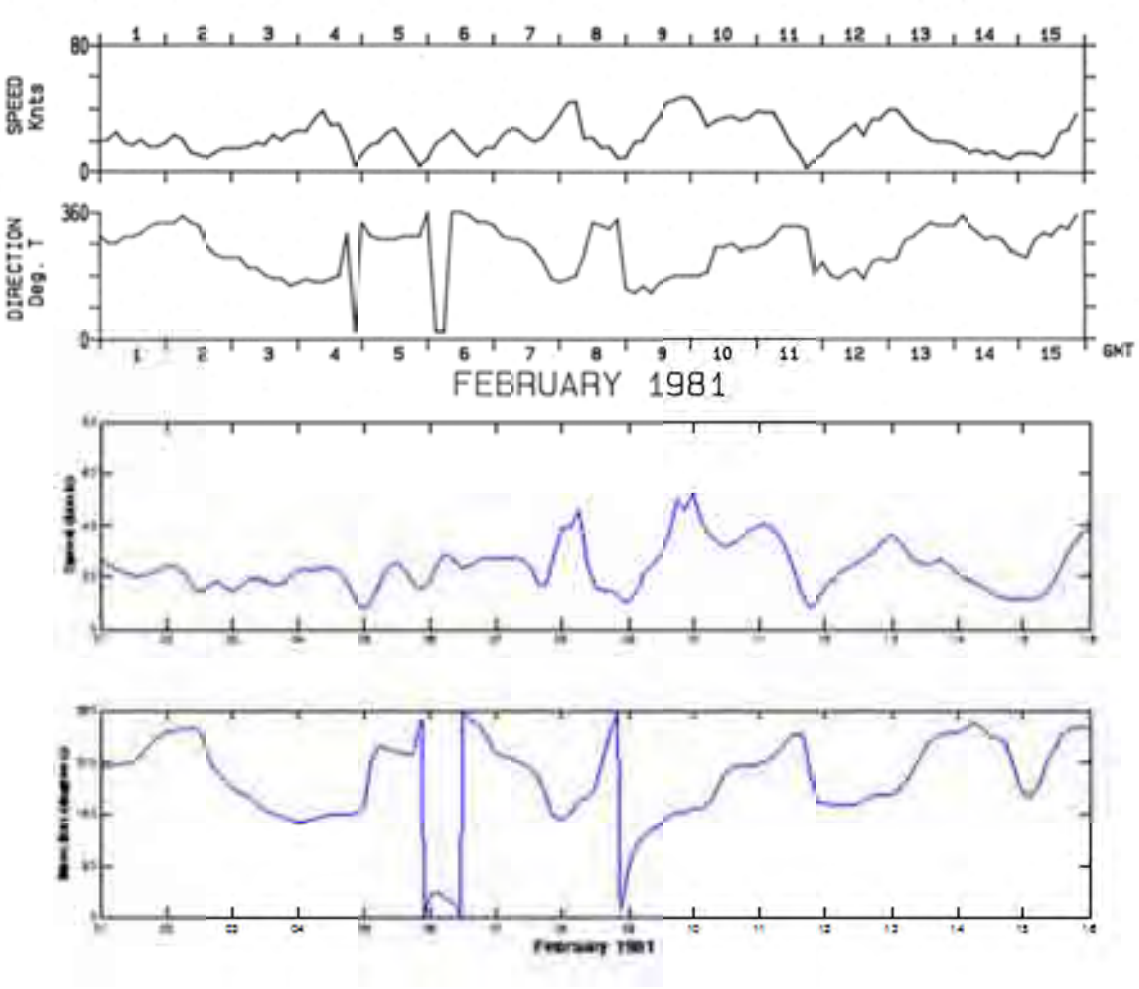


Figure 2.4-8. Comparison of wind speed and direction data collected at the Hibernia well site (top plot) with data from the MSC50 model hindcast site M6010632 (bottom plot) for the first 15 days in February, 1981.

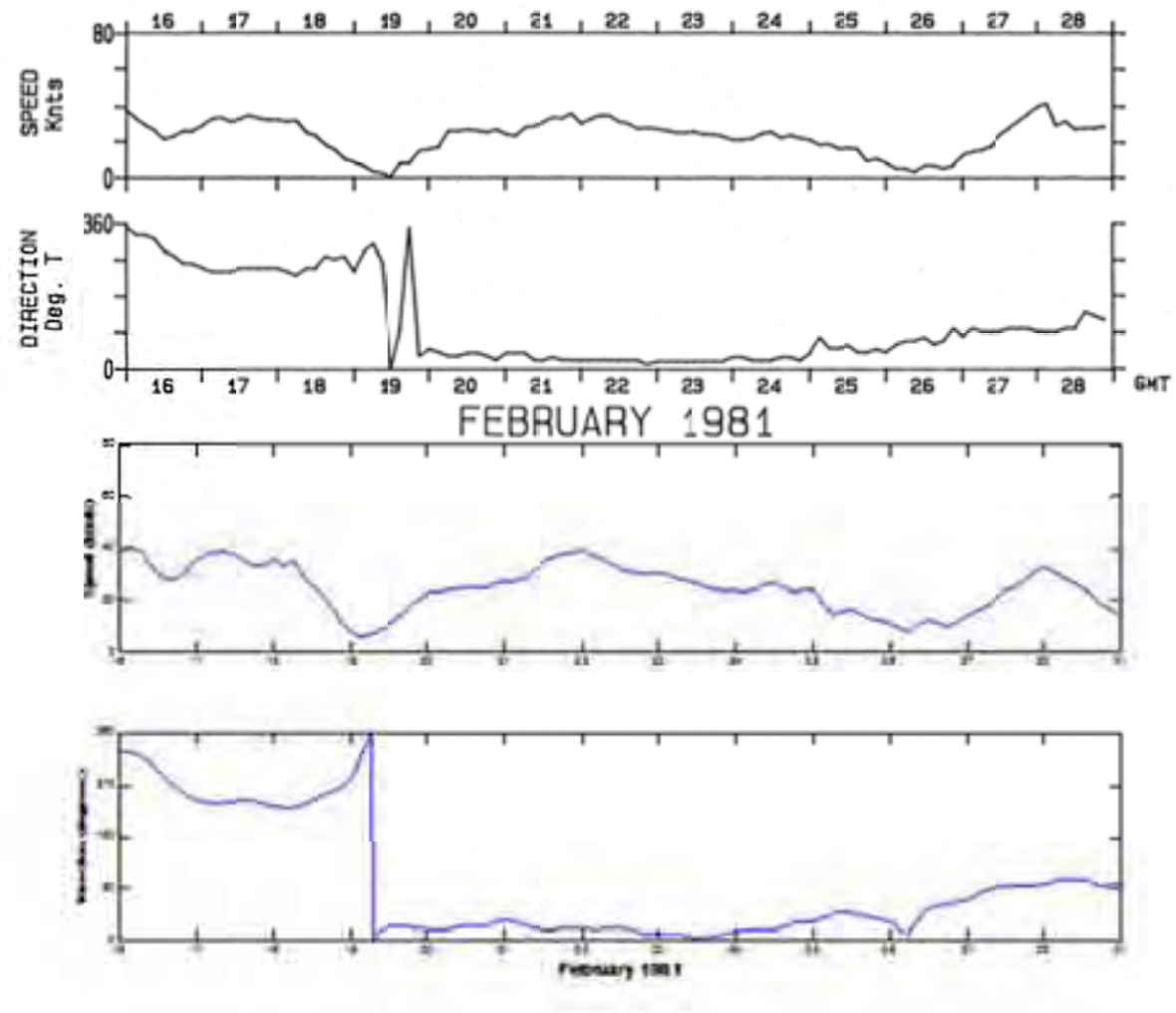


Figure 2.4-9. Comparison of wind speed and direction data collected at the Hibernia well site (top plot) with data from the MSC50 model hindcast site M6010632 (bottom plot) for the last 13 days in February, 1981.

2.5 Current Data

The Labrador Current dominates the large-scale ocean circulation in the Newfoundland region. This current originates in the Arctic Ocean and flows south along the coasts of Labrador and Newfoundland (see the map in Figure 2.5-1). This southerly current intensifies as waters are funneled primarily through the offshore branch, which follows the Flemish Pass between the Grand Bank and Flemish Cap. The Hebron platform is located on the western edge of this pass. To a lesser extent, the Labrador Current is funneled through inshore branch, which follows the Avalon Channel between Newfoundland and the Grand Bank (USCG-International Ice Patrol (IIP)). The strong southerly current dominates the yearly average flow and winds may only account for approximately 10% of current variability in this region (Petrie and Isenor, 1985).

The North Atlantic current is found farther offshore to the south and east of the Grand Banks, flowing towards the north and east with speeds up to 1 m/s. The boundary where these two currents converge produces extremely energetic and variable frontal systems and eddies on smaller scales (on the order of kilometers) (Volkov, 2005). At any point in time, local forcing may advect parcels of water in nearly any direction. Satellite and drifter studies of current dynamics reiterate this complexity; however, drifting parcels generally move to the south and east (Han and Tang, 1999; Petrie and Anderson, 1983; Richardson, 1983) where they intersect with the North Atlantic current. This region is consistently investigated by the USCG-IIP as "one of the most complex and variable regions in the world for its highly dynamic surface currents" (USCG-IIP). For these reasons, it was necessary to develop hydrodynamic model datasets to describe the currents at the offshore site sufficient to simulate the movement of spilled oil.

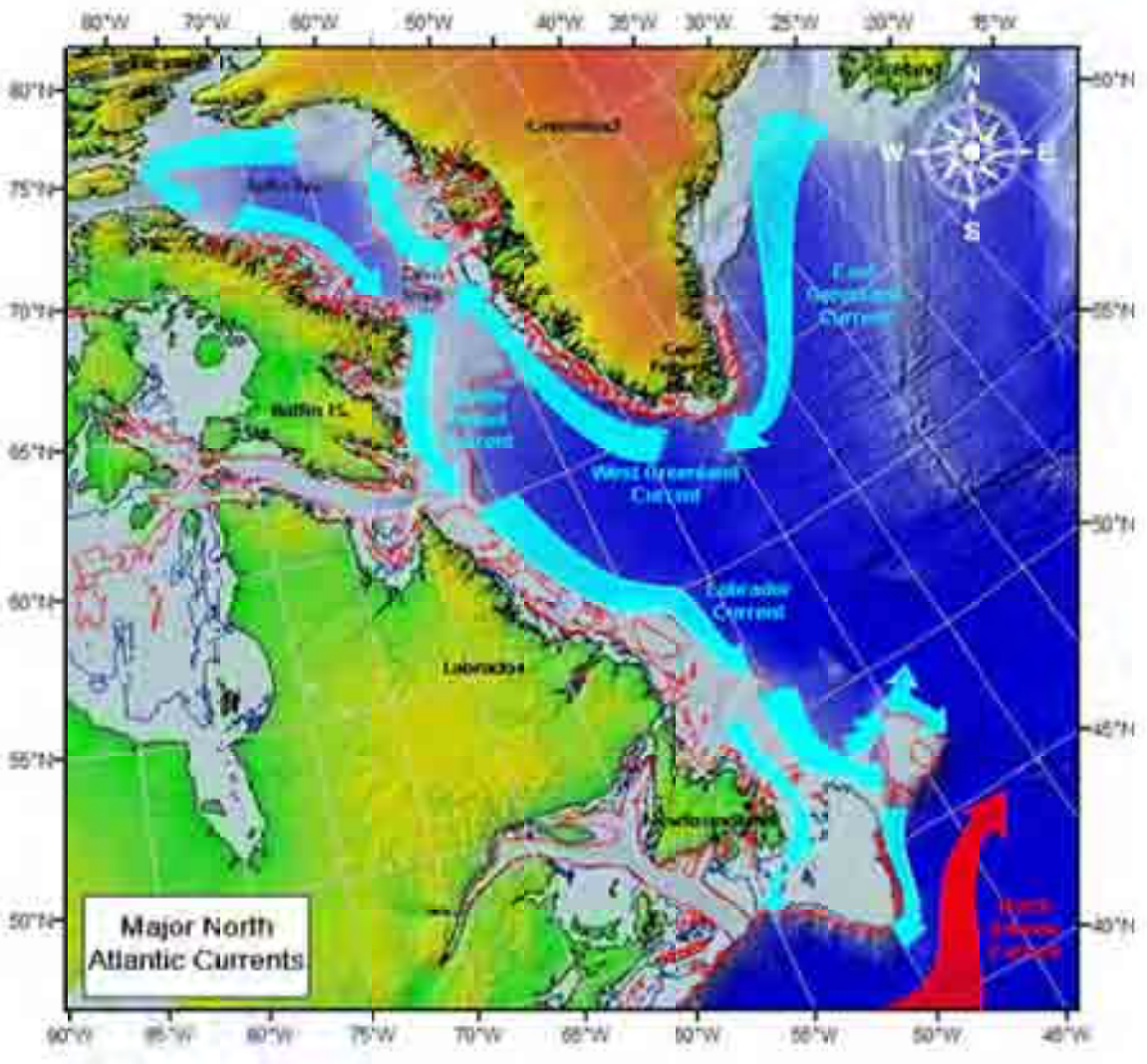


Figure2.5-1.Map of t he large sc ale ocean currents in t he Ne wfoundland regio n. (Source : U. S. Coast Guard, International Ice Patrol).

For this study, currents for the North Atlantic region were acquired from the HYCOM (HYbrid Coordinate Ocean Model) circulation model. HYCOM is a primitive-equation ocean general circulation model that evolved from the Miami Isopycnic-Coordinate Ocean Model (MICOM) (Halliwell et al., 1998, 2000; Bleck, 2002). MICOM has become one of the premier ocean circulation models, having been subjected to validation studies (Chassignet et al., 1996; Roberts et al., 1996; Marsh et al., 1996) and used in numerous ocean climate studies (New and Bleck, 1995; New et al., 1995; Hu, 1996, 1997; Halliwell, 1997, 1998; Bleck 1998).

The HYCOM global ocean system is a 3-D dynamical model that is run each day, providing a 5-day hindcast and 5-day forecast of oceanic currents. Hindcast data are used to validate the accuracy of each run to determine if modeled forcings produce results that match observational data. HYCOM uses Mercator projections between 78°S and 47°N and a bipolar patch for regions north of 47°N to avoid computational problems associated with the convergence of the meridians at the pole. The 1/12° equatorial resolution provides gridded ocean data with an average spacing of ~7km between each point. Several studies have shown that at least 1/10° horizontal resolution is required to resolve boundary currents and mesoscale variability in a realistic manner (Hurlburt and Hogan, 2000; Smith and Maltrud, 2000; Chassignet and Garaffo, 2001).

The HYCOM model works effectively in both deep and shallow waters. There are 32 vertical layers in a hybrid vertical coordinate scheme, where isopycnics are used in the deep ocean stratified interior (Halliwell, 2002). These isopycnals smoothly transition to z-level coordinates (isobaric) in the weakly stratified upper-ocean mixed layer, to terrain-following sigma coordinates in shallow water regions, and back to z-level coordinates in very shallow waters (Halliwell, 2002). Differential vertical mixing models improve performance including any one of the three available differential vertical mixing models: 1) non-local K-Profile Parameterization, 2) NASAGISS level 2 turbulence closure, and 3) Mellor-Yamada level 2.5 turbulence closure (Halliwell, 2004). Bathymetry is derived from the NRL DBDB2 dataset. Surface forcing is derived from the Navy Operational Global Atmospheric Prediction System (NOGAPS), which includes wind stress, wind speed, heat flux (using bulk formula), and precipitation.

Data is assimilated through the Navy Coupled Ocean Data Assimilation (NCODA) system (Cummings, 2005). The NCODA system employs a Multi-Variate Optimal Interpolation (MVOI) scheme, which uses model forecasts as a first guess and then refines estimates from available satellite and in-situ temperature and salinity data that are applied through the water column using a downward projection of surface information (Cooper and Haines, 1996).

One may expect approximately 5-10% sea ice coverage during the winter months in the area of interest (Deser et al., 2002). Sea ice affects the energy balance of the ocean through variations in albedo and the energy dynamics of phase change, which would impact ocean circulation. An energy loan sea ice model was developed to manage the energetics of water phase changes (Semtner, 1976). The model focuses on the stabilization of ocean temperature near the freezing point through ice formation and melting, as well as the impact of the ice surface on the ocean-atmosphere energy fluxes. When the model is run with hybrid vertical coordinates and a

non-slab mixed layer model, no attempt is made to reduce the thickness of layer one at a given grid point when ice forms (Bleck, 2000).

Hindcast currents generated using HYCOM were obtained for the period November 2003 through September 2010 for the North Atlantic region. Daily average current speed and direction data provided at locations on a regular grid spaced at a distance of 1/12 degree were used in SIMAP for modeling the Hebron oil spills in this study. Current measurements made at the Hibernia and other sites nearby the Hebron site could not be compared to the currents predicted by the HYCOM hindcast because these data sets do not cover the same time period.

While the HYCOM model hindcast also provides wind data for the North Atlantic region, the MSC50 wind data were used for the oil spill simulations because it is the best dataset for the purposes of spill risk assessment in eastern Canadian waters. The MSC50 data have superior coverage to the HYCOM data, especially near shore, and have better temporal and spatial resolution within the Canadian east coast region.

2.6 Ice Data

Sea ice is formed in the autumn in the Arctic and sub-Arctic regions of the world. The growth rate of sea ice depends on surface temperature, the depth of snow cover, and the heat flux in the underlying water. The formation and development of sea ice follows a progression of stages. The exact timing of these stages at any location is not the same from year to year because of subtle differences in climatic conditions. In the Northern Hemisphere during September and October, the air temperature lowers sufficiently to form a thin sheet of ice on the sea. Freezing temperature for average northern ocean salt water of about 3.5 percent salt composition by weight (usually designated 35 parts per thousand) is -1.8ºC (28.8ºF).

The presence of sea ice in Newfoundland and Labrador waters was below normal during the winter of 2009-2010 (CIS, 2010). In fact, the total accumulated ice coverage in eastern Newfoundland waters set a new record low during the 2009-2010 winter season. Figure 2.6-1 shows the total accumulated ice coverage offshore the Canadian east coast measured by the Canadian Ice Service since the winter of 1968-69. Ice coverage over the past 17 years over eastern Canada has been below the 40-year average, showing a decline in overall ice area.

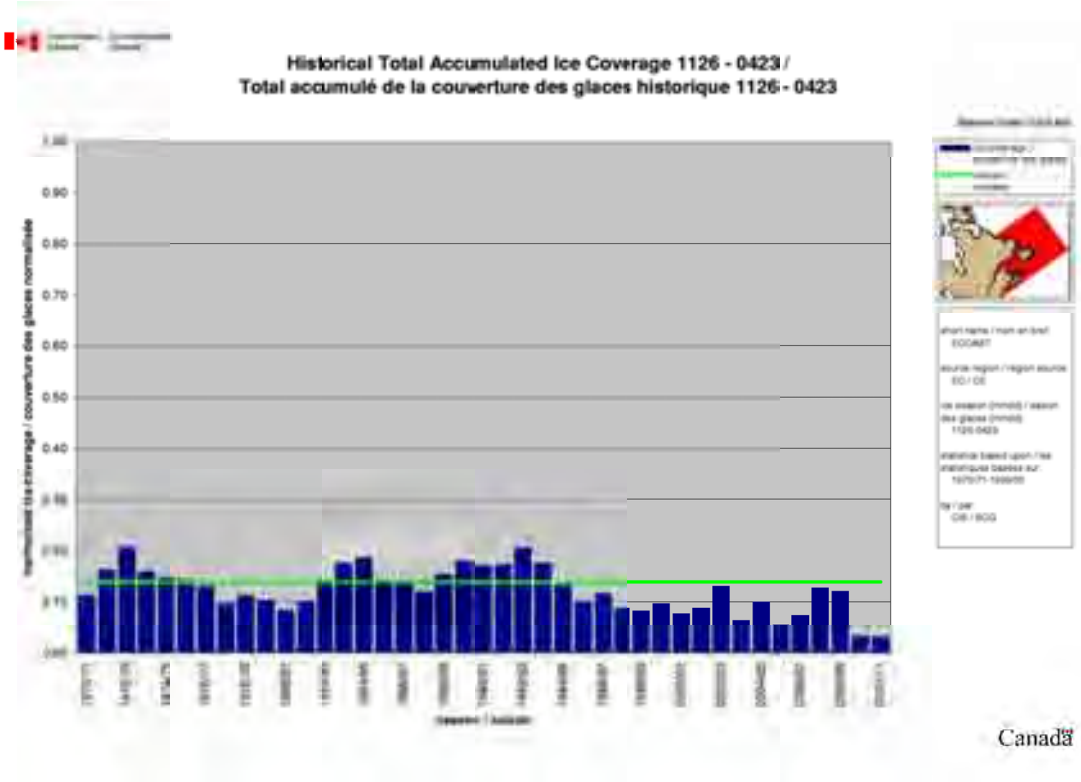


Figure 2 .6-1. Total accumulated ice co verage for the period of r ecord from the Canadi an Ice Service.

Ice coverage in the winter of 1989-1990 was at a maximum extent in the region around the Hebron site according to the data collected by the Canadian Ice Service. Figure 2.6-2 shows a map of ice concentration in the Newfoundland region for the week of March 12, 1990. The red areas on the map indicate ice concentrations greater than 90% and cover a large extent of the offshore area east of Newfoundland. The Hebron platform, located at 48.498° W, 46.544° N, is just outside this area.

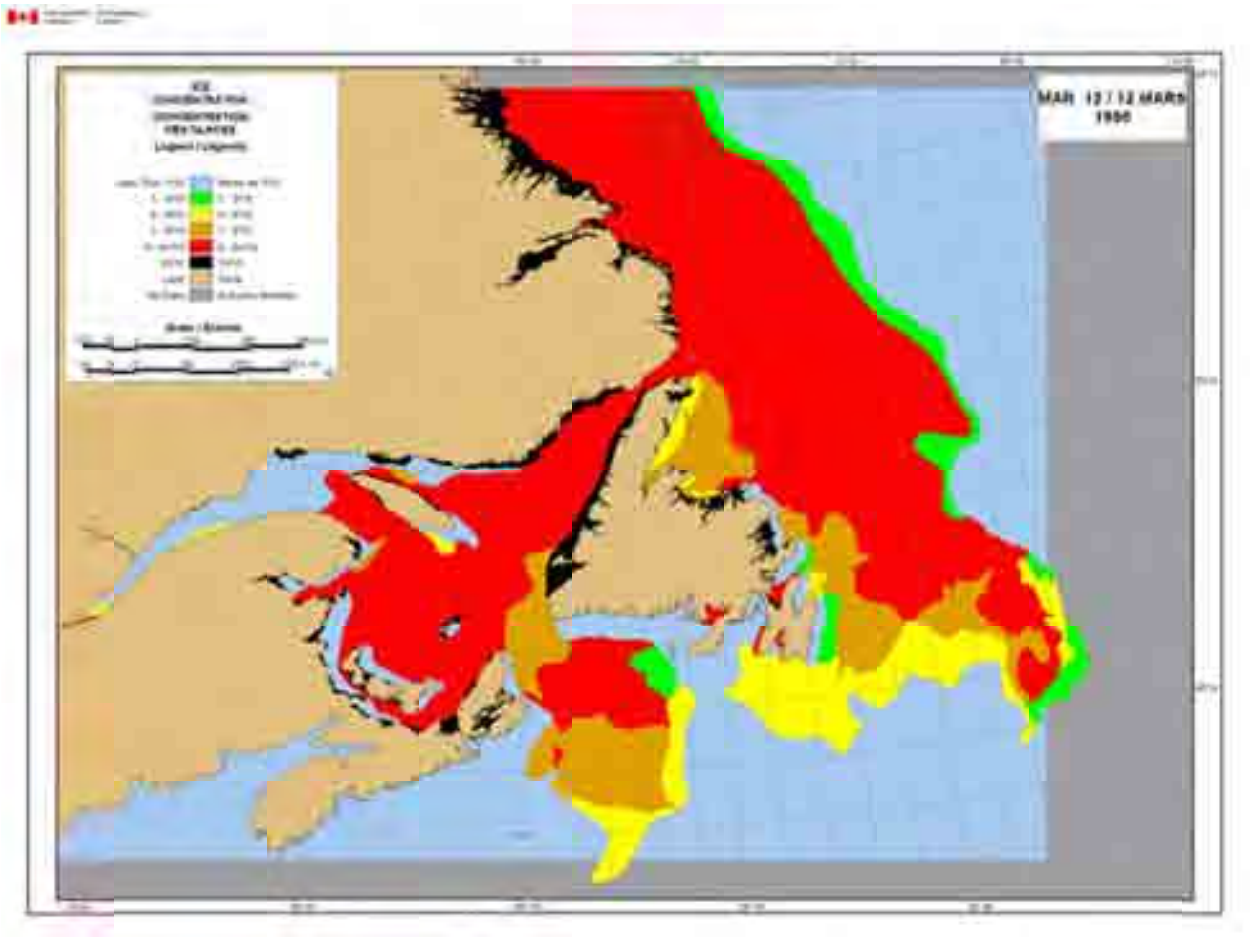


Figure 2.6-2.Ice concentration chart from the Canadian Ice Service for the week of 12March, 1990.

The fate and behavior of spilled oil is greatly affected by the presence of ice. Oil spilled before, during or after freeze-up will follow an arrested pattern of weathering compared to oil spilled on open water. Implementation of algorithms in SIMAP for modeling the movement and fate of oil in the presence of sea ice is based on the percent of ice coverage. From 0 to 30% coverage, the ice has no effect on the advection or weathering of a surface oil slick. From 30 to 80% ice coverage, oil advection is steered to the right in the northern hemisphere, surface oil thickness generally increases due to ice-restricted spreading, and evaporation and entrainment are both reduced. Above 80% ice coverage, surface oil moves with the ice, evaporation and entrainment cease and oil thickness, which can vary widely, is calculated as a function of ice thickness. Appendix A contains a brief summary of the algorithms implemented in the SIMAP model for oil spills in sea ice conditions.

The SIMAP model algorithms are based on an early (1980's - 1990's) understanding of oil/ice interactions. Since that time various studies (mostly Norwegian) have improved the understanding of oil/ice interactions, but most of that work was focused on developing oil spill response strategies, not oil spill model algorithms.

The impediment to more robust simulation of the interactions of oil in ice is not a lack of understanding of those processes as much as it is a lack of data to define the characteristics of the ice over small spatial scales (centimeters to tens of meters) and short time periods (hours to days). A review of oil spill models by Reed *et. al*. (1999) identified this as the overriding issue holding back realistic modeling of oil in ice:

> *"… the prognosis for improved representation of oil behavior in ice-infested waters remains bleak until our capability to model ice alone improves. … the processes governing oil behavior occur at scales of a few centimeters to a few tens of meters within an ice field. Ice model resolutions are typically at scales of kilometers, to account for effects at active boundaries, such that very crude, ad hoc parameterizations become necessary."*

Ice data used in the oil spill model simulations were obtained from the National Snow and Ice Data Center (http://nsidc.org/index.html) for the months of February and March, 1990. Since 1990 showed the greatest extent of ice coverage at the Hebron offshore site, this year was selected as the representative year for the purposes of spill trajectory modeling. These data are in the form of ice concentration grids with values from 0 to 100% ice coverage. The winter scenarios that were run with ice present use these data to define the ice coverage for the months of February and March regardless of the year of the simulation. Figure 2.6-3 shows the ice concentration for February; Figure 2.6-4 is a map of the ice concentration for March.

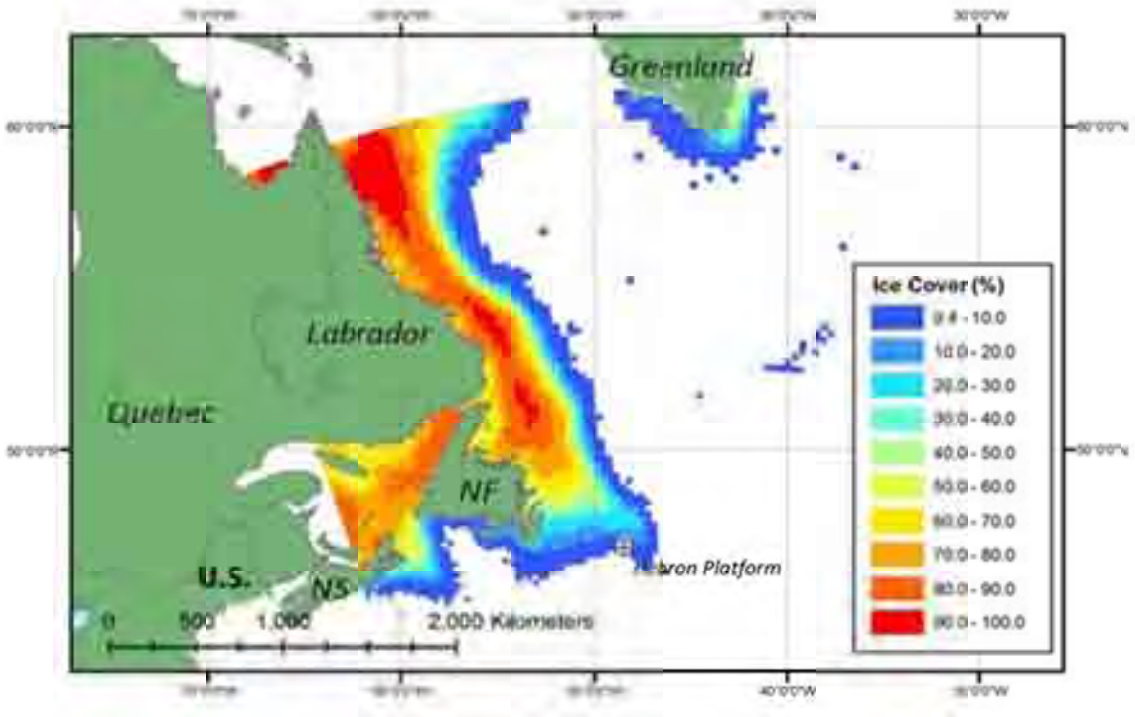


Figure 2.6-3. Sea ice coverage used in the oil spill model simulations for the month of February.

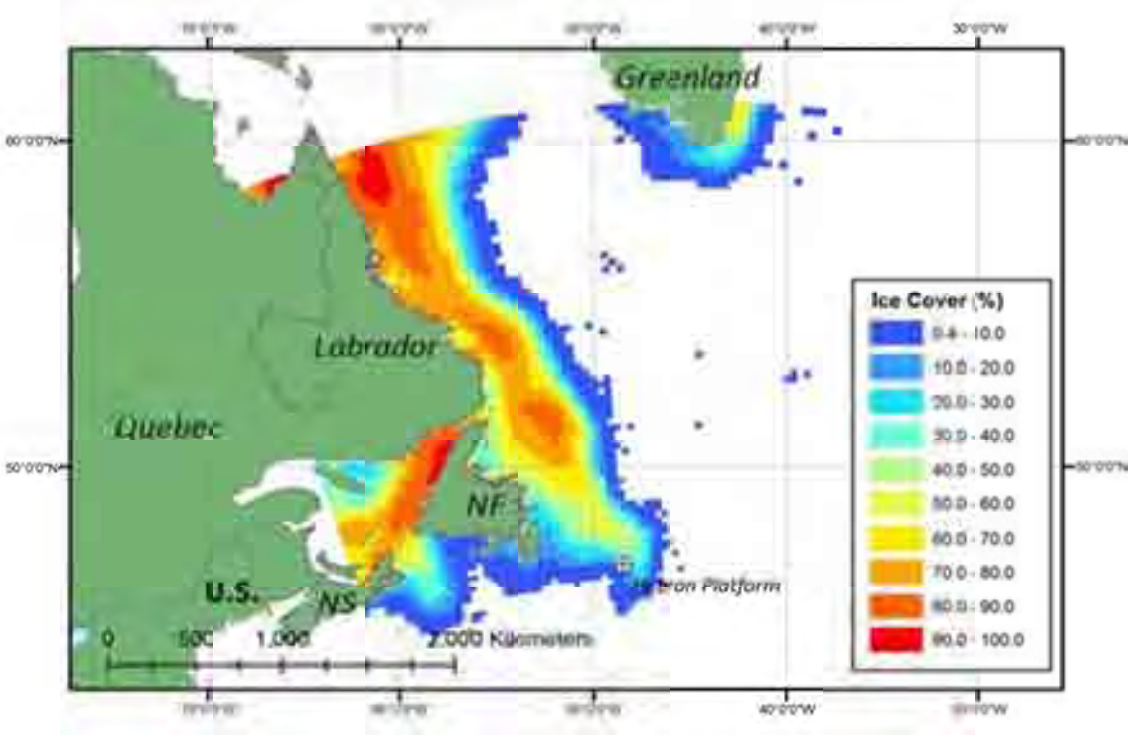


Figure 2.6-4. Sea ice coverage used in the oil spill model simulations for the month of March.

2.7 Shoreline Type Data

The SIMAP model utilizes a specification of the shoreline type in order to simulate oil interactions with the shoreline (see the description of these interactions in Appendix A). The Newfoundland shoreline was defined as Seaward Rocky Shore. Table 2.7-1 lists the shoreline width, maximum oil thickness and oil removal half-times used in the oil spill modeling.

Table 2. 7-1Shorelinecharacteristics for th e shore t ype used in the spill simul ations (ba sed on Gundlach, 1987).

Shore Type	Width (m)	Maximum Oil Thickness (mm)	Oil Removal Half-time (days)
Exposed Rocky Shore	3	2.0	1

The shoreline width and maximum thickness are used by the SIMAP model to calculate the maximum amount of oil that may reside on the shoreline (width x thickness). Once a section of shoreline has reached its holding capacity, oil coming ashore at this site will remain in or on the water, but the shoreline cannot hold more than its specified capacity. Oil on the shoreline may be washed off and return to the water surface as changes in water elevation due to tides expose the intertidal portions of the shore to wave action. This process is calculated in the oil spill

model using the oil removal half-time, which in the case of Exposed Rocky Shore means that 1% of the stranded oil mass is removed from the shoreline each day.

Interactions of oil with the shoreline are calculated in the SIMAP model based on the study of shoreline oiling, fates and removal processes performed as part of the development of the COZOIL model for the U.S. Minerals Management Service (Reed et al., 1986, 1988, 1989; Gundlach, 1987; Reed and Gundlach, 1989). Appendix A describes some of the details of these interactions while the references listed provide a more in-depth discussion of the COZOIL model.

3. Modeling Description

3.1 Overall Modeling Approach

This modeling study utilized a stochastic approach to determine the potential fate of spills from the Hebron offshore site. In a stochastic approach, a spill trajectory model is run repeatedly with a start date that is randomly selected within the time period covered by the available wind and/or currents data. Using wind model hindcast data to define the wind field and currents generated by a hydrodynamic model, each oil spill simulation was run using a wind time series that started on the randomly selected date. In this approach, a sufficient number of model runs will adequately sample the variability in the wind speed and direction in the region of interest and will result in a prediction of the probability of oil pathways for a spill at the prescribed location. Running multiple spill simulations during a single season will provide a reliable prediction of the oiling probability for a spill starting during that season and extending into subsequent seasons.

The oil spill scenarios listed in Table 2.2-1 were simulated using the SIMAP model and environmental conditions from the summer and winter seasons. The initial simulations were run for 30, 60, 100 and 120-day periods to determine the fate of the oil released from both the platform and subsurface blowouts. The platform spill scenarios have subsequently been modeled for extended periods of time to determine the fate of the oil within the defined model domain (i.e., to determine if the oil leaves the model domain, and/or if oil contacts the Newfoundland shoreline). The 30-day release was run an additional 200 days for a total of 230 days. The 100- and 120-day blowouts were also run for an additional 200 days. The results from the extended run simulations are presented in the addendum to this report.

Seasonal wind roses of the 30-year wind time series from the MSC50 model hindcast location closest to the Hebron site (M6010632) are presented in Section 2 of this report. Based on the MSC50 wind data for the period 1978 - 2008, wind climatology in the summer and winter exhibit two distinct regimes characterized by predominant wind directions. Summer winds are most frequently from the southwest, while winter winds are of higher speed and come most often from the west. The summer and winter wind regimes are periods where winds show a pattern of predominant direction while the spring and fall wind regimes represent periods of transition between them. The direction of spring and fall winds is highly variable and extended duration spills occurring during these months tend to remain closer to the spill source because the wind does not blow from the same direction for extended periods of time. The variability in direction seen in the spring and fall seasons is also contained within the summer and winter winds. And finally, while all of the spill simulations start during the summer or winter months, the simulations extend into the following season so that its winds are also used. In the case of the extended period simulations, run for an additional 200 days, the simulations run through most of the year. In the case of the extended runs, Figure 3.1-1 illustrates the time span covered by the blowout releases and the total model simulation period over a full year.

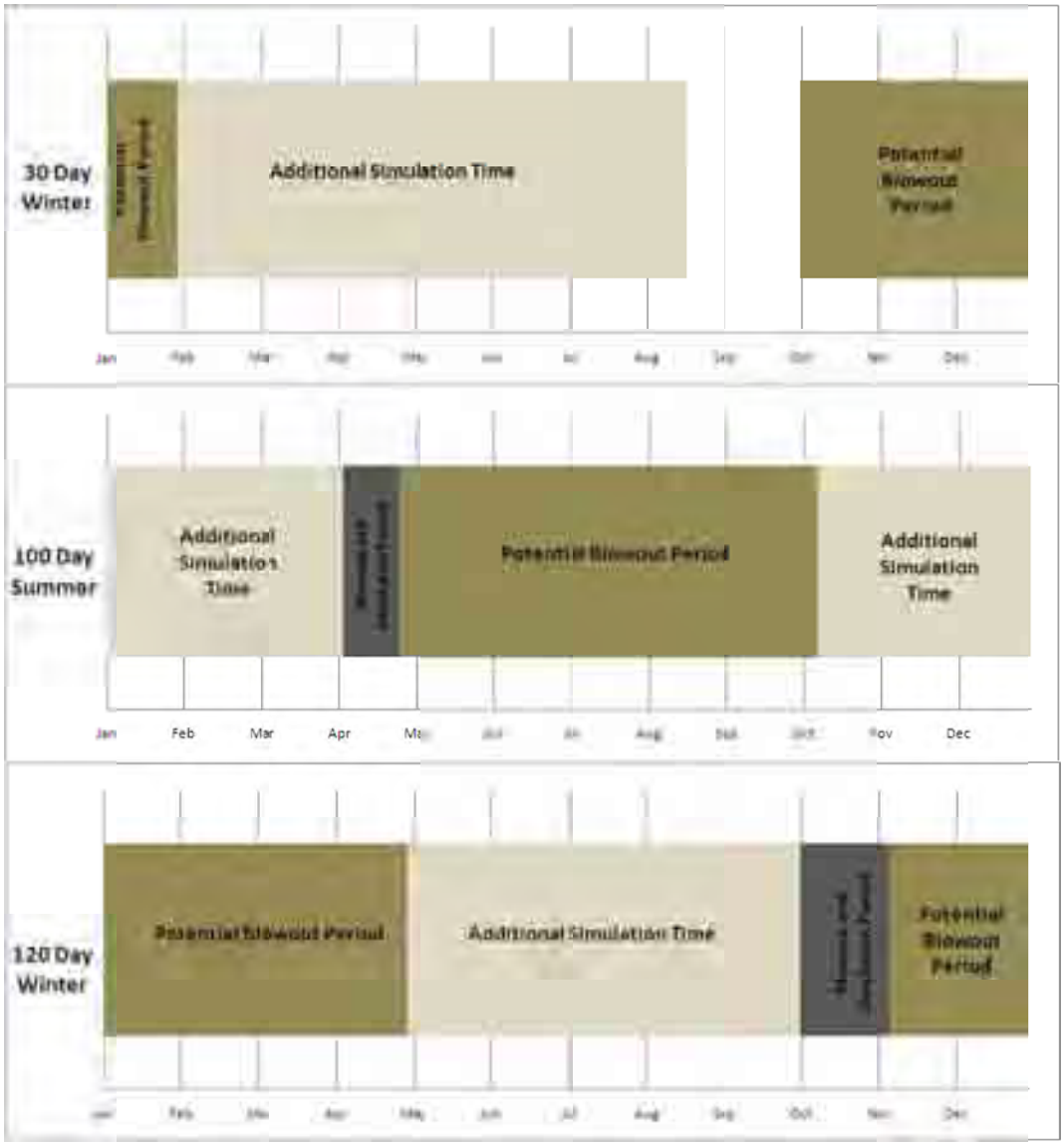


Figure 3.1-1. Time coverage for blowout simulations.

Each simulation of the spill scenarios using the stochastic model consisted of 100 individual runs of the spill model, each with a randomly selected start time so that a different time slice of wind data was used for each model run. In order to demonstrate that 100 simulations is sufficient to obtain an adequate sample of the wind within all seasons, plots of the wind data from the entire 30 year wind record are compared with plots of the wind data sampled by the stochastic model for each season. These wind plots, shown in Figures 3.1-2 through 3.1-4, demonstrate that the 100 stochastic model simulations performed for each spill scenario adequately sampled the relevant environmental data within the season the spill began, but also within the subsequent season. For example, in Figure 3.1-4, the bottom two wind roses show

good agreement between the entire wind record and the wind sampled by the spill model for the spring months for the 120 day spills started in the winter.

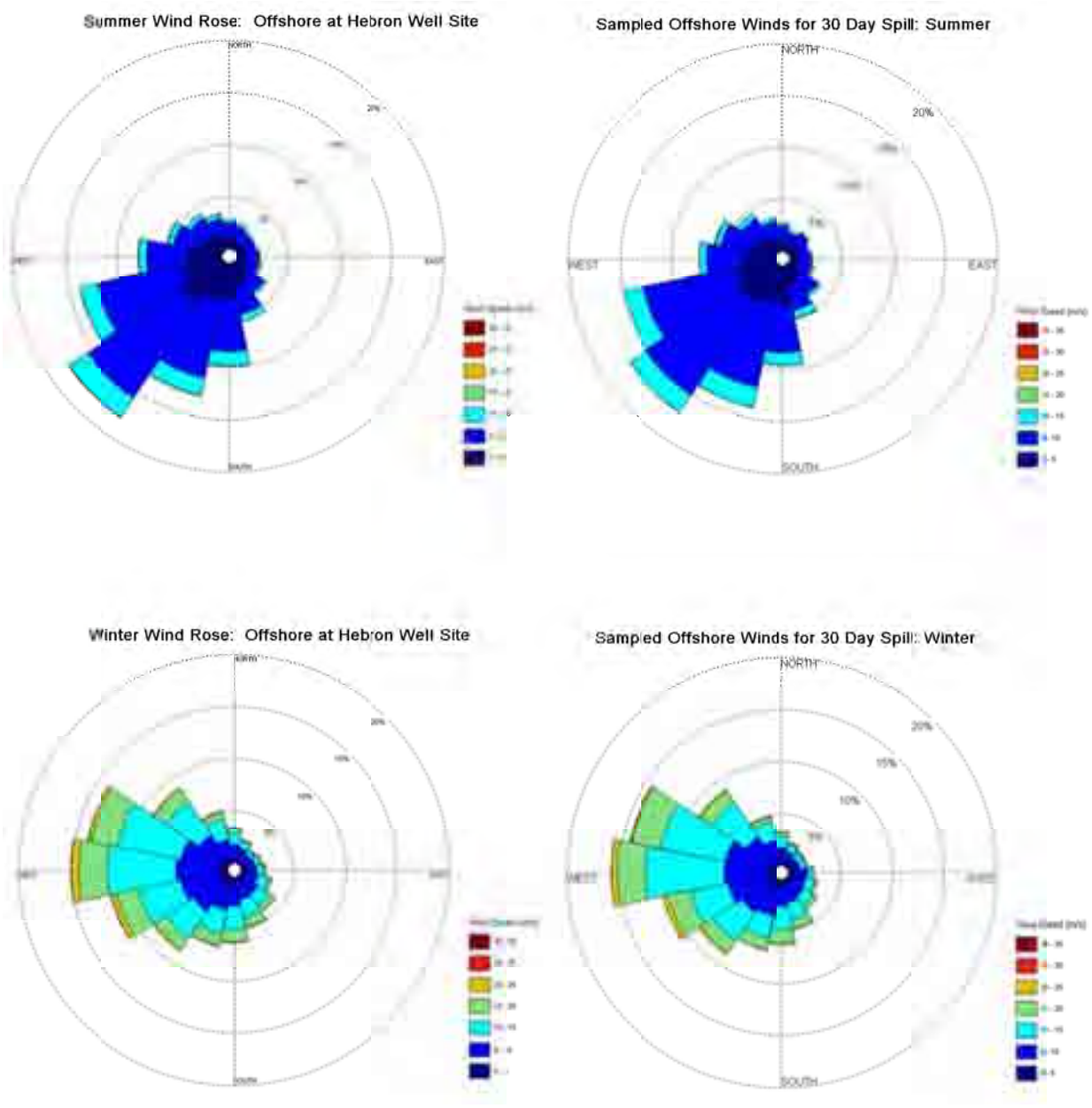


Figure 3.1-2. Comparison between the 30-year MSC50 wind data occurring at site M6010632 (left rose plots) and the wind data from the same source that was used by the SIMAP model to simulate spills (right rose plot) for the 30 day platform blowout. The top pair of plots is from the summer season, the bottom pair compares winter data.

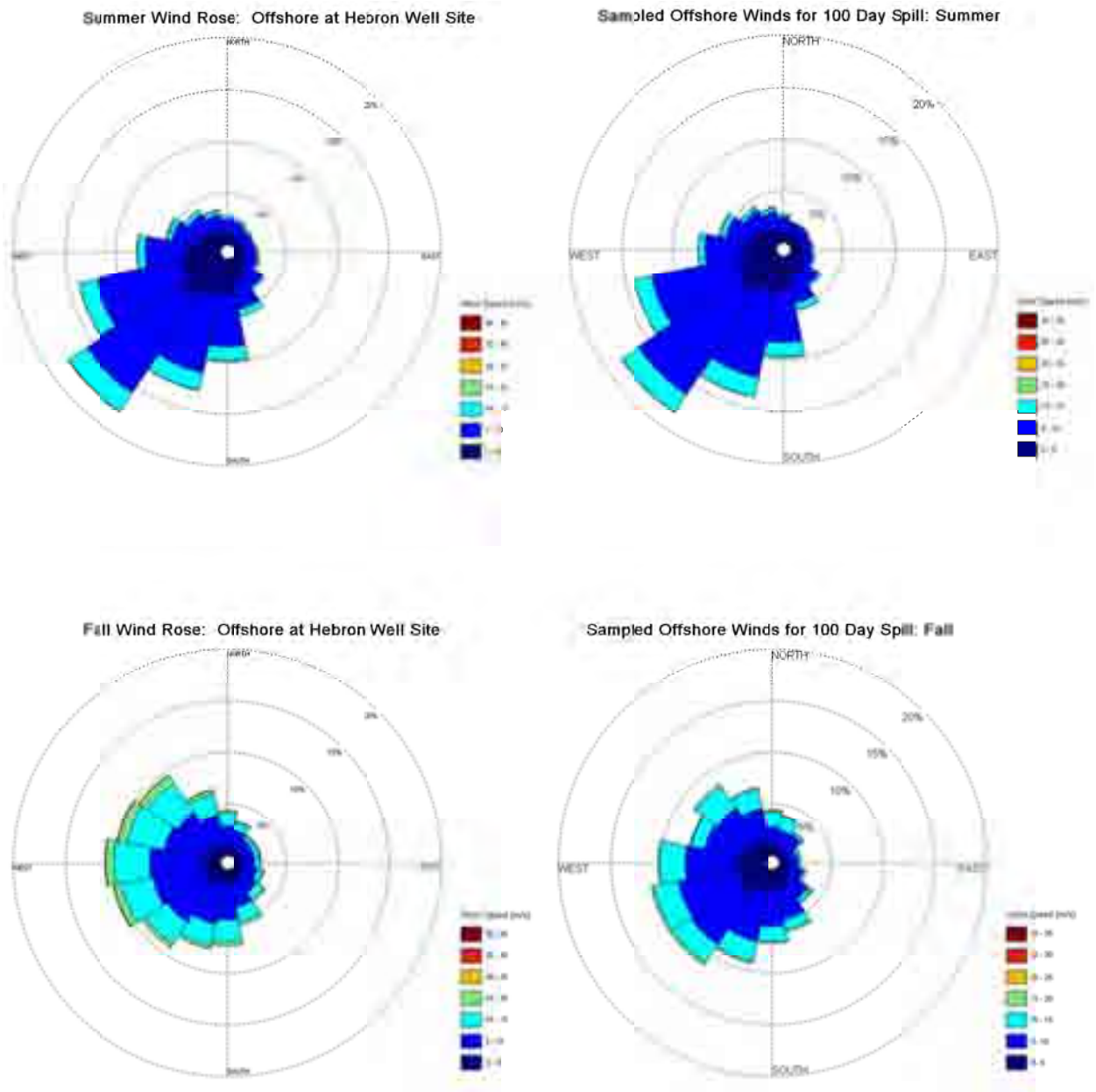


Figure 3.1-3. Comparison between the 30-year MSC50 wind data occurring at site M6010632 (left rose plots) and the wind data from the same source that was used by the SIMAP model to simulate spills (right rose plot) for the 100 day platform blowout. The top pair of plots is from the summer season, the bottom pair compares fall data.

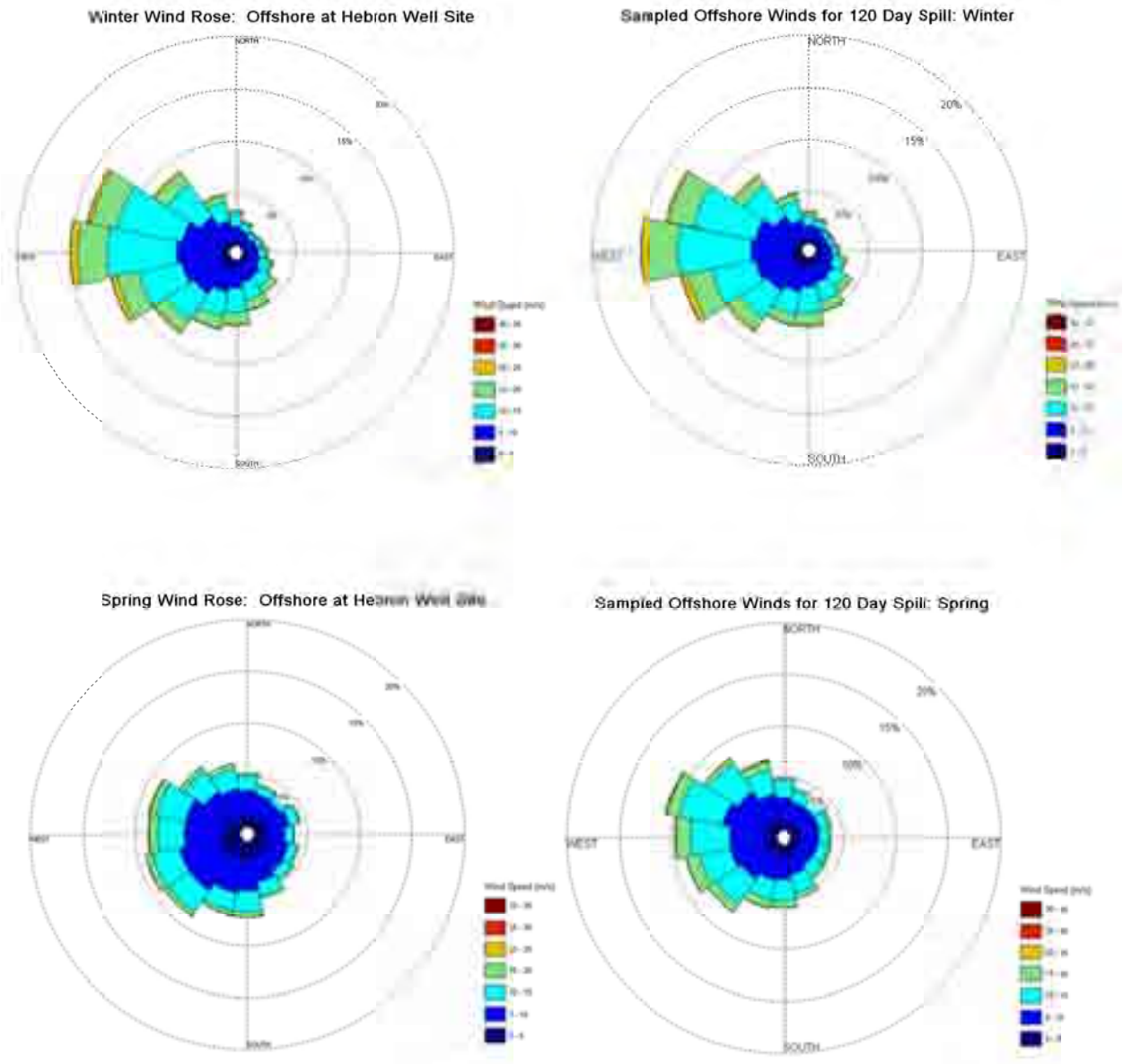


Figure 3.1-4. Comparison between the 30-year MSC50 wind data occurring at site M6010632 (left rose plots) and the wind data from the same source that was used by the SIMAP model to simulate spills (right rose plot) for the 120 day platform blowout. The top pair of plots is from the winter season, the bottom pair compares spring data.

3.2 Blowout Releases of Crude Oil

Blowouts

Two blowout scenarios were simulated at the Hebron offshore site. One discharge originates from the platform deck at a height of 70m above the sea surface, the second blowout scenario involves the subsea release of crude oil at the seabed in approximate 98 meter water depth. The platform blowout was simulated using the SIMAP stochastic and 3D fates deterministic models. The seabed release was modeled using the ASA blowout model in combination with the SIMAP stochastic and 3D fates models.

ASA's blowout model was used to determine the near field dynamics of the oil plume for the release occurring at the seabed. When blowouts occur in deep water it is necessary to use a model that considers the effects of gas hydrate formation and calculates the size of oil droplets discharged from the source in order to determine the movement of oil through the water column to the sea surface. In this case the 98 meter water depth at the Hebron offshore site is too shallow for hydrate formation so that process is not included in this modeling study.

ASA's blowout plume model predicts the dynamics of deep-water blowouts by solving equations for the conservation of water mass, momentum, buoyancy, and oil/gas mass using integral plume theory, following McDougall (1978). Equilibrium hydrate formation and dissociation for gas hydrates are determined by a multi-phase flash calculation developed by Bishnoi et *al*., (1979, 1989). Appendix B describes the blowout plume model. Results from the blowout plume modeling provide the initial dynamics of the oil plume for the 3D fates simulations (i.e. far field analysis) of the seafloor blowout.

In a blowout, an oil and gas mixture is released from the seabed and is driven into the water column where it initially forms a momentum jet. Depending on the velocity of the gas/oil mixture exiting the well, the jet portion of the discharge can be confined to the vicinity of the seabed or extend vertically into the water column for hundreds of meters. As the jet-driven plume rises, it continues to entrain sea water, reducing the plume's velocity and buoyancy and increasing its radius, forming the shape of an inverted cone. Figure 3.2-1 shows a perspective view of an idealized terminated plume for a simple case with no currents to distort the plume. At the point above the seabed where the jet is no longer driven by the discharge momentum and buoyancy of the gas, the oil droplets are driven towards the sea surface by buoyant force. If the momentum driven jet reaches the sea surface, the plume is deflected in a radial, surface flow zone without appreciable loss of momentum. This radial jet carries the oil particles rapidly away from the center of the plume. The velocity and oil concentrations in this surface flow zone decrease while the depth of the zone increases. In the far field, where the plume buoyancy has been dissipated, ambient currents and wind generated waves determine the subsequent transport and dispersion of the oil. If the momentum driven plume does not reach the sea surface then the oil droplets rise through the water column driven by buoyant force.

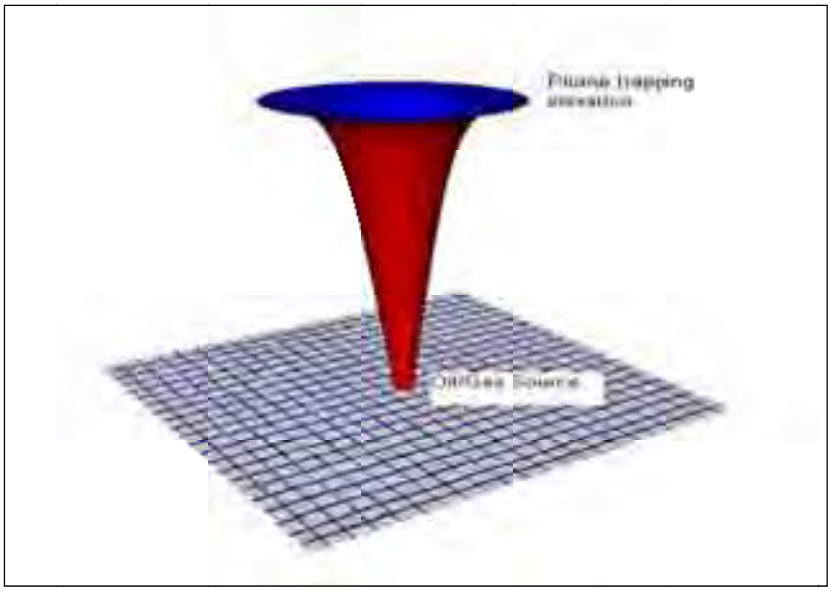


Figure 3.2-1. Perspective view of example oil/gas plume reaching termination depth.

Blowout Plume Dynamics

Oil ascends to the surface essentially with the same path as the gas. The oil initially rides on the buoyant plume, after leaving the plume it rises with the free rise velocities determined by Stokes law. The free rise velocities of oil are significantly slower than that of gas due to the lower density difference (water/oil) and a much smaller range of oil droplet sizes.

The size range of the oil droplets produced during the blowout has a profound effect on how oil travels after leaving the plume. Large droplets will reach the surface faster and small droplets will stay longer in the water column and be subjected to the subsurface advection-diffusion transport from ocean currents and turbulence for a longer period. Long residence time in the water column means that oil droplets have the potential to be transported long distances from the blown out well before reaching the sea surface.

The oil droplet size distribution used in the blowout model is based on the Rosin-Rammler distribution (Rye et al., 1998, Lefebvre, 1989), and primarily depends on the exit velocity of the discharged oil and gas. For a given exit dimension, exit velocity is a function of total discharge rate. Table 3.2-1 lists the inputs to the blowout model defining the seabed blowout. Table 3.2-2 lists the droplet size distribution calculated by the blowout model. Once a size distribution is determined, rise velocities are a function of droplet size. The oil droplet size distributions in Table3-2.2, as well as the width and height of the plume determined using the blowout model, were used in the SIMAP 3D fates model to initialize the subsurface blowout simulations. The blowout model predicts that the oil will be delivered to the top 10 meters of the water column as oil droplets with the size distribution listed in Table 3.2-2.

Table 3.2-1.Blowout model inputs defining the seafloor blowout.

Parameter	Value
Gas/Oil Ratio (GOR)	655 scf/stb
Discharge Diameter (m)	0.1594
Discharge Temperature (°C)	58
Temperature/Density Profile	From NODC, winter and summer

Table 3.2-2.Oil droplet size distribution for the subsea blowout at the Hebron platform.

Droplet Size (microns)	Volume %
64.5	16.5
129.0	26.0
193.5	23.6
258.0	17.2
322.5	10.8
387.0	6.0

The blowout originating on the Hebron platform 70m above the sea surface does not require use of the blowout model. This release was simulated using the SIMAP 3D fates model as a surface release. The gas/oil mixture exiting the well pipe will form a jet extending tens of meters into the air before the oil that is discharged settles on the water surface in a circular area surrounding the platform, defined in the model as a circle of 200 meters in diameter.

3.3 Batch Transfer Spills

Small volume crude oil and marine diesel spills were simulated at the Hebron well site. Both of these spills are short-term releases at the sea surface (Table 2.2-1 lists the spill volumes and durations).

3.4 Oil Weathering

Understanding the weathering process of oil in the marine environment is critical for determining the fate and effects of spilled oil from blowouts. While the weathering of numerous oils has been studied through laboratory and field studies, each individual oil type behaves slightly differently based on a variety of physical and chemical properties including viscosity, pour point, and density.

In general, viscosity increases with time due to weathering processes. As the oil emulsifies, the oil emulsion is even more viscous than the residual oil product as is illustrated in Figures 3.4-1 and 3.4-2. The increase in viscosity tends to increase the persistence of oil on the water surface and reduce the likelihood of entrainment into the water column. This reduces the water column hydrocarbon concentration and potential exposure to organisms residing in the water column.

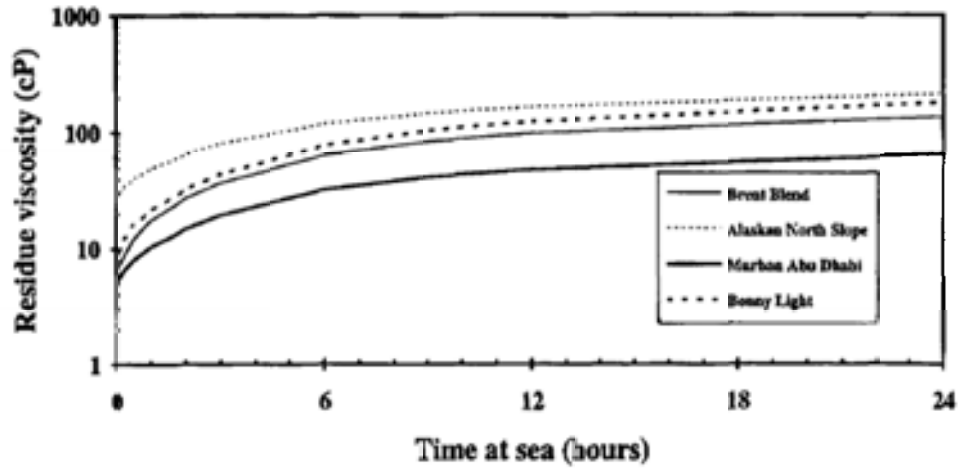


Figure 3.4-1. Change in residue viscosity with time for 4 types of oil according to the IKU Oil Weathering Model with 5 m/s wind and water temperature of 15°C (Nordiv, 1995).

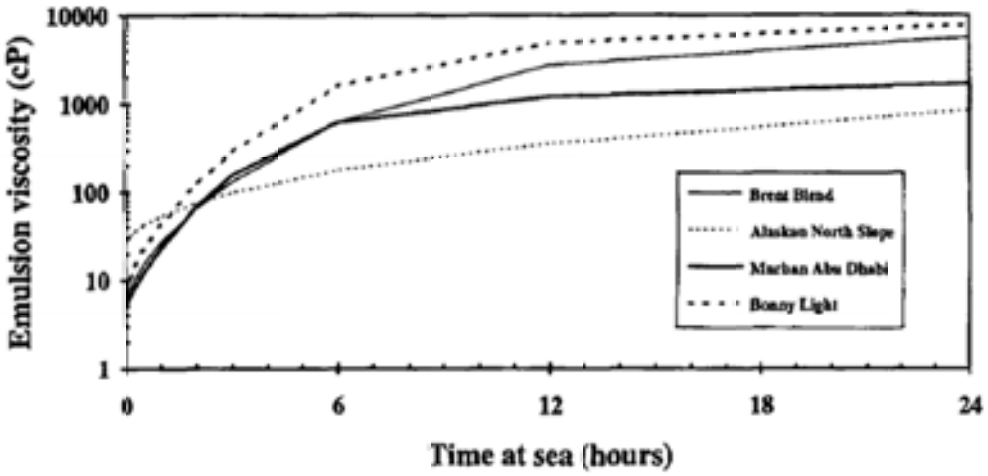


Figure 3.4-2. Change in emulsion viscosity with time for 4 types of oil according to the IKU Oil Weathering Model with 5 m/s wind and water temperature of 15°C (Nordiv, 1995).

While increases in viscosity increase the persistence of the oil on the sea surface, many processes serve to degrade the oil and reduce the toxicity and the mass of the oil in the environment. Oil mass is removed from the sea surface through evaporation and degradation. Evaporation results in the loss of the components of the oil that have low boiling points to the atmosphere (Blumer et al., 1973). Figure 3.4-3 shows a time series of oil loss due to evaporation for a variety of oils, with a range from about a 5% to 40% loss in the first 24 hours. Evaporation tends to level off within this time frame as the constituents with low boiling point are removed from the oil.

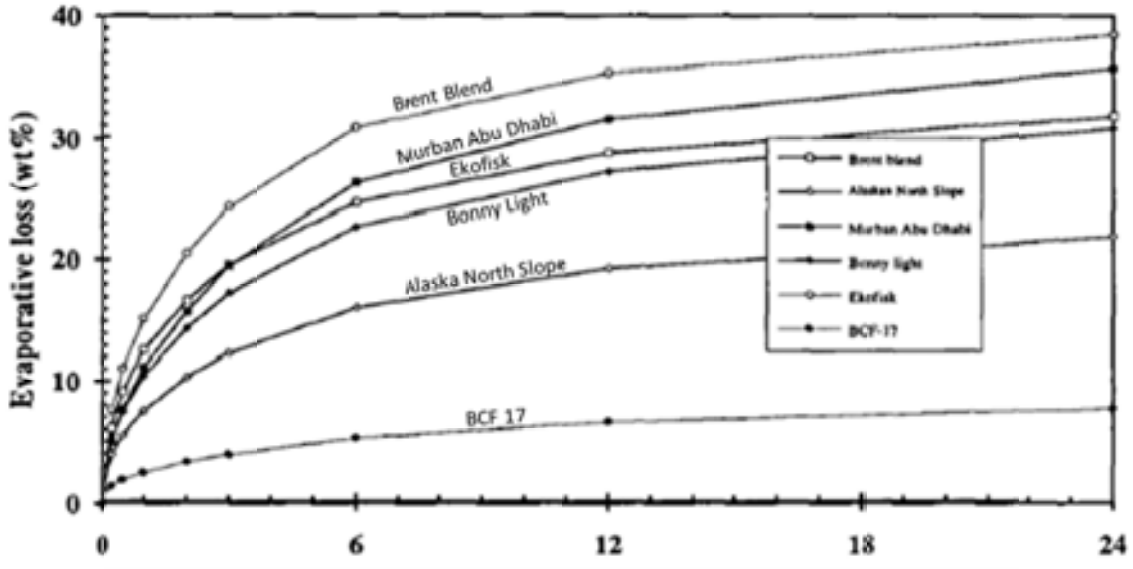
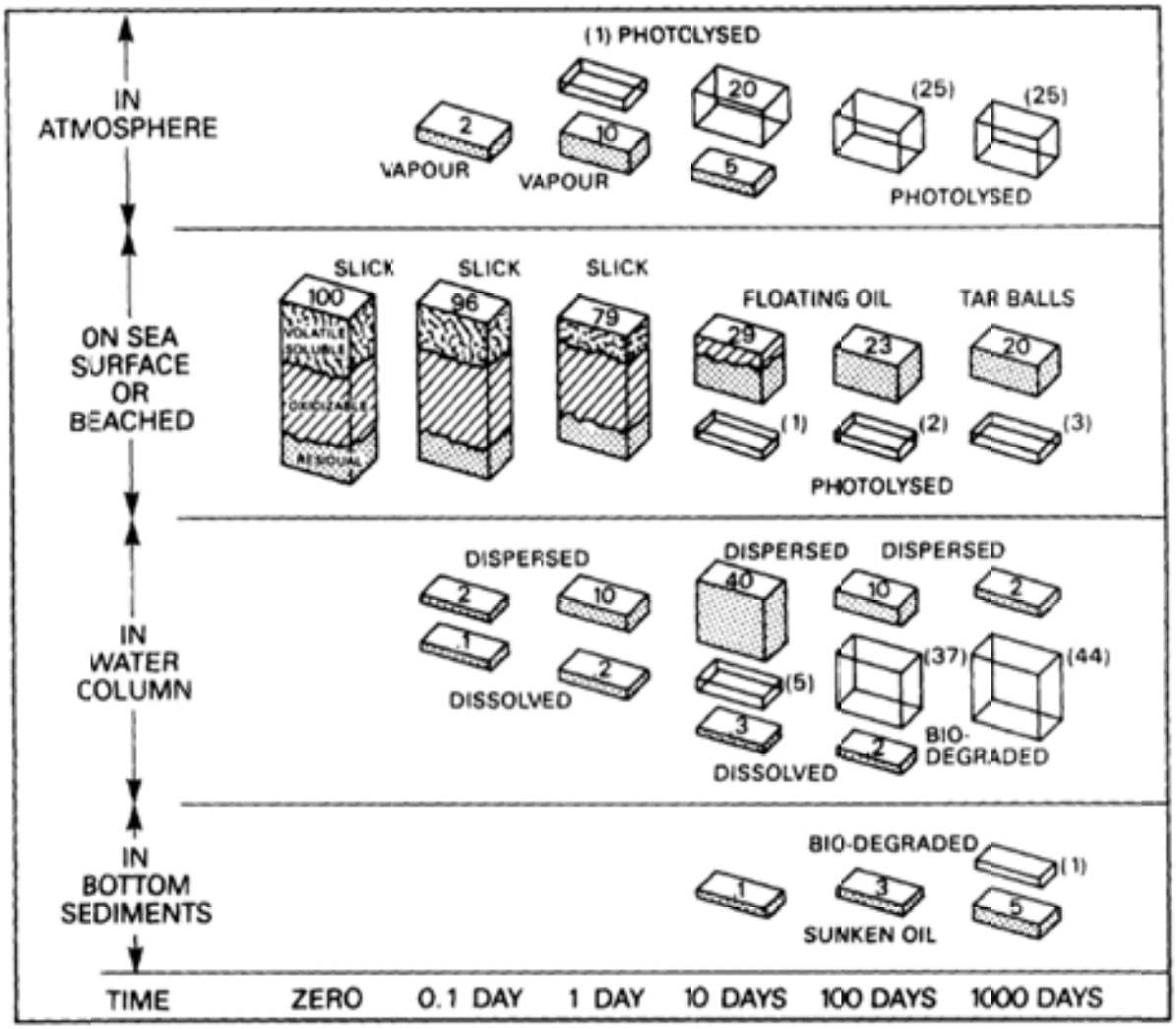


Figure 3.4-3. Evaporative loss with time for 6 types of oil according to the IKU Oil Weathering Model with 5 m/s wind and water temperature of 15°C (Nordiv, 1995).

During long duration spills, oil degradation plays an increasingly important role in removal and alteration of oil in the environment. Degradation may occur as the result of photolysis, which is a chemical process energized by ultraviolet light from the sun, and by biological breakdown, termed biodegradation. The rate of degradation can vary depending on the biological productivity and environmental conditions. In the SIMAP model, degradation acts on oil in the surface slick, on the shore and on the entrained oil and aromatics in the water column. A constant decay rate of 0.01/day(1% of available oil mass each day) is assumed in this application of oil spill trajectory modeling, resulting in a continually reducing mass of oil in the marine environment from these processes.

Figure 3.4-4 illustrates a conceptual model of the timing and location of the different oil weathering effects. The volatile, soluble, and oxidizable constituents of the oil are lost due to weathering through time, with only the residual component of the oil remaining after 100 days. Given enough time, the right environmental conditions and oil attributes, crude oil may form tar balls.

While there may be oil remaining on the water surface after an extended period of time, the literature also suggests that the area associated with an oil slick levels off after some period. Figure 3.4-5 shows a potential increase in the size of a surface slick with time for various oil volumes. While larger spill volumes result in correspondingly larger surface slicks, spreading of the surface slick stops within days of its release. Oil that is predicted to travel over the sea surface for weeks and even months will have reached its minimum thickness and not grow in area, suggesting that the surface slick becomes discontinuous and patchy.



Note: Empty unshaded boxes represent oil converted to another chemical form.

Figure 3.4-4. Conceptual model oil weathering over time (Hume, et al., 1983).

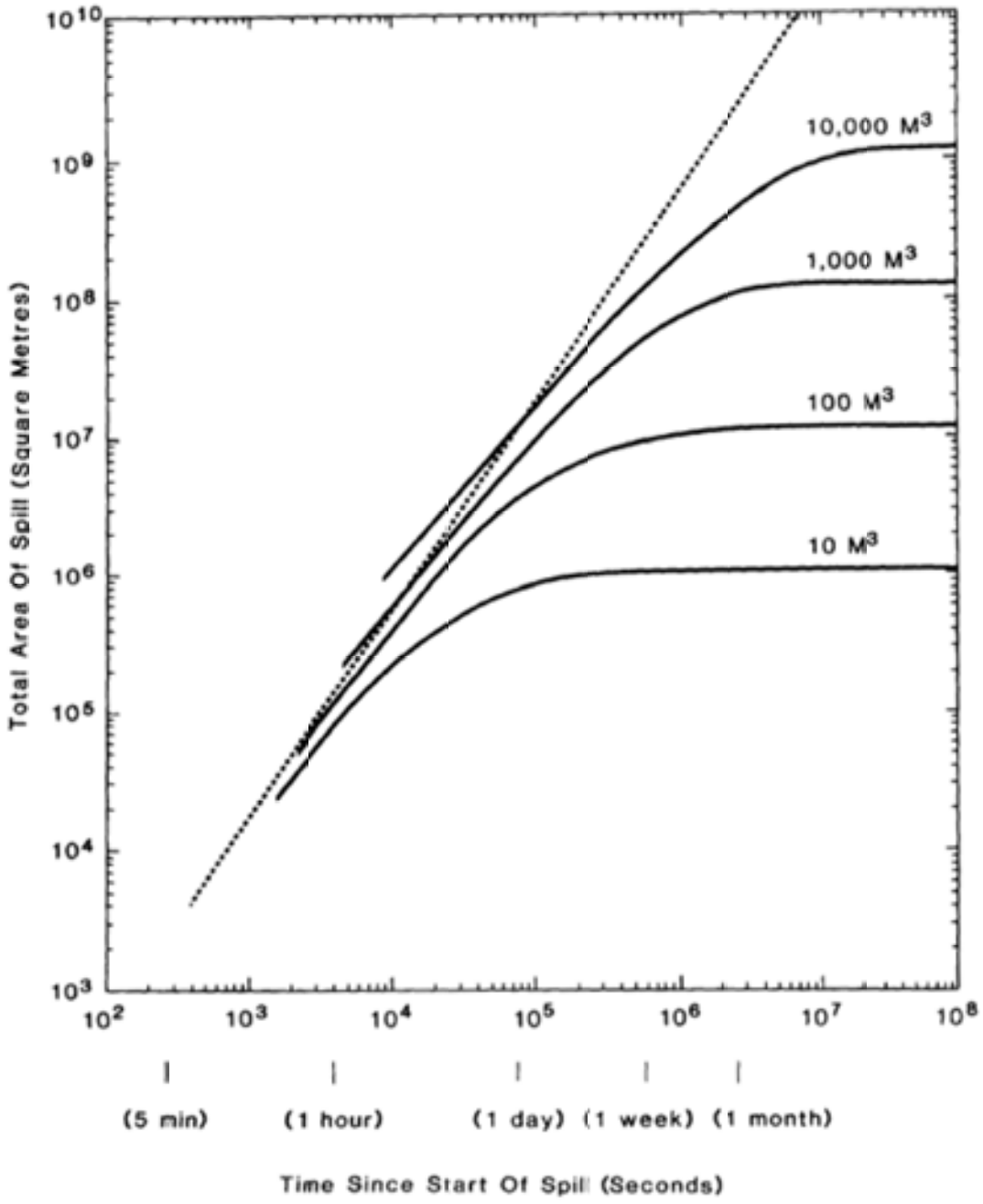


Figure 3.4-5. A prediction of swept spill area with time (Hume, et al., 1983).

Weathering of oil has an impact on the ultimate fate and effect from oil spills. For spills of Hebron D-94 and Ben Nevis crudes off the coast of Newfoundland, the weathering processes will reduce the amount of oil that remains on the water surface and thus the amount that

potentially arrives at Newfoundland shorelines. The Hebron-D94 crude, with an API gravity of 20.1, is able to contain up to 75% water when fully emulsified, allowing for the formation of a stable mousse. This emulsification places a limit on the mass of oil that can be entrained in the water column. Evaporation and decay reduce the mass of oil with time. Using a degradation rate of 0.01/day, as much as75% of the spilled oil could decay over the course of 320 days, while about 20% may evaporate (Figure 3.4-6).

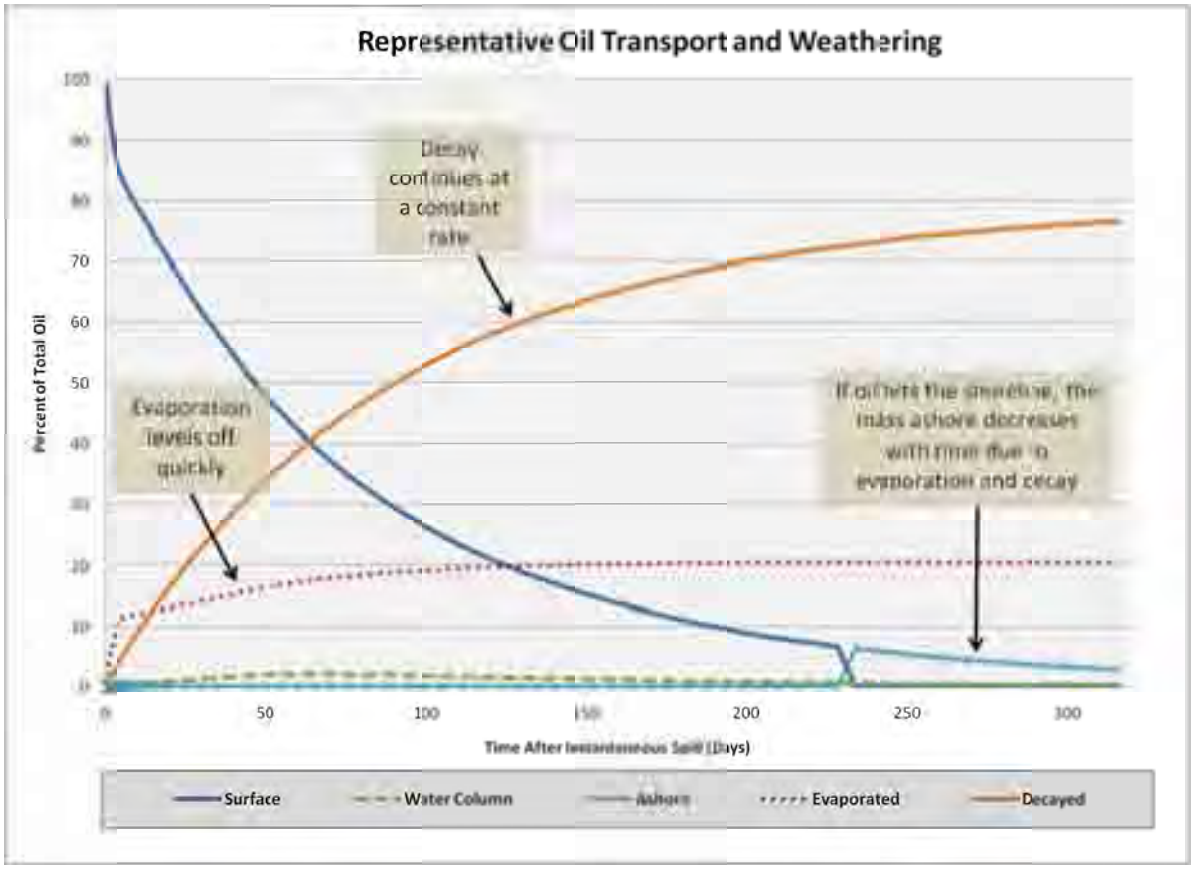


Figure 3.4-6. Mass balance from a representative instantaneous spill of Hebron D-94 oil.

4. Model Results

The stochastic and deterministic model results are presented and discussed in Section 4. Maps of the stochastic modeling results are presented in Appendix C, followed by results from the 3D fates deterministic modeling in Appendix D. Model results from the extended run simulations are presented and discussed in the Addendum.

4.1 Stochastic Model Results

The stochastic model is used to determine the probability that oil on the water surface and the shoreline will exceed the thickness threshold of 0.01mm and that oil dispersed into the water column by natural processes will exceed a concentration threshold of 10ppb (parts per billion).

Maps of the stochastic model results in Appendix C show the predicted probability of oil exceeding the thickness and concentration thresholds as well as the minimum time required for thresholds to be exceeded within the oil probability footprint.

The 0.01 mm (10 micron) surface oil thickness was selected because it is sufficient to provide a lethal dose to seabirds provided they move through the slick a minimum distance (French-McCay, 2009). Smaller surface oil thicknesses that may result in a sub-lethal dose to seabirds were not considered. French-McCay (2009) provides a good summary of recent work and discusses the details of wildlife oiling from surface slicks.

Summary of Stochastic Model Results for Blowouts

Table 4.1-1 summarizes the results from the stochastic modeling of the platform and seafloor blowouts. The table lists the results from the stochastic model for individual simulations ranked as the 50^{th} and 95^{th} percentile for oiled sea surface area, oiled shoreline length and entrained oil volume.

Table 4.1-1. Summary of the stochastic simulations of the platform and seafloor blowouts at the Hebron well site. The 50 th and 95 th percentile values are determined by ranking all 100 spills in each scenario according to the area of sea surface exposed to oil, the length of shoreline exposed to oil and the volume of entrained (naturally dispersed) oil above the stated thresholds.

Oil Release	Season	Sea Surface Area Oiled at > 0.01mm (km^2)		Shoreline Length Oiled at > 0.01mm (km)		Entrained Oil Volume after 30 days (m^3)	
		50th Percentile	95th Percentile	50th Percentile	95th Percentile	50th Percentile	95th Percentile
Platform Blowout	Summer 30-Day	205,661	388,892	0	0	20,717	31,200
	Winter 30-Day	416,325	586,907	0	0	27,428	71,582
	Winter 30-Day Ice	446,821	646,973	0	0	27,478	55,122
	Summer 30/60 Day	963,319	1,383,242	0	0	434	501
	Winter 30/60 Day	1,462,785	1,901,033	0	47.7	480	573
	Winter 30/60 Day Ice	1,382,033	1,791,808	0	42.4	476	550
	Summer 100-Day	1,855,219	2,306,565	0	10.6	134,106	159,925
	Winter 120-Day	3,353,447	4,225,306	63.6	636.2	198,454	263,493
	Winter 120-Day Ice	3,981,644	4,841,586	148.4	742.2	198,454	263,493
Seafloor Blowout	Summer 100-Day	1,942,295	2,416,717	0	5.3	3,403,664	3,706,057
	Winter 120-Day	3,535,976	4,415,367	42.4	466.5	3,777,843	4,309,446
	Winter 120-Day Ice	3,741,889	4,615,041	53	471.8	3,814,887	4,182,299

Note that the 30-day duration blowout scenarios were also run using a 60-day duration in order to track the oil for an additional 30 days. These extended simulations use the same blowout duration, rate of release and total release volume as the 30-day scenarios, however the model run time was extended to 60 days. The purpose of the extended period 30-day spill scenarios is

to determine when and where oil contacts the Newfoundland shoreline. A summary of the spills resulting in oil contact with the Newfoundland shoreline are presented in a subsequent subsection later in section 4.1.

Winds and currents at the Hebron well site are such that the majority of spills are predicted to travel eastward. The distance traveled is controlled by the blowout duration and the strength and consistency of direction of the wind. Winter wind speeds are higher than in summer and more frequently from the west and north which drives oil greater distances to the east than summer winds. A subset of the summer and winter spill simulations of greater than 30 days duration are predicted to reach segments of the Newfoundland shoreline.

Both of the crude oils used in the simulations are persistent and do not disperse into the water column readily from natural processes. This characteristic, combined with the long duration release of oil into the water, result in a large fraction of the oil remaining on the sea surface. The area of sea surface exposed to floating oil increases linearly with an increase in total spill volume.

Summary of Stochastic Model Results for Batch Transfer Spills

Table 4.1-2 summarizes the results from the stochastic modeling of the batch transfer spills performed at the Hebron well site location. The table lists the results from the stochastic model for individual simulations ranked as the 95th percentile for oiled sea surface area, oiled shoreline length and entrained oil volume. The 95th percentile results correspond to the maps of deterministic model results shown in Appendix D.

Table 4.1-2. Summary of stochastic simulations of the batch transfer spills modeled at the Hebron well site. The 95th percentile values are determined by ranking all 100 spills in each scenario according to the area of sea surface exposed to oil, the length of shoreline exposed to oil and the volume of entrained (naturally dispersed) oil above the stated thresholds.

Oil Release	Season	Surface Area Oiled at > 0.01mm (km^2)	Shoreline Oiled at > 0.01mm (km)	Entrained Oil Volume after 30 days (m^3)
		95th Percentile	95th Percentile	95th Percentile
Batch Transfer	Summer	251,672	0	496
	Winter	447,298	0	548
	Winter w/ Ice	461,520	0	547
Batch OLS Transfer	Summer	250,351	0	25
	Winter	433,132	0	28
	Winter w/ Ice	454,550	0	32

Similar to the blowout releases of crude oil reported above, marine diesel and crude oil released in the batch transfer spills is predicted to travel primarily toward the east away from Newfoundland. The marine diesel fuel is more easily dispersed into the water column than the crude oil as can be seen in the quantity of entrained oil in Table 4.1-2. The marine diesel is capable of achieving a smaller minimum thickness than the crude oil, resulting in a relatively higher sea surface area exposed to oil. None of the batch transfer spills are predicted to reach the Newfoundland shoreline.

4.2 Deterministic Model Results

This section presents and discusses the results from the deterministic model simulations of platform and seafloor blowouts and from the batch transfer spills. Maps of the deterministic model output in Appendix D depict the results from one model simulation chosen from the 100 individual simulations completed by the stochastic model. The simulations were selected because they rank as the 95th percentile for sea surface area exposed to oil, shoreline length exposed to oil, or entrained (water column) oil volume exceeding the stated thresholds. It should be kept in mind that each map in Appendix D displays the results from an individual spill simulation.

Platform blowout scenarios simulated a release of 35,000 bbl of Hebron D94 crude onto the sea surface daily for a period of between 30 and 120 days. Winter and summer environmental conditions were used to determine the seasonal variability in the oil trajectory and weathering. Seafloor blowouts were simulated by releasing 20,000 bbl of Ben Nevis crude daily into the water column above the well for a period of 100 and 120 days. Winter season conditions were simulated with and without sea ice present for both the platform and seafloor blowouts. Batch transfer spills include an instantaneous release of 5,031 bbl of marine diesel and 31,449 bbl of D-94 crude oil over 24 hours at the sea surface.

Table 4.2-1 summarizes the results from the deterministic model runs.

Table 4.2-1. Summaryof the de terministic model results. The perce ntages in the table are the fraction of oil volume in each location or weathering category at the end of the simulation.

Release Type	Spill Scenario	Total Spill Volume (bbl)	Surface Oil (%)	Evap. (%)	Water Column (%)	Oil Ashore (%)	Oil Decayed (%)
Platform Blowout	Summer 30-day	1,050,000	79	8.2	0.2	0	12.6
	Winter 30-day	1,050,000	79	8.3	0.2	0	12.5
	Winter – ice 30-day	1,050,000	79	7.8	0.2	0	13
	Summer 30/60-day	1,050,000	56	11.7	0.3	0	32.0
	Winter 30/60-day	1,050,000	56	11.3	0.3	0.2	32.2
	Winter – ice 30/60-day	1,050,000	56	11.3	0.3	0.01	32.4
	Summer 100-day	3,500,000	56	10.2	0.2	0.02	33.6
	Winter 120-day	4,200,000	51	11.4	0.3	0.4	36.9
	Winter – Ice 120-day	4,200,000	51	11.2	0.3	0.4	37.1
Seafloor Blowout	Summer	2,000,000	35	28.6	9.9	0	26.5
	Winter	2,400,000	31	29.8	9	0.09	30.1
	Winter - ice	2,400,000	29	32.3	9.1	0.2	29.4
Batch Transfer	Summer	5,031	0	45.2	39.6	0	15.2
	Winter	5,031	0	6.4	69.7	0	23.9
	Winter - ice	5,031	0	6.2	69.8	0	24.0
Batch OLS Transfer	Summer	31,449	64	12.9	0.5	0	22.6
	Winter	31,449	64	12.5	0.5	0	23.0
	Winter - Ice	31,449	64	12.6	0.4	0	23.0

Platform Blowout

The volume of oil remaining on the sea surface at the end of each model simulation ranges from 51% to 79% of the total volume released. In general, as the oil release duration increases, the fraction of oil remaining on the sea surface decreases. This relative decrease in surface oil corresponds with an increase in the rate of natural decay. Decay, which accounts for 12% to 37% of the total platform blowout spill volume, occurs as the result of photolysis, a chemical process energized by ultraviolet light from the sun, and by biological breakdown from organisms

in the water. The decrease in surface oil over time may in some instances correspond to surface oil stranding on the shoreline, reducing the amount of oil on the surface.

While the fraction of surface oil volume is predicted to decrease over time, the sea surface area covered by oil thicker than 0.01mm is predicted to increase as the duration of the blowout increases. The increase in sea surface area exposed to oil is due to the rapid and continual spreading of the surface slick.

The fraction of oil lost to evaporation does not vary greatly, ranging from 7.8% to 11.4% of the total volume released. The amount of oil entrained in the water column through natural dispersion processes is less than 0.5% for all platform blowout spill scenarios.

Seafloor Blowout

The volume of oil remaining on the sea surface at the end of each of the seafloor blowout simulations ranges from 29% to 35%, considerably less than the platform blowouts. The seafloor blowout introduces oil directly into the water column where it makes up 9-10% of the spilled volume throughout the duration of the blowout. As with the platform blowout, as the oil release duration increases, the fraction of oil remaining on the sea surface decreases due to an increasing rate of natural decay. Decay accounts for 26 – 30% of the released oil.

Oil lost to evaporation in the seafloor blowout spills is predicted to be more than twice the amount in the platform blowouts, ranging from approximately 29% to 32%. This is due primarily to differences in the physical and chemical makeup of the Ben Nevis crude compared to the Hebron D94 crude oil.

Batch Transfer Spills

None of the marine diesel oil released in the batch transfer spill remains on the sea surface at the end of the 30-day simulation. This is primarily because the diesel is more readily entrained into the water column than the crude oil and in the summer season has a higher rate of evaporation. Between 40 and 70% of the diesel is predicted to become entrained in the water column while 0.4 – 0.5% of the crude will entrain. The model predicts between 15 and 24% of the diesel and 22 – 23% of the crude will decay.

4.3 Newfoundland Shoreline Oiling

Not all of the stochastic model simulations of the platform and seafloor blowouts predict oil will hit the Newfoundland coast. The stochastic model simulations predict a less than 10% probability that oil from either the platform or the seafloor blowouts will reach the Newfoundland shore. Spill scenarios where oil is predicted to reach the Newfoundland shoreline are listed in Table 4.3-1. The values listed in the table are from the individual spill from each stochastic model scenario that resulted in the maximum amount of oil on the Newfoundland shore. A zero probability of oiling means that none of the 100 spills completed in the stochastic model scenario reached the Newfoundland coastline.

Table 4.3-1. Newfoundland shoreline oiling summary. Values listed are from the individual spill within each stochastic scenario that resulted in the largest volume of oil stranded on the shore.

Scenario	Probability of Oiling (%)	First Arrival of Oil (days)	Shoreline Length Oiled (km)	Shoreline Area Oiled (m^2)	Expected Mean Mass (g/m^2)
Surface 30-day Summer	0	-	-	-	-
Surface 30-day Winter	0	-	-	-	-
Surface 30-day Extended Run Summer	0	-	-	-	-
Surface 30-day Extended Run Winter	1	41	142.7	428,100	20
Surface 30-day Extended Run Winter w/ice	0	-	-	-	-
Surface 100-day Summer	1	23	5.3	15,900	0.2
Surface 120-day Winter	1	108	285.5	856,500	20
Surface 120-day Winter w/ice	3	21	137.8	413,500	60
Subsurface 100-day Summer	1	39	5.3	15,900	0.8
Subsurface 120-day Winter	3	21	127.2	381,600	39
Subsurface 120-day Winter w/ice	1	40	116.6	349,900	20
Batch Transfer Summer	0	-	-	-	-
Batch Transfer Winter	0	-	-	-	-
Batch Transfer Winter – w/ice	0	-	-	-	-
Batch OLS Transfer Summer	0	-	-	-	-
Batch OLS Transfer Winter	0	-	-	-	-
Batch OLS Transfer Winter –w/ice	0	-	-	-	-

5. References

AMEC, 2010. Spill Trajectory Modeling for the Hebron Project, AMEC Earth & Environmental, St. John's, Newfoundland. April, 2010.

ASCE Task Committee on Modeling Oil Spills, 1996. State-of-the-art Review of Modeling Transport and Fate of Oil Spills, Water Resources Engineering Division, ASCE, Journal of Hydraulic Engineering, 122(11), 594-609.

Becker,J., D. T. Sandwell, 2008, "SRTM30_PLUS: Data fusion of SRTM land topography with measured and estimated seafloor topography",SRTM30_PLUS V4.0 May 20, 2008.

Blumer, M., Ehrhardt, M., and J.H. Jones, 1973.The environmental fate of stranded crude oil, Deep Sea Research and Oceanographic Abstracts, 20(3, March), 239-259.

Boyer, T., S. Levitus, H. Garcia, R. A. Locarnini, C. Stephens, and J. Antonov, 2004 Objective Analyses of Annual, Seasonal, and Monthly Temperature and Salinity for the World Ocean on a ¼ E Grid, Submitted to International Journal of Climatology April 16, 2004, Ocean Climate Laboratory, National Oceanographic Data Center, Silver Spring, MD.

Bishnoi, P. R. and Mainik B. B., 1979.Laboratory study of behaviour of oil and gas particles in salt water, relating to deepwater blowouts, Spill Technology Newsletter, Vol. 4(1), 24-36.

Bishnoi, P. R., Gupta, A. K., Englezos, P., Kalogerakis, N., 1989. Fluid Phase Equilibria, 83, 97.

Bleck, R., 1998: Ocean modeling in isopycnic coordinates. Chapter 18 in Ocean Modeling and Parameterization, E. P. Chassignet and J. Verron, Eds., NATO Science Series C: Mathematical and Physical Sciences, 516, 4223-448.

Bleck, R., 2002: An oceanic general circulation model framed in hybrid isopycnic-Cartesian coordinates. Ocean Modeling, 4, 55-88.

Boyer, T., S. Levitus, H. Garcia, R. A. Locarnini, C. Stephens, and J. Antonov, 2004 Objective Analyses of Annual, Seasonal, and Monthly Temperature and Salinity for the World Ocean on a ¼ E Grid, Submitted to International Journal of Climatology April 16, 2004, Ocean Climate Laboratory, National Oceanographic Data Center, Silver Spring, MD.

Canadian Ice Service, 2010: Seasonal Summary for Eastern Canada, Winter 2009-2010. Produced by the Canadian Ice Service, July, 2010.

Chassignet, E. P., L. T. Smith, R. Bleck, and F. O. Bryan, 1996: A model comparison: numerical simulations of the North and Equatorial Atlantic oceanic circulation in depth and isopycnic coordinates. J. Phys. Oceanogr., 26, 1849-1867.

Chassignet, E.P., Z.D. Garraffo, 2001. Viscosity parameteriation and gulf stream separation. In: Hawaii U., Muller P., Henderson, D. (Eds.). String to Mixing in Stratified Ocean, Proceedings of Aha Huliko'a Hawaiian Winter Workshop, pp. 27-41.

Cummings, J.A., 2005. Operational multivariate ocean data assimilation. Quarterly Journal of the Royal Meteorological Society. Part C, 131(613), 3583-3604.

Cooper, M. and K.A. Haines, 1996.Altimetric assimilation with water property conservation. Journal of Geophysical Research, 24, 1059-1077.

Deser, C., M. Holland, G. Reverdin, M. Timlin, 2002. Decadal variations in Labrador Sea ice cover and North Atlantic sea surface temperatures. Journal of Geophysical Research, 107, C5, doi:10.1029/2000JC000683.

Egbert, G.D., Bennett, A.F., and M.G.G. Foreman (1994), TOPEX/POSEIDON tides estimated using a global inverse model, J. Geophysical Research, 99, 24821-24852.

Environmental Technology Centre, Environment Canada, 2004. Spills Technology Databases. Oil Properties database. http://www.etc-cte.ec.gc.ca/databases/OilProperties/Default.aspx

French, D., M. Reed, K. Jayko, S. Feng, H. Rines, S. Pavignano, T. Isaji, S. Puckett, A. Keller, F. W. French III, D. Gifford, J. McCue, G. Brown, E. MacDonald, J. Quirk, S. Natzke, R. Bishop, M. Welsh, M. Phillips and B.S. Ingram, 1996a. The CERCLA type A natural resource damage assessment model for coastal and marine environments (NRDAM/CME), Technical Documentation, Vol. I - Model Description. Final Report, submitted to the Office of Environmental Policy and Compliance, U.S. Dept. of the Interior, Washington, DC, April, 1996, Contract No. 14-0001-91-C-11.

French, D., M. Reed, S. Feng and S. Pavignano, 1996b. The CERCLA type A natural resource damage assessment model for coastal and marine environments (NRDAM/CME), Technical Documentation, Vol. III - Chemical and Environmental Databases. Final Report , Submitted to the Office of Environmental Policy and Compliance, U.S. Dept. of the Interior, Washington, DC, April, 1996, Contract No. 14-01-0001-91-C-11.

French-McCay, D., 2009, State of the Art Research Needs for Oil Spill Impact Assessment Modeling. Proceedings of the 32nd AMOP Technical Seminar on Environmental Contamination and Response, Emergencies Science Division, Environment Canada, pp. 601-653.

Gundlach, E.R., 1987. Oil Holding Capacities and Removal Coefficients for Different Shoreline Types to Computer Simulate Spills in Coastal Waters, in Proceedings of the1987 Oil Spill conference, pp. 451-457.

Halliwell, G. R., Jr., 1997.Simulation of decadal/interdecadal variability the North Atlantic driven by the anomalous wind field. Proceedings, Seventh Conference on Climate Variations, Long Beach, CA, pp. 97-102.

Halliwell, G. R., Jr., 1998. Simulation of North Atlantic decadal/multi-decadal winter SST anomalies driven by basin-scale atmospheric circulation anomalies. Journal of Physical Oceanography, 28, 5-21.

Halliwell, G. R., Jr., R. Bleck, and E. Chassignet, 1998. Atlantic Ocean simulations performed using a new hybrid-coordinate ocean model. EOS, Fall 1998 AGU Meeting.

Halliwell, G .R, R. Bleck, E. P. Chassignet, and L.T. Smith, 2000: mixed layer model validation in Atlantic Ocean simulations using the Hybrid Coordinate Ocean Model (HYCOM). EOS, 80, OS304.

Halliwell, G.R. 2002.HYCOM Overview. http://www.hycom.org. June 27, 2011.

Halliwell, G. 2002. Documentation for the HYbrid Coordinate Ocean Model; Energy Loan Sea Ice Model (Bleck, R. 6 September, 2000).

Halliwell, G.R. 2004.Evaluation of vertical coordinate and vertical mixing algorithms in the HYbrid-Coordinate Ocean Model (HYCOM). Ocean Modelling, 7(3-4), 285-322.

Han, G. and C.L. Tang, 1999. Velocity and transport of the Labrador Current determined from altimetric, hydrographic, and wind data. Journal of Geophysical Research, 104(C8), 18047-18057.

Hu, D., 1996: On the Sensitivity of Thermocline Depth and Meridional Heat Transport to Vertical Diffusivity in OGCMs. J. Physical Oceanography, 26, 1480-1494.

Hume, H.R., Buist, I., Betts, D., and R. Goodman, 1983. Arctic marine oil spill research, Cold Regions Science and Technology, 7(June), 313-341.

Hurlburt, H.E., Hogan, P.J., 200. Impact of 1/8 to 1/64 resolution on Gulf stream model-data comparisons in basin-scale Atlantic Ocean models. Dynamics of Atmospheres and Oceans, 32, 283-329.

IOC, IHO and BODC (GEBCO) 2003. Centenary Edition of the GEBCO Digital Atlas, published on behalf of the Intergovernmental Oceanographic Commission (IOC) and the International Hydrographic Organization (IHO) as part of the General Bathymetric Chart of the Oceans; British Oceanographic Data Centre (BODC), Liverpool.

Isaji T., E. Howlett, C. Dalton, and E. Anderson, 2001: "Stepwise -Continuous-Variable-Rectangular Grid Hydrodynamics Model", in Proceedings of the Twenty-fourth Arctic and Marine Oil Spill Program (AMOP) Technical Seminar, Edmonton (Alberta) Canada, pp. 597-610, June 12, 2001.

Kalnay, E., M. Kanamitsu, R. Kistler, W. Collins, D. Deaven, L. Gandin, M. Iredell, S. Saha, G. White, J. Woollen, Y. Zhu, A. Leetmaa, R. Reynolds, M. Chelliah, W. Ebisuzaki, W. Higgins, J. Janowiak, K. C. Mo, C. Ropelewski, J. Wang, Roy Jenne, Dennis Joseph, 1996. The NCEP/NCAR 40-year reanalysis project, Bulletin of the American Meteorological Society, 77, 437-471.

Kullenberg, G. (editor), 1982. Pollutant transfer and transport in the sea. Volume I. CRC Press, Boca Raton, FL. 227 pp.

Lefebvre, A. H., 1989, Atomization and Sprays, Hemisphere Publishing Corp., New York.

Marsh, R., M. J. Roberts, R. A. Wood, and A. L. New, 1996: An intercomparison of a Bryan-Cox-type ocean model and an isopycnic ocean model, part II: the subtropical gyre and meridional heat transport. J. Phys. Oceanogr., 26, 1528-1551.

McAuliffe, C.D., 1987. Organism exposure to volatile/soluble hydrocarbons from crude oil spills – a field and laboratory comparison. Proceedings of the 1987 Oil Spill Conference, API, pp. 275-288.

McDougall, T.J., 1978. Bubble plumes in stratified environments, Journal of Fluid Mechanics, 85(4), 655-672.

Nafaa, M.G. and O.E. Frihy, 1993. Beach and Nearshore Features Along the Dissipative Coastline of the Nile Delta, Egypt. Journal of Coastal Research, 9(2, Spring), 423-433.

National Research Council (NRC), 1985. Oil in the Sea: Inputs, Fates and Effects, National Academy Press, Washington, DC. 601 pp.

New, A. and R. Bleck, 1995: An isopycnic model of the North Atlantic, Part II: interdecadal variability of the subtropical gyre. J. Phys. Oceanogr., 25, 2700-2714.

New, A., R. Bleck, Y. Jia, R. Marsh, M. Huddleston, and S. Barnard, 1995: An isopycnic model of the North Atlantic, Part I: model experiments. J. Phys. Oceanogr., 25, 2667-2699.

Nordvik, A.B., 1995. The technology windows-of-opportunity for marine oil spill response as related to oil weathering and operations, Spill Science & Technology Bulletin, 2(1, March 1995), 17-46.

Okubo, A. 1971. Oceanic diffusion diagrams. Deep-Sea Research 8:789-802.

Okubo, A. and R.V. Ozmidov, 1970. Empirical dependence of the coefficient of horizontal turbulent diffusion in the ocean on the scale of the phenomenon in question. Atmospheric and Ocean Physics, 6(5), 534-536.

Petrie, B., 1983. Circulation of the Newfoundland Continental Shelf. Atmosphere-Ocean, 21(2), 207-226.

Petrie, B. A. Isenor, 1985. The Near-Surface Circulation and Exchange in the Newfoundland Grand Banks Region. Atmosphere-Ocean, 23(3), 209-227.

Reed, M., E. Gundlach and T. Kana, 1989. A coastal zone oil spill model: development and sensitivity studies. Oil & Chemical Pollution 5: 411-449.

Reed, M., T. Kana, and E. Gundlach, 1988. Development, testing and verification of an oil spill surf-zone mass-transport model. Final Report to: Mineral Management Service, Alaska OCS Region, Contract No. 14-12-0001-30130; by Applied Science Associates, Inc. (ASA), Coastal Science & Engineering, Inc. (CSE), and E-Tech, Inc., June 1988, 343 pp.

Reed, M., M.L. Spaulding, E.R. Gundlach, T.W. Kana and S.J. Siah, 1986.Formulation of a shoreline/oil spill interaction model. In: Proceedings 1986 Arctic Marine Oil Program (AMOP), Edmonton, Canada, Ottawa, Ontario, pp. 77-101.

Reed, M. and E. Gundlach. 1989. Hindcast of the Amoco Cadiz event with a coastal zone oil spill model. Oil and Chemical Pollution, 5, 451-476.

Richardson, P.L., 1983. Eddy Kinetic Energy in the North Atlantic From Surface Drifters. Journal of Geophysical Research, 88(C7), 4355-4367.

Roberts, M. J., R. Marsh, A. L. New, and R. A. Wood, 1996: An intercomparison of a Bryan-Cox-type ocean model and an isopycnic ocean model, part I: the subpolar gyre and high latitude processes. J. Phys. Oceanogr., 26, 1495-1527.

Rye, H., Johansen, O., and Kolderup, H. 1998. Drop size formation from deep water blowouts. *SINTEF Report*.

Semtner, A.J. Jr., 1976. A model of the thermodynamic grown of sea ice in numerical simulations of climate. Journal of Physical Oceanography, 6, 379-389.

Smith, R.D. Maltrud, M.E., 2000. Numerical simulations of the North Atlantic Ocean at 1/10. Journal of physical Oceanography, 30, 1532-1561.

Statoil Memo, "ElDabaa Field – Monthly metocean data", Martin Mathiesen, Polytec Foundation, 9 July 2010.

Swail, V.R., Cardone, V.J., Ferguson, M., Gummer, D.J., Harris, E.L., Orelup, E.A. and A.T. Cox. 2006: The MSC50 Wind and Wave Hindcast Reanalysis, Ninth International Workshop on Wave Hindcasting and Forecasting, September 25-29, 2006. Victoria, BC.

VLIZ (2009). Maritime Boundaries Geodatabase, version 5. Available online at http://www.vliz.be/vmdcdata/marbound. Consulted on 2010-10.

Volkov, D.L., 2005. Interannual Variability of the Altimetry-Derived Eddy Field and Surface Circulation in the Extratropical North Atlantic Ocean in 1993-2001. Journal of Physical Oceanography, 35, 405-426.

Appendix A: SIMAP Model Description

This appendix provides a discussion of the SIMAP model and its important oil fates model algorithms. It is intended to supplement information provided in the spill modeling technical reportand help the reader understand the application of the model to the spill simulations performed. It includes an extensive reference list for oil spill modeling in general and a supplementary list of model applicationand validation study references.

SIMAP includes (1) an oil physical fates model, (2) interfacing to a hydrodynamics model for simulation of currents, (3) a biological effects model, (4) an oil physical, chemical and toxicological database, (5) environmental databases (winds, currents, salinity, temperature), (6) geographical data (in a GIS), (7) a biological database, (8) a response module to analyze effects of response activities, (9) graphical visualization tools for outputs, and (10) exporting tools to produce text format output.

SIMAP originated from the oil fates and biological effects sub-models in the Natural Resource Damage Assessment Model for Coastal and Marine Environments (NRDAM/CME), which ASA developed in the early 1990s for the US Department of the Interior for use in Natural Resource Damage Assessment (NRDA) regulations under the Comprehensive Environmental Response, Compensation and Liability Act of 1980 (CERCLA). The NRDAM/CME (Version 2.4, April 1996) was published as part of the CERCLA type A NRDA Final Rule (Federal Register, May 7, 1996, Vol. 61, No. 89, p. 20559-20614). The technical documentation for the NRDAM/CME is in French et al. (1996a,b,c). This technical development involved several in-depth peer reviews, as described in the Final Rule.

While the NRDAM/CME was developed for simplified natural resource damage assessments of small spills in the United States, SIMAP is designed to evaluate fates and effects of both real and hypothetical spills in marine, estuarine and freshwater environments worldwide. SIMAP may be run in stochastic mode to evaluate a distribution of spill results, rather than just a single result for a specific hind-cast. Additions and modifications to prepare SIMAP were made to increase model resolution, allow modification and site-specificity of input data, allow incorporation of temporally varying current data, evaluate subsurface releases and movements of subsurface oil, track multiple chemical components of the oil, enable stochastic modeling, and facilitate analysis of results. The consideration of the impacts of subsurface oil is important, particularly in the evaluation of impacts on aquatic organisms. Surface floating oil primarily impacts wildlife and intertidal biota, and not aquatic biota in subtidal habitats. At higher wind speeds than about 12 knots (or at lower wind speeds if dispersant is applied), oil will entrain into the water column, unless it has become too viscous to do so after weathering and the formation of mousse. Once oil is entrained in the water in the form of small droplets, monoaromatics (MAHs) and polynuclear aromatic hydrocarbons (PAHs) dissolve into the water column. The dissolved MAHs and PAHs are the most bioavailable and toxic portion of the oil. The dissolution rate is very sensitive to the droplet size (because it involves mass transfer across the surface area of the droplet), and the amount of hydrocarbon mass dissolved is a function of the mass entrained and droplet size distribution. These are in turn a function of soluble

hydrocarbon content of the oil, the amount of evaporation of these components before entrainment, oil viscosity (which increases as the oil weathers and emulsifies), oil surface tension (which may be reduced by surfactant dispersants), and the energy in the system (the higher the energy the smaller the droplets). Large droplets (greater than a few hundred microns in diameter) resurface rapidly, and so dissolution from those is also inconsequential. Dispersant application facilitates the entrainment of oil into the water in a smaller size distribution than would occur naturally, with the median droplet size about 20 microns (Lunel, 1993a,b).

Thus, the fate of MAHs and PAHs in surface oil is primarily volatilization to the atmosphere, rather than to the water. If wind speeds exceed 12 knots, entrainment of the surface oil into the water becomes significant. Dispersant application can also facilitate entrainment into the water column. If oil is entrained before it has weathered and lost the lower molecular weight aromatics to the atmosphere, dissolved MAHs and PAHs in the water can reach concentrations where they can affect water column organisms or bottom communities (French McCay and Payne, 2001).

Below is a brief description of the physical fates model implemented in SIMAP. Detailed descriptions of the algorithms and assumptions in the model are in published papers (French McCay 2002, 2003, 2004). The model has been validated with more than 20 case histories, including the Exxon Valdez and other large spills (French and Rines, 1997; French McCay, 2003, 2004; French McCay and Rowe, 2004) as well as test spills designed to verify the model (French et al., 1997).

The three dimensional physical fates model estimates distribution (as mass and concentrations) of whole oil and oil components on the water surface, on shorelines, in the water column, and in sediments. Oil fate processes included are spreading (gravitational and by shearing), evaporation, transport, randomized dispersion, emulsification, entrainment (natural and facilitated by dispersant), dissolution, volatilization of dissolved hydrocarbons from the surface water, adherence of oil droplets to suspended sediments, adsorption of soluble and semi-soluble aromatics to suspended sediments, sedimentation, and degradation.

Oil is a mixture of hydrocarbons of varying physical, chemical, and toxicological characteristics. Thus, oil hydrocarbons have varying fates and impacts on organisms. In the model, oil is represented by component categories, and the fate of each tracked separately. The “pseudo-component” approach (Payne et al., 1984, 1987; French et al., 1996a; Jones 1997; Lehr et al. 2000) is used, where chemicals in the oil mixture are grouped by physical-chemical properties, and the resulting component category behaves as if it were a single chemical with characteristics typical of the chemical group.

SIMAP fates model focuses on tracking the lower molecular weight aromatic components divided into chemical groups based on volatility, solubility, and hydrophobicity. In the model, the oil is treated as eight components (defined in Table A-1). Six of the components (all but the two non-volatile residual components) evaporate at rates specific to the pseudo-component. Solubility is strongly correlated with volatility, and the solubility of aromatics is higher than aliphatics of the same volatility, with the MAHs the most soluble, the 2-ring PAHs semi-soluble,

and the 3-ring PAHs slightly soluble Mackay et al. (1992a,b,c,d). Both the solubility and toxicity of the non-aromatic hydrocarbons are much less than for the aromatics and dissolution (and water concentrations) of non-aromatics is safely ignored. Thus, dissolved concentrations are calculated only for each of the three soluble aromatic pseudo-components.

Table A-1. Definition of four distillation cuts and the eight pseudo-components in the model (monoaromatic hydrocarbons, MAHs; benzene + toluene + ethybenzene + xylene, BTEX; polynuclear aromatic hydrocarbons, PAHs).

Characteristic	Volatile and Highly Soluble	Semi-volatile and Soluble	Low Volatility and Slightly Soluble	Residual (non-volatile and insoluble)
Distillation cut	1	2	3	4
Boiling Point (^{o}C)	< 180	180 - 265	265 - 380	>380
Molecular Weight	50 - 125	125 - 168	152 - 215	> 215
Log(K_{ow})	2.1-3.7	3.7-4.4	3.9-5.6	>5.6
Aliphatic pseudo-components: Number of Carbons	volatile aliphatics: C4 – C10	semi-volatile aliphatics: C10 – C15	low-volatility aliphatics: C15 – C20	non-volatile aliphatics: > C20
Aromatic pseudo-component name: included compounds	MAHs: BTEX, MAHs to C3-benzenes	2 ring PAHs: C4-benzenes, naphthalene, C1-, C2-naphthalenes	3 ring PAHs: C3-, C4-naphthalenes, 3-4 ring PAHs with log(K_{ow}) < 5.6	$\geq$4 ring aromatics: PAHs with log(K_{ow}) > 5.6 (insoluble)

This number of components provides sufficient accuracy for the evaporation and dissolution calculations, particularly given the time frame (minutes) over which dissolution occurs from small droplets and the rapid resurfacing of large droplets (see discussion above). The alternative of treating oil as a single compound with empirically-derived rates (e.g., Mackay et al, 1980; Stiver and Mackay, 1984) does not provide sufficient accuracy for impact analyses because the impacts to water column organisms are caused by MAHs and PAHs, which have specific properties that differ from the other volatile and soluble compounds. Use of more pseudo components does not improve accuracy, as the major constituents of concern are well characterized (sufficiently similar in properties within the pseudo-component group of chemicals) by the modeled component properties used in SIMAP. The model has been validated both in predicting dissolved concentrations and resulting toxic effects, supporting the adequacy of the use of this number of pseudo-components (French McCay, 2003).

The lower molecular weight aromatics dissolve from the whole oil and are partitioned in the water column and sediments according to equilibrium partitioning theory (French et al., 1996a; French McCay 2004). The residual fractions in the model are composed on non-volatile and insoluble compounds that remain in the “whole oil” that spreads, is transported on the water

surface, strands on shorelines, and disperses into the water column as oil droplets or remains on the surface as tar balls. This is the fraction that composes black oil, mousse, and sheen.

Lagrangian elements (spillets) are used to simulate the movements of oil components in three dimensions over time. Surface floating oil, subsurface droplets, and dissolved components are tracked in separate spillets. Transport is the sum of advective velocities by currents input to the model, surface wind drift, vertical movement according to buoyancy, and randomized turbulent diffusive velocities in three dimensions. The vertical diffusion coefficient is computed as a function of wind speed in the wave-mixed layer. The horizontal and deeper water vertical diffusion coefficients are model inputs.

The oil (whole and as pseudo-components) separates into different phases or parts of the environment, i.e., surface slicks; emulsified oil (mousse) and tar balls; oil droplets suspended in the water column; dissolved lower molecular weight components (MAHs and PAHs) in the water column; oil droplets adhered and hydrocarbons adsorbed to suspended particulate matter in the water; hydrocarbons on and in the sediments; dissolved MAHs and PAHs in the sediment pore water; and hydrocarbons on and in the shoreline sediments and surfaces. The physical fates model creates output files recording the distribution of a spilled substance in three dimensional space and time. The quantities recorded are:

- area covered by oil and thickness on the water surface ("swept area")
- volumes in the water column at various concentrations of dissolved aromatics
- volumes in the water column at various concentrations of total hydrocarbons in suspended droplets
- total hydrocarbon concentrations and dissolved aromatic concentrations in surface sediment
- lengths and locations of shoreline impacted and volume of oil ashore in each segment

Important Oil Fates Processes

The following section describes the details of the important processes simulated in the SIMAP model.

Wind Drift

If the wind drift of the surface wave-mixed layer is not included in three-dimensional and time varying current data supplied to the fates model, wind drift is added to the advective particle velocity within the oil fates model. Wind drift for surface slicks may be added as a user-specified, constant percentage of wind speed, with the option of including a drift angle clockwise of the down wind direction. Alternatively, wind drift is calculated in the SIMAP fates model.

The wind drift rate is the ratio of oil drift speed relative to the wind speed. Drift velocities due to a wind, u_{wc} and v_{wc} (m/sec), toward the east and north, respectively, are

$$u_{wc} = C_w u_w$$

$$v_{wc} = C_w v_w$$

where:

- u_w - east component of wind speed (m/sec)
- v_w - north component of wind speed (m/sec)
- C_w - drift factor (fraction)

The drift factor, C_w, may be set by the user as a constant (Lange and Hufnerfuss, 1978; Wu, 1980; Samuels et al., 1982), where C_w varies between 2.5 and 4.5%. These are values based on observations. The default value in the model is 3.5%, which may be reset by the user.

The wind drift angle is the angle the oil drifts clockwise (to the right in the northern hemisphere, use negative values for southern hemisphere) of the wind direction. The drift angle may be entered by the user as a constant angle in degrees. The default value is zero. For open waters a small positive value may be appropriate. A mean of 20^o has been observed in several spills in mid-latitudes. The angle increases with latitude.

Oil Degradation

Degradation may occur as the result of photolysis, which is a chemical process energized by ultraviolet light from the sun, and by biological breakdown, termed biodegradation.

Most studies of microbe-hydrocarbon interactions have been carried out under controlled laboratory conditions and results are not always applicable to the marine environment. Several parameters can limit biodegradation including the microbial population, temperature, oil composition, toxicity and state of weathering; and availability of nutrients and dissolved oxygen.

In the SIMAP model, degradation occurs on the surface slick, oil on the shore and the entrained oil and aromatics in the water column. A first order decay algorithm is used. The degradation rate, $\overset{o}{M}_b$ (g/sec), can be defined as:

$$\overset{o}{M}_b = \frac{dM_{b,i}}{dt} = -K_i M_i$$

i	environmental compartment (water or shoreline surface, water column, and sediments)
$M_{b,I}$	mass of oil lost by degradation from i (g)
M_i	mass of oil subjected to degradation from i (g)
K_i	degradation constant for compartment i (1/day)

Many types of marine organisms ingest, metabolize and utilize oil as a carbon source, producing carbon dioxide and water as by-products. The biodegradable fraction of various crude oils ranges from 11 to 90% (NRC, 1985, 1989). A typical degradation rate results in the loss of 1% of the available oil mass per day.

Shoreline Interactions

The fate of spilled oil that reaches the shoreline depends on characteristics of the oil, the type of shoreline, and the energy environment (Reed et al., 1986, 1988, 1989; Gundlach, 1987; Reed and Gundlach, 1989; Harper and Harvey-Kelly, 1994; Humphrey, 1994). Even when beached, oil will continue to weather. However, several additional processes become important: refloatation, penetration into the substrate, and retention/transport in the beach-groundwater system. Erosion of oiled substrate from the beach to offshore sediments may also occur. Considerable study of shoreline oiling, fates and removal processes was performed as part of the development of the COZOIL model for the U.S. Minerals Management Service (Reed et al., 1986, 1988, 1989; Gundlach, 1987; Reed and Gundlach, 1989). The shoreline interaction algorithms in SIMAP are based on this model.

The maximum oil holding thickness is a function of oil viscosity and shore type (CSE/ASA/BAT, 1986; Gundlach, 1987). Oil removal from the shoreline is by water penetration and flushing, and by wave erosion. Thus, removal is faster on exposed coasts than sheltered shorelines. Each shoreline cell in the SIMAP model grid has an oil holding capacity based on oil type, shore type, beach slope, beach width (Table A2) and shoreline grid length.

Oil deposition occurs when oil intersects the shore surface. Deposition ceases when the holding capacity for the shore surface is reached. Subsequent oil deposited is not allowed to remain on the shore surface, and is refloated as slicks that continue to move along shore. After stranding permanently, the shoreline oil is removed exponentially with time. The removed oil is returned to the water column on a rising tide (sufficiently high to wet the oiled surface) and offshore winds.

Table A-2: Typical beach widths by shore type (CERC, 1984; French et al, 1996).

Shore Type	Mean Beach Width (m)				
East	Coast[2]	Gulf of Mexico[3]	California[4]	Pacific NW[5]	Gulf of Alaska[6]
1. Exposed rocky	2	1	2	3	3
2. Wave cut platform	2	1	2	3	3
3. Fine sand	10	5-15	10	15	20
4. Coarse sand	10	5	10	15	20
5. Mixed sand/gravel	5	5	5	7	10
6. Gravel	3	2	3	4	6
7. Exposed tidal flats	10	10	10	15	20
8. Sheltered rocky	2	1	2	3	3
9. Sheltered tidal flats	140	20	120	210	300
10. Sheltered marsh	140	50	120	210	300
11. Glacier edge	-	-	-	-	3
12. Artificial[1]	0.1	0.1	0.1	0.1	0.1

[1] Assumed value for vertical bulkhead

[2] These shore widths, as well as the data in Tables 3-4 and 3-5, are included in the default data file "CME-East_Coast.SHR" supplied with the model.

[3] These shore widths, as well as the data in Tables 3-4 and 3-5, are included in the default data file "CME-Gulf_of_Mexico.SHR" supplied with the model.

[4] These shore widths, as well as the data in Tables 3-4 and 3-5, are included in the default data file "CME-California.SHR" supplied with the model.

[5] These shore widths, as well as the data in Tables 3-4 and 3-5, are included in the default data file "CME-Pacific_NW.SHR" supplied with the model.

[6] These shore widths, as well as the data in Tables 3-4 and 3-5, are included in the default data file "CME-Gulf_of_Alaska.SHR" supplied with the model.

Oil Entrainment

As oil on the sea surface is exposed to wind and waves, it is entrained (and dispersed) into the water column. Entrainment is a physical process where globules of oil are transported from the sea surface into the water column by breaking waves. It has been observed that entrained oil is broken into droplets of varying sizes. Smaller droplets spread and diffuse in the water column, while larger ones rise rapidly back to the surface (Delvigne and Sweeney, 1988; Delvigne, 1991). Breaking waves created by the action of wind and waves on the ocean surface are the primary sources of energy for entrainment, although other sources of turbulence can entrain oil (Delvigne et al., 1994). Entrainment is strongly dependent on turbulence and is greater in areas of high wave energy.

It has been observed that entrained oil is subjected to enhanced dissolution and biodegradation processes. The increased surface area represented by these droplets increases the rates of dissolution and photo-oxidation.

Delvigne and Sweeney (1988), using laboratory and flume experimental observations, developed relationships for oil entrainment rate and resulting suspended oil droplet size distribution as functions of turbulent energy level and oil viscosity. Droplet sizes decrease and entrainment rate increases with increasing turbulence. The higher the oil viscosity, the larger is the maximum droplet size and the lower the entrainment rate. Oil viscosity is increased by emulsification, which slows entrainment rate (Spaulding et al., 1992; French et al., 1996; Dahling et al., 1997). The data and relationships in Delvigne and Sweeney (1988) are used to calculate mass and particle size distribution of droplets entrained in SIMAP (as it is in the NRDAM/CME, French et al., 1996). Particle size decreases with higher turbulent energy level and lower oil viscosity, from a low-turbulence and high-viscosity condition where droplet sizes range up to a maximum of 5 mm, to a high-turbulence and low-viscosity condition where droplet sizes range up to a maximum of 0.2 mm (200 m). The natural dispersion particle sizes observed by Delvigne and Sweeney (1988) are confirmed by field observations by Lunel (1993a,b).

Entrained droplets in the water column rise according to Stokes Law, where velocity is related to the difference in density between the particle (droplet) and the water, and to the particle diameter. In addition to rising according to Stokes Law, entrained droplets are transported by currents and mixed vertically by randomized turbulent diffusion. When droplets intersect the water surface, if their buoyancy can overcome vertical mixing they surface and form sheens and tar balls (modeled as surface spillets of <0.1mm average thickness).

Oil Evaporation

Evaporation can result in the transfer of 20-40% of spilled oil from the sea surface to the atmosphere, depending on the type of oil (Gundlach and Boehm, 1981). The rate of evaporation depends on surface area, thickness, vapor pressure and mass transport coefficient, which in turn are functions of the composition of the oil, wind speed and temperature. As oil evaporates its composition changes, affecting its density and viscosity as well as subsequent evaporation. The most volatile hydrocarbons (low carbon number) evaporate most rapidly, typically in less than a day and sometimes in under an hour (McAuliffe, 1989). As the oil continues to weather, and particularly if it forms a water-in-oil emulsion, evaporation will be significantly decreased.

Evaporation models assume the oil to be well-mixed within the slick. For thick, viscous slicks, the well-mixed assumption is not valid, and virtually fresh oil may remain for several days or even weeks, trapped within viscous oil-water emulsions. A diagram of the evaporative process is in Figure A1.

The Mackay evaporative exposure algorithm (Stiver and Mackay, 1984) is used in many oil spill models such as the Mackay et al. models (Mackay and Leinonen 1977; Mackay et al. 1980a,b, 1982), ADIOS (Lehr et al. 1992), OILMAP (Spaulding et al. 1992), and earlier versions of SIMAP (French et al. 1999). The algorithm is based on accepted evaporation theory, which follows Raoult's Law that each component will evaporate with a rate proportional to the saturation vapor pressure and mole fraction present for that component. For the evaporative exposure model the assumption is that the oil mixture behaves as a single component. It uses

an analytical approach to predict the volume fraction evaporated, using distillation data to estimate parameters needed for the analytic equation.

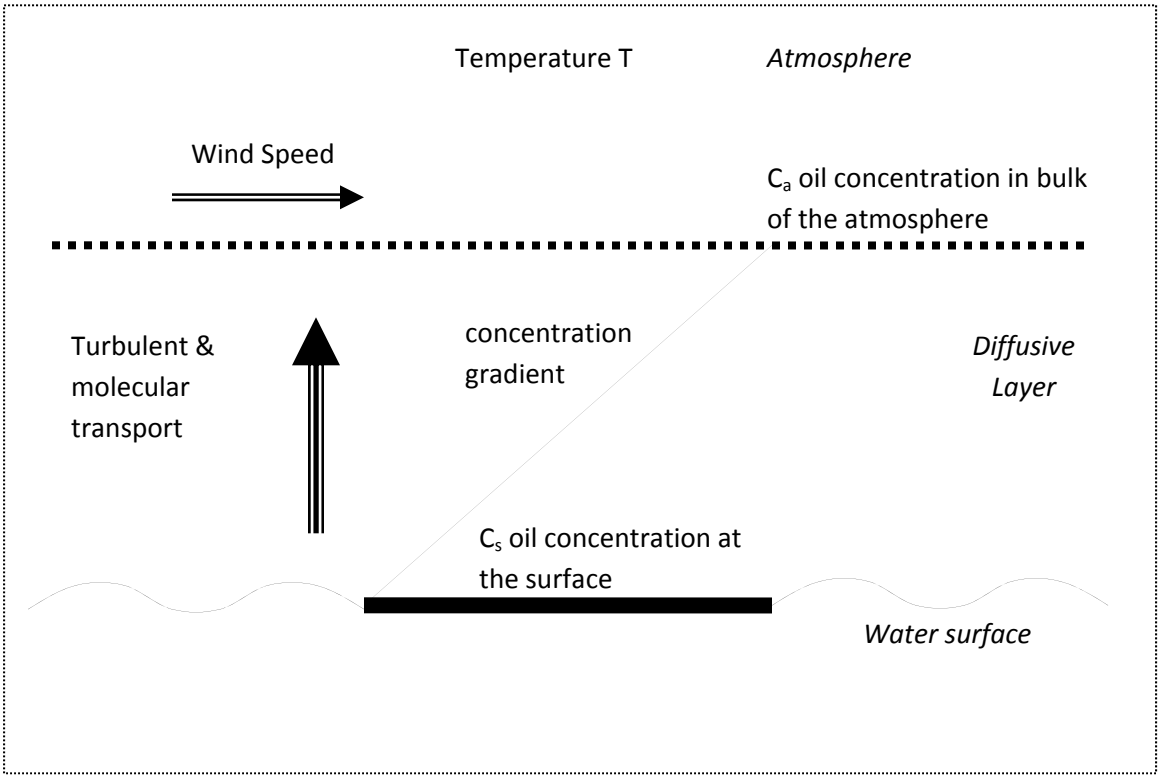


FIGURE A1. SCHEMATIC DIAGRAM OF EVAPORATION PROCESS.

In other models (Payne et al. 1984, 1987; Kirstein et al. 1985; French et al. 1996; Jones 1997; Lehr et al. 2000; Reed et al. 2000) and in SIMAP, so-called pseudo-components (chemical component classes) are evaporated according to an analogous evaporative exposure algorithm, where the flux to the atmosphere is specific to the component's molar volume, vapor pressure, and molecular weight. Jones (1997) simplified this approach into a simplified pseudo-component (SPC) model, relating molar volume, vapor pressure, and molecular weight to the boiling point of the component. Thus, only the boiling points and initial volume fractions of the components need to be specified to implement the model.

Oil/Ice Interactions

The SIMAP model accounts for the presence of ice when calculating surface oil advection, evaporation, entrainment into the water column and surface oil spreading. Table A-3 briefly summarizes how the model deals with oil advection and weathering in the presence of different ice concentrations.

Table A-3: Summary of oil-in-ice advection and weathering effects accounted for in the SIMAP model.

Ice Cover (Percent)	Advection	Evaporation	Entrainment	Spreading
0 – 30	No change	No change	No change	No change
30 – 80	15° to right	Linear reduction with ice cover	Linear reduction with ice cover	Terminal thickness increased in proportion to ice coverage
80 - 100	Oil moves with pack ice	No weathering	No weathering	Oil thickness computed as a function of ice thickness

References

CSE/ASA/BAT, 1986.Development of a Coastal Oil Spill Smear Model. Phase 1: Analysis of Available and Proposed Models, Prepared for Minerals Management Service by Coastal Science & Engineering, Inc. (CSE) with Applied Science Associates, Inc. (ASA) and Battelle New England Research Laboratory (BAT), 121p.

French, D., M. Reed, K. Jayko, S. Feng, H. Rines, S. Pavignano, T. Isaji, S. Puckett, A. Keller, F. W. French III, D. Gifford, J. McCue, G. Brown, E. MacDonald, J. Quirk, S. Natzke, R. Bishop, M. Welsh, M. Phillips and B.S. Ingram, 1996a. The CERCLA type A natural resource damage assessment model for coastal and marine environments (NRDAM/CME), Technical Documentation, Vol. I - Model Description. Final Report, submitted to the Office of Environmental Policy and Compliance, U.S. Dept. of the Interior, Washington, DC, April, 1996, Contract No. 14-0001-91-C-11.

French, D., M. Reed, S. Feng and S. Pavignano, 1996b. The CERCLA type A natural resource damage assessment model for coastal and marine environments (NRDAM/CME), Technical Documentation, Vol. III - Chemical and Environmental Databases. Final Report , Submitted to the Office of Environmental Policy and Compliance, U.S. Dept. of the Interior, Washington, DC, April, 1996, Contract No. 14-01-0001-91-C-11.

French, D., S. Pavignano, H. Rines, A. Keller, F.W. French III and D. Gifford, 1996c. The CERCLA type A natural resource damage assessment model for coastal and marine environments (NRDAM/CME), Technical Documentation, Vol.IV- Biological Databases. Final Report , Submitted to the Office of Environmental Policy and Compliance, U.S. Dept. of the Interior, Washington, DC, April, 1996, Contract No. 14-01-0001-91-C-11.

French, D.P., and H. Rines, 1997. Validation and use of spill impact modeling for impact assessment. Proceedings, 1997 International Oil Spill Conference, Fort Lauderdale, Florida, American Petroleum Institute Publication No. 4651, Washington, DC, pp-829-834.

French, D.P., H. Rines and P. Masciangioli, 1997.Validation of an Orimulsion spill fates model using observations from field test spills. In: Proceedings of the Twentieth Arctic and Marine Oilspill Program (AMOP) Technical Seminar, Vancouver, Canada, June 10-13, 1997, Emergencies Science Division, Environment Canada, Ottawa, Ontario, Canada, pp.933-961.

French, D., H. Schuttenberg, and T. Isaji, 1999. Probabilities of oil exceeding thresholds of concern: examples from an evaluation for Florida Power and Light. in Proceedings of the 22nd Arctic and Marine Oil Spill Program (AMOP) Technical Seminar, June 2-4, 1999, Environment Canada, pp.243-270.

French McCay, D.P., 2002. Development and Application of an Oil Toxicity and Exposure Model, OilToxEx. Environmental Toxicology and Chemistry 21(10): 2080-2094.

French McCay, D.P., 2003. Development and Application of Damage Assessment Modeling: Example Assessment for the North Cape Oil Spill. Marine Pollution Bulletin, Volume 47, Issues 9-12, September-December 2003, pp. 341-359.

French McCay, D.P., 2004. Oil spill impact modeling: Development and validation. Environmental Toxicology and Chemistry 23(10): in press.

French McCay, D. and James R. Payne, 2001.Model of oil fate and water concentrations with and without application of dispersants. In: Proceedings of the Twenty-fourth Arctic and Marine Oil spill Program (AMOP) Technical Seminar, Emergencies Science Division, Environment Canada, Ottawa, Ontario, Canada, pp.611-645.

French McCay, D.P., and J.J. Rowe, 2004.Evaluation of Bird Impacts in Historical Oil Spill Cases Using the SIMAP Oil Spill Model. In Proceedings of the 27th Arctic and Marine Oil Spill Program (AMOP) Technical Seminar, Emergencies Science Division, Environment Canada, Ottawa, ON, Canada, pp. 421-452.

Gundlach, E.R., 1987. Oil holding capacities and removal coefficients for different shoreline types to computer simulate spills in coastal waters. In: Proceedings of the 1987 Oil Spill conference, pp. 451-457.

Gundlach, E.R. and P. Boehm, 1981. Fates of several oil spills in coastal and offshore waters. Report to NOAA/Seattle. NOAA Grant No.NA80RAD00060, RPI/R/81/12/31-30.

Gundlach, E.R., P.D. Boehm, M. Marchand, R.M. Atlas, D.M. Ward, and D.A. Wolfe. 1983. The tale of Amoco Cadiz oil. Science.Vol. 332, pp. 122-129, July.

Harper, J. R. and F. Harvey-Kelly, 1994.Subsurface oil retention in coarse sediments beaches. Ottawa, Ontario: Environmental Technology Centre, Environment Canada; Jan 1994; Report Series No. EE-147.

Humphrey, B., 1994. Stranded oil in coarse sediments (SOCS) model. Ottawa, Ontario: Environmental Technology Centre, Environment Canada; Jan 1994; Report Series No. EE-146. 27p.

Jones, R.K., 1997. A Simplified Pseudo-Component of Oil Evaporation Model, in Proceedings of the 20th Arctic and Marine Oil Spill Program (AMOP) Technical Seminar, Environment Canada, pp. 43-61.

Kirstein, B.E., J.R. Clayton, C. Clary, J.R. Payne, D. McNabb, Jr., G. Fauna and R. Redding, 1985 Integration of suspended particulate matter and oil transportation study. Minerals Management Service, Anchorage, Alaska.

Lehr, W.J., R. Overstreet, R. Jones, and G. Watabayashi, 1992. ADIOS-Automatic Data Inquire for Oil Spill, in Proceedings of the 15th Arctic Marine Oilspill Program, Technical Seminar,Environment Canada, Ottawa, Ontario, pp. 31-45.

Lehr, W.J., D. Wesley, D. Simecek-Beatty, R. Jones, G. Kachook and J. Lankford, 2000. Algorithm and interface modifications of the NOAA oil spill behavior model. Proceedings

of the 23rd Arctic and Marine Oil Spill Program (AMOP) Technical Seminar, Vancouver, BC, Environmental Protection Service, Environment Canada, pp. 525-539.

Lunel, T. 1993a. Dispersion: Oil droplet size measurements at sea. in Proceedings of the 16th Arctic Marine Oilspill Program (AMOP) Technical Seminar, Environment Canada, Calgary, Alberta, June 7-9, 1993, pp. 1023-1056.

Lunel, T. 1993b. Dispersion: Oil droplet size measurements at sea. InProceedings of the 1993 Oil Spill Conference, pp. 794-795.

Mackay, D. and P.J. Leinonen, 1977. Mathematical model of the behavior of oil spills on water with natural and chemical dispersion. Prepared for Fisheries and Environment Canada. Economic and Technical Review Report EPS-3-EC-77-19, 39p.

Mackay, D.,S. Paterson and K. Trudel, 1980b. A mathematical model of oil spill behavior, Department of Chemical and Applied Chemistry, University of Toronto, Canada, 39p.

Mackay, D., I. Buist, R. Mascarenhas and S. Peterson, 1980a. Oil spill processes and models. Report EE-8, Environment Protection Service, Canada.

Mackay, D, W.Y. Shiu, K. Hossain, W. Stiver, D. McCurdy and S. Peterson, 1982. Development and calibration of an oil spill behavior model. Report No. CG-D-27-83, U.S. Coast Guard, Research and Development Center, Groton, Connecticut, 83p.

Mackay, D., W.Y. Shiu, and K.C. Ma, 1992a.Illustrated Handbook of Physical-Chemical Properties and Environmental Fate for Organic Chemicals, Vol.I, Monoaromatic Hydrocarbons, Chlorobenzenes, and PCBs. Lewis Publ., Chelsea, Michigan, 668p.

Mackay, D., W.Y. Shiu, and K.C. Ma, 1992b.Illustrated Handbook of Physical-Chemical Properties and Environmental Fate for Organic Chemicals, Vol. II, Polynuclear Aromatic Hydrocarbons, Polychlorinated Dioxins, and Dibenzofurans.Lewis Publ., Chelsea, Michigan, 566p.

Mackay, D., W.Y. Shiu, and K.C. Ma, 1992c. Illustrated Handbook of Physical-Chemical Properties and Environmental Fate for Organic Chemicals, Vol. III, Volatile Organic Chemicals. Lewis Publ., Chelsea, Michigan, 885p.

Mackay, D., W.Y. Shiu and D.C. Ma, 1992d.Illustrated Handbook of Physical-Chemical Properties and Environmental Fate for Organic Chemicals.Volume IV Oxygen, Nitrogen, and Sulfur containing compounds. Lewis Publishers, Inc. Chelsea, Michigan, 930p.

McAuliffe, C.D., 1989. The weathering of volatile hydrocarbons from crude oil slicks on water. In: Proceedings of the 1989 Oil Spill conference. San Antonio, TX. pp. 357-364.

National Research Council (NRC), 1985. Oil in the Sea: Inputs, Fates and Effects, National Academy Press, Washington, D.C., 601 p.

National Research Council (NRC) 1989.Review of the State-of-Knowledge Regarding Dispersant Usage in Open-Ocean Spill Responses. NRC Marine Board, Washington, DC., 306p.

O'Clair, C.E., J.W. Short, and S.D. Rice, 1996.Contamination of intertidal and subtidal sediments by oil from the *Exxon Valdez* oil spill. In Rice SD, Spies RB, Wolfe DA, Wright BA, eds. *Proceedings* of the *Exxon Valdez* oil spill symposium. American Fisheries Society Symposium 18:17-28.

Payne, J.R., B.E. Kirstein, G.D. McNabb, Jr., J.L. Lambach, R. Redding R.E. Jordan, W. Hom, C. deOliveria, G.S. Smith, D.M. Baxter, and R. Gaegel, 1984. Multivariate analysis of petroleum weathering in the marine environment – sub Arctic , Environmental Assessment of the Alaskan Continental Shelf, OCEAP, Final Report of Principal Investigators, Vol. 21 and 22, Feb. 1984, 690p.

Payne, J.R., B.E. Kirstein, J.R. Clayton, Jr., C. Clary, R. Redding, G.D. McNabb, Jr., and G. Farmer, 1987. Integration of suspended particulate matter and oil transportation study.Final Report.Minerals Management Service, Environmental Studies Branch, Anchorage, AK. Contract No. 14-12-0001-30146, 216 p.

Reed, M. and E. Gundlach. 1989. Hindcast of the Amoco Cadiz event with a coastal zone oil spill model. Oil and Chemical Pollution, Vol. 5, pp. 451-476.

Reed, M., E. Gundlach and T. Kana, 1989. A coastal zone oil spill model: development and sensitivity studies. Oil & Chemical Pollution 5:411-449.

Reed, M., T. Kana, and E. Gundlach, 1988. Development, testing and verification of an oil spill surf-zone mass-transport model. Final Report to: Mineral Management Service, Alaska OCS Region, Contract No. 14-12-0001-30130; by Applied Science Associates, Inc. (ASA), Coastal Science & Engineering, Inc. (CSE), and E-Tech, Inc., June 1988, 343p.

Reed, M., M.L. Spaulding, E.R. Gundlach, T.W. Kana and S.J. Siah, 1986.Formulation of a shoreline/oil spill interaction model. In: Proceedings 1986 Arctic Marine Oil Program (AMOP), Edmonton, Canada, Ottawa, Ontario, pp. 77-101.

Spaulding, M.L., E. Howlett, E. Anderson and K. Jayko, 1992. OILMAP: A global approach to spill modeling. 15th Arctic and Marine oil Spill Program, Technical Seminar, Edmonton, Alberta, Canada, June 9-11, 1992, pp. 15-21.

Stiver, W. and D. Mackay, 1984. Evaporation rate of oil spills of hydrocarbons and petroleum mixtures. Environmental Science and Technology 18: 834-840.

References - SIMAP Example Applications and Validations

French, D.P., and H. Rines, 1997. Validation and use of spill impact modeling for impact assessment. In *Proceedings, 1997 International Oil Spill Conference*, Fort Lauderdale, Florida, American Petroleum Institute Publication No. 4651, Washington, DC, pp-829-834.

French, D. P., 1998a. Estimate of Injuries to Marine Communities Resulting from the North Cape Oil Spill Based on Modeling of Fates and Effects. Report to US Department of

Commerce, National Oceanic and Atmospheric Administration (NOAA), Damage Assessment Center, Silver Spring, MD, January 1998.

French, D. P., 1998b. Updated Estimate of Injuries to Marine Communities Resulting from the North Cape Oil Spill Based on Modeling of Fates and Effects. Report to US Department of Commerce, National Oceanic and Atmospheric Administration (NOAA), Damage Assessment Center, Silver Spring, MD, December 1998.

French, D.P., 1998c. Modeling the Impacts of the *North Cape,* p. 387-430.In *Proceedings, 21st Arctic and Marine Oilspill Program (AMOP) Technical Seminar*, June 10-12, 1998, West Edmonton Mall Hotel Edmonton, Alberta, Canada, Emergencies Science Division, Environment Canada, Ottawa, ON, Canada.

French McCay, D. and James R. Payne, 2001.Model of Oil Fate and Water concentrations with and with out application of dispersants. In *Proceedings of the 2001 24th Arctic and Marine Oil spill Program (AMOP) Technical Seminar*, June 12-14, 2001, Environment Canada, pp.611-645.

French, D. P., Jones, M. A., and Coakley, L., 2001. Use of Oil Spill Modeling for Contingency Planning and Impact Assessment: Application for Florida Power and Light. In *Proceedings of the 2001 International Oil Spill Conference & Exposition*, American Petroleum Institute, March 26-29, 2001, Tampa, Florida.

French, D.P. and H. Schuttenberg, 1999.Evaluation of net environmental benefit using fates and effects modeling. Paper ID #321. In *Proceedings, 1999 International Oil Spill Conference*, American Petroleum Institute.

French McCay, D. 2002. Modeling Evaluation of Water Concentrations and Impacts Resulting from Oil Spills With and Without the Application of Dispersants. International Marine Environmental Seminar 2001, Journal of Marine Systems, Special Issue 2002.

French McCay, D., N. Whittier, S. Sankaranarayanan, J. Jennings, and D. S. Etkin, 2002.Modeling Fates and Impacts for Bio-Economic Analysis of Hypothetical Oil Spill Scenarios in San Francisco Bay. In *Proceedings of the Twenty Fifth Arctic and Marine Oil Spill Program (AMOP) Technical Seminar*, Environment Canada, Calgary, AB, Canada, 2002, p. 1051-1074.

French McCay, D., N. Whittier, T. Isaji, and W.Saunders, 2003. Assessment of the Potential Impacts of Oil Spills in the James River, Virginia. In Proceedings of the 26th Arctic and Marine Oil Spill Program (AMOP) Technical Seminar, Emergencies Science Division, Environment Canada, Ottawa, ON, Canada, p. 857-878.

French McCay, D., N. Whittier, S. Sankaranarayanan, J. Jennings, and D. S. Etkin, 2003.Estimation of Potential Impacts and Natural Resource Damages of Oil. J. Hazardous Materials (in press).

French McCay, D. and N. Whittier, 2003.Modeling Assessment of Potential Fates and Exposure for Orimulsion and Heavy Fuel Oil Spills. In: Proceedings, International Oil Spill Conference, April 2003, Paper 157, American Petroleum Institute, Washington, DC.

French McCay, D.P., 2003. Development and Application of Damage Assessment Modeling: Example Assessment for the North Cape Oil Spill. Marine Pollution Bulletin, Volume 47, Issues 9-12, September-December 2003, pp. 341-359.

French McCay, D.P., and J.J. Rowe, 2004.Evaluation of Bird Impacts in Historical Oil Spill Cases Using the SIMAP Oil Spill Model. In Proceedings of the 27th Arctic and Marine Oil Spill Program (AMOP) Technical Seminar, Emergencies Science Division, Environment Canada, Ottawa, ON, Canada, pp. 421-452.

French-McCay, D.P., J.J. Rowe, N. Whittier, S. Sankaranarayanan, D. S. Etkin, and L. Pilkey-Jarvis, 2005. Evaluation of the Consequences of Various Response Options Using Modeling of Fate, Effects and NRDA Costs of Oil Spills into Washington Waters. In: Proceedings, International Oil Spill Conference, May 2005, Paper 395, American Petroleum Institute, Washington, DC.

French-McCay, D.P., N. Whittier, C. Dalton, J.J. Rowe, and S. Sankaranarayanan, 2005.Modeling fates and impacts of hypothetical oil spills in Delaware, Florida, Texas, California, and Alaska waters, varying response options including use of dispersants. In: Proceedings, International Oil Spill Conference, May 2005, Paper 399, American Petroleum Institute, Washington, DC.

French McCay, D., N. Whittier, J.J. Rowe, S. Sankaranarayanan and H.-S.Kim, 2005.Use of Probabilistic Trajectory and Impact Modeling to Assess Consequences of Oil Spills with Various Response Strategies. In Proceedings of the 28th Arctic and Marine Oil Spill Program (AMOP) Technical Seminar, Emergencies Science Division, Environment Canada, Ottawa, ON, Canada, pp. 253-271, 2005.

Appendix B: Blowout Model Description

ASA's oil blowout model is based on the work of McDougall (gas plume model, 1978), Fanneløp and Sjøen (1980a, plume/free surface interaction) and Spaulding (1982) oil concentration model. A simplified integral jet theory is employed for the vertical as well as for the horizontal motions of the gas-oil plume. The necessary model parameters defining the rates of entrainment and spreading of the jet are obtained from laboratory studies (Fanneløp and Sjøen 1980a). The gas plume analysis is described in McDougall (1978), Spaulding (1982), and Fanneløp and Sjøen (1980a). The hydrate formation and dissociation is formulated based on a unique equilibrium kinetics model developed by R. Bishnoi and colleagues at the University of Calgary. A brief description of the governing equations used in the model and the solution methodology can be found in Spaulding et al., 2000.

In shallow water (< 200 m) oil and gas released from the sea bed are driven into the water column as a jet due to the momentum of the discharge. The jet region is confined to the vicinity of the seabed and is relatively short in length (< 1 m). As the discharge moves upward the density difference between the expanding gas bubbles in the plume and the receiving water result in a buoyant force which drives the plume. The resulting plume is analogous to a thermal plume, with the important exception that for blowouts the plume is bubble starved, because the bubbles are few in number and large. The presence of the bubbles leads to a two-layer structure with an inner core bubble plume and an outer ring of mostly entrained water. As the plume rises, it continues to entrain ambient sea water due to the velocity difference between the rising plume and the receiving water. This entrainment reduces the plume's velocity and buoyancy and increases its radius. The oil in the release is rapidly mixed by the turbulence in the rising plume causing it to break up into small droplets. These droplets (typically a few micrometers to millimeters in diameter) are rapidly transported upward by the rising plume; their individual rise velocities contributing little to their upward motion. As the plume reaches the sea surface it is deflected in a radial, surface flow zone without appreciable loss of momentum. This radial jet, with its origin at the surface directly above the blowout, carries the oil particles rapidly away from the center of the plume. The velocity and oil concentrations in this surface flow zone decrease while the depth of the zone increases. Finally in the far field, where the plume buoyancy has been dissipated, ambient currents and wind generated waves determine the subsequent transport and dispersion of the oil.

There are several important modifications that may alter this basic description of jet/plume behavior. If the buoyant driving force for the plume is dissipated by entrainment before it reaches the surface, the oil droplets in the plume will be carried to the surface solely by their own rise velocities and the surface interaction zone will effectively disappear. The plume behavior can also be altered by variations in the ambient density field, which can cause trapping of the plume in the water column. Finally in the presence of ambient currents the plume path can be substantially altered as the current forces the jet to bend from its preferred vertical direction. If the current velocity profile with depth varies with time the path of the plume can become very complicated.

As water depths become deeper (> 200 m) the basic dynamics of the oil/gas jet/plume become more complicated, principally due to the increase in hydrostatic pressure at the seabed which leads to the possibility of the formation of gas hydrate solids. Gas hydrates constitute a class of solids in which small molecules occupy almost spherical holes in ice-like lattices made up of hydrogen-bonded water molecules. This class of solids is known as clathrates. Clathrate compounds are characterized by the structural combinations of two substances which remain associated not through strong attractive forces, but because strong mutual binding of the molecules of one sort makes possible the firm enclosure of the other. The hydrate-forming gases include light alkanes, carbon dioxide, hydrogen sulphide, nitrogen, and oxygen. Gas hydrates can exist in one of four structures: Structure I and Structure II, Structure H and a new, as of yet unnamed structure. Methane, the most typical gas likely to be released during a blowout is known to form Structure I hydrates. A portion or the entire volume of released gas may be converted to hydrates. These hydrates, which typically form on the gas bubbles close to the release location, have specific gravities on the order of 0.92 to 0.96. The hydrate solids break into small particles and are transported by their rise velocity and the ambient currents. The conversion of the gas into gas hydrates, to the extent that it occurs, deprives the plume of its principal source of buoyancy, leaving the oil droplets and gas hydrates free to rise under the action of their own buoyancy. The oil and gas hydrates in this much less vigorously mixed plume may be carried over very large distances in the water column before ultimately reaching the sea surface.

A review of the literature shows that our understanding and ability to model the dynamics of rising oil and gas plumes in shallow water is extensively developed. Early work by Fannelop and Sjoen (1980a,b), Spaulding (1982), and Milgram (1983), using integral plume theory, has been extended by Rye (1994) and Kolluru (1993) into operational models to predict plume dynamics and oil concentrations. Zheng and Yapa (1997a,b, 1998) have further developed and refined this basic approach for buoyant oil jets and smoke plumes. Their model has been extensively tested against analytic and theoretical results and laboratory and field experiments. Rye (1996) and Rye et al. (1996) describe a 1995 experiment in the North Sea. In all cases the models performed well against theory and field observations. They also correctly predicted the height of the transition zone from when oil transport was dominated by plume dynamics to when oil droplet rise velocities dominated its movement.

The most critical issue for deepwater blowouts is the formation rate of gas hydrates under the gas/oil flow rates, hydrostatic pressures, temperatures, and salinity at typical blowout sites. Topham (1977) performed field experiments using simulated natural gas at a release depth of 650 m, with and without oil, and observed the formation of hydrates in both cases. He was unable to determine the rates of formation but did note that hydrates did not form at depths shallower than about 300 m. Bishnoi and Mainik (1979) performed a set of laboratory experiments using a high pressure test facility (2000 psi) (equal to a seawater depth of 1370 m). According to their work, gas to hydrate conversion was complete when starting pressures were in excess of 700 psi (480 m) and ceased when the pressure was lower than 450 psi (310 m). It is noted that the hydrate formation pressures are highly dependent on the gas or hydrocarbon liquid compositions. For very light condensate oils or rich gases the pressure could be even

lower than 450 psi. Quantitative estimates of the rates were not provided. Zheng and Yapa (1999) have recently extended their model to include a very simplified hydrate formation component. The approach ignores the kinetics of hydrate formation, assumes that all hydrates are formed at the very beginning of the release and that the conversions are based on ideal gas laws.

References

Bishnoi, P.R. and Mainik B.B., 1979.Laboratory study of behaviour of oil and gas particles in salt water, relating to deepwater blowouts, Spill Technology Newsletter, Vol. 4 (1), pp. 24-36.

Bishnoi, P.R., Gupta, A.K., Englezos, P., Kalogerakis, 1989. N., Fluid Phase Equilibria, 83, 97.

Fanneløp, T.K. and K. Sjoen , 1980a. Hydrodynamics of underwater blowouts, AIAA 8th Aerospace Sciences Meeting, January 14-16, Pasadena, California, AIAA paper, pp. 80-0219.

Fanneløp, T. K. and K. Sjoen, 1980b.Hydrodynamics of underwater blowouts, Norwegian Maritime Research, No. 4, pp. 17-33.

Kolluru, V., M. L. Spaulding, and E. Anderson, 1993.Application and verification of WOSM to selected spill events, 16th Arctic and Marine Oil Spill Program, Technical Seminar, June 7-9, 1993, Calgary, Alberta, Canada, pp. 647-668.

McDougall, T.J., 1978. Bubble plumes in stratified environments, Journal of Fluid Mechanics, Vol. 85, Part 4, pp. 655-672.

Milgram, J.H., 1983. Mean flow in round bubble plumes, Journal of Fluid Mechanics, Vol. 133, pp. 345-376.

Rye, H., 1994. Model for calculation of underwater blowout plume. Proceedings of the 17th Arctic and Marine Oilspill Program Technical Seminar, Canada, p. 849-865.

Rye, 1996. NOFO exercise 1995. Dispersants and underwater release experiments-Observations and modelling of the underwater plume behaviour. Data report", IKU Report No.41.514.00/03/95 dated 19 January.

Rye, H. P. Brandvik, and M. Reed, 1996. Subsurface oil release field experiment- observations and modeling of subsurface plume behavior. Proceedings of the 19th Arctic Marine Oilspill Program, Technical Seminar, Calgary, Alberta, Canada, p 1417-1435.

Spaulding, M.L., 1982. User's manual for a simple gas blowout plume model, Continental Shelf Institute, Trondheim, Norway.

Topham, D.R., 1977. Observations of the formation of hydrocarbon gas hydrates at depth in seawater, Spill Technology Newsletter, July-August, Vol. 2, No. 4, pp. 23-28.

Yapa, P.D andZheng, L, 1997b. Simulation of oil spills from underwater accidents I: model development, Journal of Hydraulic Research, International Association of Hydraulic Research, The Netherlands, Vol 35, No. 5, p. 673-688.

Zheng, L. and P. Yapa, 1997a. A numerical model for buoyant oil jets and smoke plumes, Proceedings of the 20th Arctic Marine Oilspill Program, Technical Seminar, Vancouver, BC, Canada, p. 963-979.

Zheng, L. And Yapa, P.D., 1998. Simulation of oil spills from underwater accidents II: Model verification, Journal of Hydraulic Research, International Association of Hydraulic Research, The Netherlands, Vol 36, No. 1, p. 117-134.

Zheng, L. and P. D. Yapa, 1999.A deepwater jet/plume model and a parametric analysis, p. 285-299.

Appendix C - Stochastic Model Results

The following spill scenarios have been defined for the offshore site. Results from the stochastic model platform and subsea blow-out cases are presented in this Appendix.

Release Type	Season	Flow Rate (m^3/day)	Duration	Total Release Volume (m^3)	Ice
Platform Blow-out	Summer	5,600	30 days	168,000	No
	Winter	5,600	30 days	168,000	No
	Winter	5,600	30 days	168,000	Yes
	Summer	5,600	100 days	560,000	No
	Winter	5,600	120 days	672,000	No
	Winter	5,600	120 days	672,000	Yes
Subsea Blow-out	Summer	3,200	100 days	320,000	No
	Winter	3,200	120 days	384,000	No
	Winter	3,200	120 days	384,000	Yes
Batch Transfer	Summer	-	Instantaneous	800	No
	Winter	-	Instantaneous	800	No
	Winter	-	Instantaneous	800	Yes
Batch OLS Transfer	Summer	208 m^3/hr	24 hours	5,000	No
	Winter	208 m^3/hr	24 hours	5,000	No
	Winter	208 m^3/hr	24 hours	5,000	Yes

The stochastic model is used to determine the probability of oiling the water surface, the shoreline and the water column based on specified thickness and concentration thresholds. The thresholds used for the stochastic model simulations in this study are as follows:

- Average thickness > 0.01 mm (10 µm)
- Average shoreline oil thickness > 0.01 mm (10 µm)
- Entrained oil (oil in water) average concentration > 10 ppb

The maps in Figures 1 through 48 show the probability for sea surface area oiling, shoreline oiling (including minimum time to reach the shoreline) and entrained oil exceeding the above thresholds for the platform and seafloor blow-outs in the winter and summer seasons. Figures 49 through 60 show the probability for sea surface area oiling and entrained oil exceeding the above thresholds for the batch transfer spills in the winter and summer seasons. **It should be noted that the maps do not show that oil will cover the entire area depicted, only the probability that surface oil will enter the area in excess of the given threshold.**

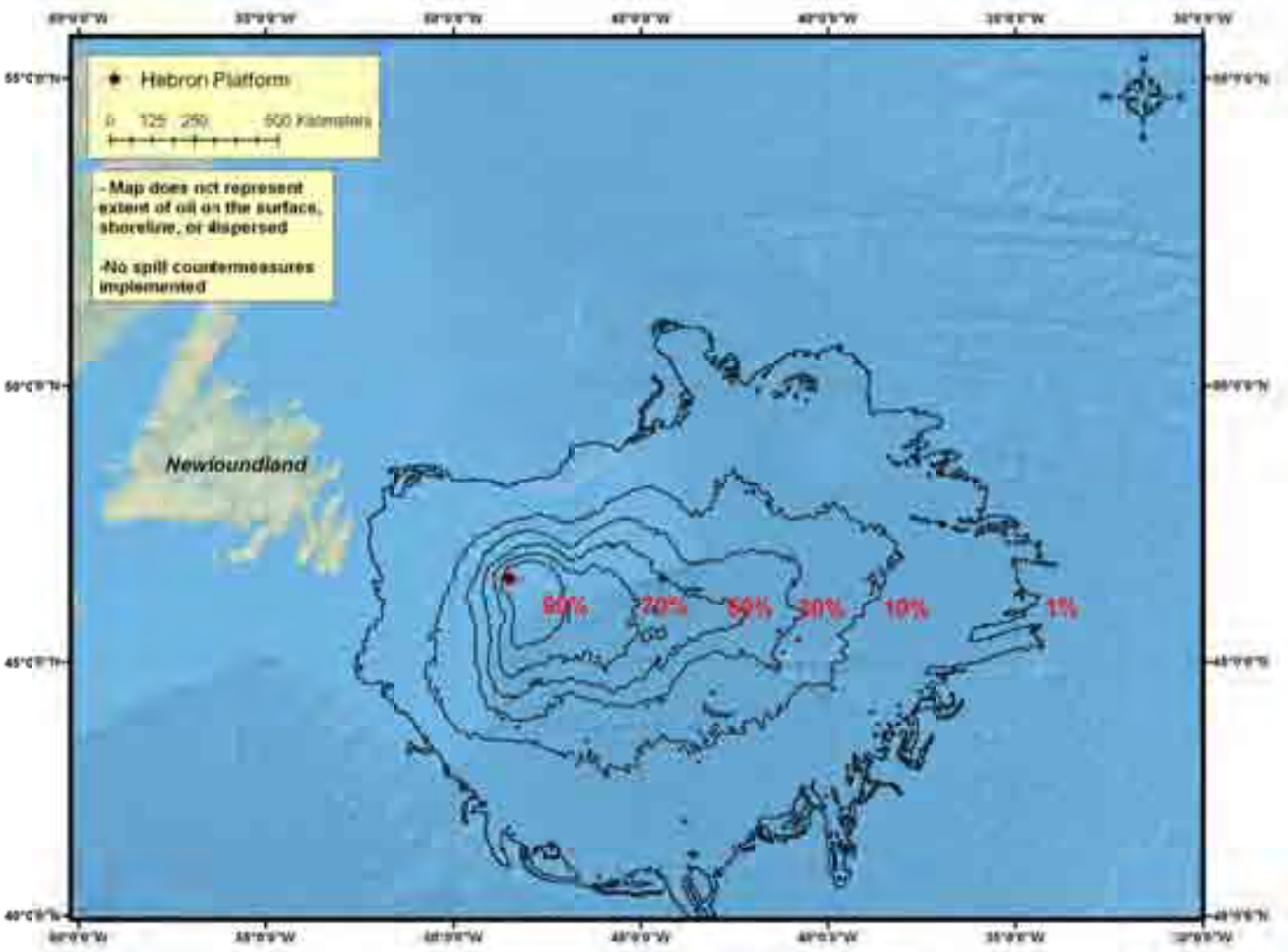


Figure 1. Surface oiling probabilities from a platform blow-out of 5,600 m^3/day of Hebron D-94 over a 30-day period during the summer.

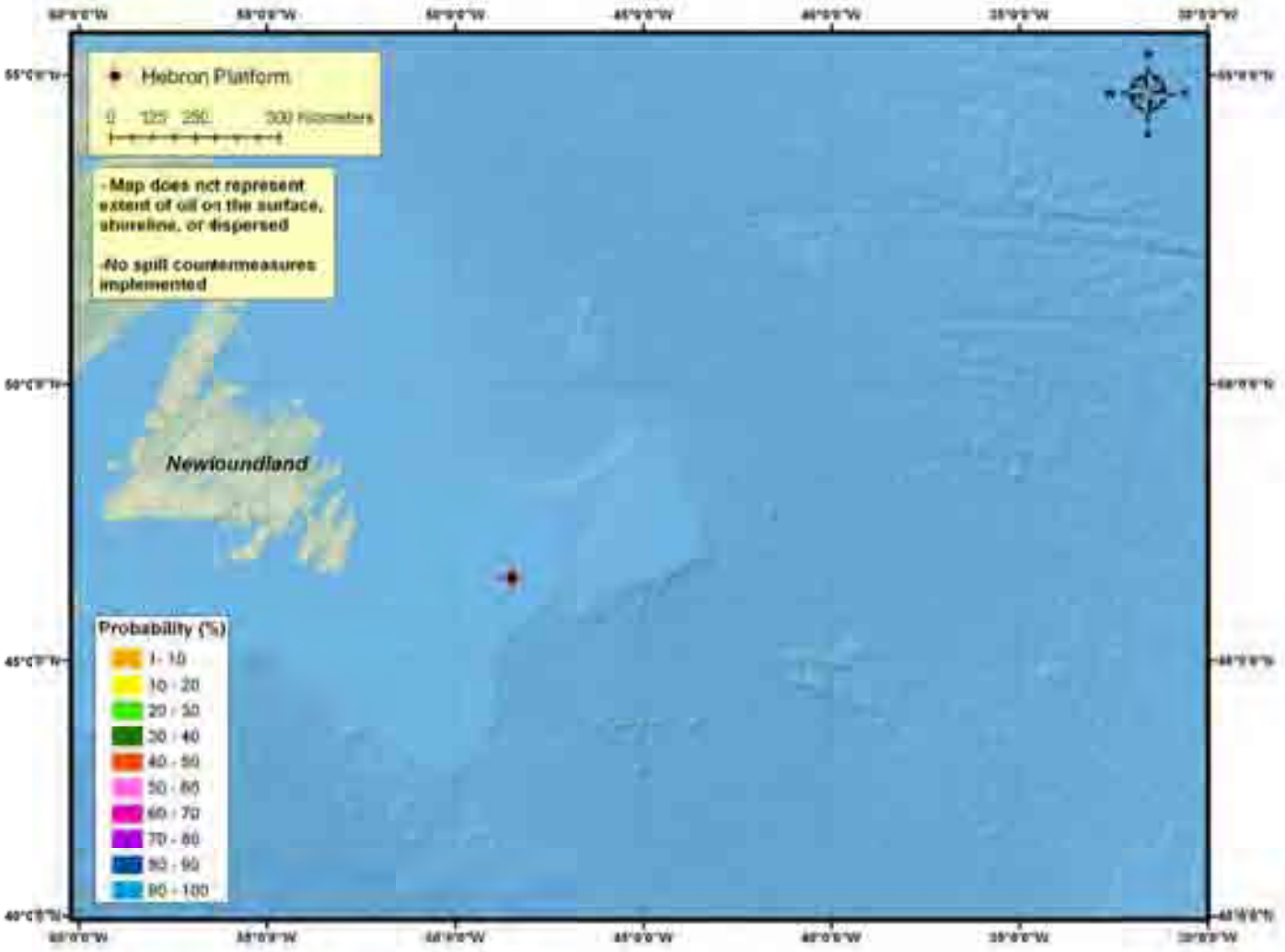


Figure 2. Shoreline oiling probabilities from a platform blow-out of 5,600 m^3/day of Hebron D-94 over a 30-day period during the summer.

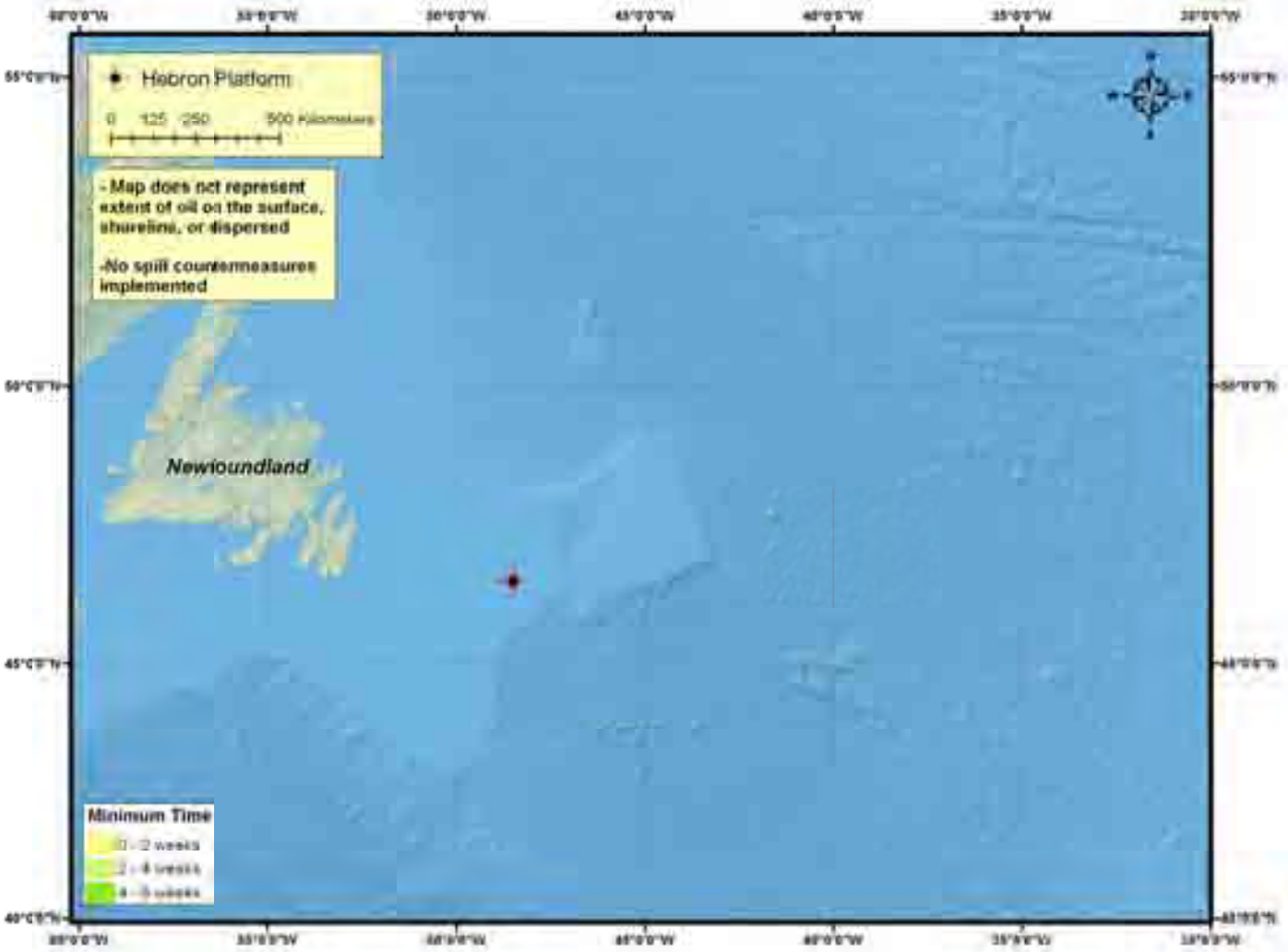


Figure 3. Minimum time to shoreline oiling from a platform blow-out of 5,600 m^3/day of Hebron D-94 over a 30-day period during the summer.

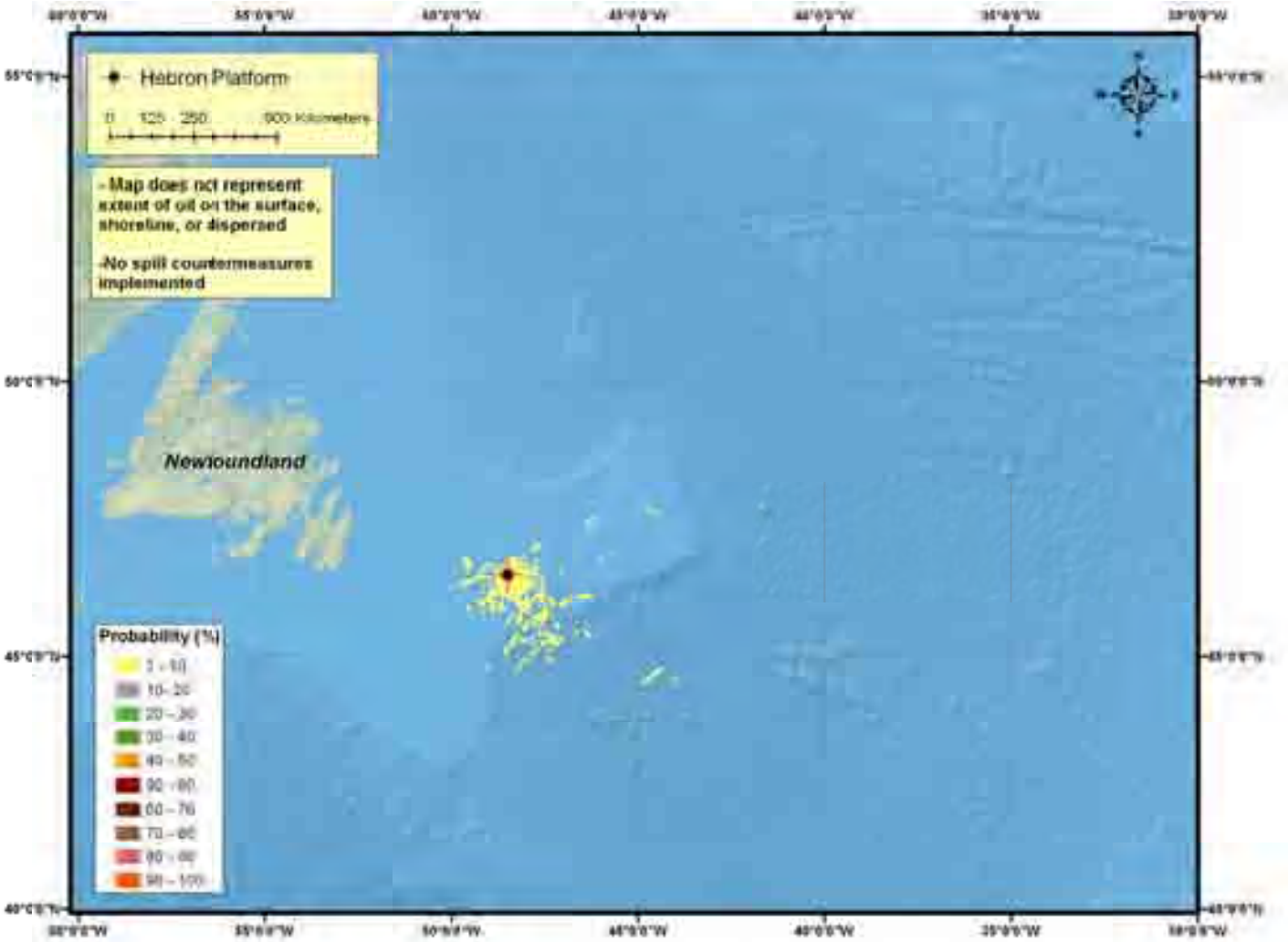


Figure 4. Entrained oiling probabilities from a platform blow-out of 5,600 m^3/day of Hebron D-94 over a 30-day period during the summer.

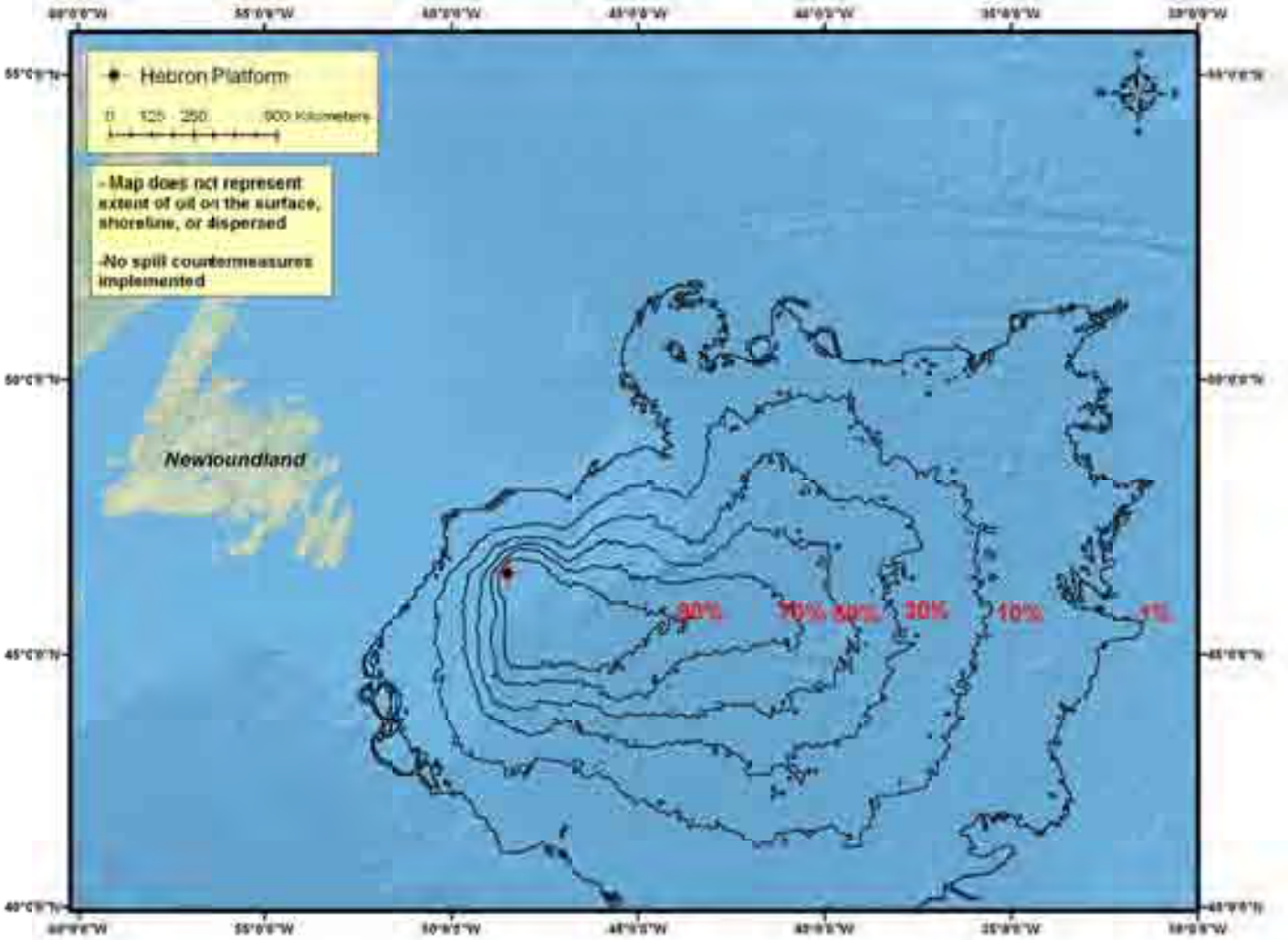


Figure 5. Surface oiling probabilities from a platform blow-out of 5,600 m^3/day of Hebron D-94 over a 30-day period during the winter.

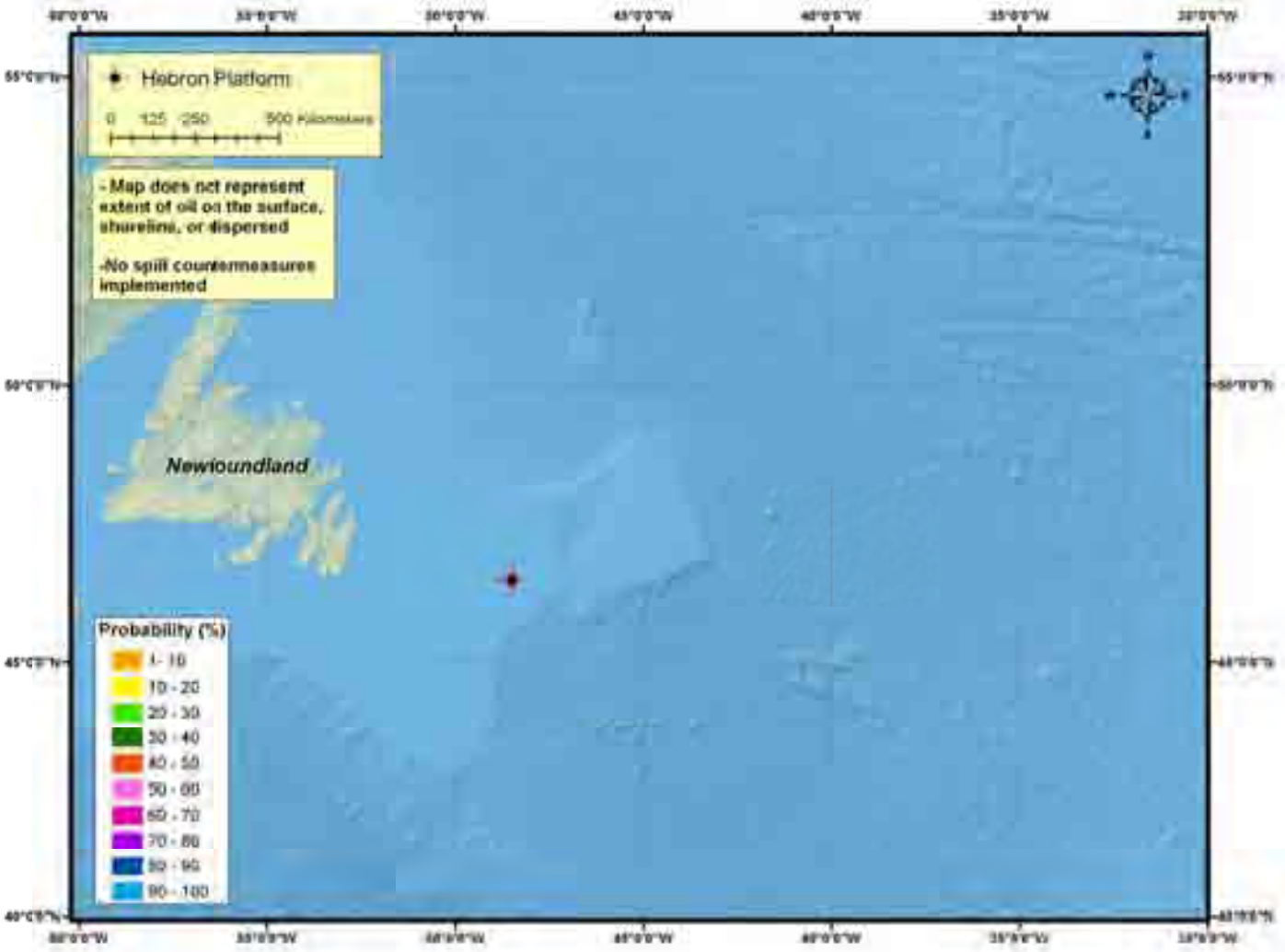


Figure 6. Shoreline oiling probabilities from a platform blow-out of 5,600 m^3/day of Hebron D-94 over a 30-day period during the winter.

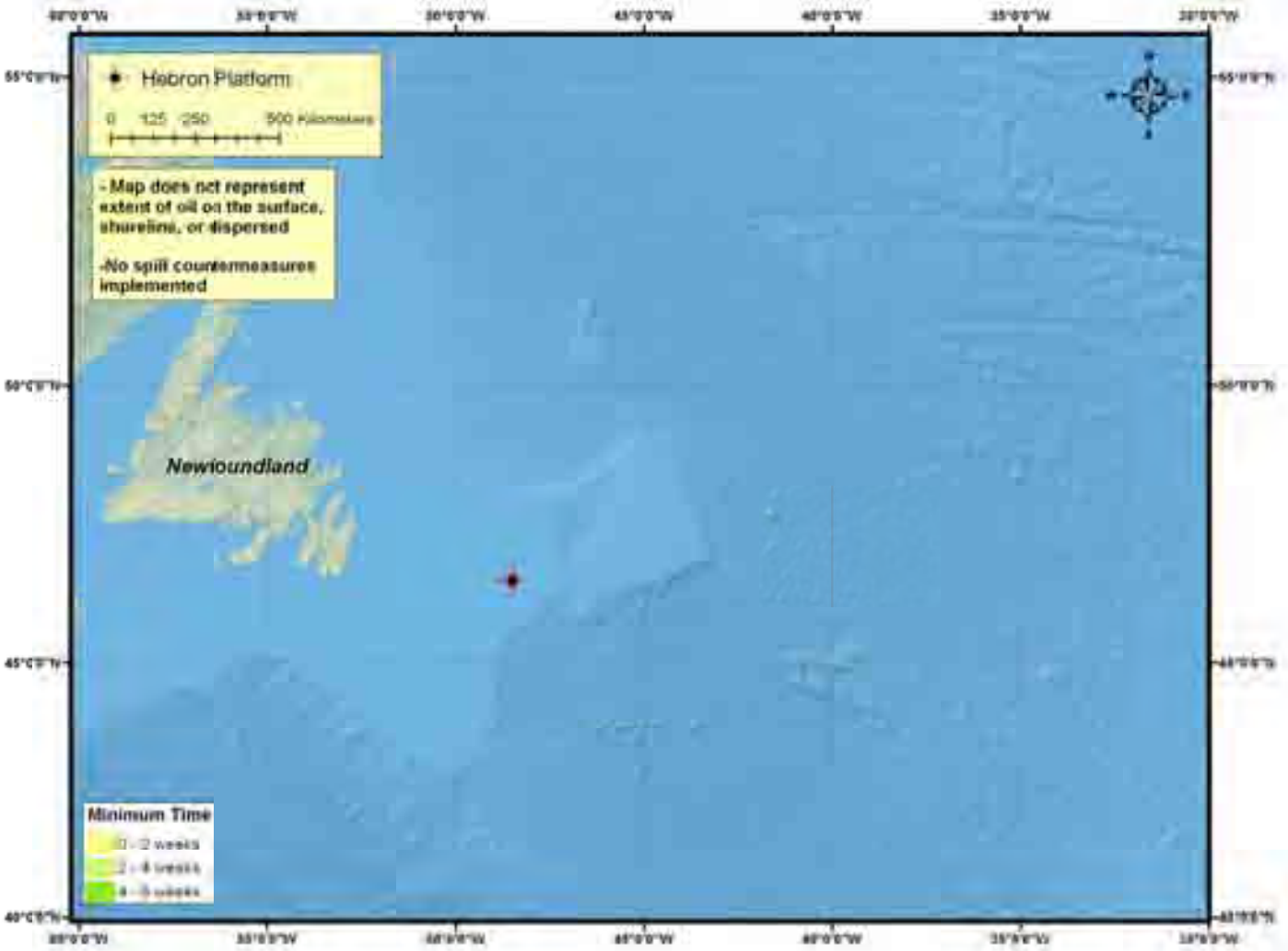


Figure 7. Minimum time to shoreline oiling from a platform blow-out of 5,600 m^3/day of Hebron D-94 over a 30-day period during the winter.

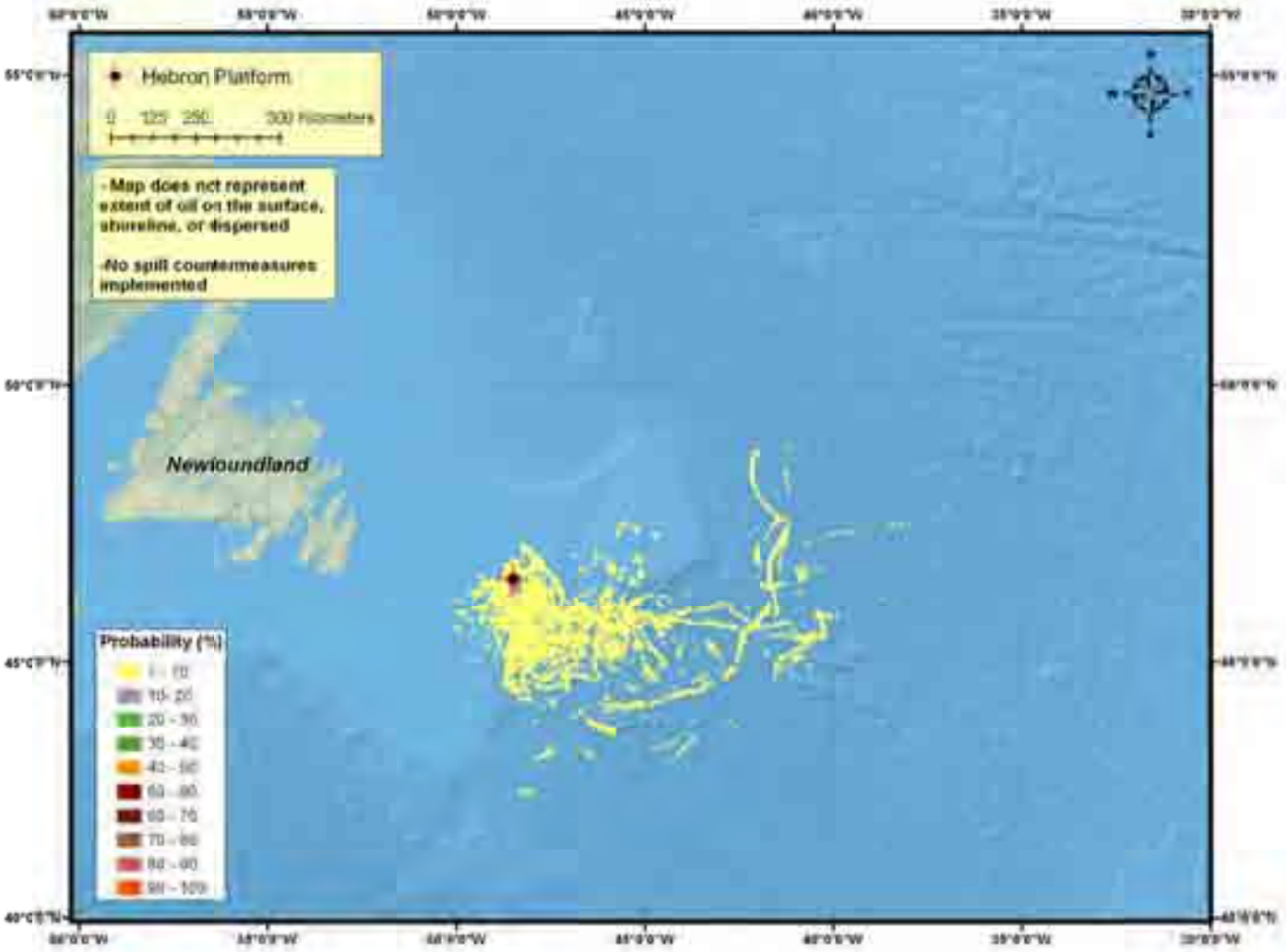


Figure 8. Entrained oiling probabilities from a platform blow-out of 5,600 m^3/day of Hebron D-94 over a 30-day period during the winter.

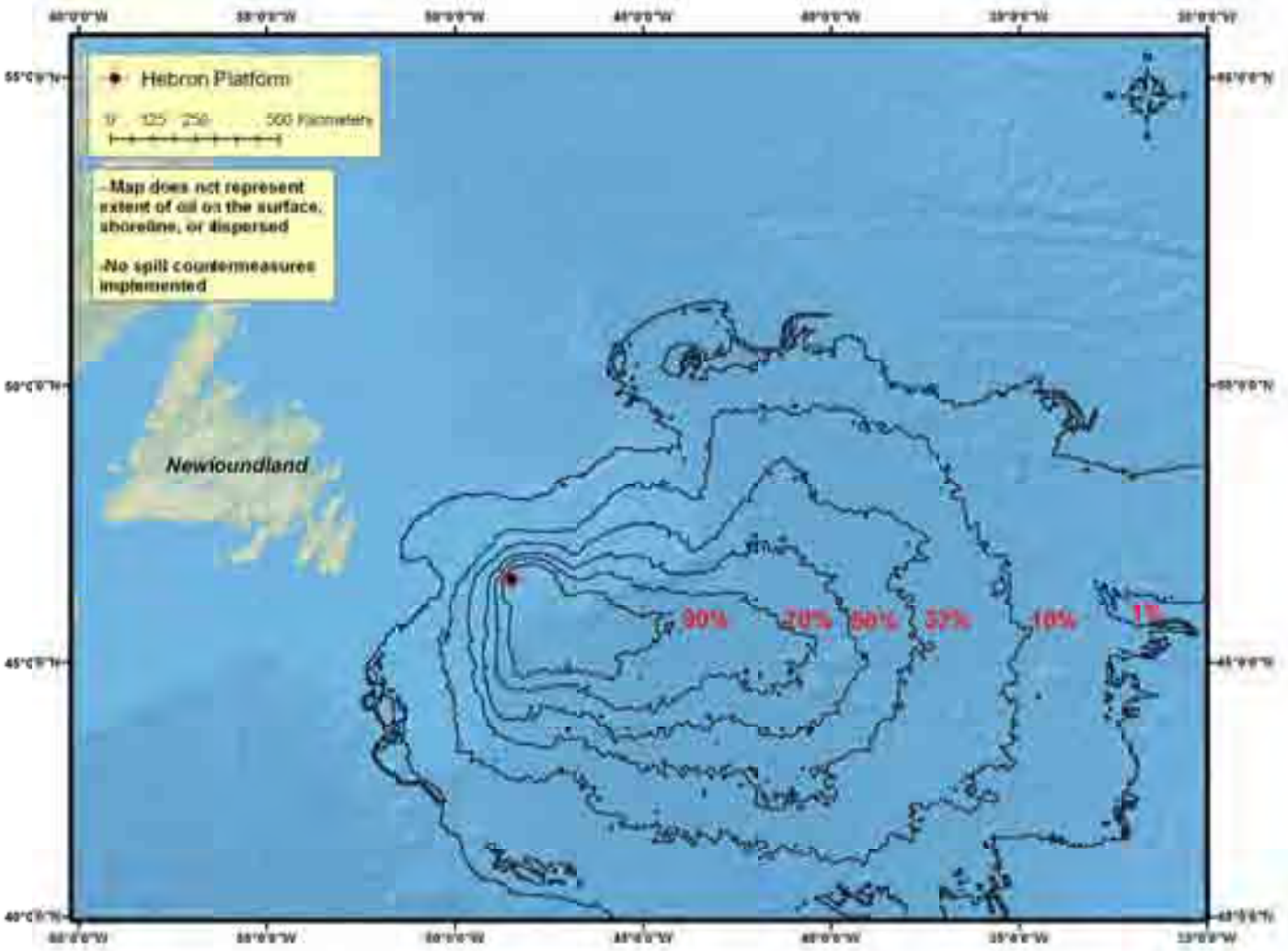


Figure 9. Surface oiling probabilities from a platform blow-out of 5,600 m^3/day of Hebron D-94 over a 30-day period during the winter with ice present.

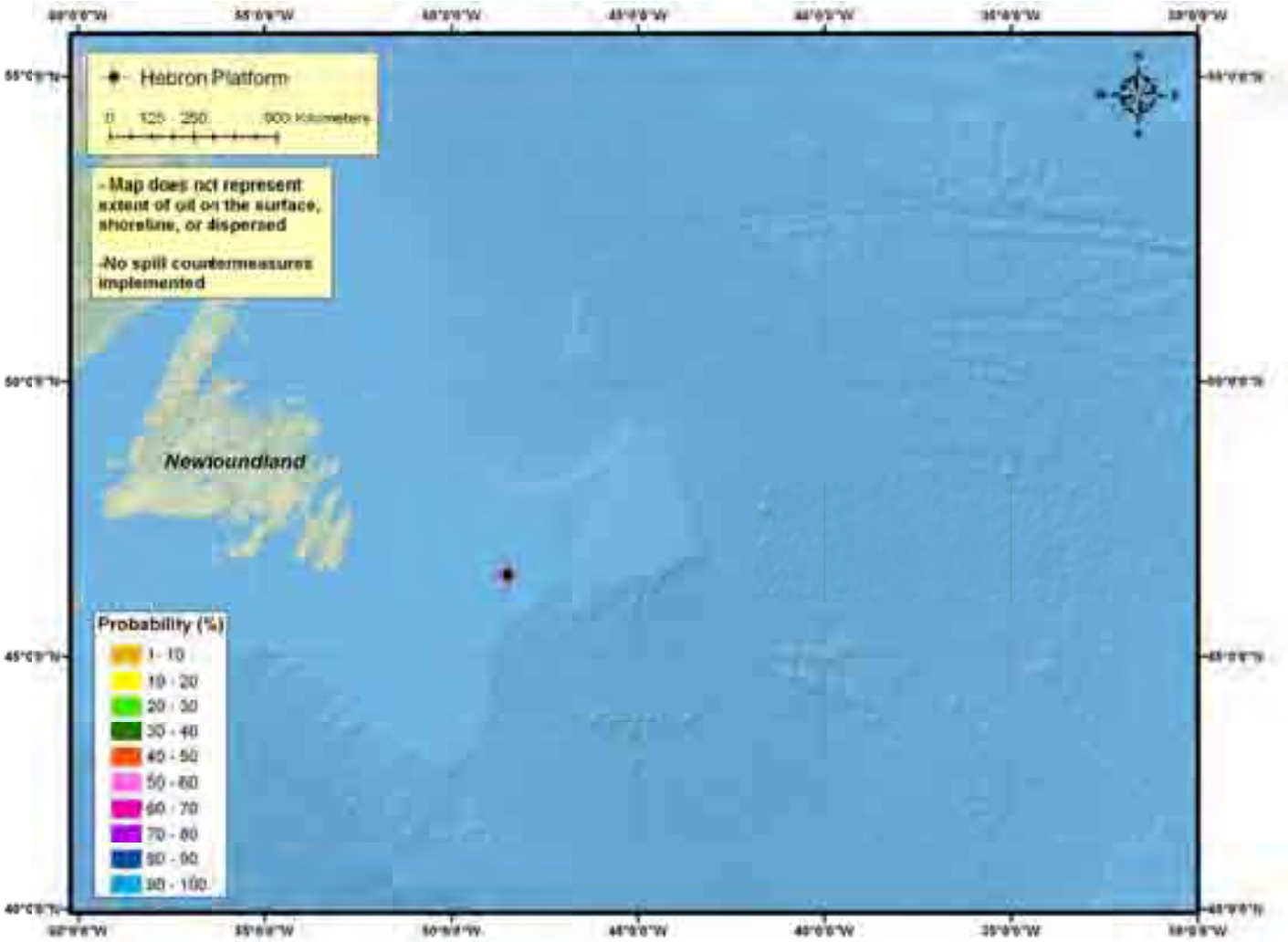


Figure 10. Shoreline oiling probabilities from a platform blow-out of 5,600 m^3/day of Hebron D-94 over a 30-day period during the winter with ice present.

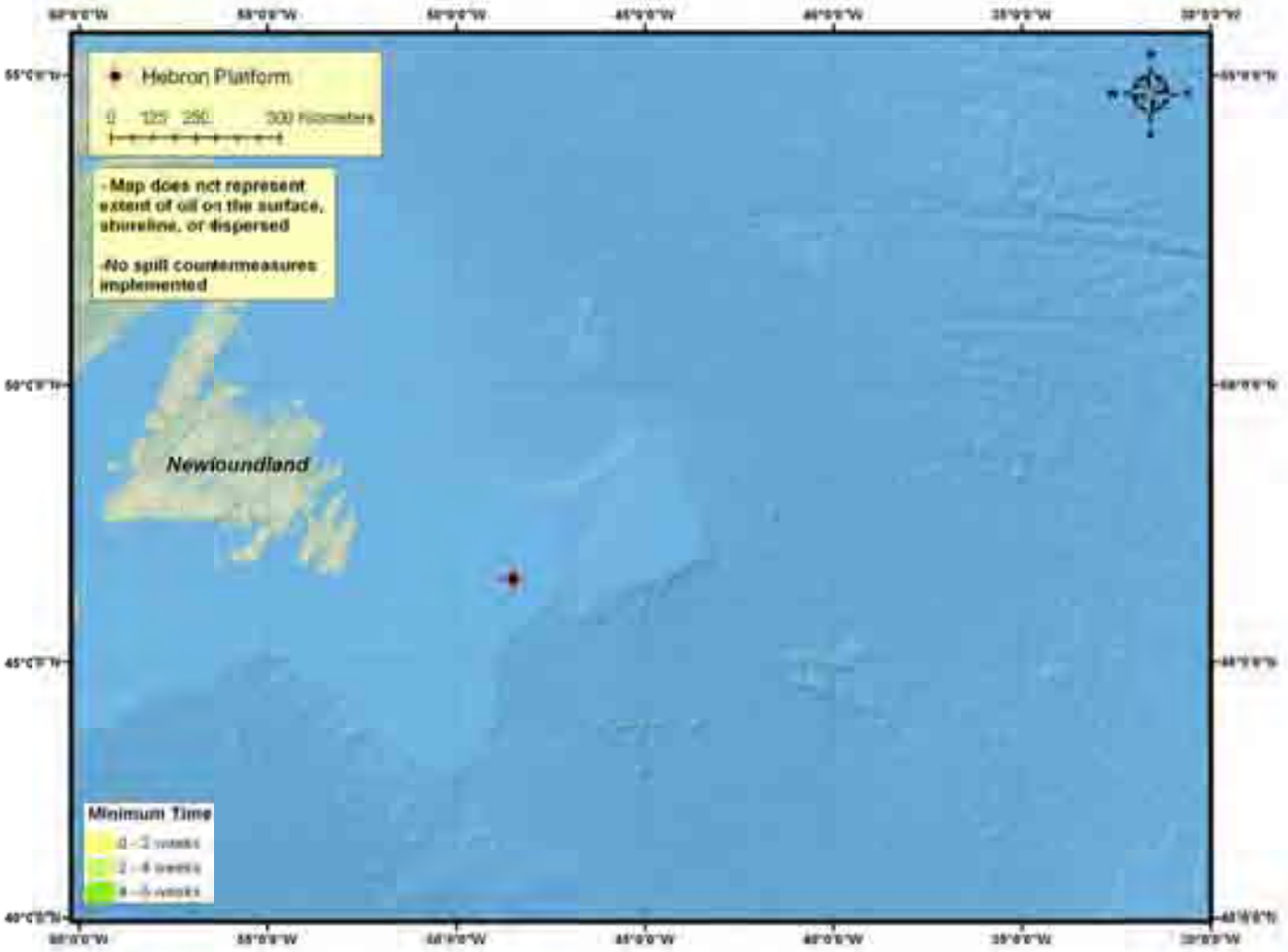


Figure 11. Minimum time to shoreline oiling from a platform blow-out of 5,600 m^3/day of Hebron D-94 over a 30-day period during the winter with ice present.

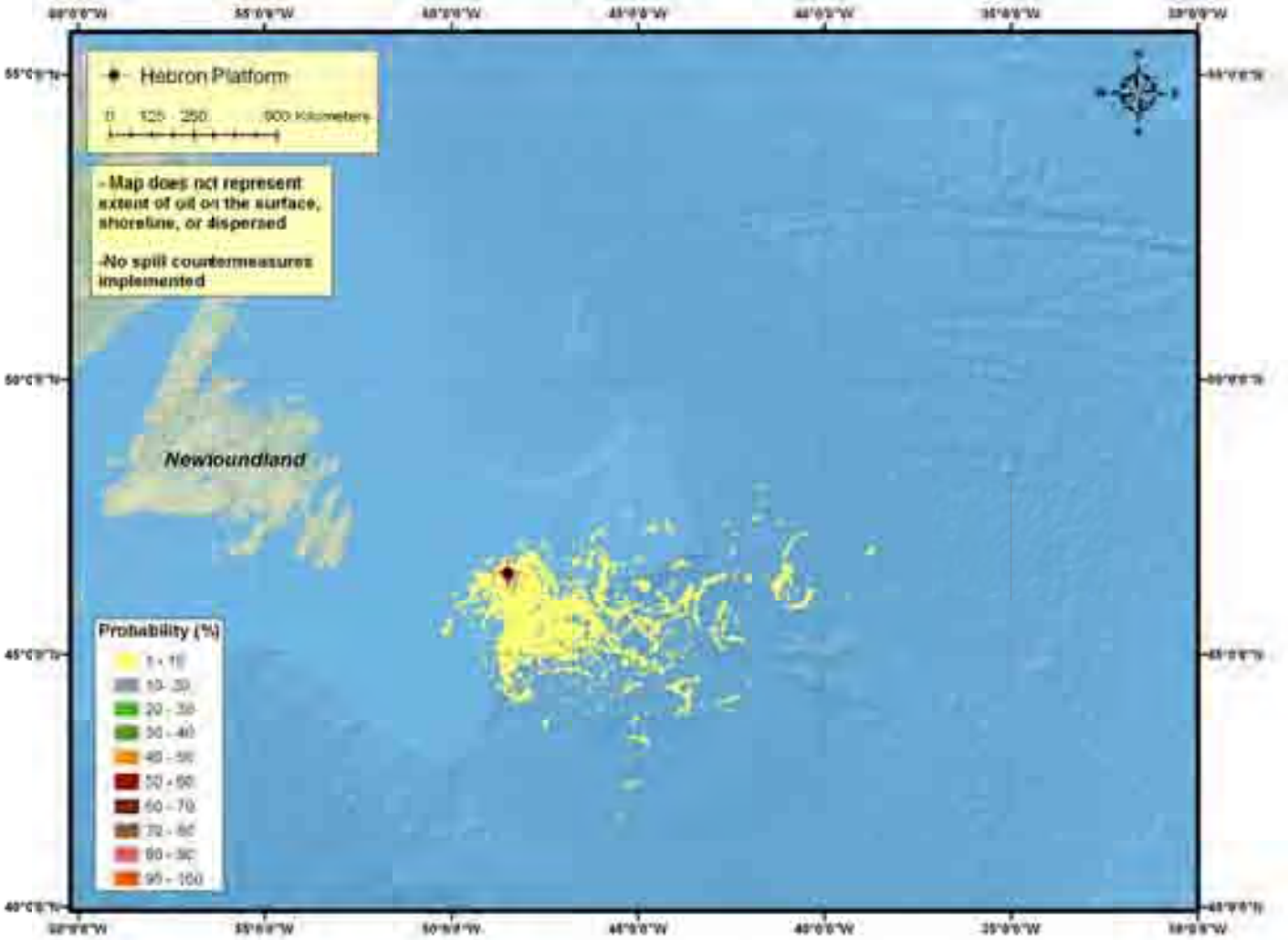


Figure 12. Entrained oiling probabilities from a platform blow-out of 5,600 m^3/day of Hebron D-94 over a 30-day period during the winter with ice present.

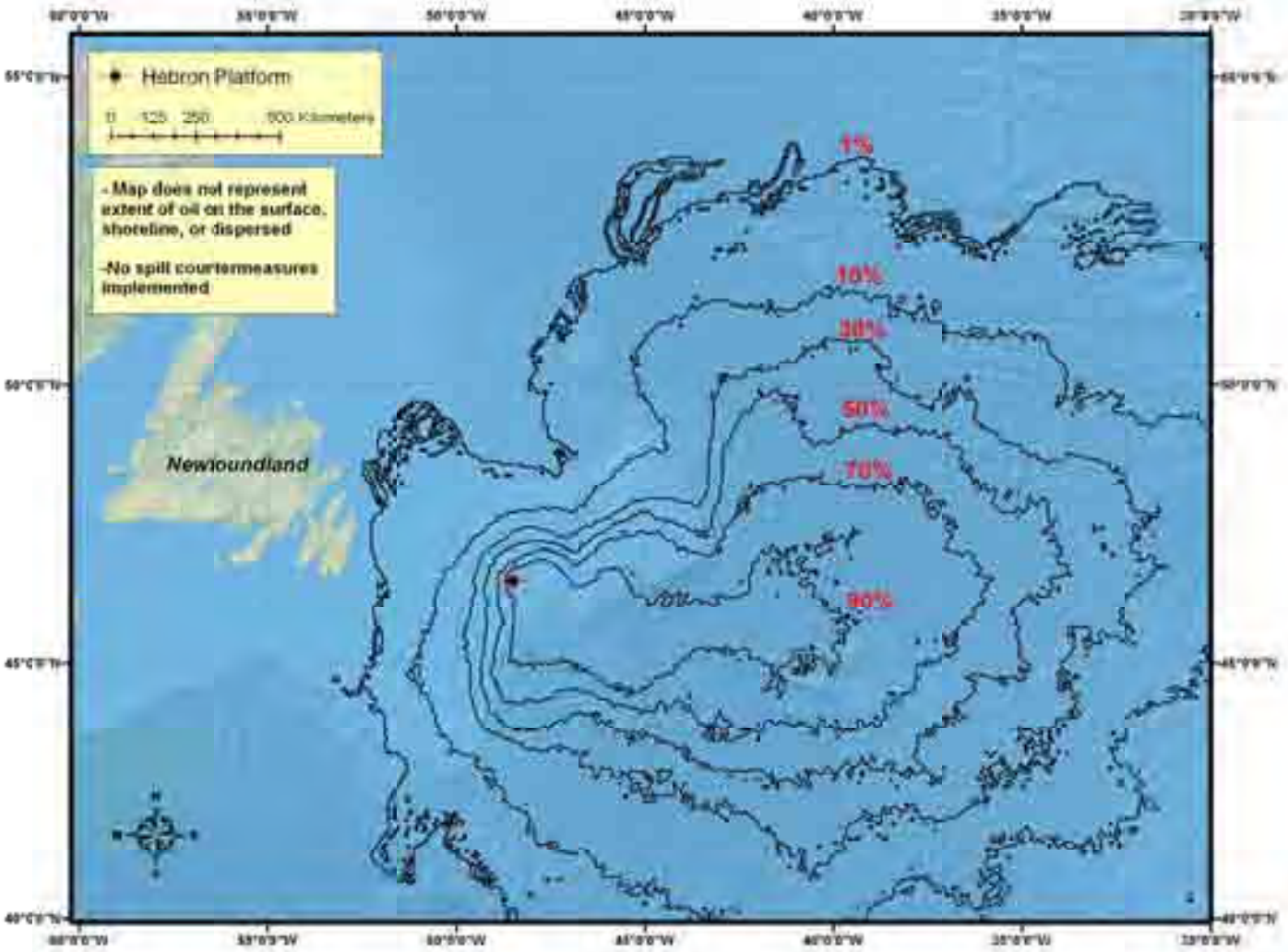


Figure 13. Surface oiling probabilities from a platform blow-out of 5,600 m^3/day of Hebron D-94 over a 30-day period during the summer run for 60 days.

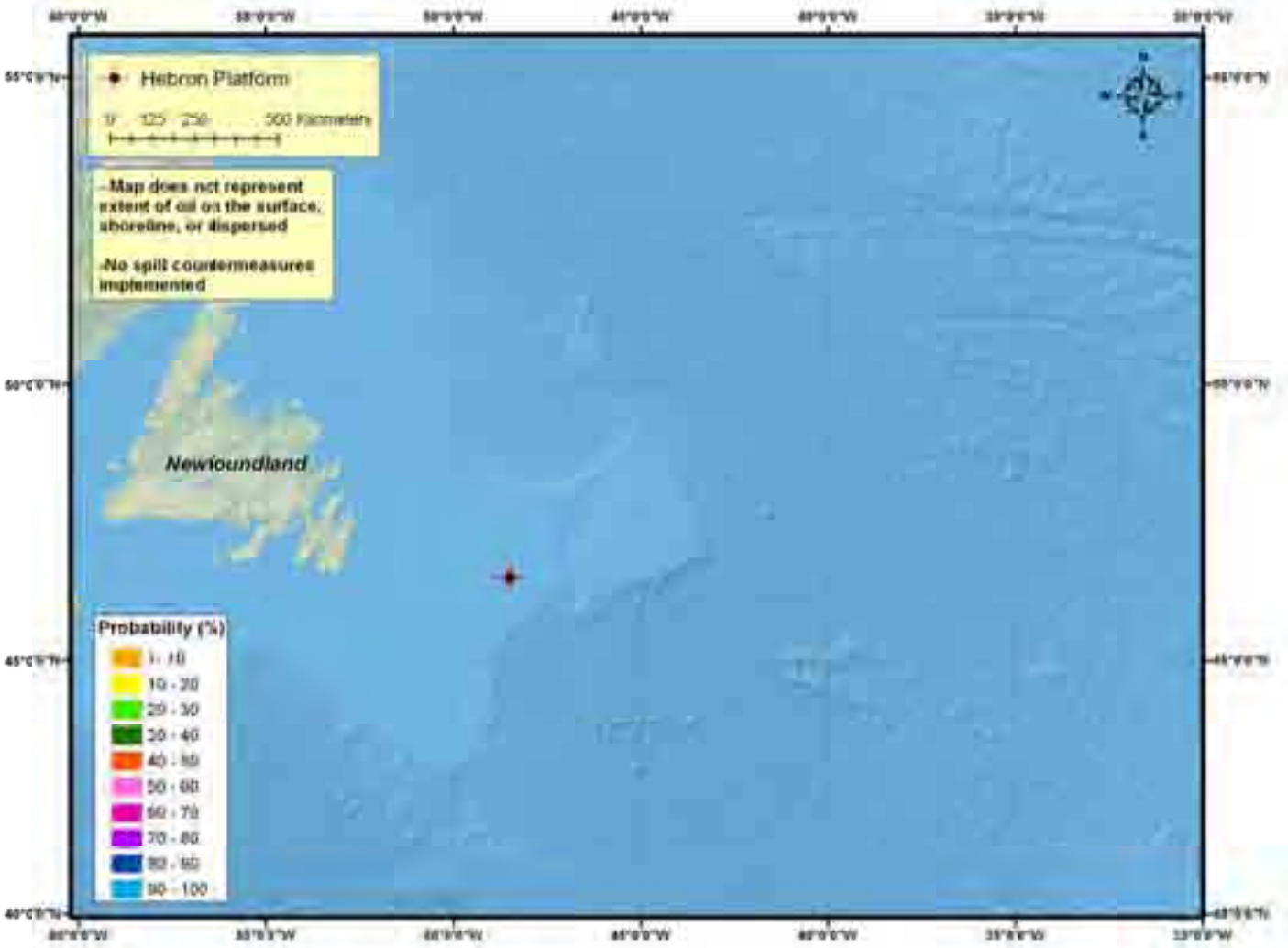


Figure 14. Shoreline oiling probabilities from a platform blow-out of 5,600 m^3/day of Hebron D-94 over a 30-day period during the summer run for 60 days.

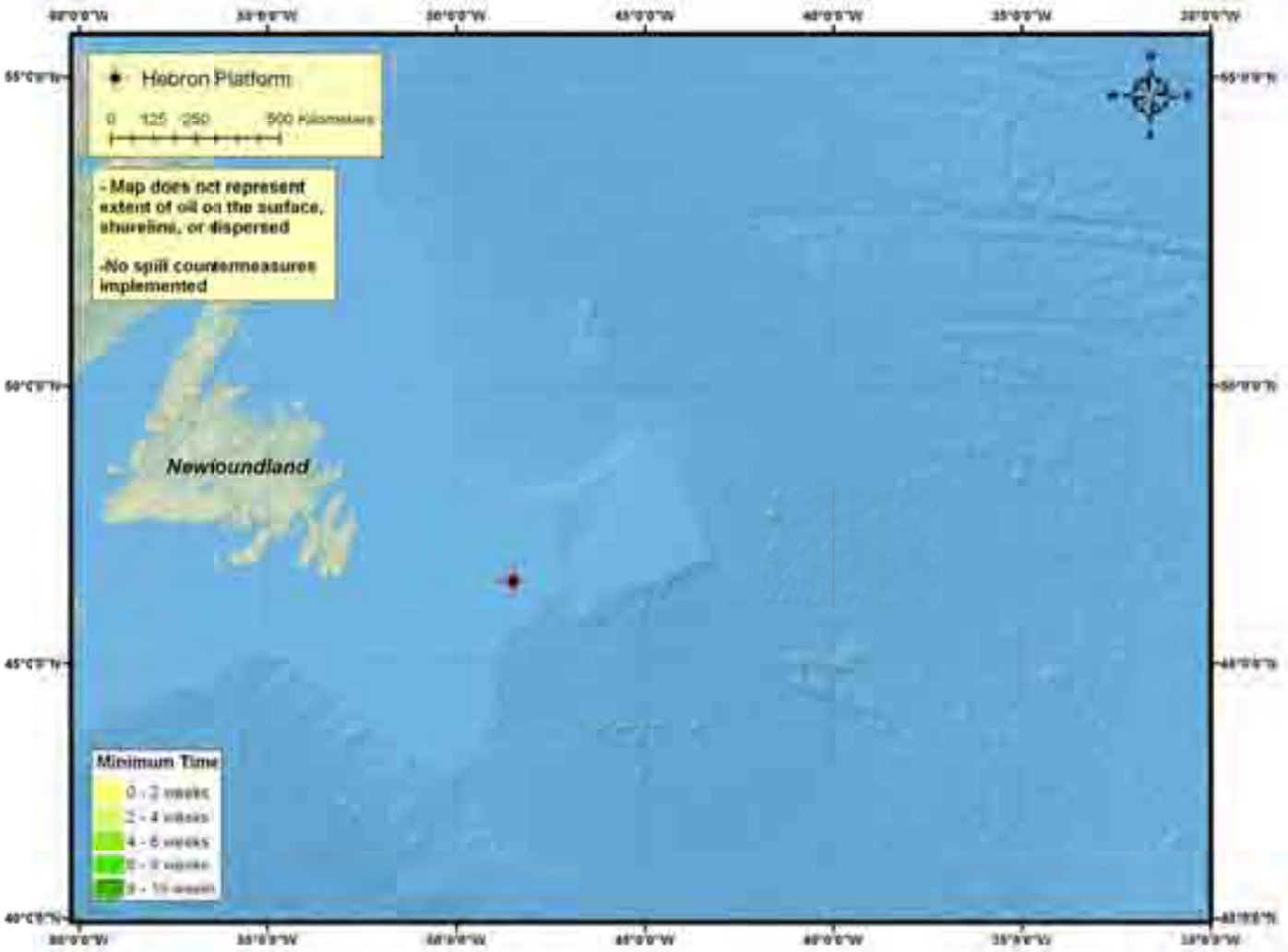


Figure 15. Minimum time to shoreline oiling from a platform blow-out of 5,600 m^3/day of Hebron D-94 over a 30-day period during the summer run for 60 days.

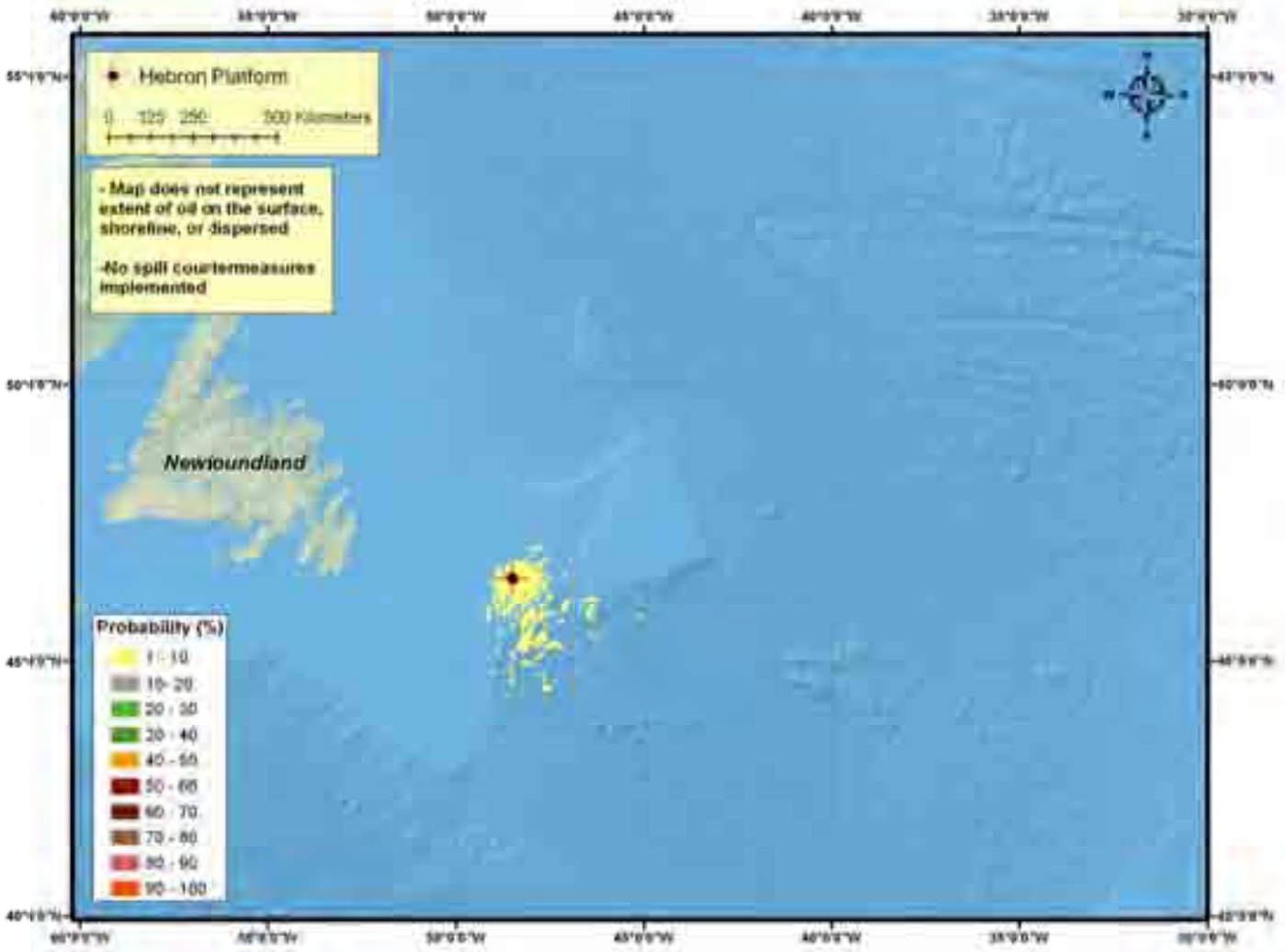


Figure 16. Entrained oiling probabilities from a platform blow-out of 5,600 m^3/day of Hebron D-94 over a 30-day period during the summer run for 60 days.

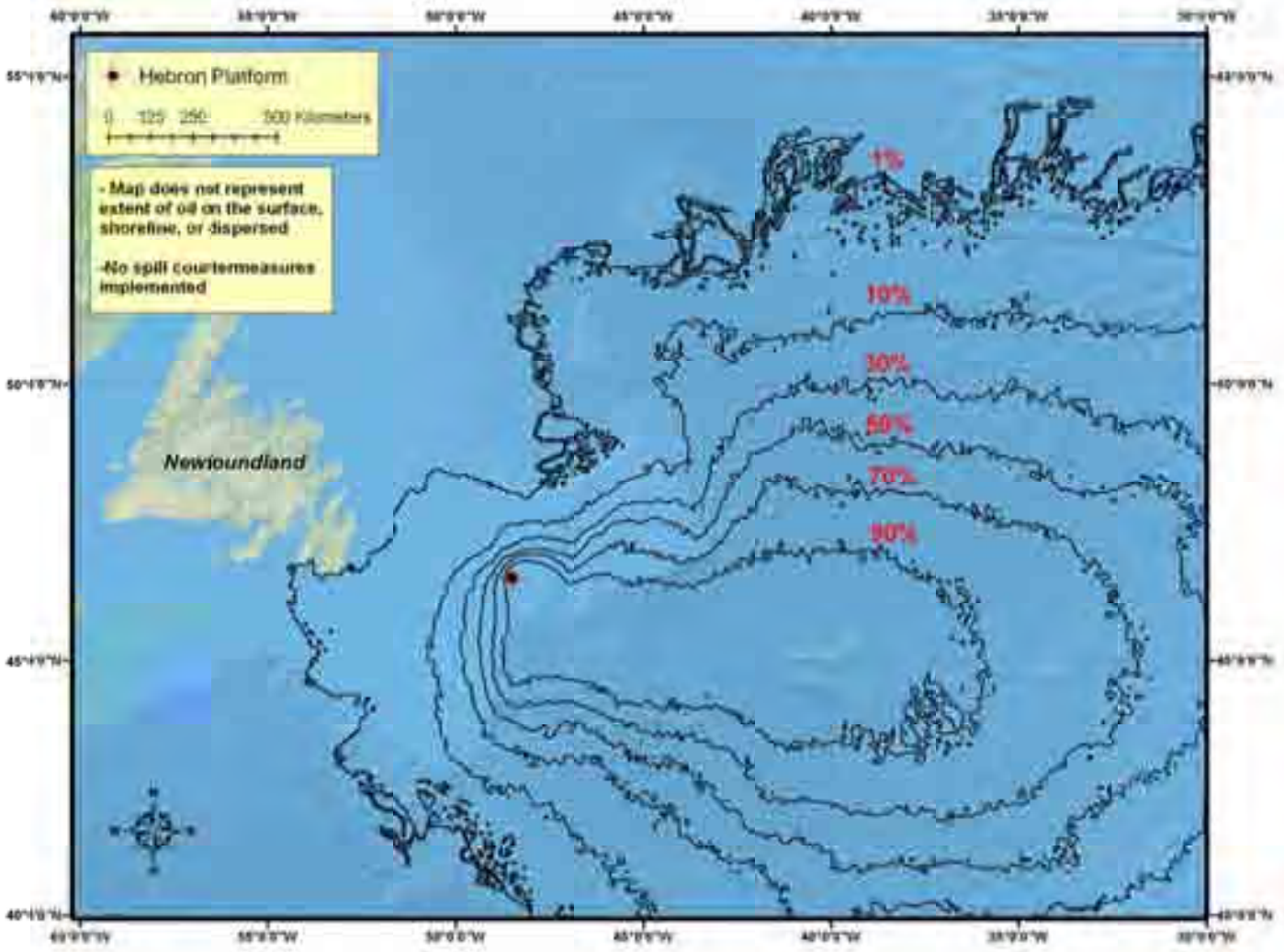


Figure 17. Surface oiling probabilities from a platform blow-out of 5,600 m^3/day of Hebron D-94 over a 30-day period during the winter run for 60 days.

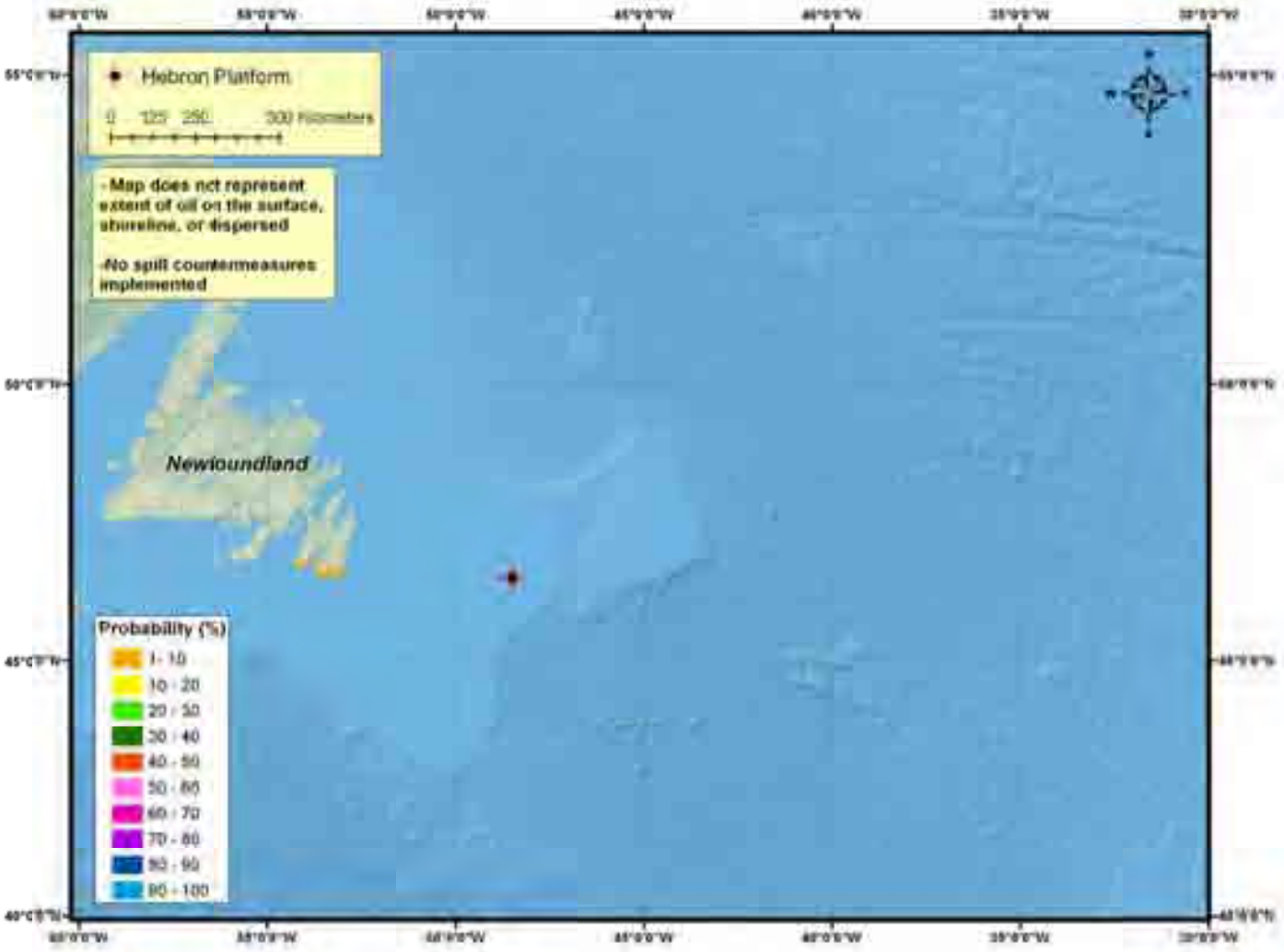


Figure 18. Shoreline oiling probabilities from a platform blow-out of 5,600 m^3/day of Hebron D-94 over a 30-day period during the winter run for 60 days.

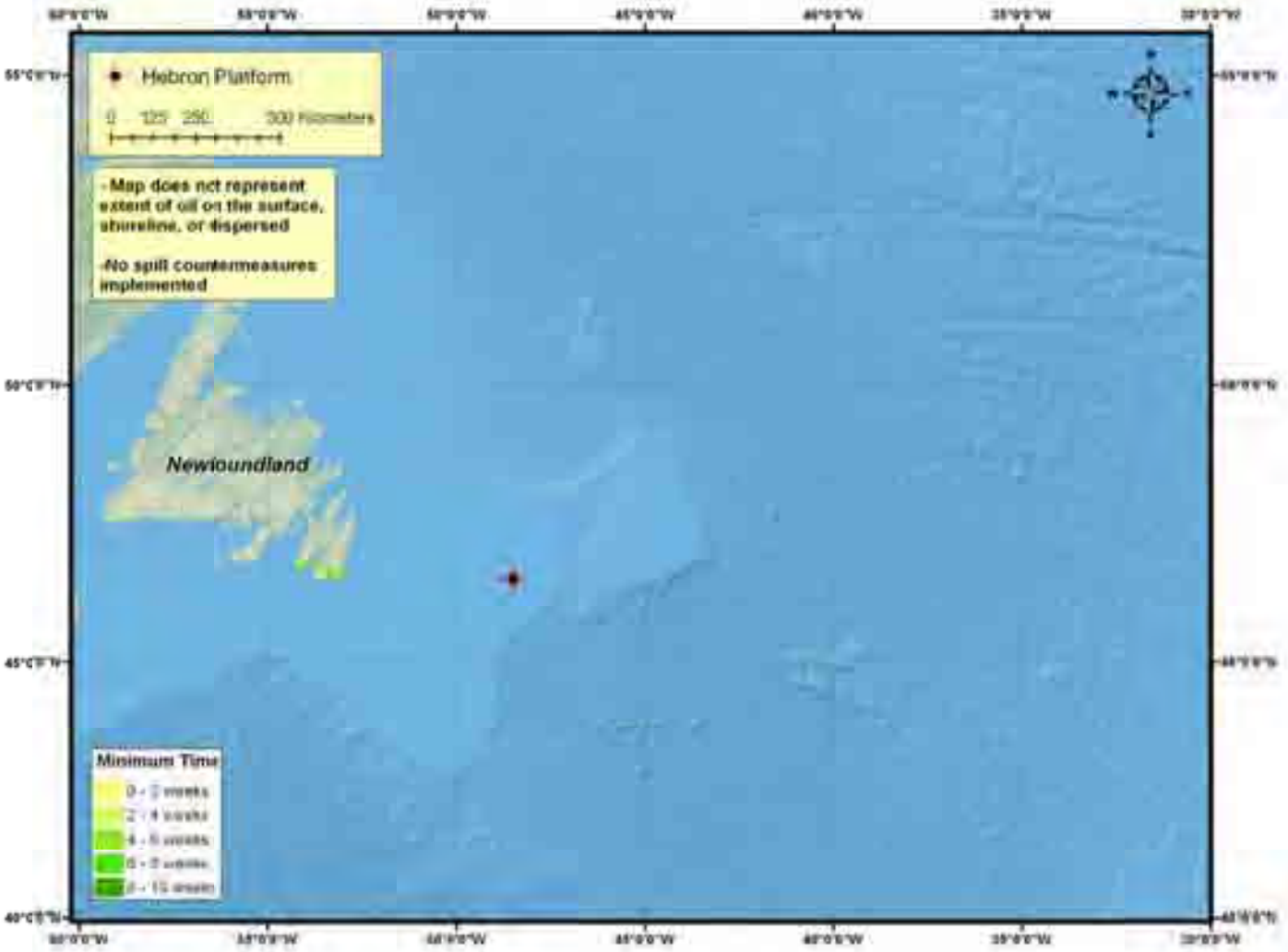


Figure 19. Minimum time to shoreline oiling from a platform blow-out of 5,600 m^3/day of Hebron D-94 over a 30-day period during the winter run for 60 days.

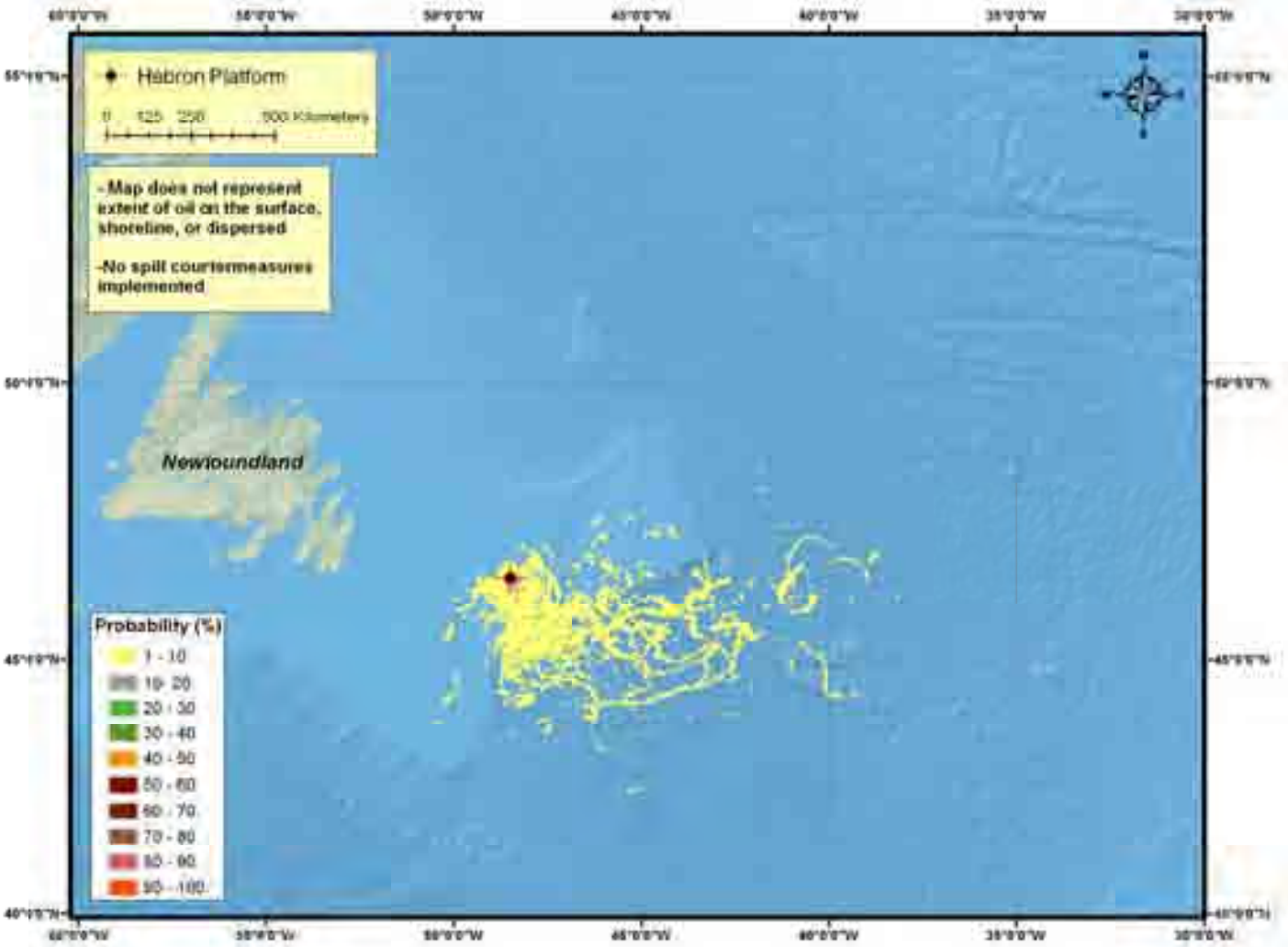


Figure 20. Entrained oiling probabilities from a platform blow-out of 5,600 m^3/day of Hebron D-94 over a 30-day period during the winter run for 60 days.

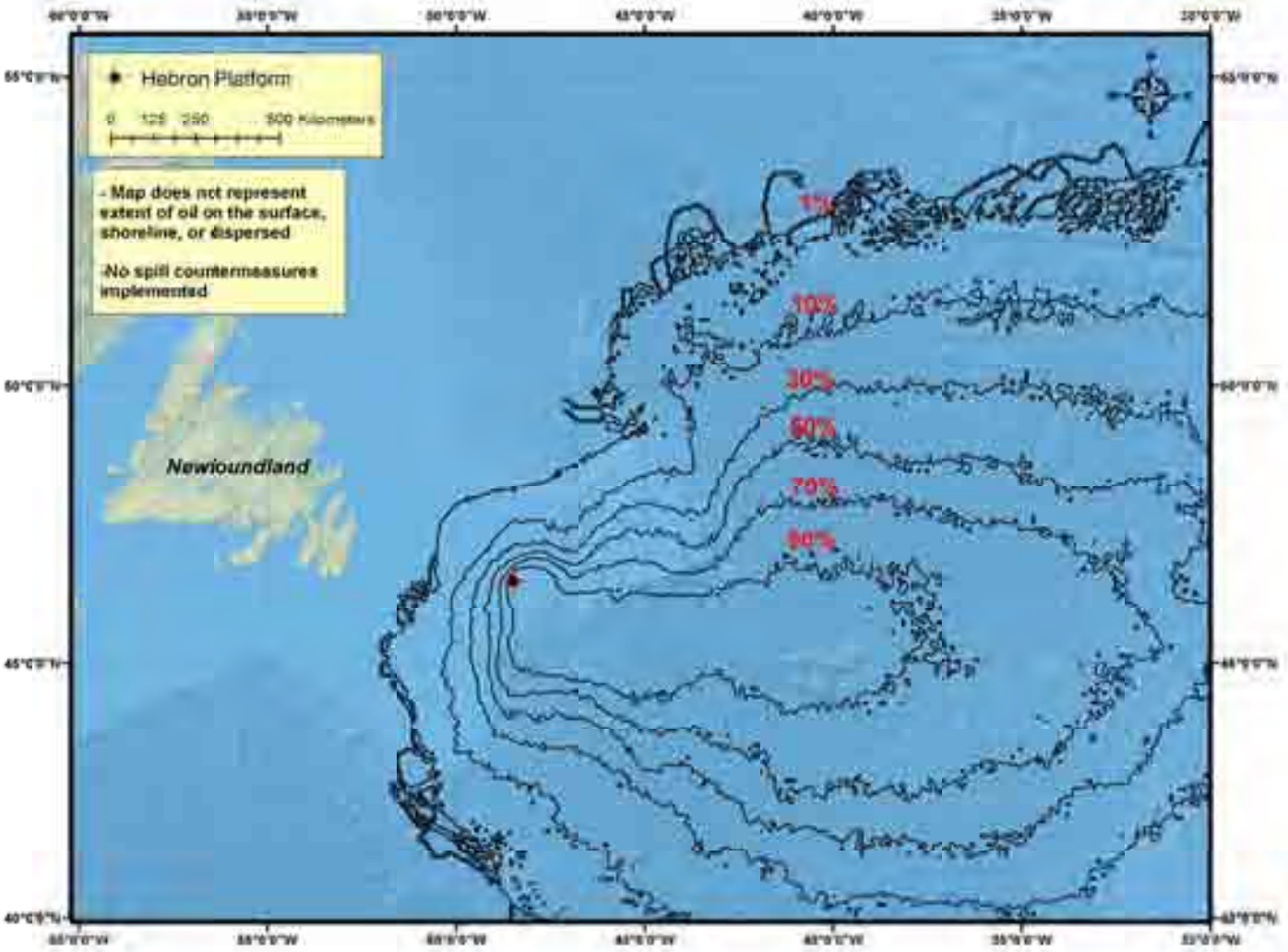


Figure 21. Surface oiling probabilities from a platform blow-out of 5,600 m^3/day of Hebron D-94 over a 30-day period during the winter run for 60 days with ice present.

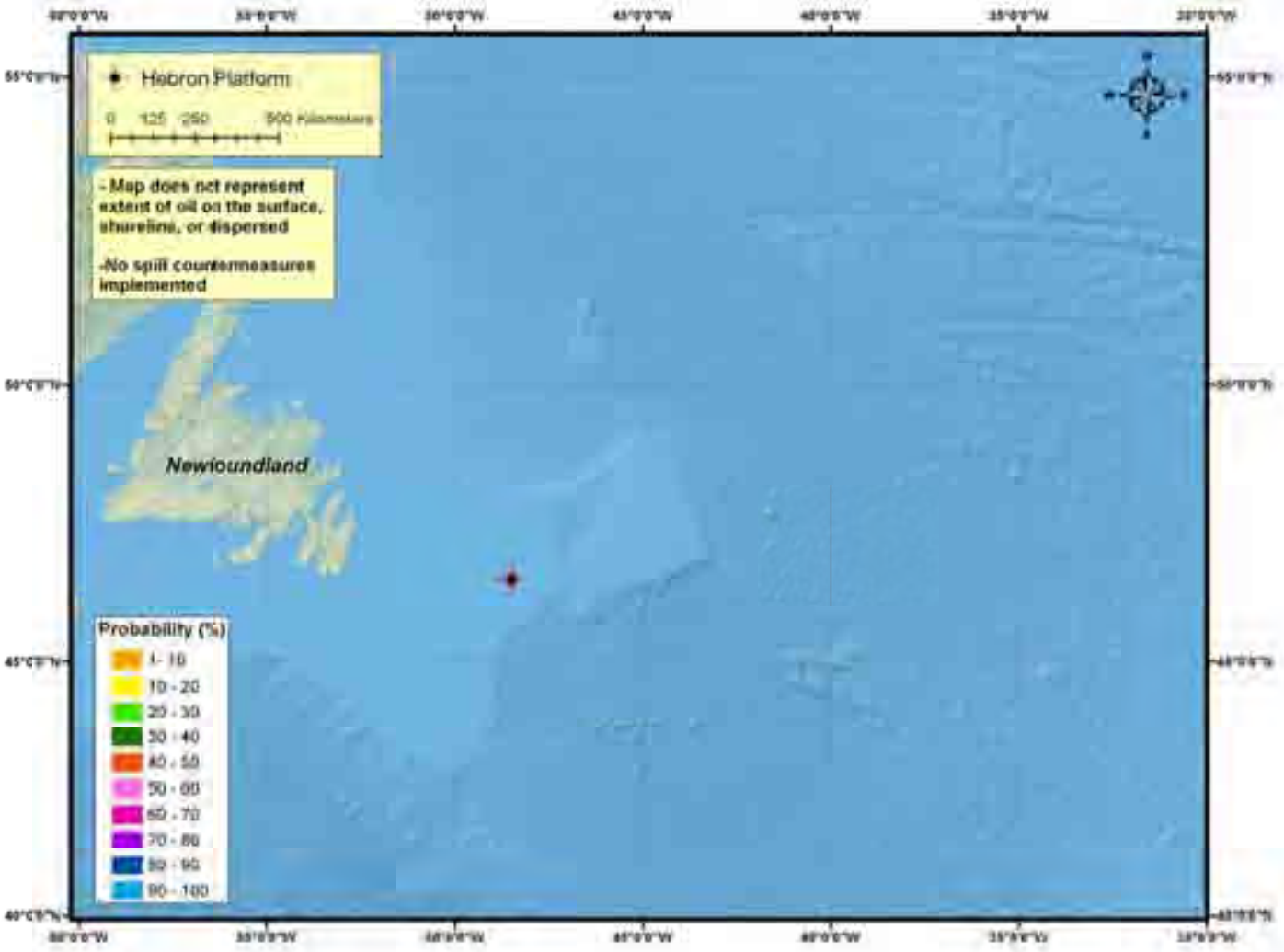


Figure 22. Shoreline oiling probabilities from a platform blow-out of 5,600 m^3/day of Hebron D-94 over a 30-day period during the winter run for 60 days with ice present.

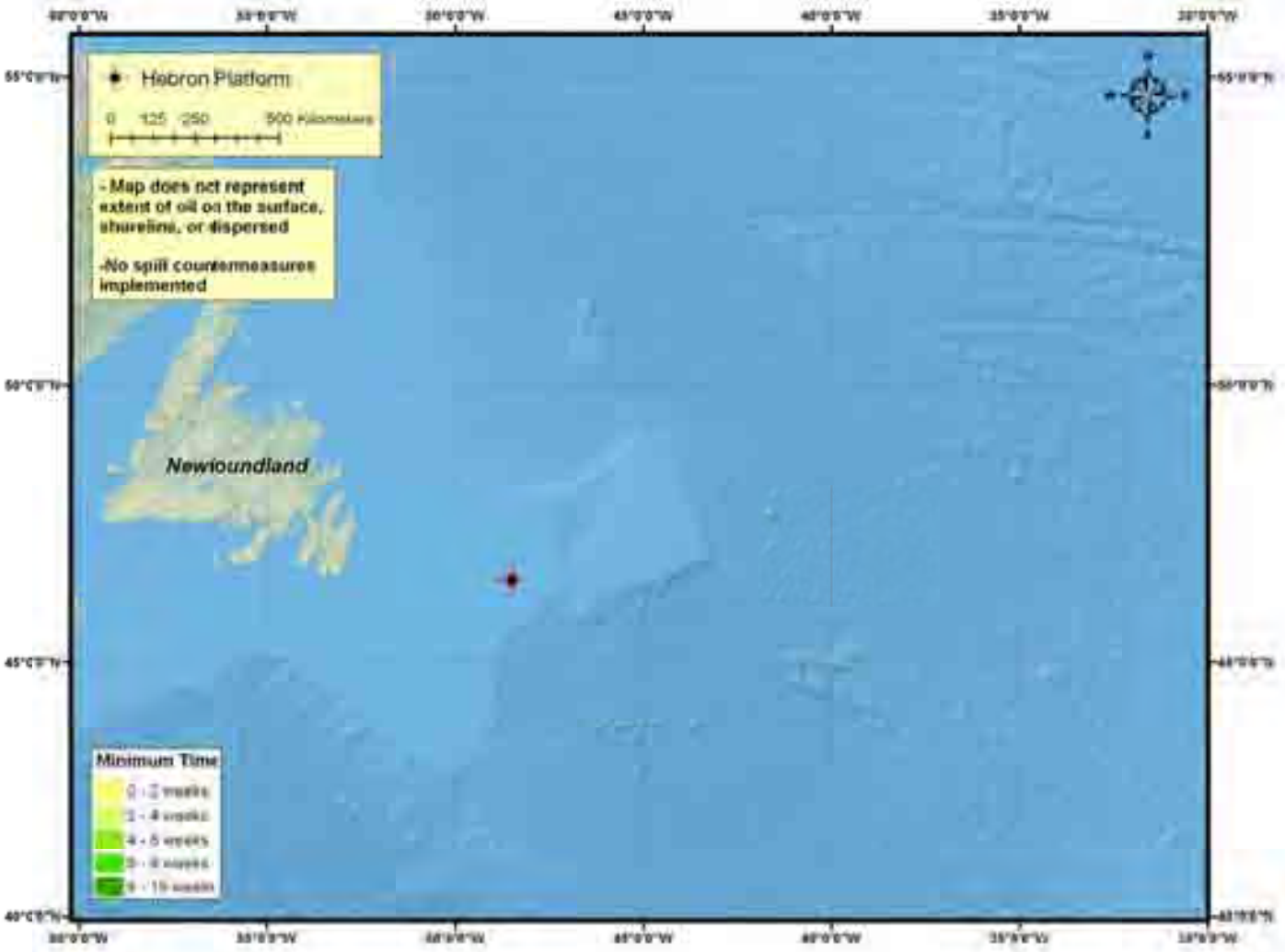


Figure 23. Minimum time to shoreline oiling from a platform blow-out of 5,600 m^3/day of Hebron D-94 over a 30-day period during the winter run for 60 days with ice present.

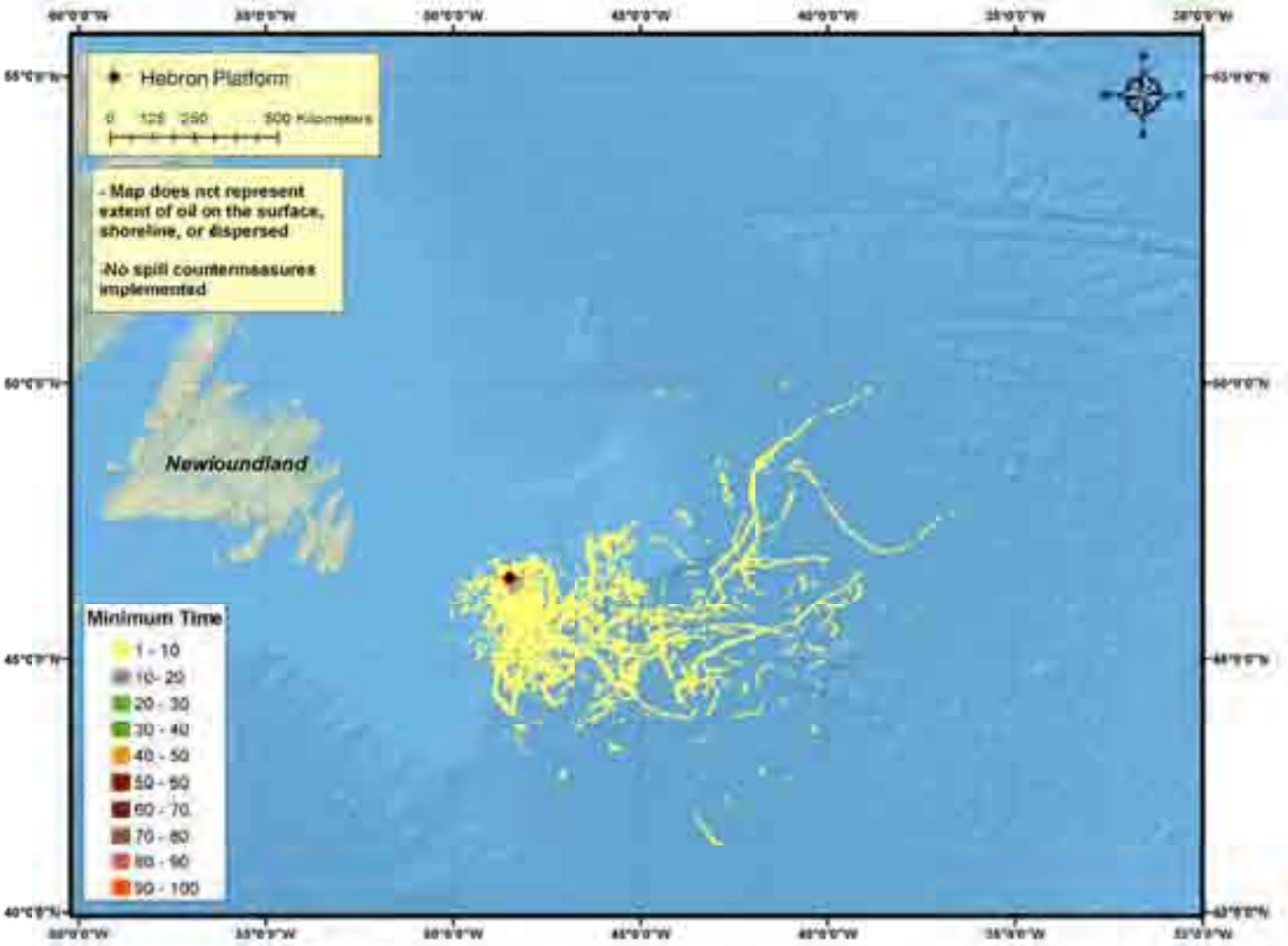


Figure 24. Entrained oiling probabilities from a platform blow-out of 5,600 m^3/day of Hebron D-94 over a 30-day period during the winter run for 60 days with ice present.

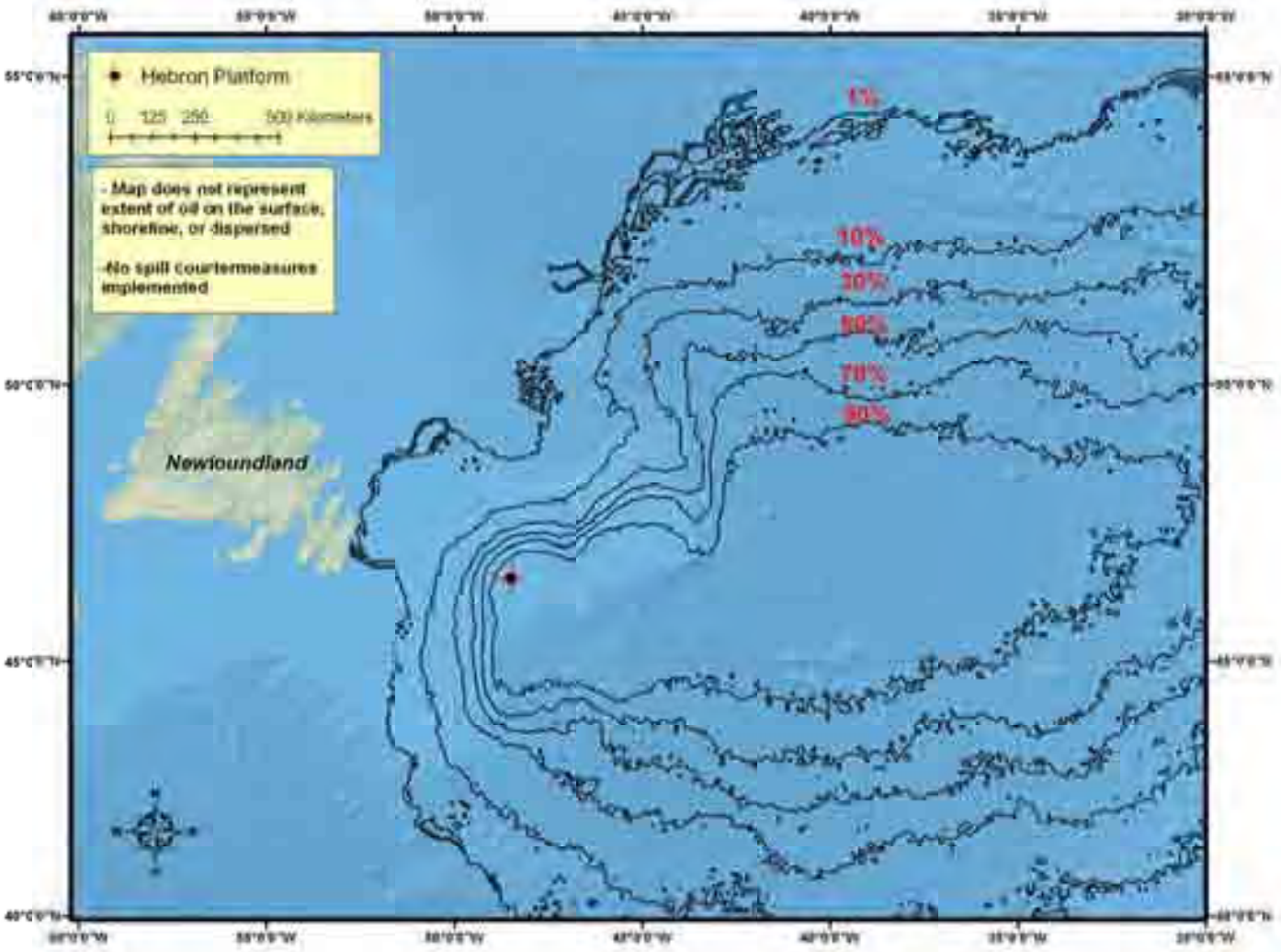


Figure 25. Surface oiling probabilities from a platform blow-out of 5,600 m^3/day of Hebron D-94 over a 100-day period during the summer.

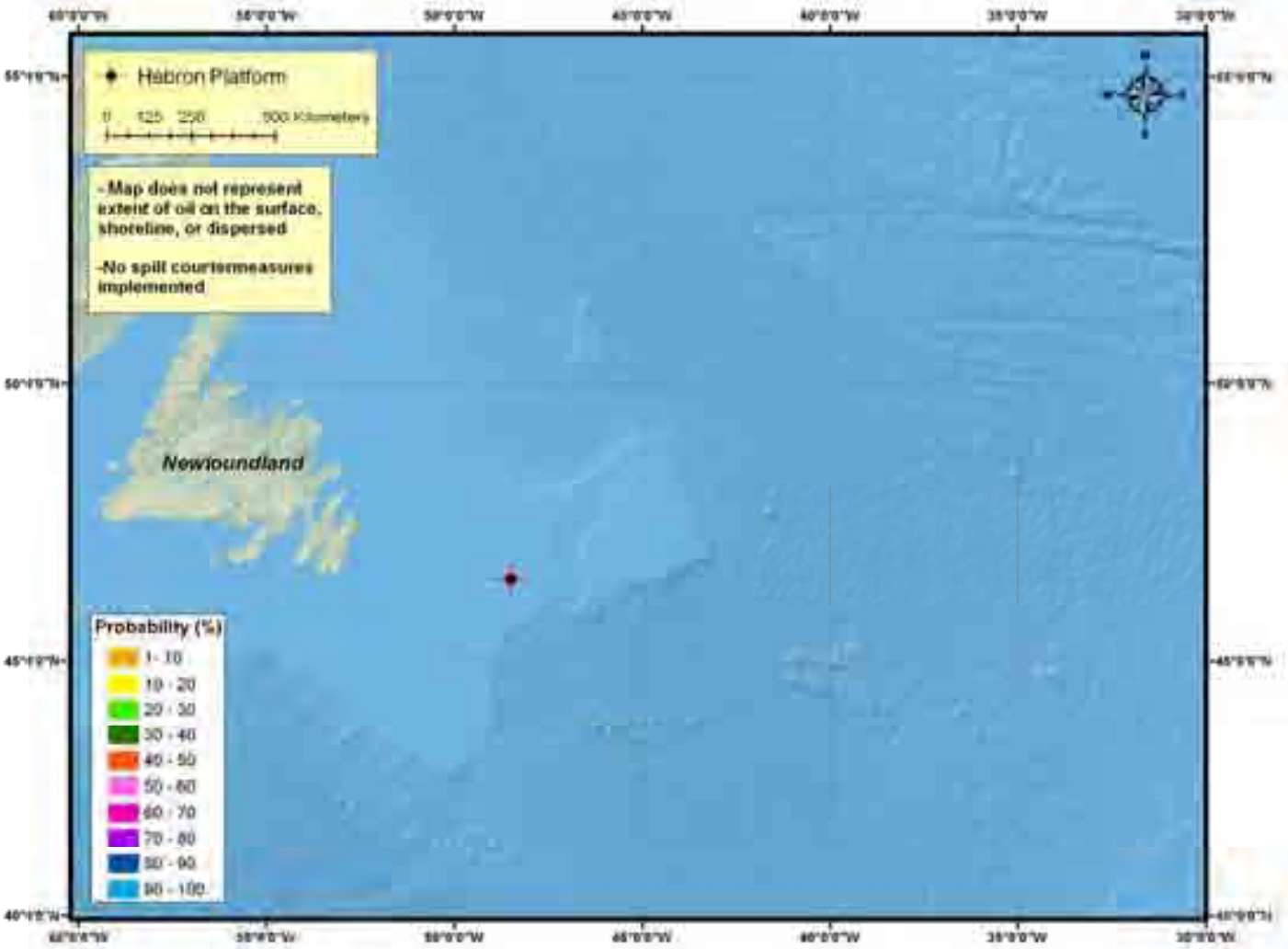


Figure 26. Shoreline oiling probabilities from a platform blow-out of 5,600 m^3/day of Hebron D-94 over a 100-day period during the summer.

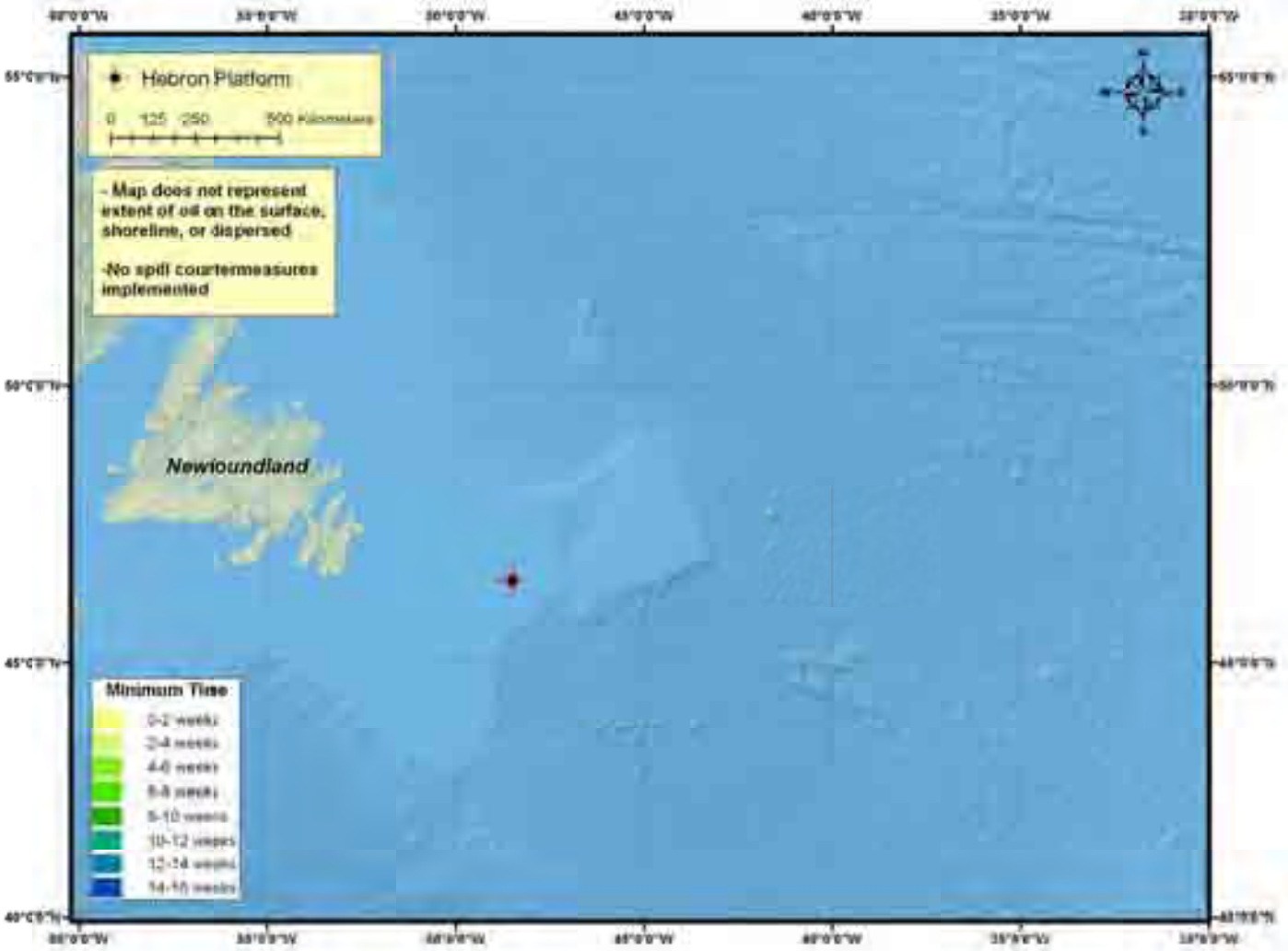


Figure 27. Minimum time to shoreline oiling from a platform blow-out of 5,600 m^3/day of Hebron D-94 over a 100-day period during the summer.

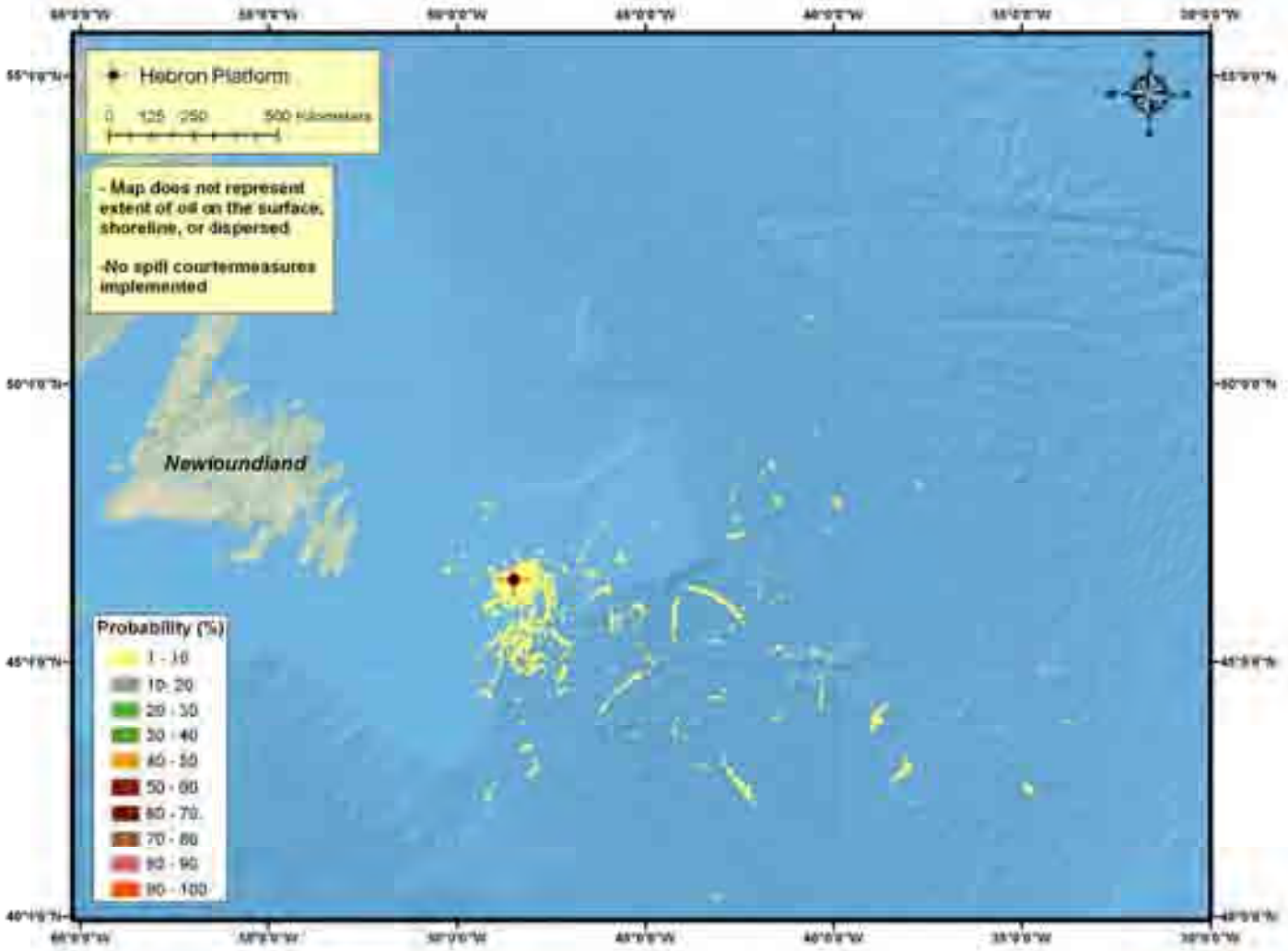


Figure 28. Entrained oil probabilities from a platform blow-out of 5,600 m^3/day of Hebron D-94 over a 100-day period during the summer.

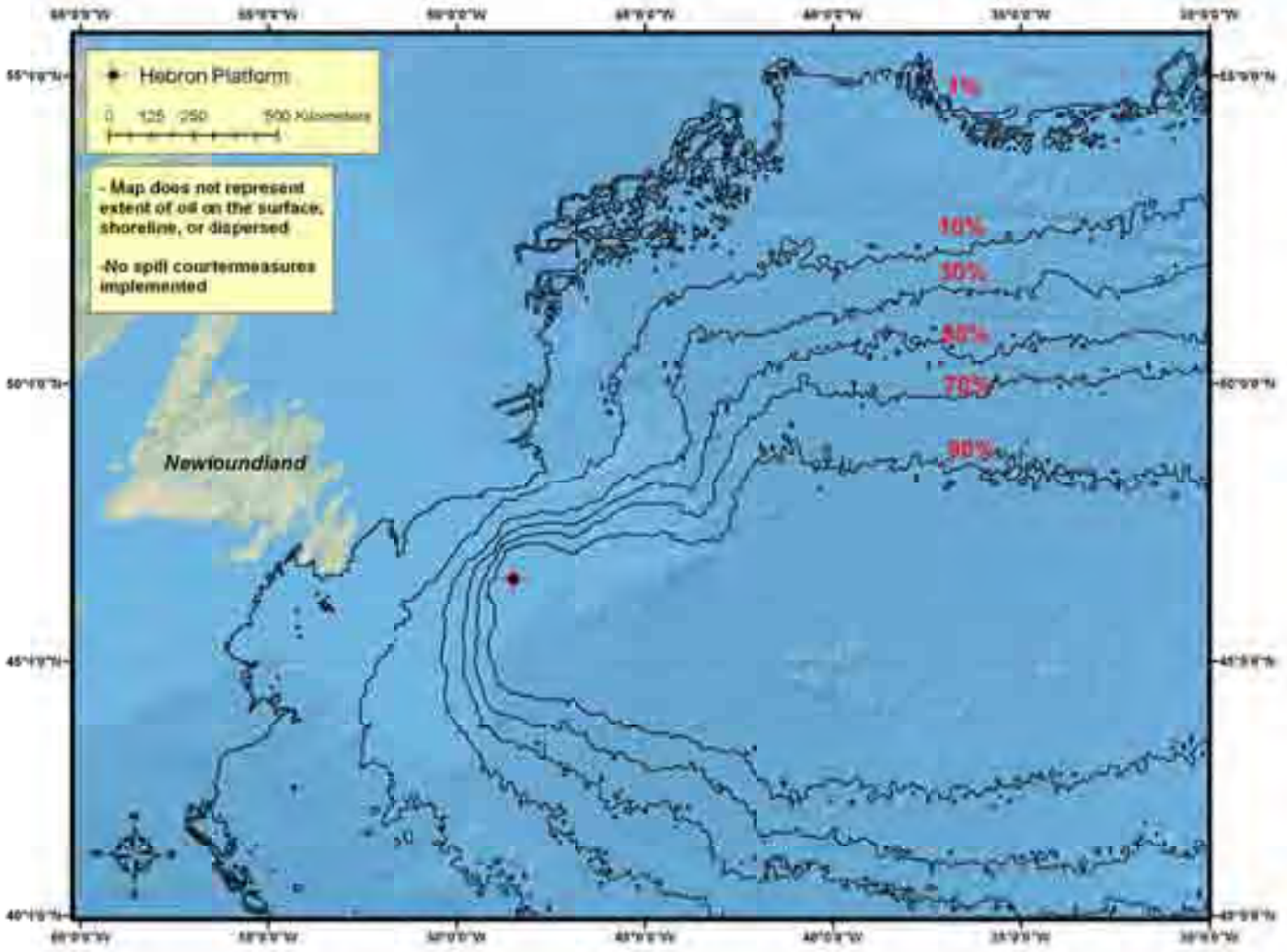


Figure 29. Surface oiling probabilities from a platform blow-out of 5,600 m^3/day of Hebron D-94 over a 120-day period during the winter.

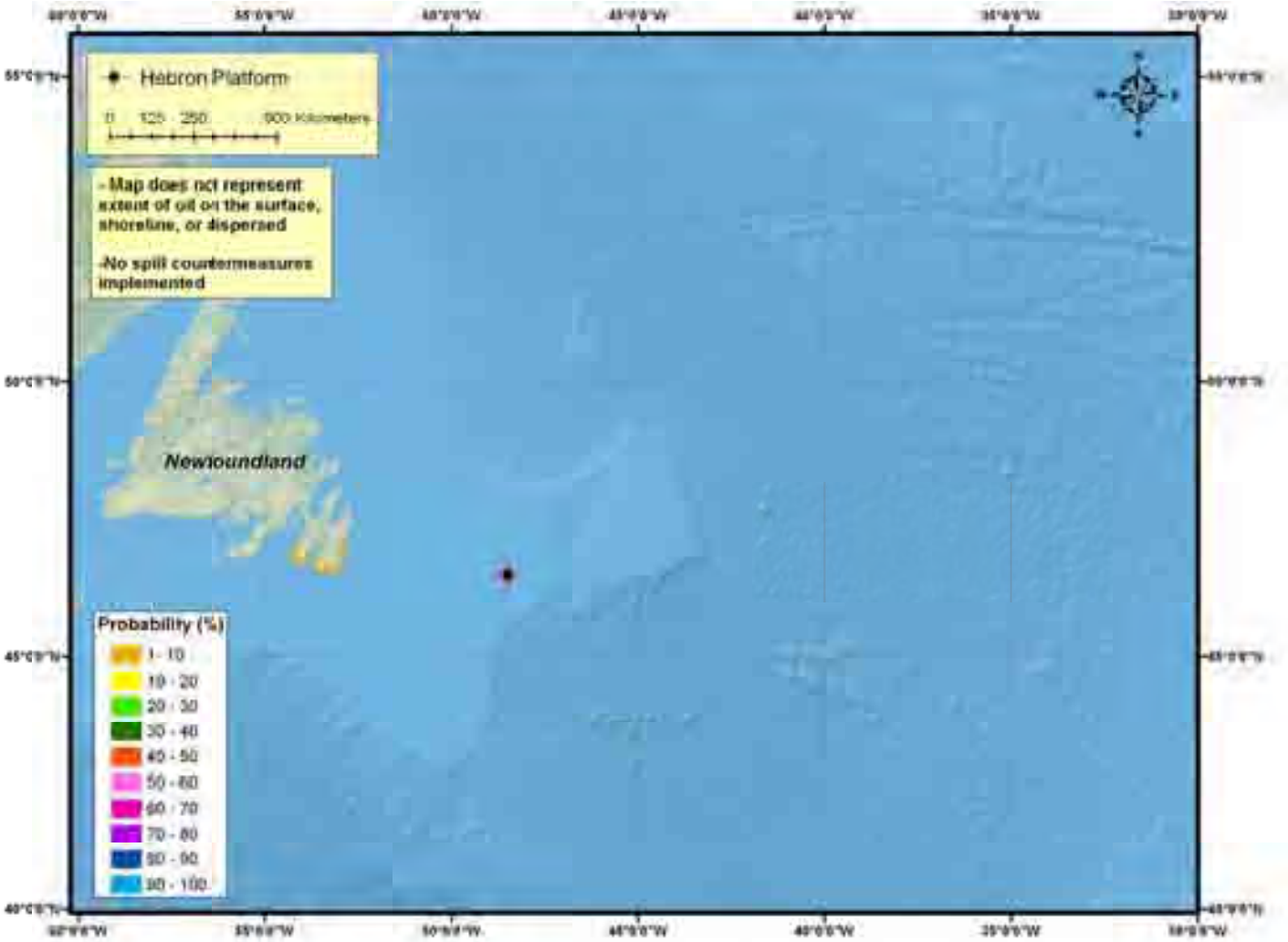


Figure 30. Shoreline oiling probabilities from a platform blow-out of 5,600 m^3/day of Hebron D-94 over a 120-day period during the winter.

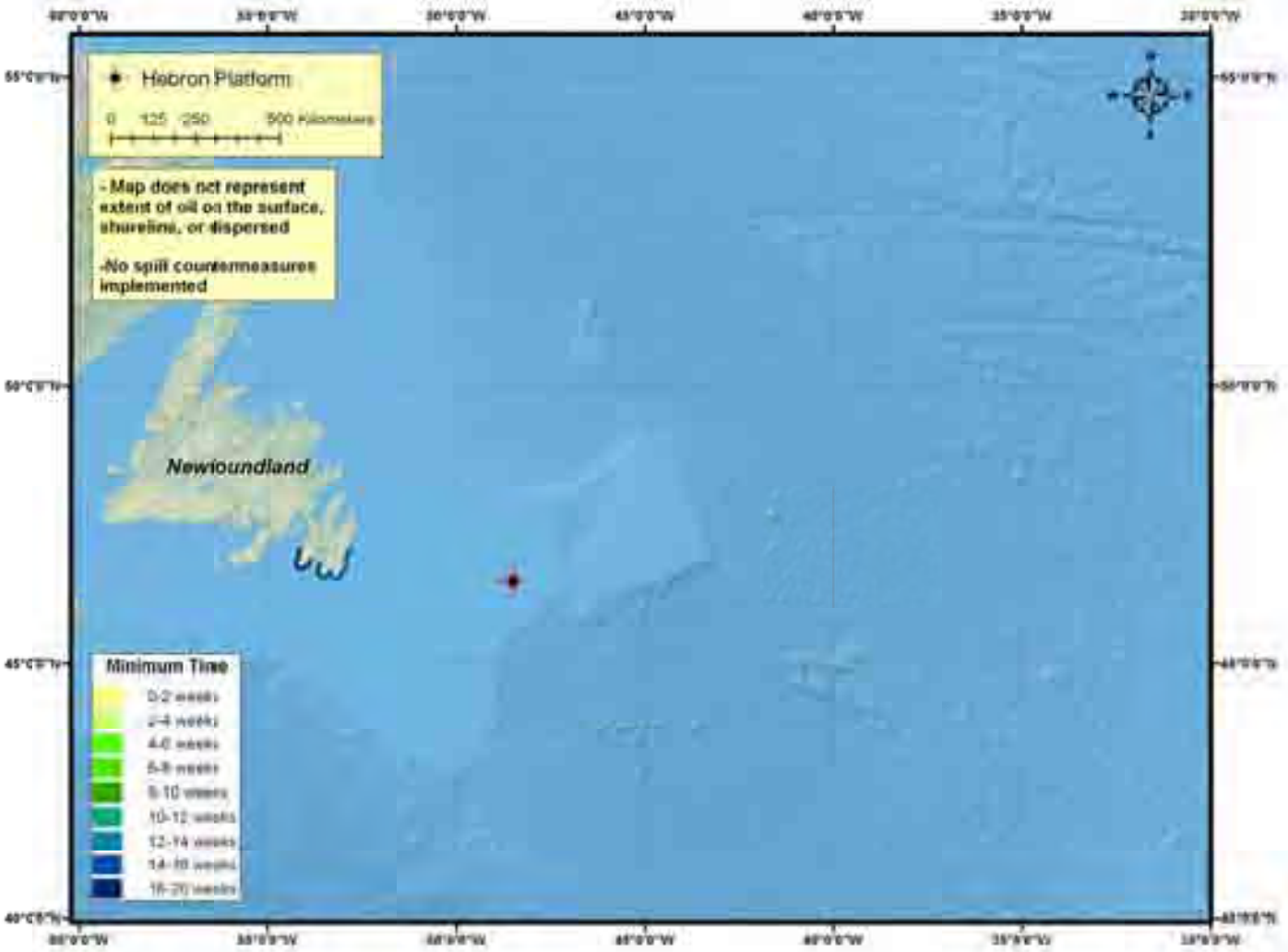


Figure 31. Minimum time to shoreline oiling from a platform blow-out of 5,600 m^3/day of Hebron D-94 over a 120-day period during the winter.

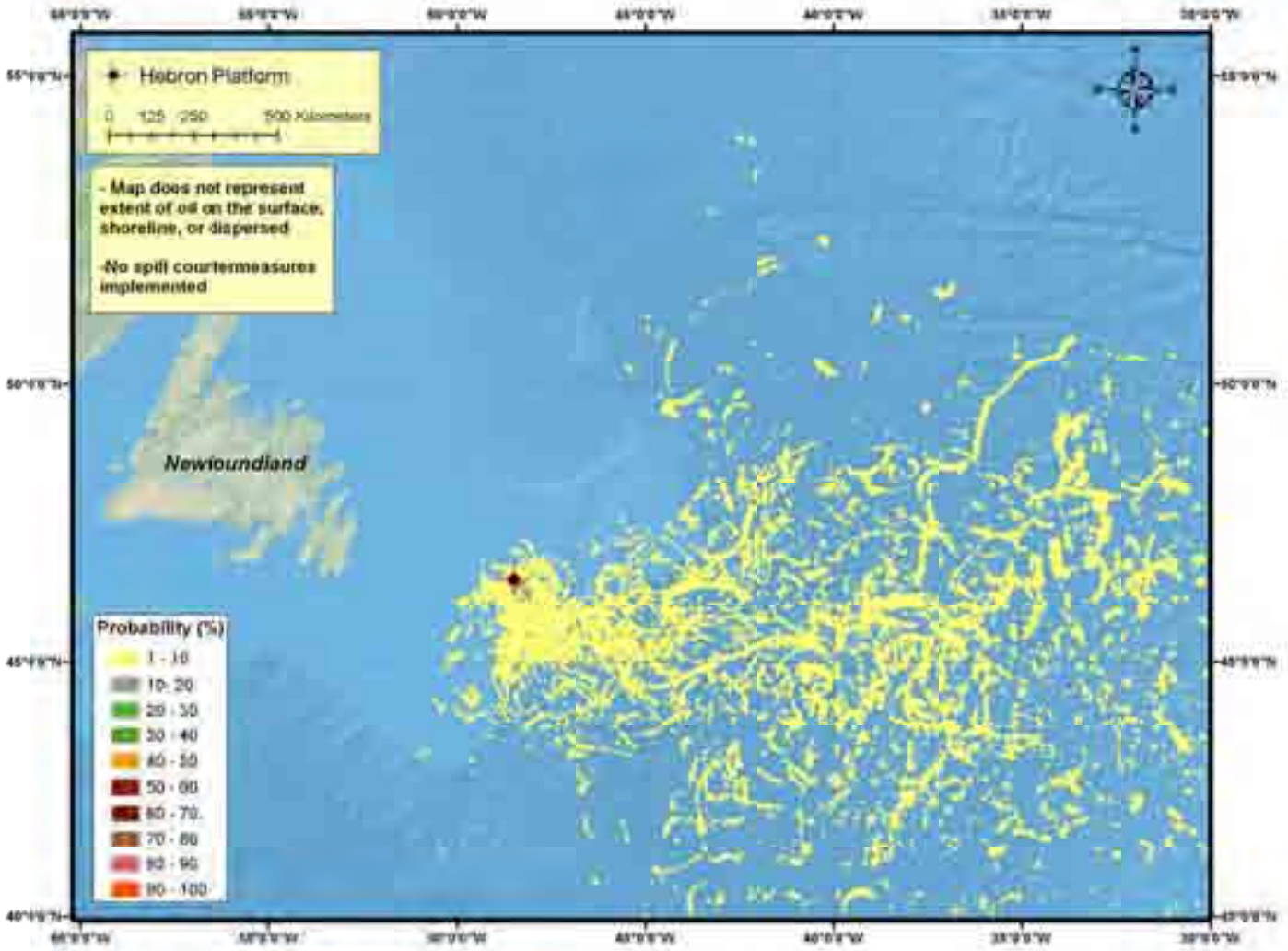


Figure 32. Entrained oil probabilities from a platform blow-out of 5,600 m^3/day of Hebron D-94 over a 120-day period during the winter.

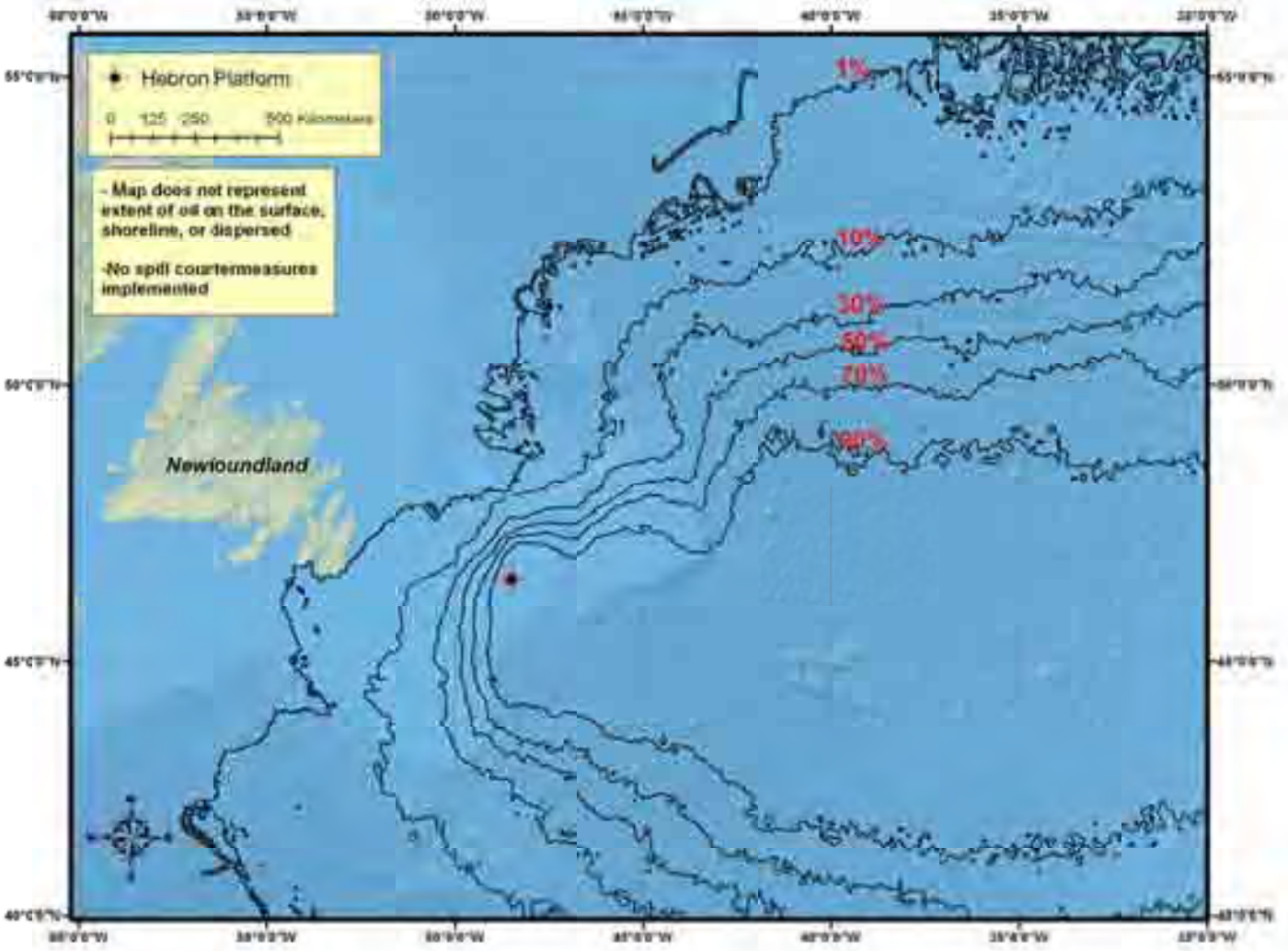


Figure 33. Surface oiling probabilities from a platform blow-out of 5,600 m^3/day of Hebron D-94 over a 120-day period during the winter with sea ice present.

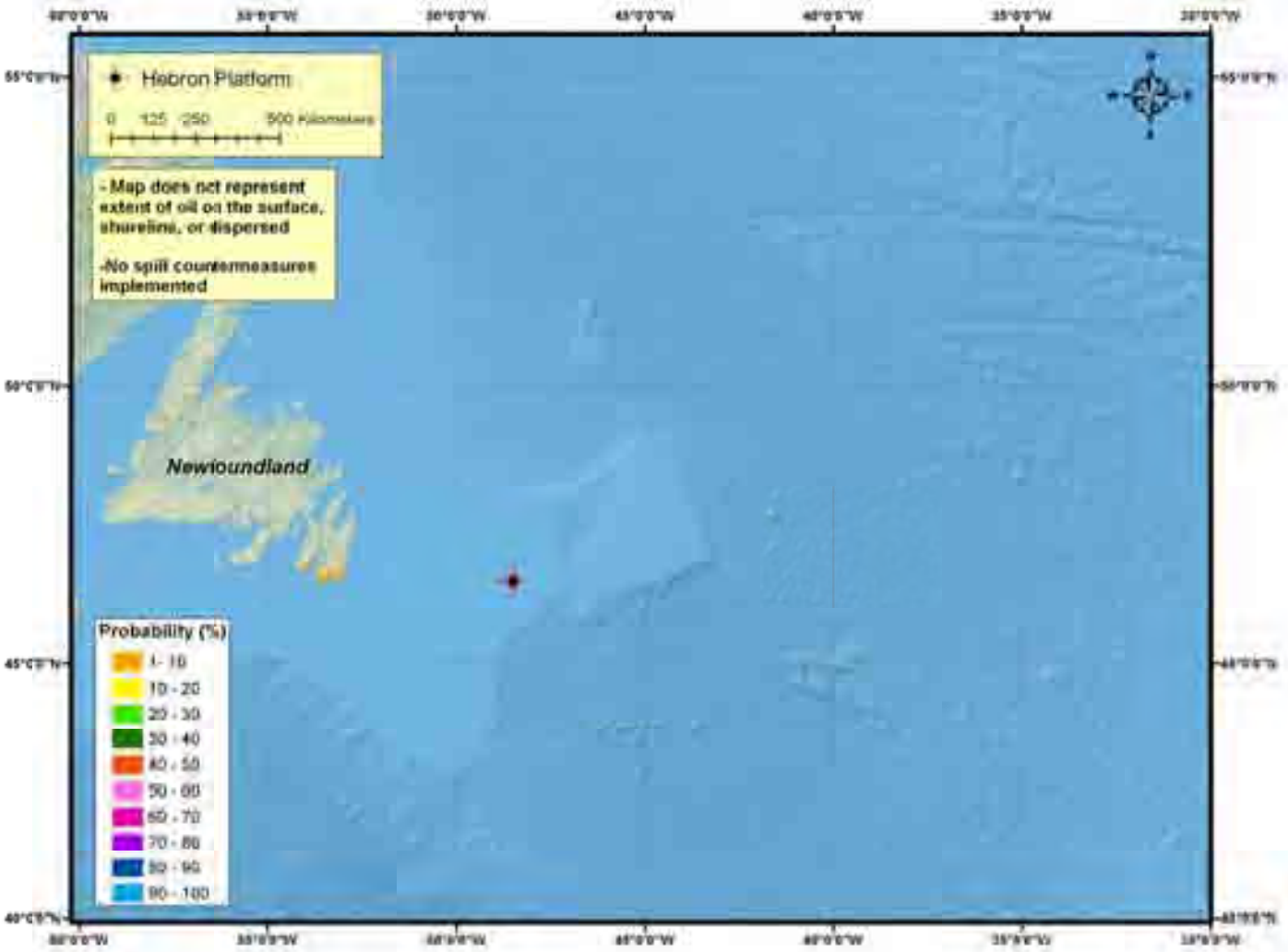


Figure 34. Shoreline oiling probabilities from a surface blow-out of 5,600 m^3/day of Hebron D-94 over a 120-day period during the winter with ice present.

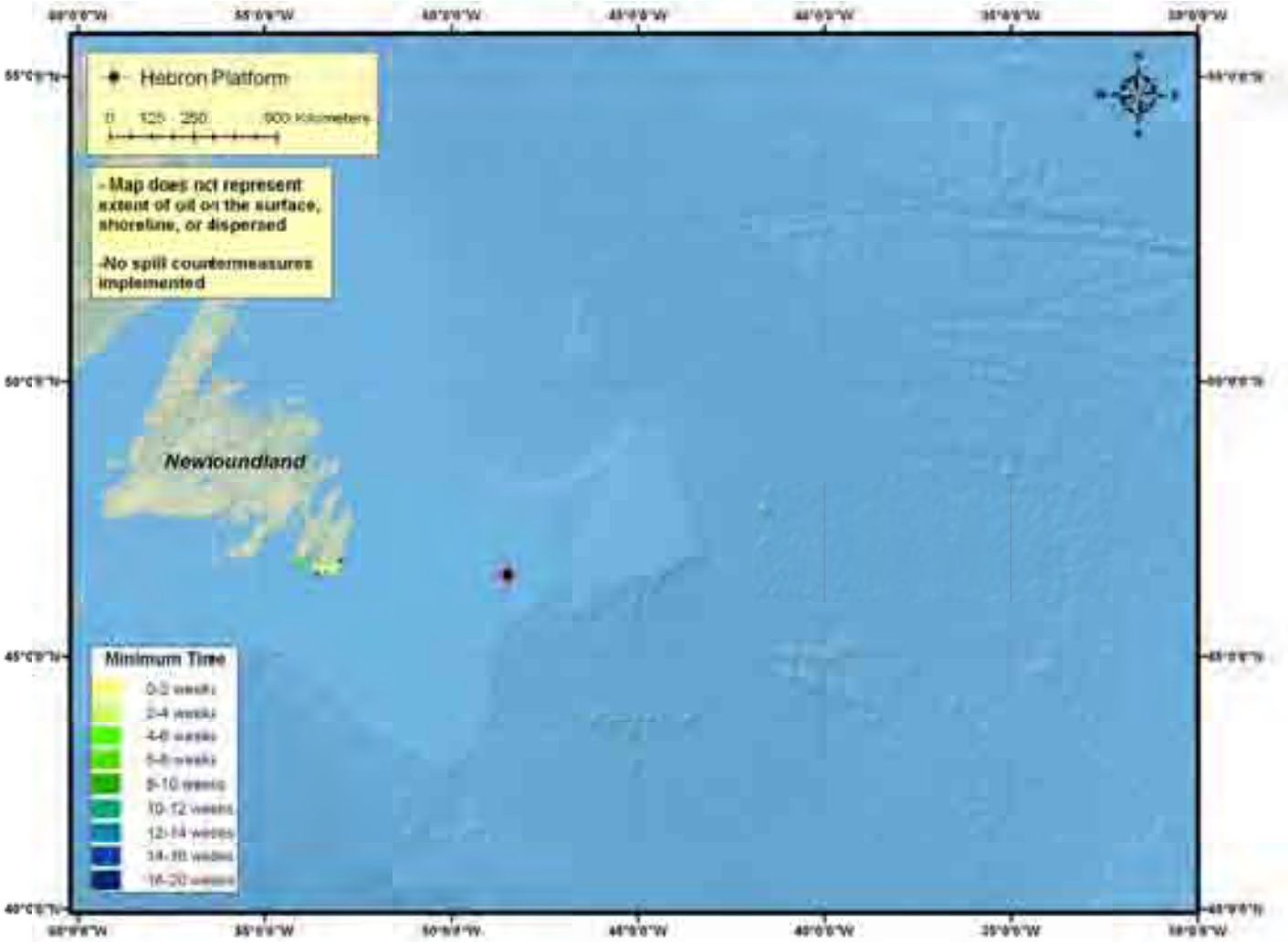


Figure 35. Minimum time to shoreline oiling from a platform blow-out of 5,600 m^3/day of Hebron D-94 over a 120-day period during the winter with sea ice present.

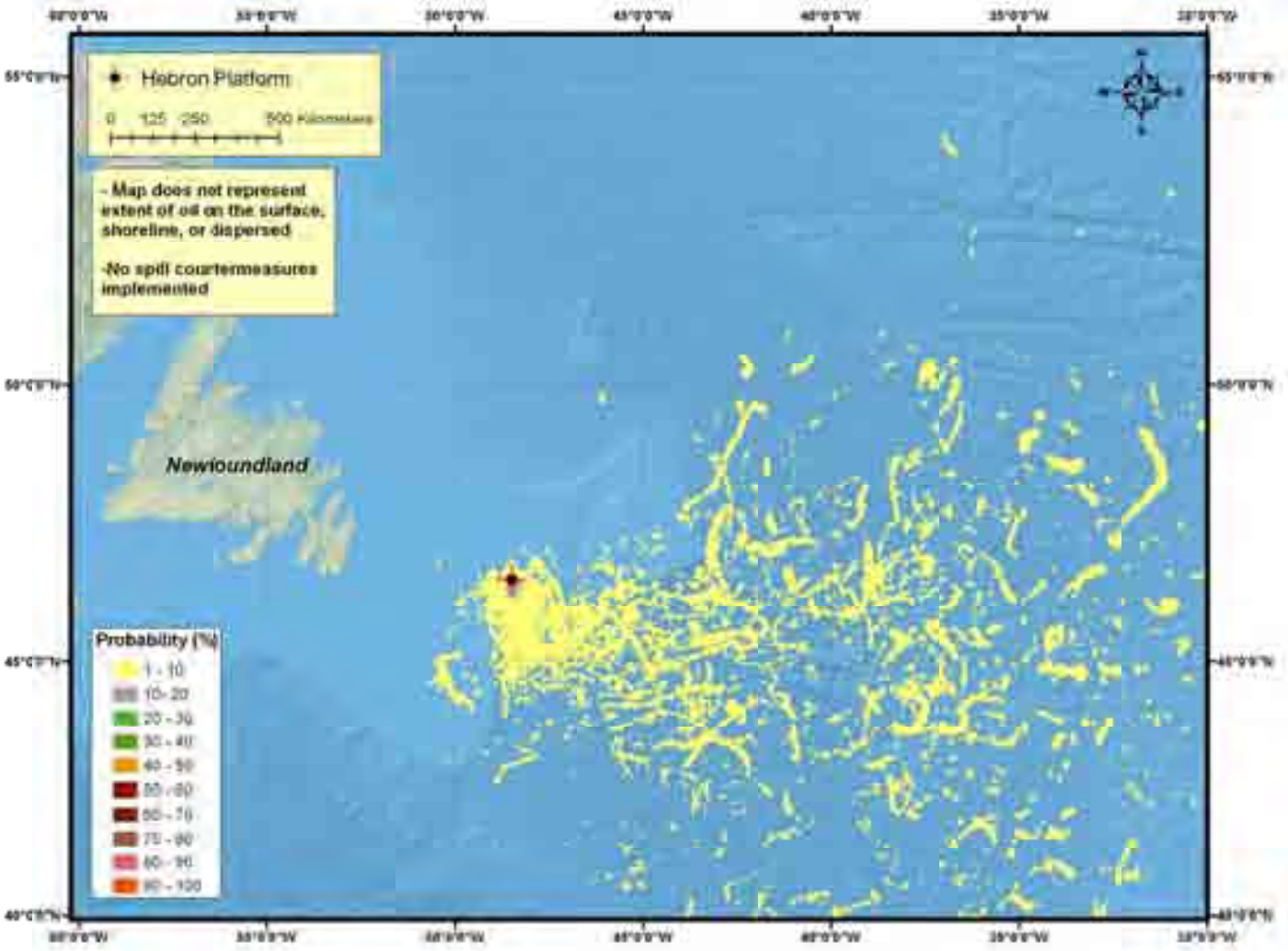


Figure 36. Entrained oil probabilities from a platform blow-out of 5,600 m^3/day of Hebron D-94 over a 120-day period during the winter with sea ice present.

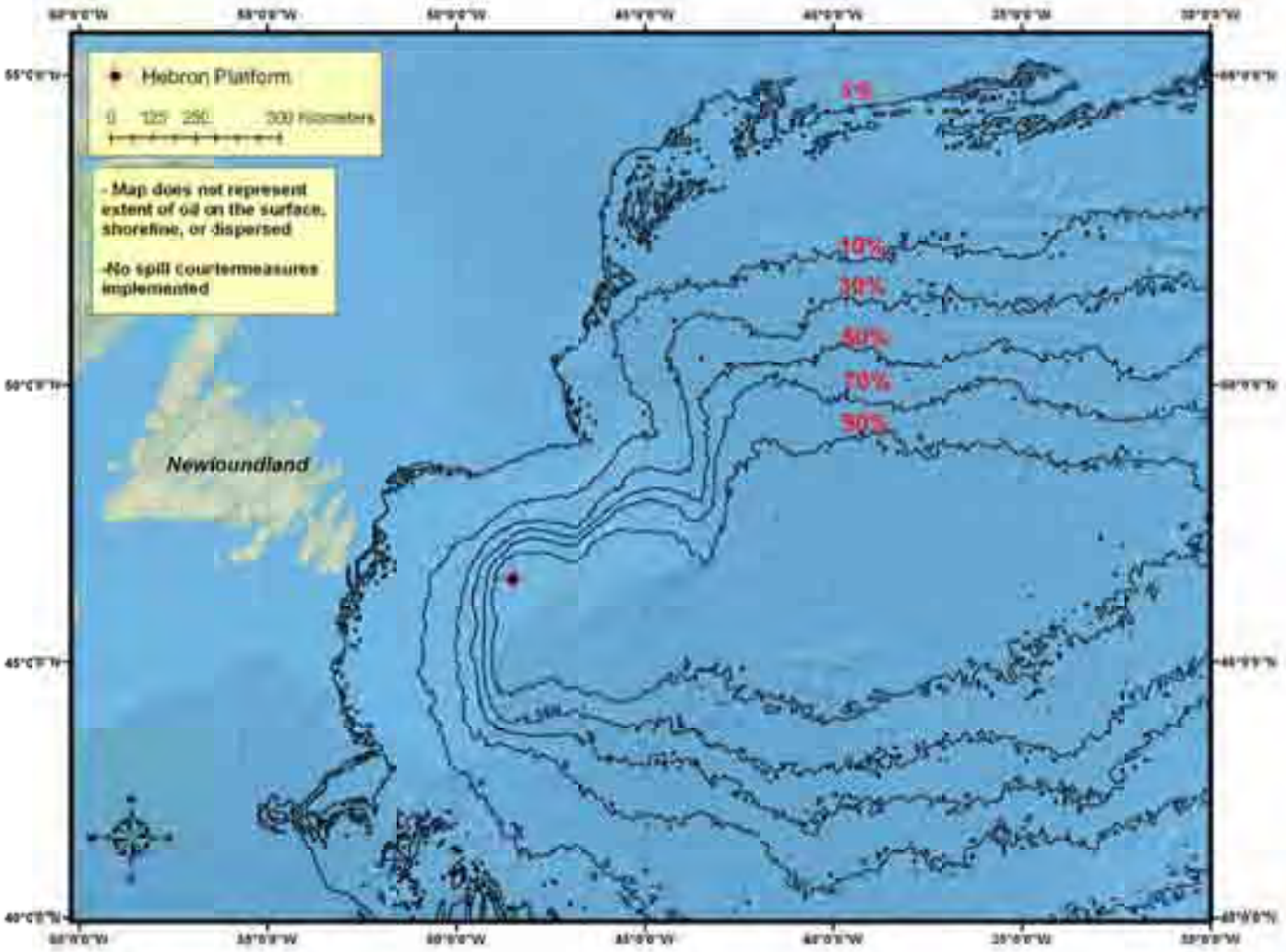


Figure 37. Surface oiling probabilities for a subsea blow-out of 3,200 m^3/day of Ben Nevis Well L55 oil over a 100-day period during the summer.

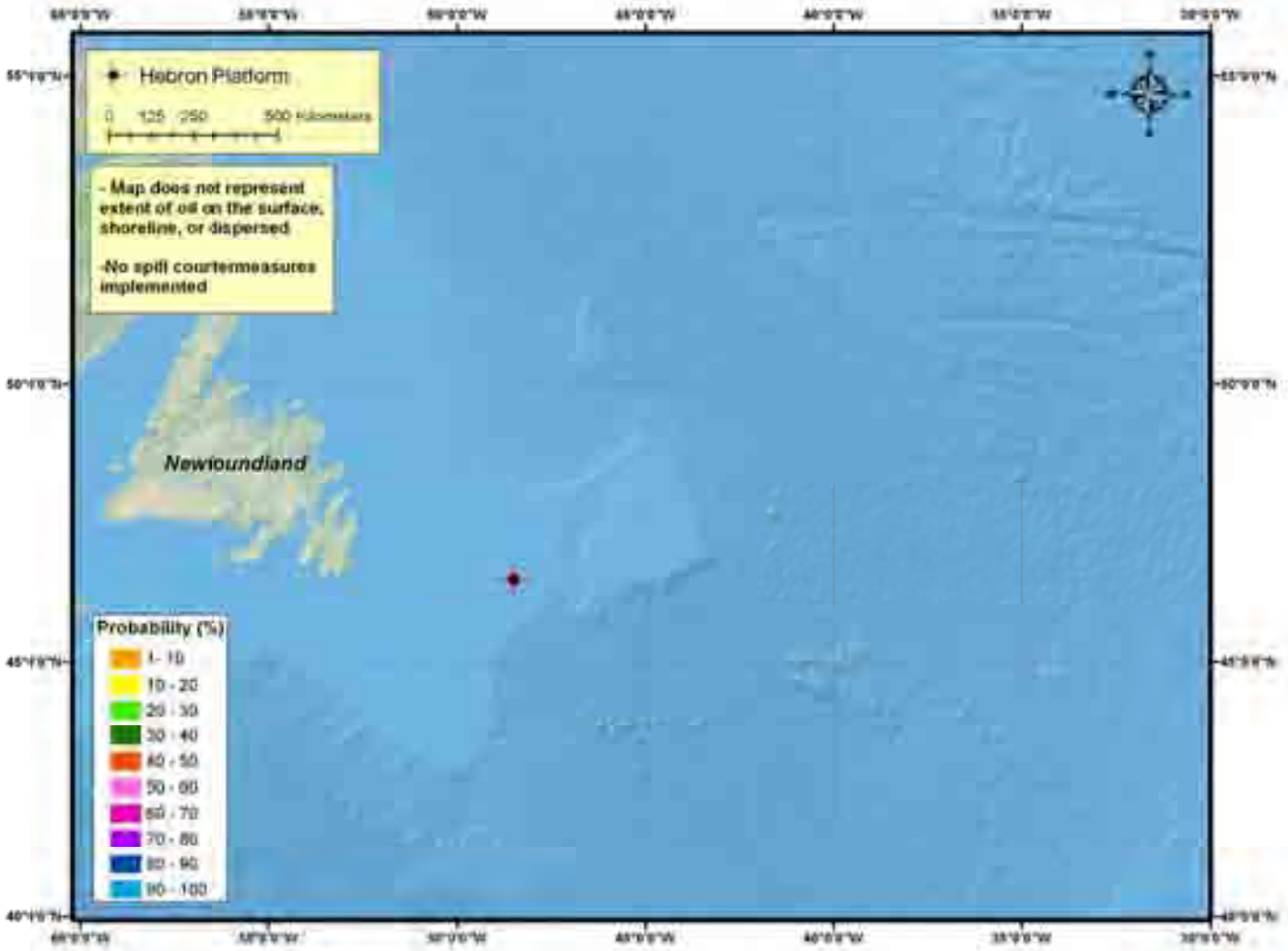


Figure 38. Shoreline oiling probabilities for a subsea blow-out of 3,200 m^3/day of Ben Nevis Well L55 oil over a 100-day period during the summer.

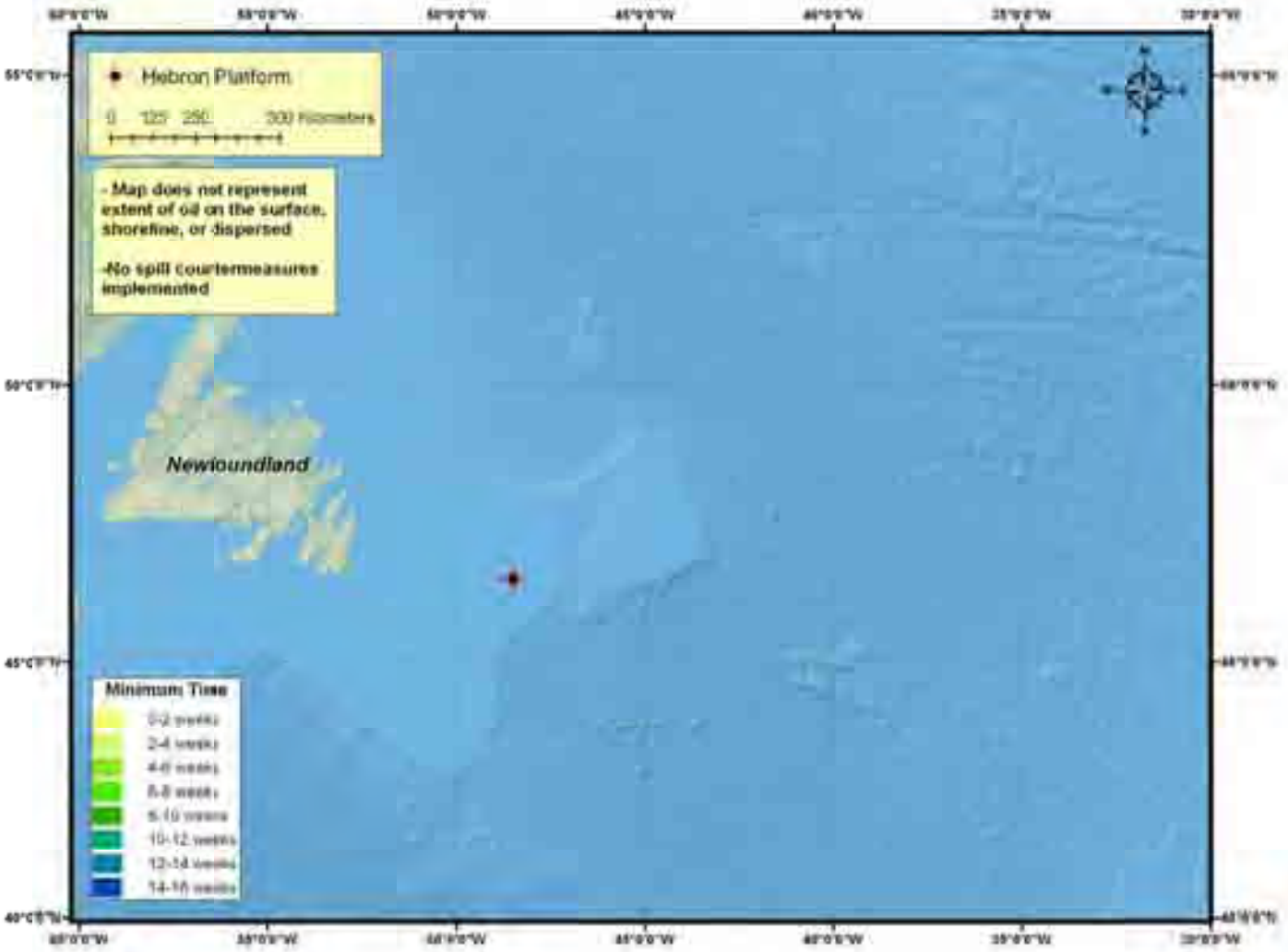


Figure 39. Minimum time to shoreline oiling from a subsea blow-out of 3,200 m^3/day of Ben Nevis Well L55 oil over a 100-day period during the summer.

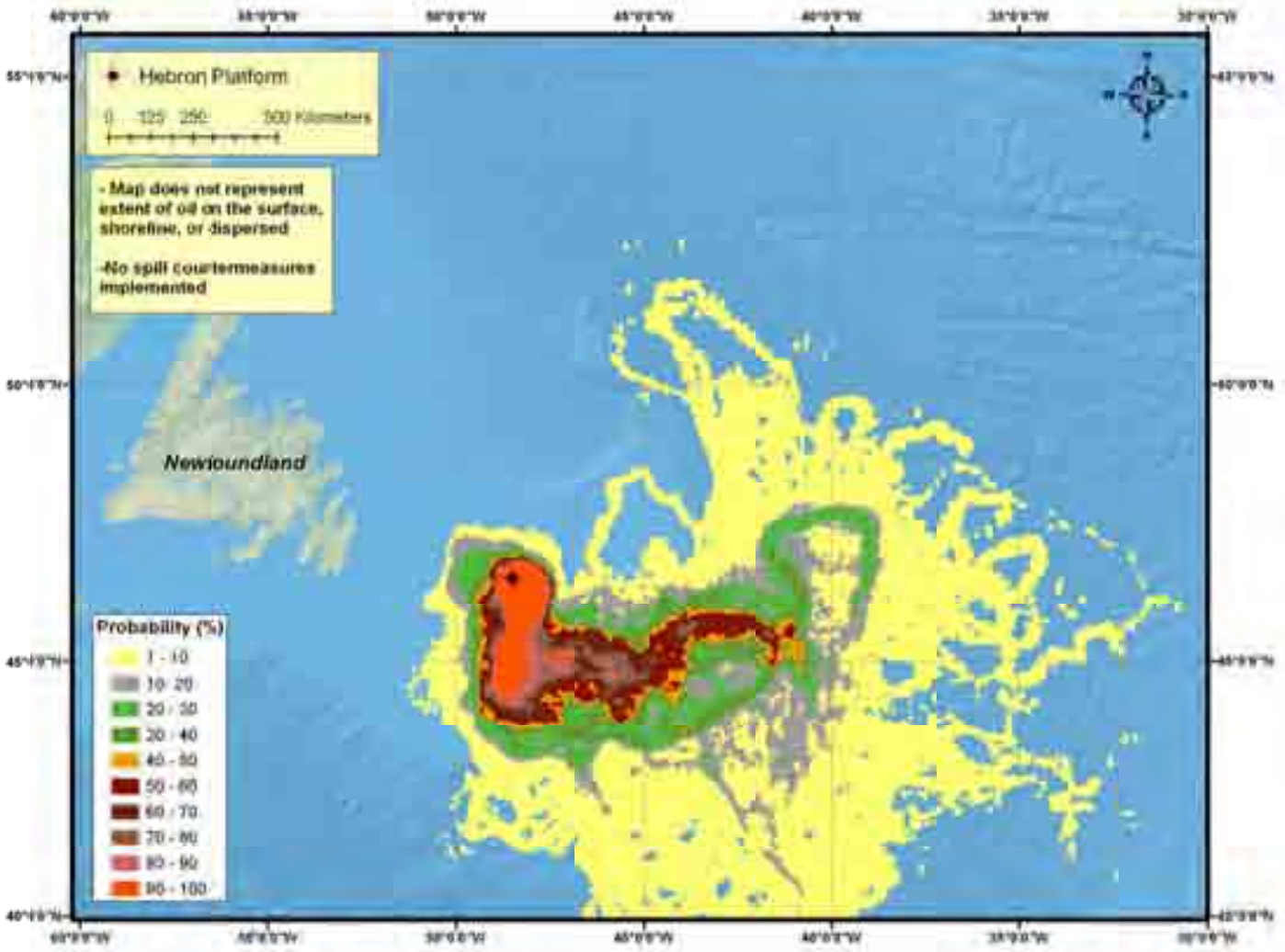


Figure 40. Entrained oil probabilities for a subsea blow-out of 3,200 m^3/day of Ben Nevis Well L55 oil over a 100-day period during the summer.

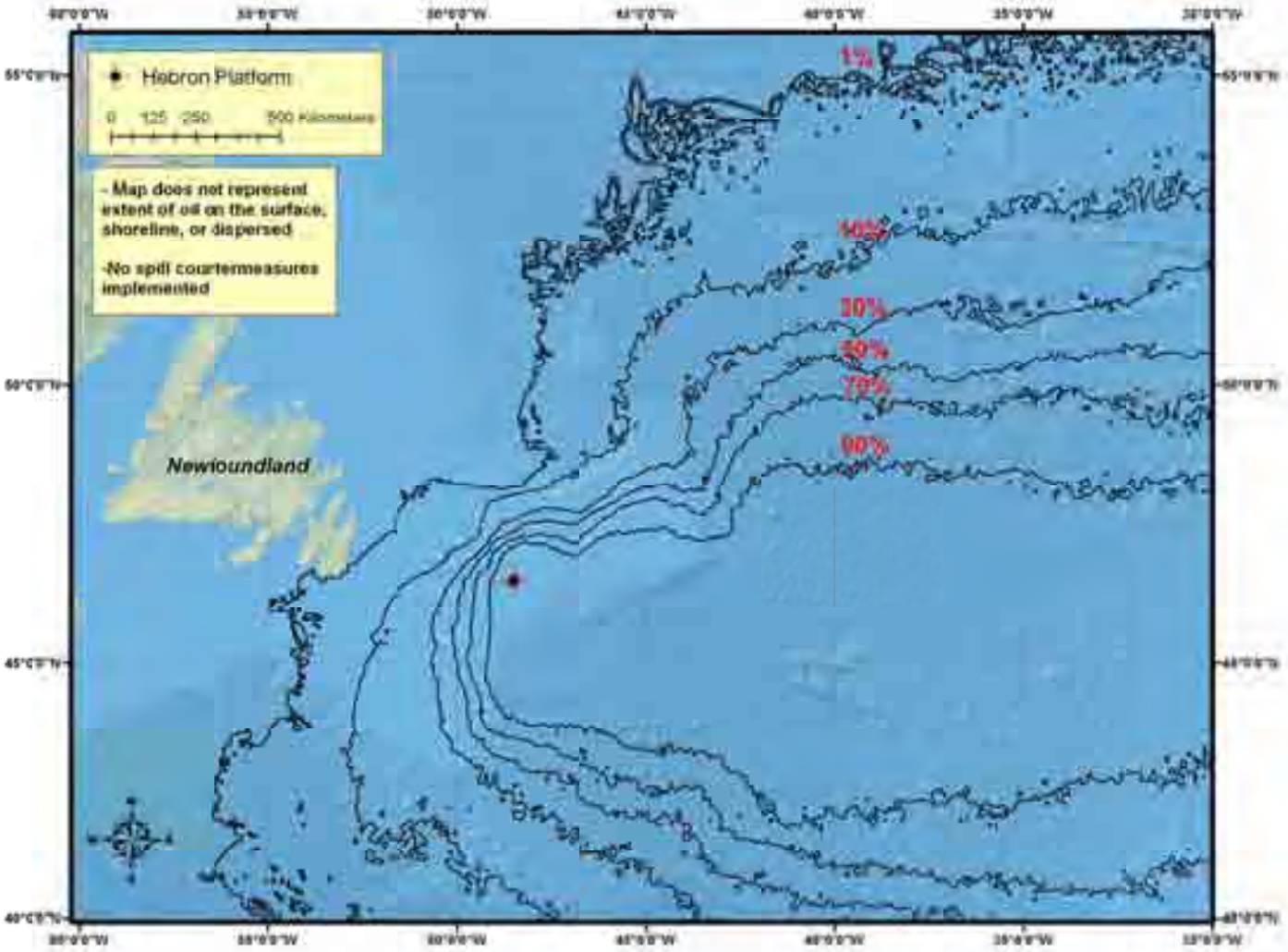


Figure 41. Surface oiling probabilities for a subsea blow-out of 3,200 m^3/day of Ben Nevis Well L55 oil over a 120-day period during the winter.

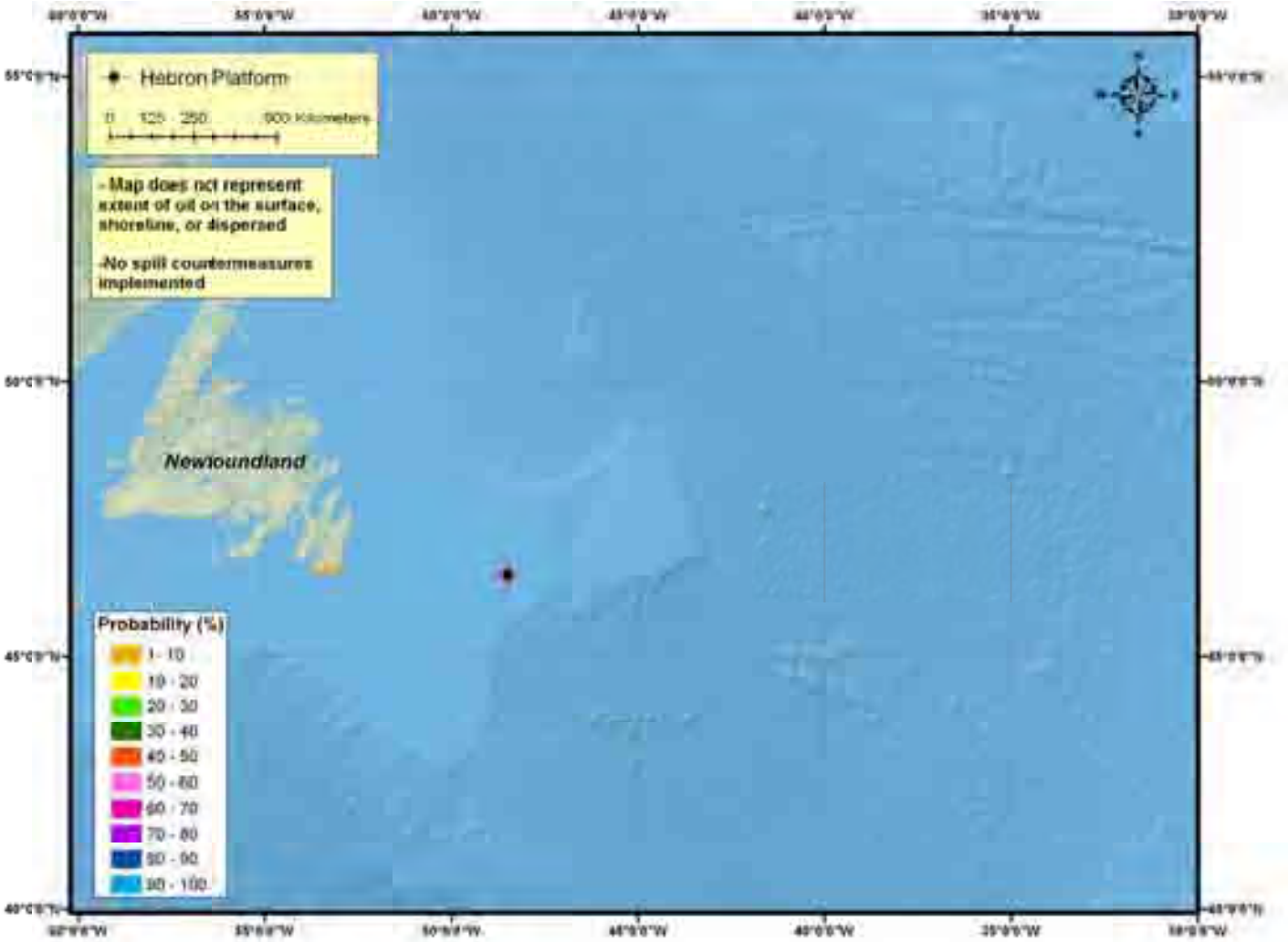


Figure 42. Shoreline oiling probabilities for a subsea blow-out of 3,200 m^3/day of Ben Nevis Well L55 oil over a 120-day period during the winter.

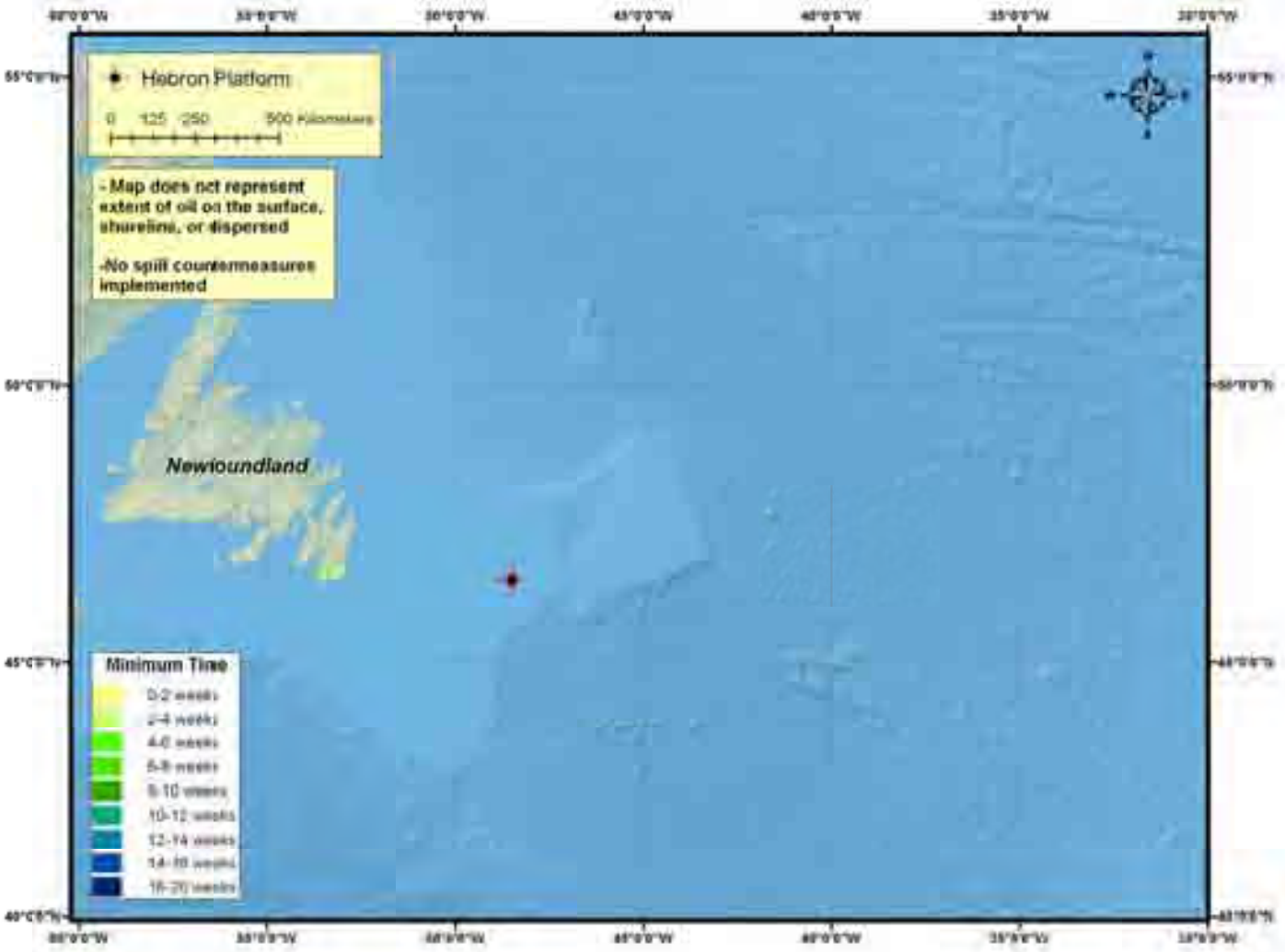


Figure 43. Minimum time to shoreline oiling from a subsea blow-out of 3,200 m^3/day of Ben Nevis Well L55 oil over a 120-day period during the winter.

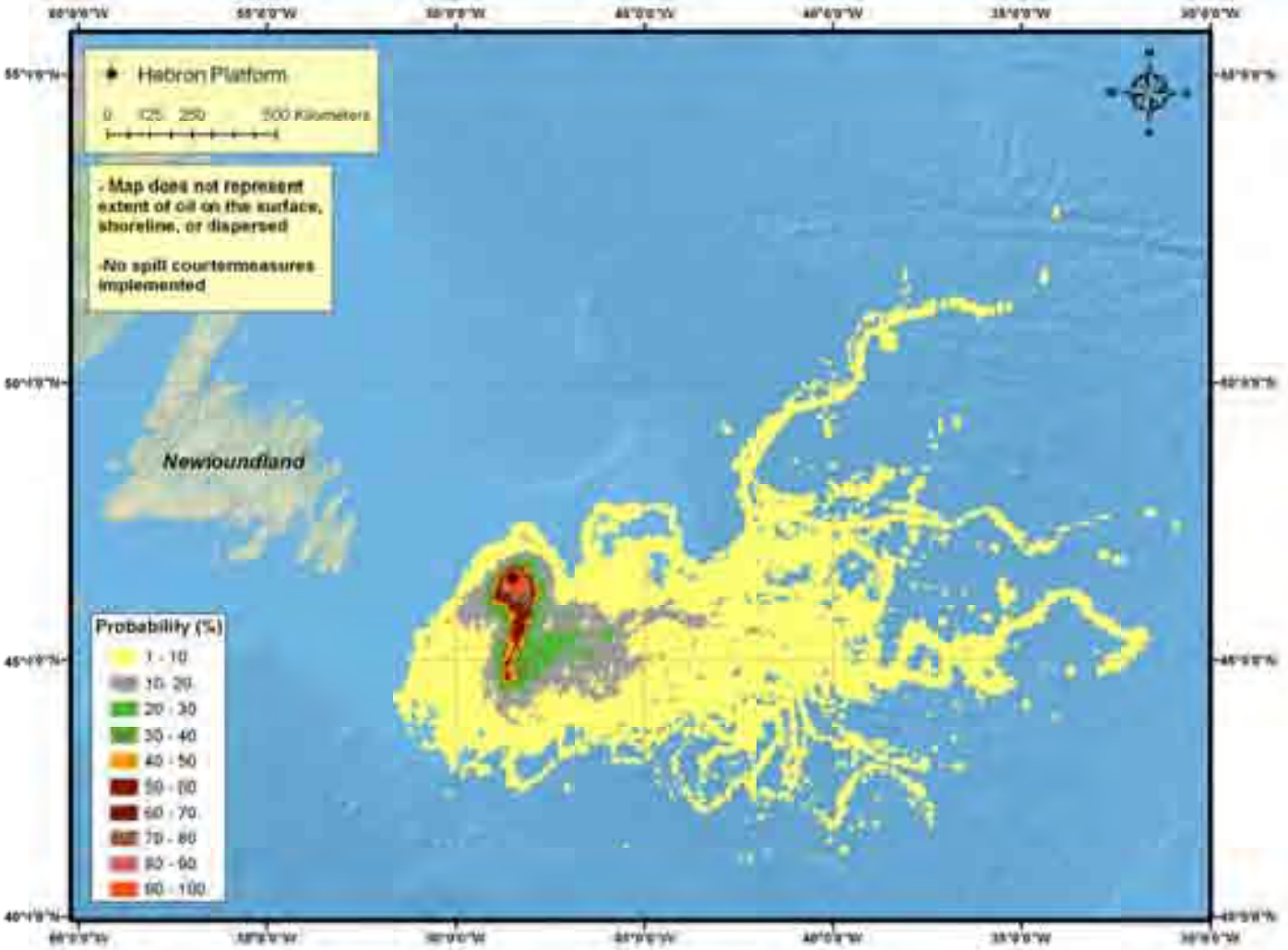


Figure 44. Entrained oil probabilities for a subsea blow-out of 3,200 m^3/day of Ben Nevis Well L55 oil over a 120-day period during the winter.

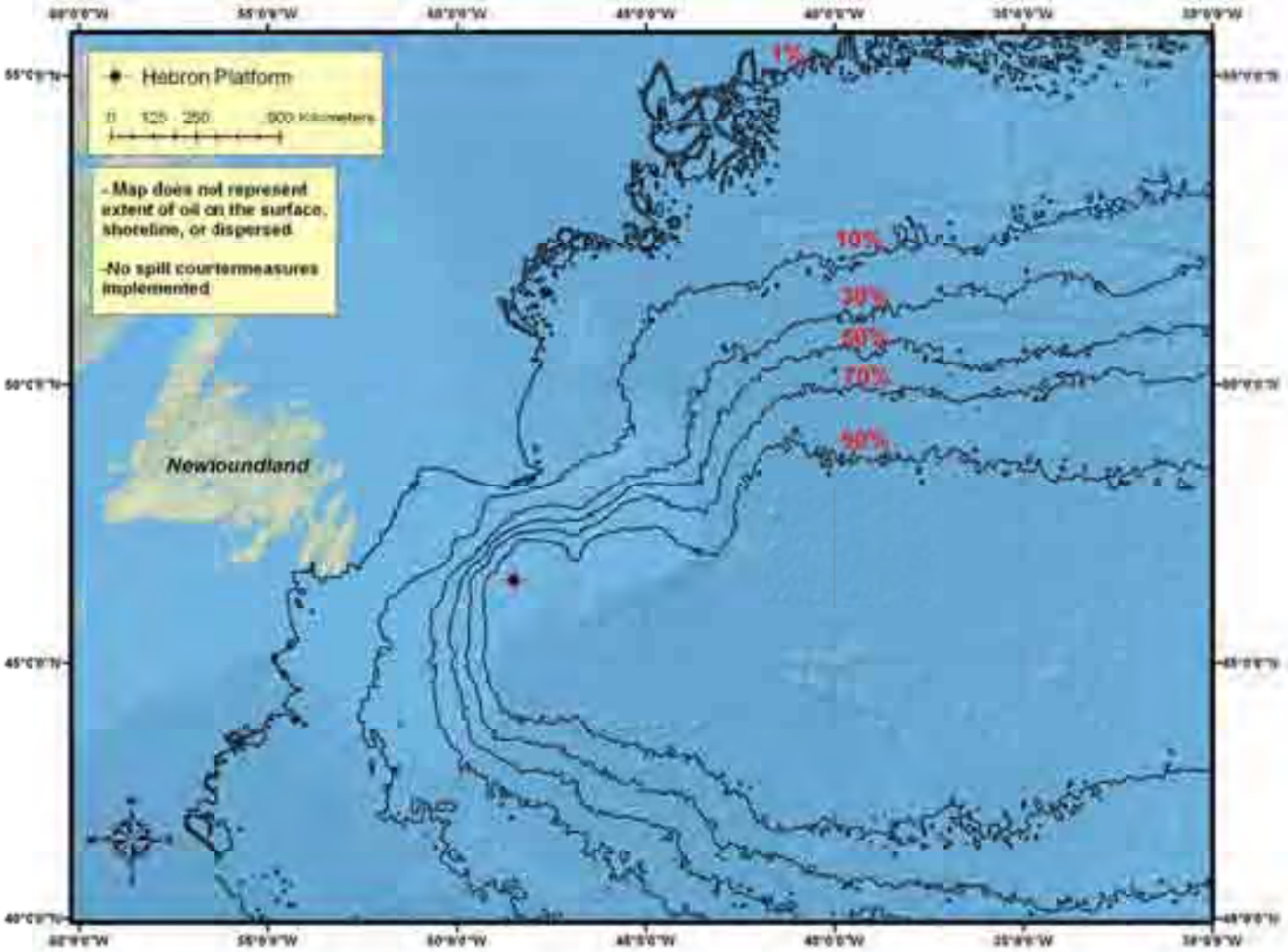


Figure 45. Surface oiling probabilities for a subsea blow-out of 3,200 m^3/day of Ben Nevis Well L55 oil over a 120-day period during the winter with ice present.

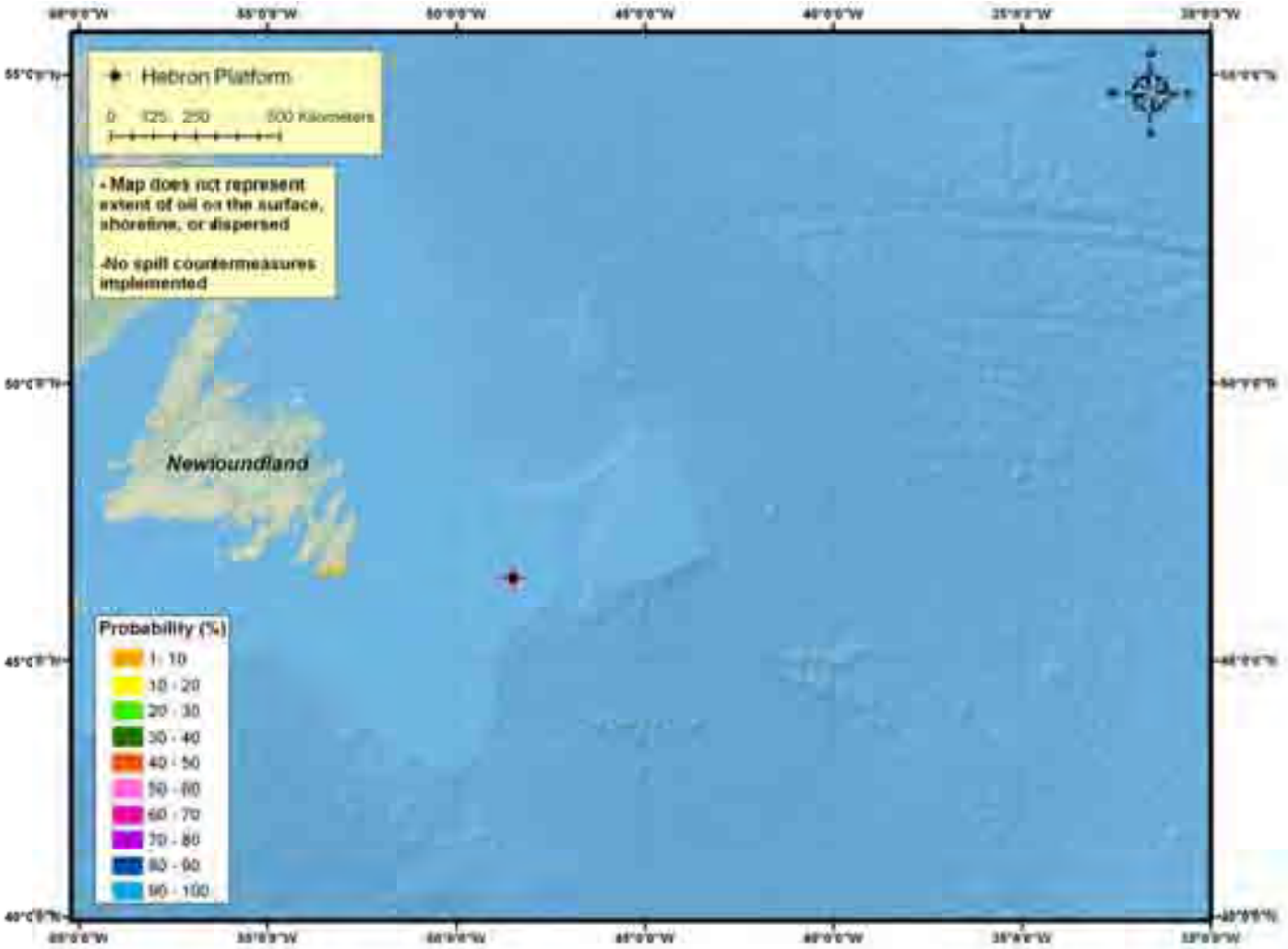


Figure 46. Shoreline oiling probabilities for a subsea blow-out of 3,200 m^3/day of Ben Nevis Well L55 oil over a 120-day period during the winter with ice present.

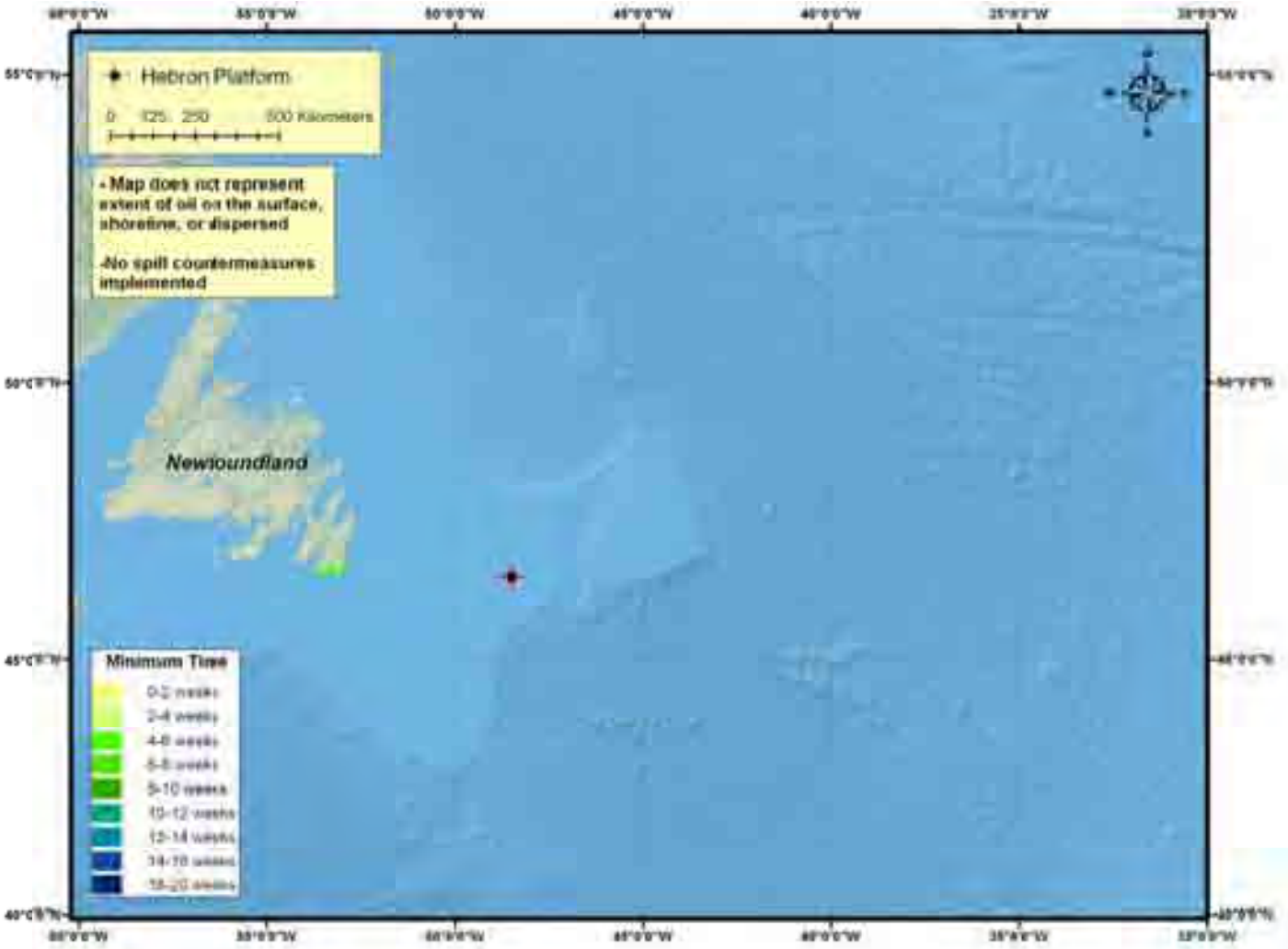


Figure 47. Minimum time to shoreline oiling from a subsea blow-out of 3,200 m^3/day of Ben Nevis Well L55 oil over a 120-day period during the winter with ice present.

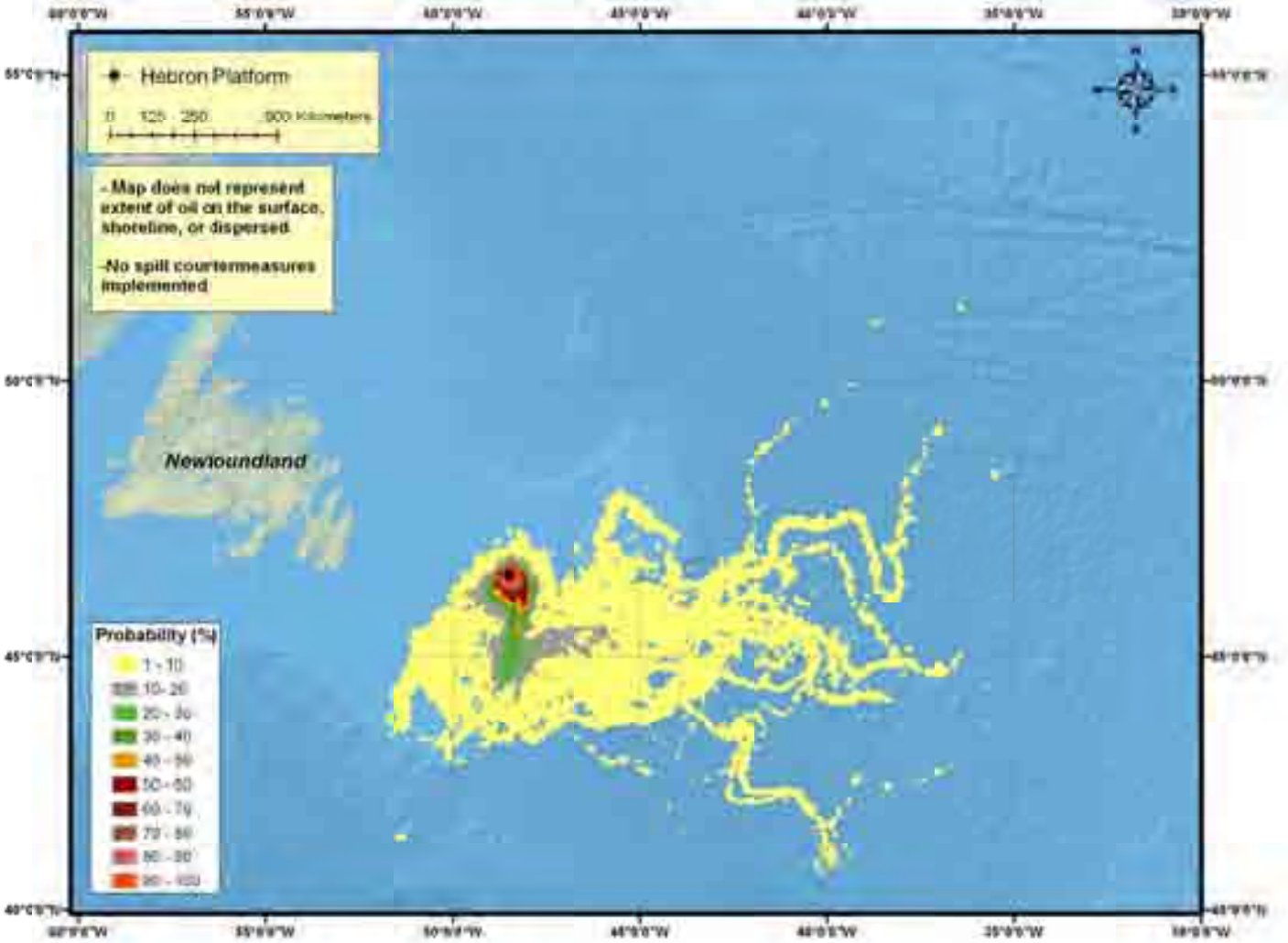


Figure 48. Entrained oil probabilities for a subsea blow-out of 3,200 m^3/day of Ben Nevis Well L55 oil over a 120-day period during the winter with ice present.

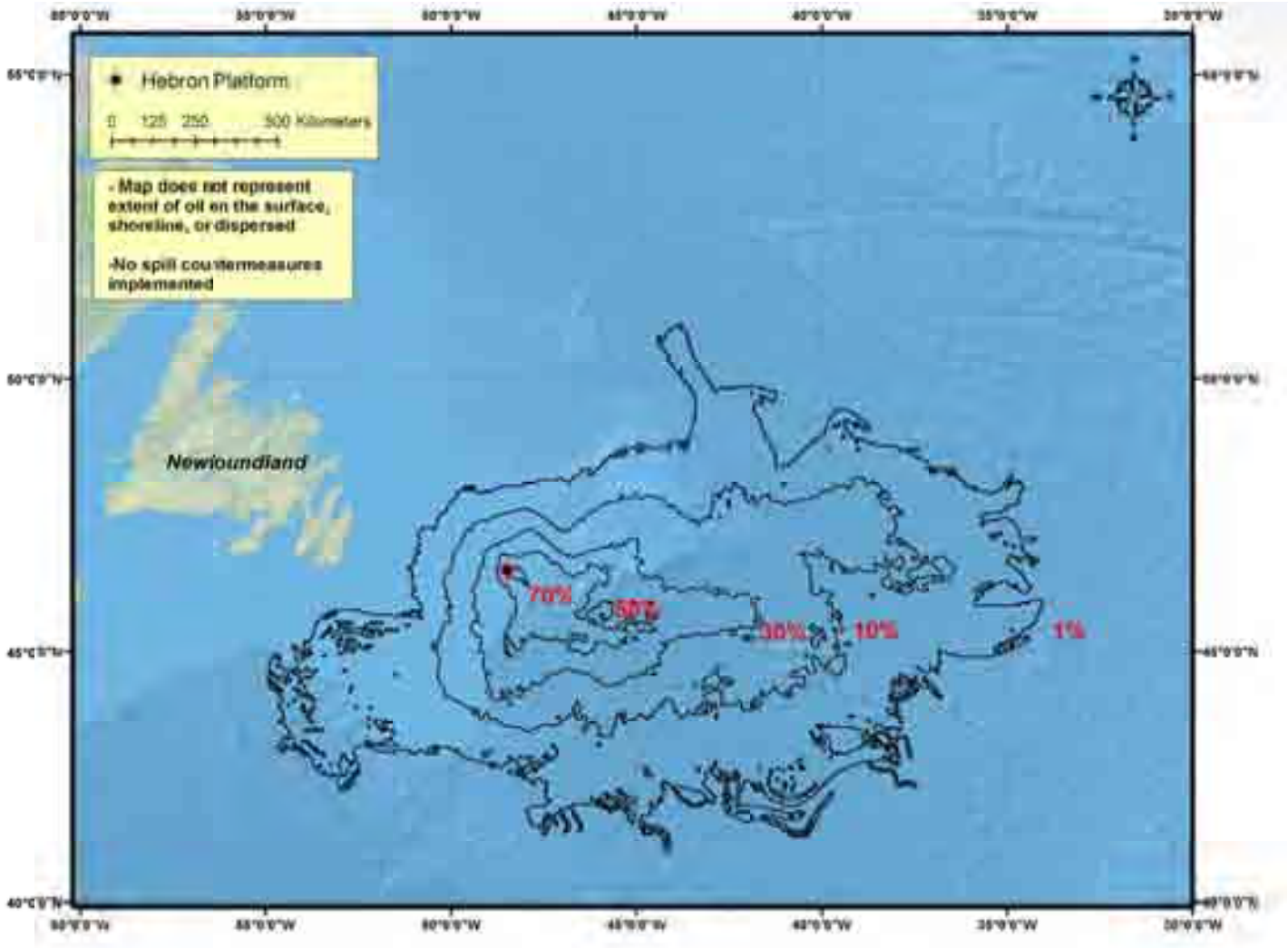


Figure 49. Surface oiling probabilities for a batch transfer release of 800 m^3 of diesel fuel oil during the summer.

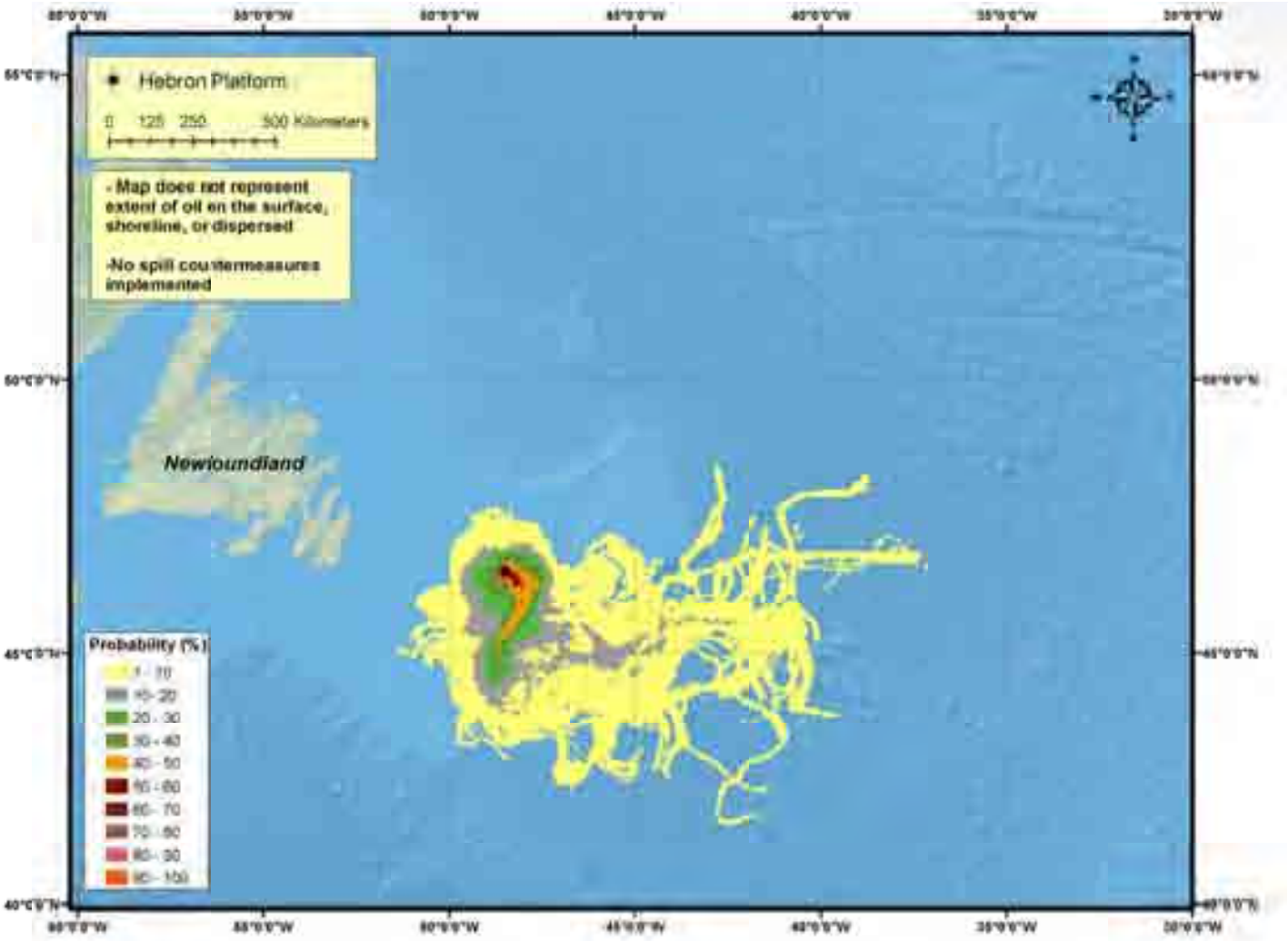


Figure 50. Entrained oil probabilities for a batch transfer release of 800 m^3 of diesel fuel oil during the summer.

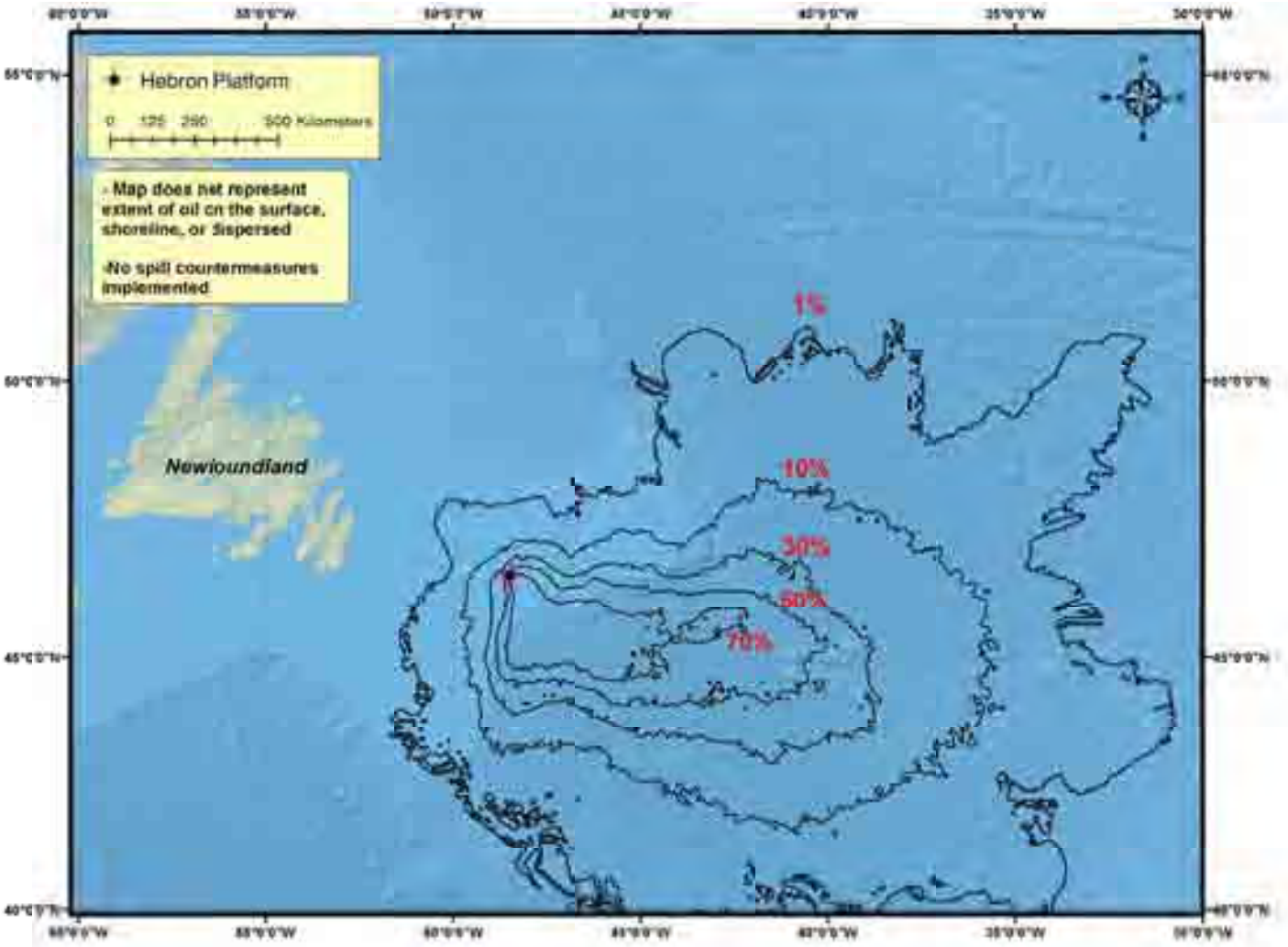


Figure 51. Surface oiling probabilities for a batch transfer release of 800 m^3 of diesel fuel oil during the winter.

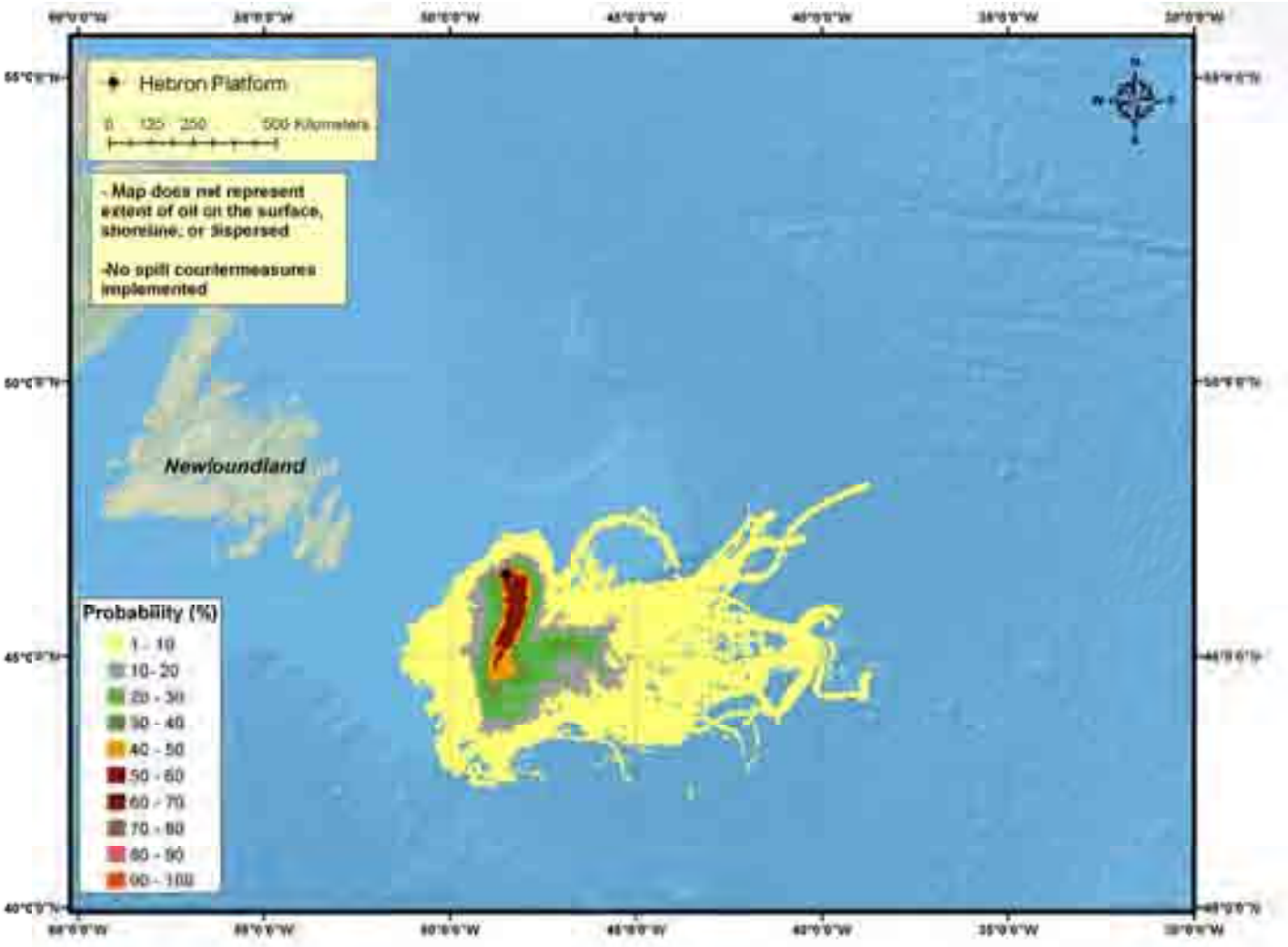


Figure 52. Entrained oil probabilities for a batch transfer release of 800 m^3 of diesel fuel oil during the winter.

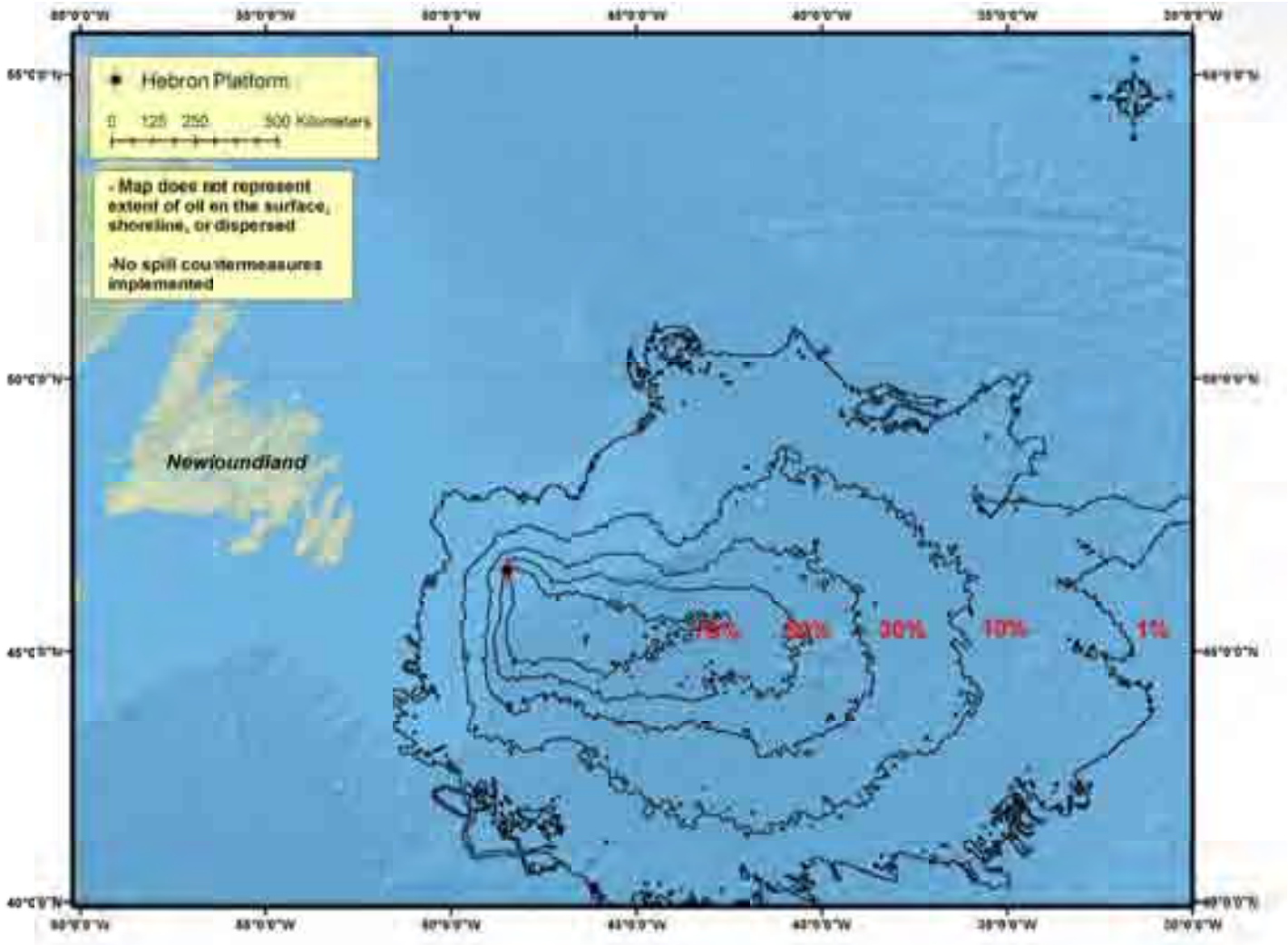


Figure 53. Surface oiling probabilities for a batch transfer release of 800 m^3 of diesel fuel oil during the winter with ice present.

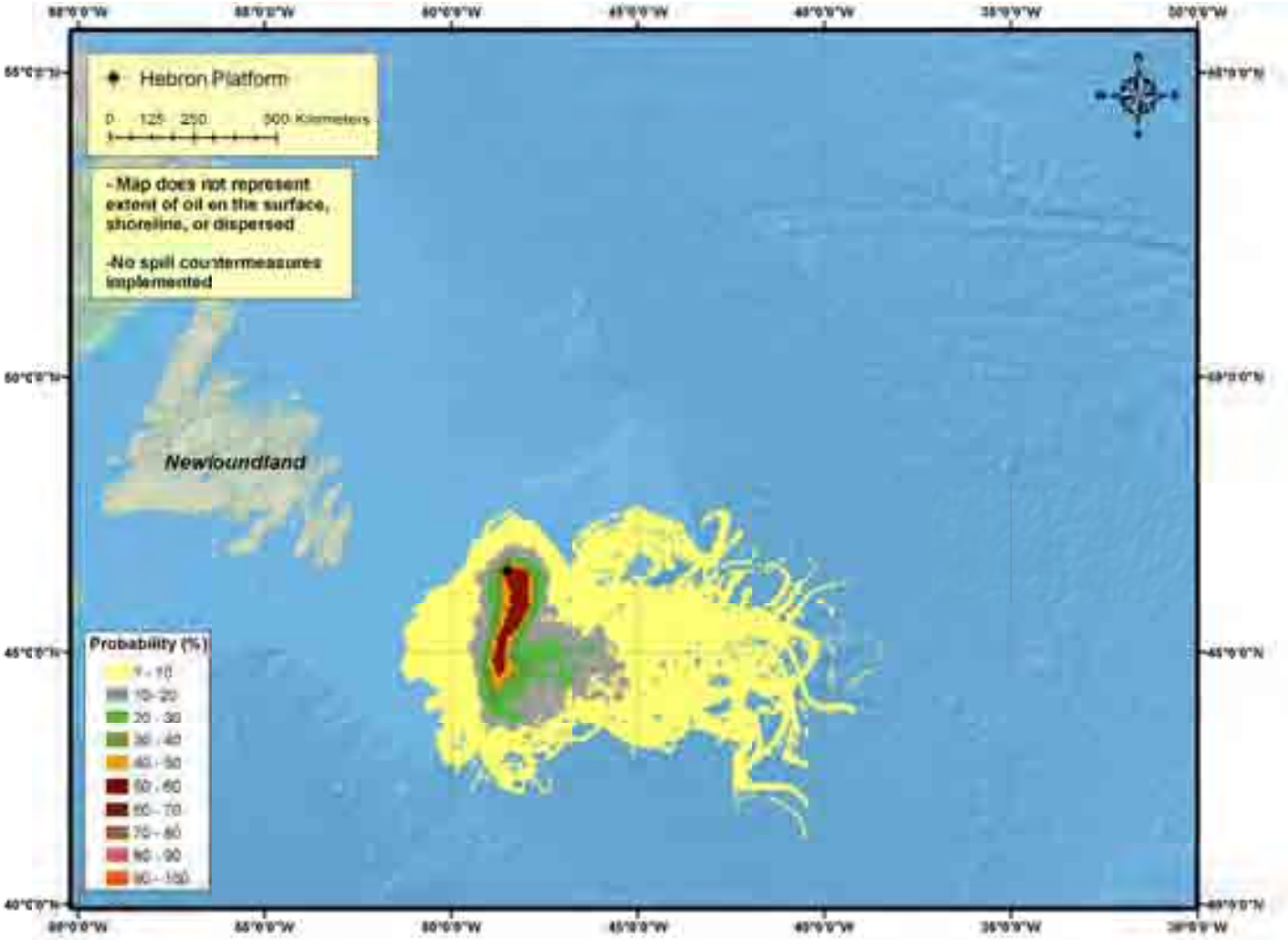


Figure 54. Entrained oil probabilities for a batch transfer release of 800 m^3 of diesel fuel oil during the winter with ice present.

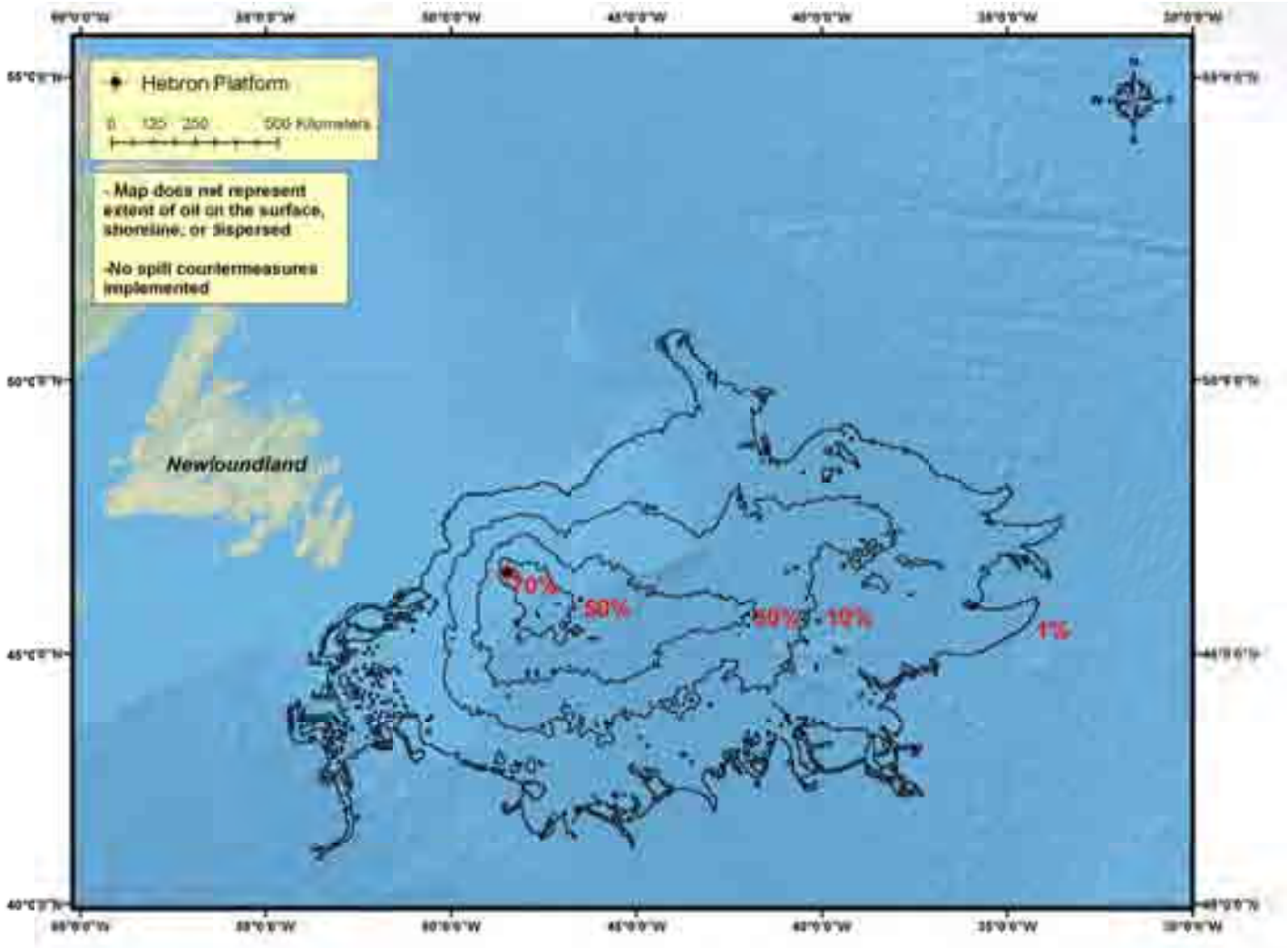


Figure 55. Surface oiling probabilities for a batch OLS transfer release of 5,000 m^3 of crude oil during the summer.

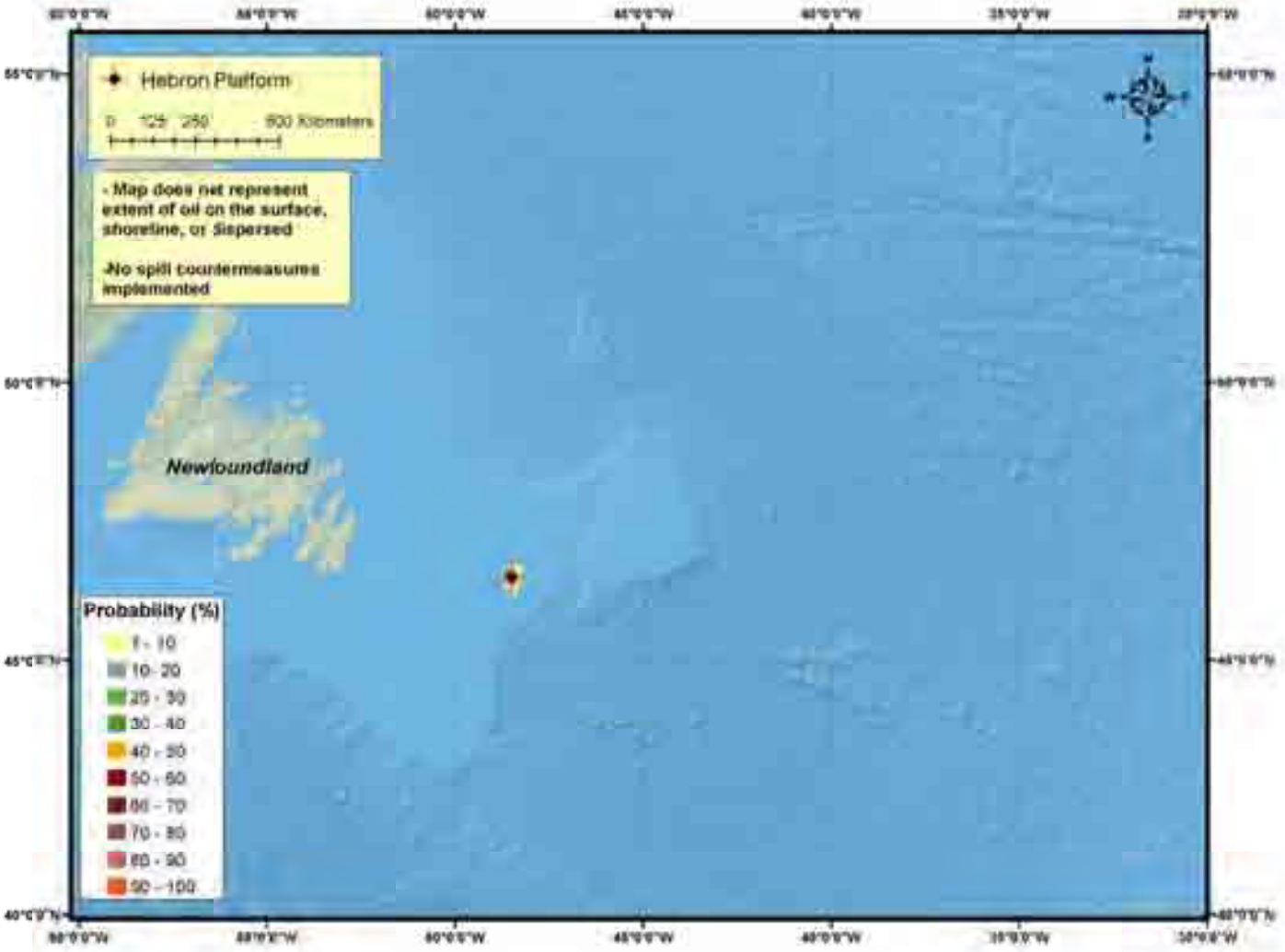


Figure 56. Entrained oil probabilities for a batch OLS transfer release of 5,000 m^3 of crude oil during the summer.

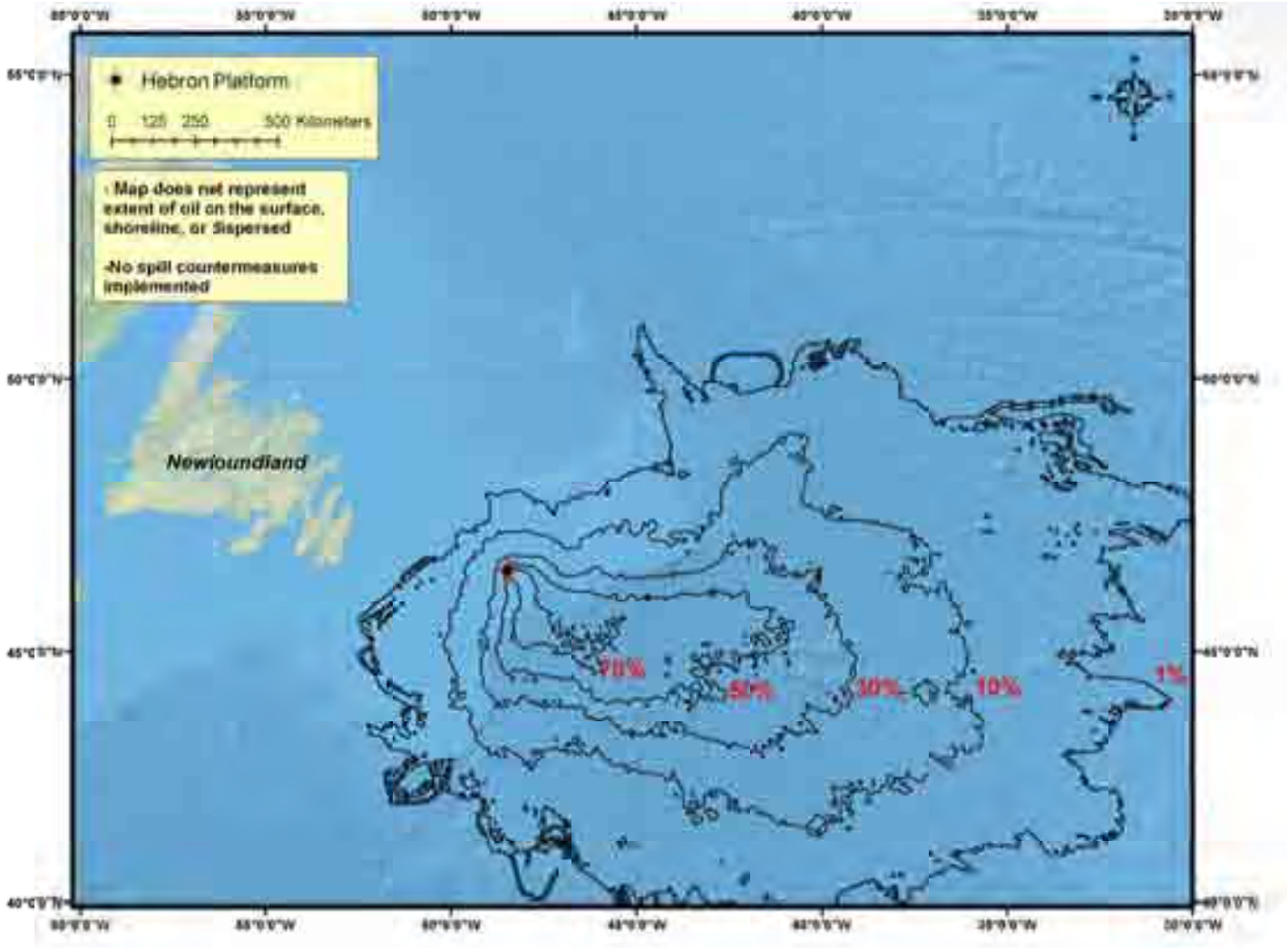


Figure 57. Surface oiling probabilities for a batch OLS transfer release of 5,000 m^3 of crude oil during the winter.

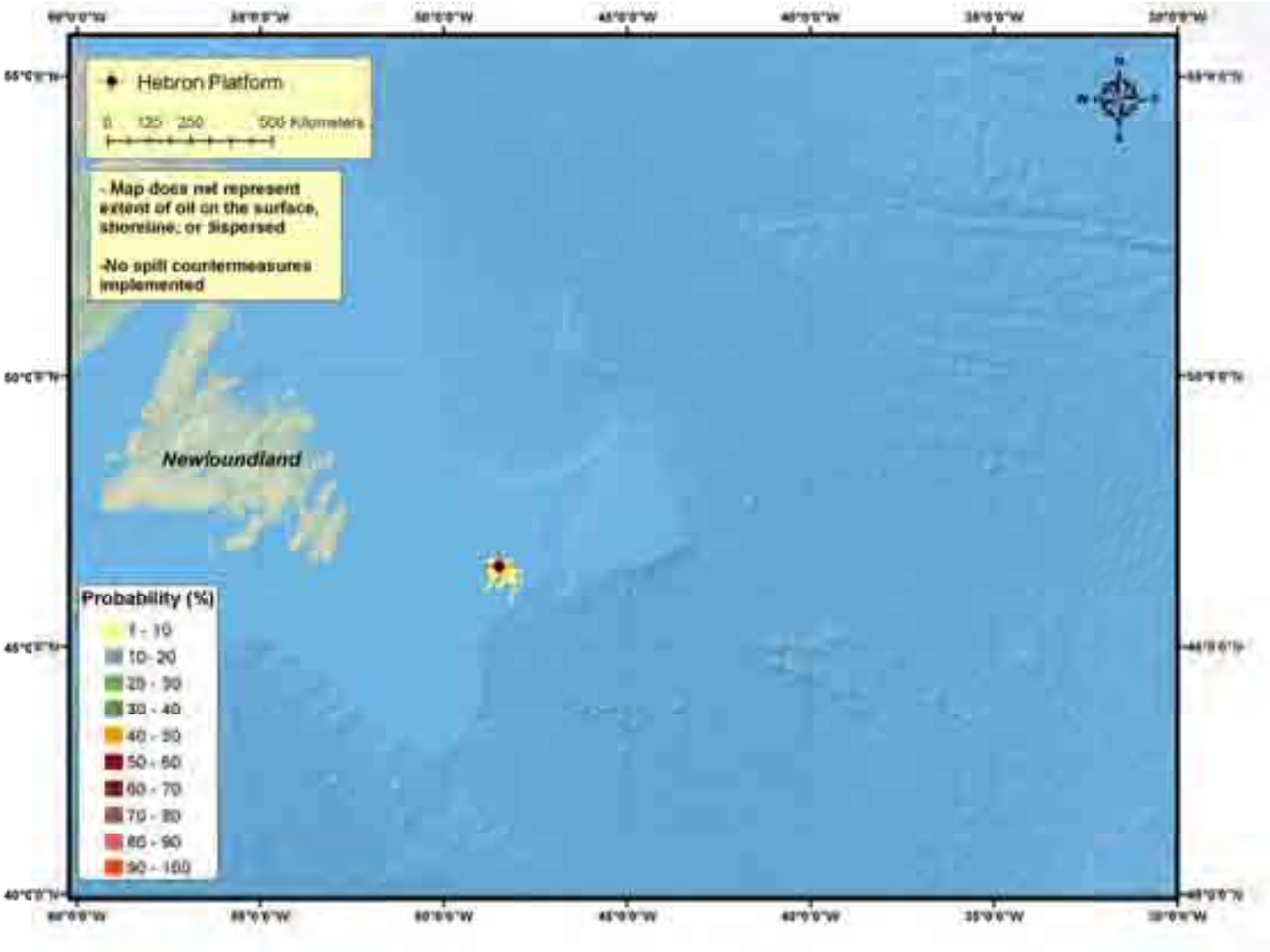


Figure 58. Entrained oil probabilities for a batch OLS transfer release of 5,000 m^3 of crude oil during the winter.

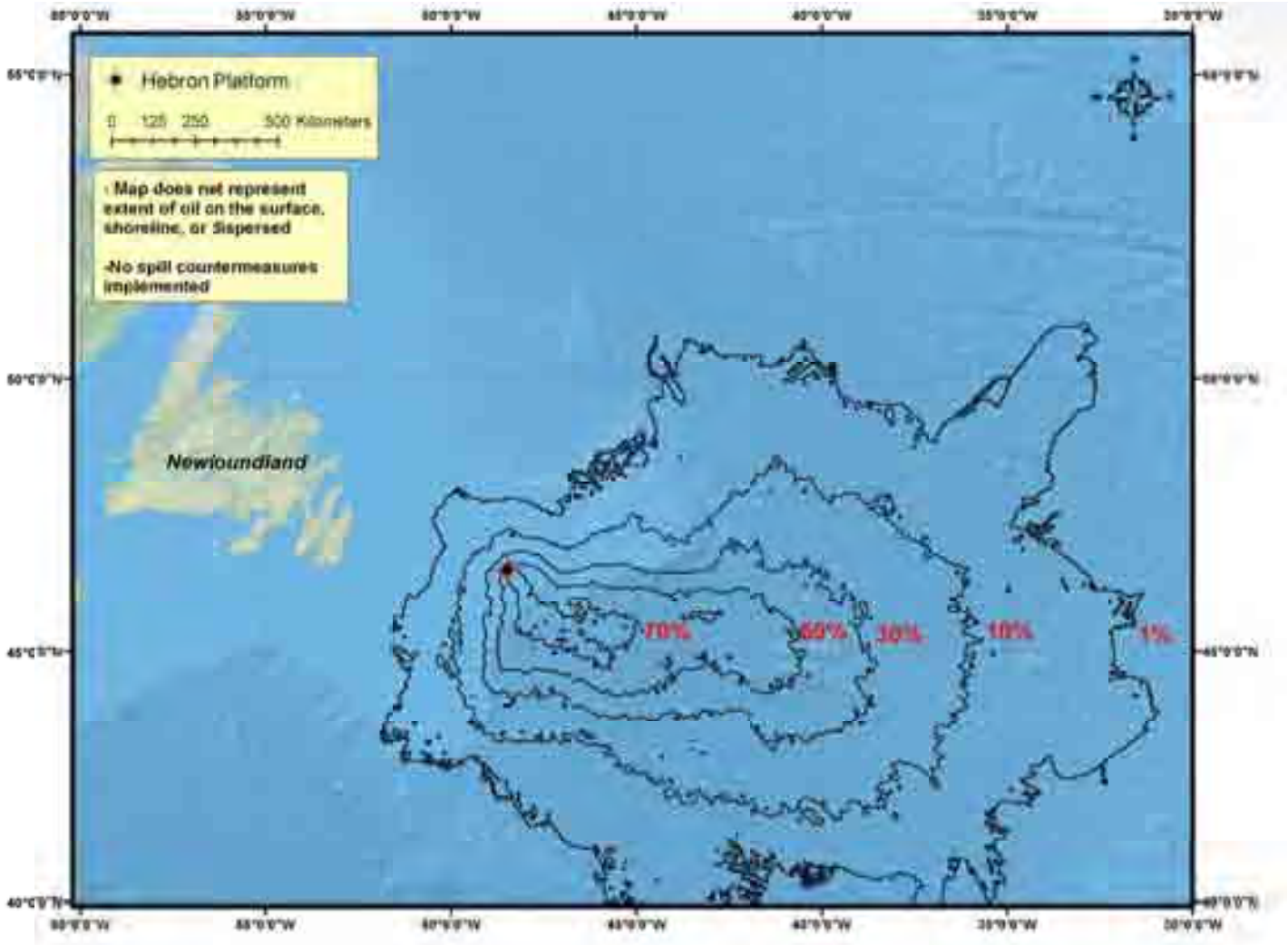


Figure 59. Surface oiling probabilities for a batch OLS transfer release of 5,000 m^3 of crude oil during the winter with ice present.

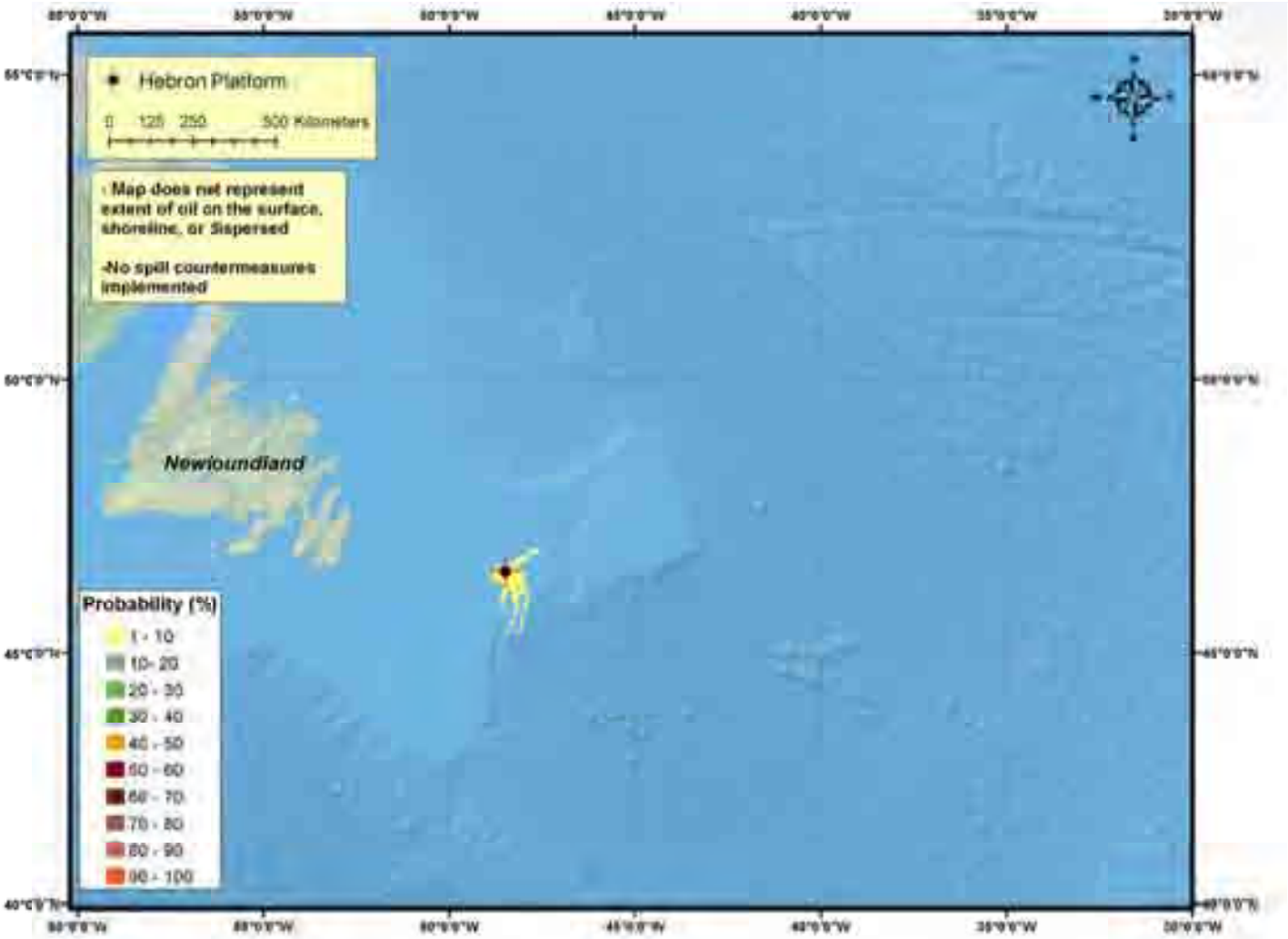


Figure 60. Entrained oil probabilities for a batch OLS transfer release of 5,000 m^3 of crude oil during the winter with ice present.

Appendix D - Deterministic Model Results

The deterministic model is used to investigate individual spill events identified in the stochastic modeling that rank in the 95th percentile for surface oiling, shoreline oiling and entrained oiling. The maps of deterministic model results show the maximum surface oil thickness or maximum shoreline oil thickness for the entire spill period as contours or areas of color corresponding to oil thickness. Maps of entrained oil show areas in the water that are predicted to exceed the 10 ppb threshold at any time during the spill.

Figures 1 through 25 contain maps of individual spills from the blow-out scenarios. Figures 26 through 37 contain the maps of individual spills from the batch transfer scenarios. It should be noted that several of the individual spill simulations ranked as the 95th percentile for shoreline oiling do not reach the Newfoundland shoreline. No shoreline oiling maps were made for those scenarios.

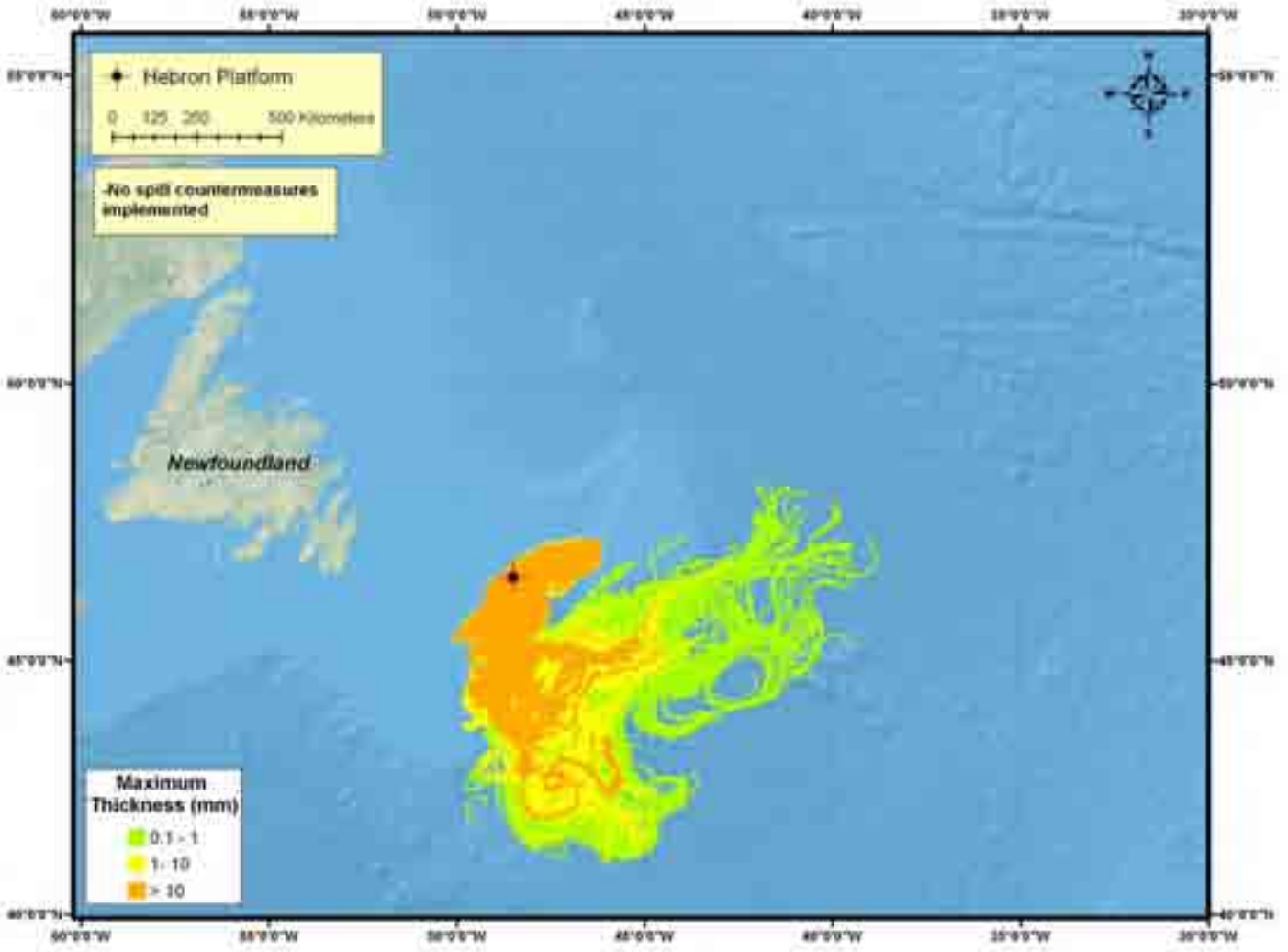


Figure 1. Maximum surface oil thickness for the 95th percentile surface oiling case based on the sea surface area oiled during a 30 day platform blow-out in the summer.

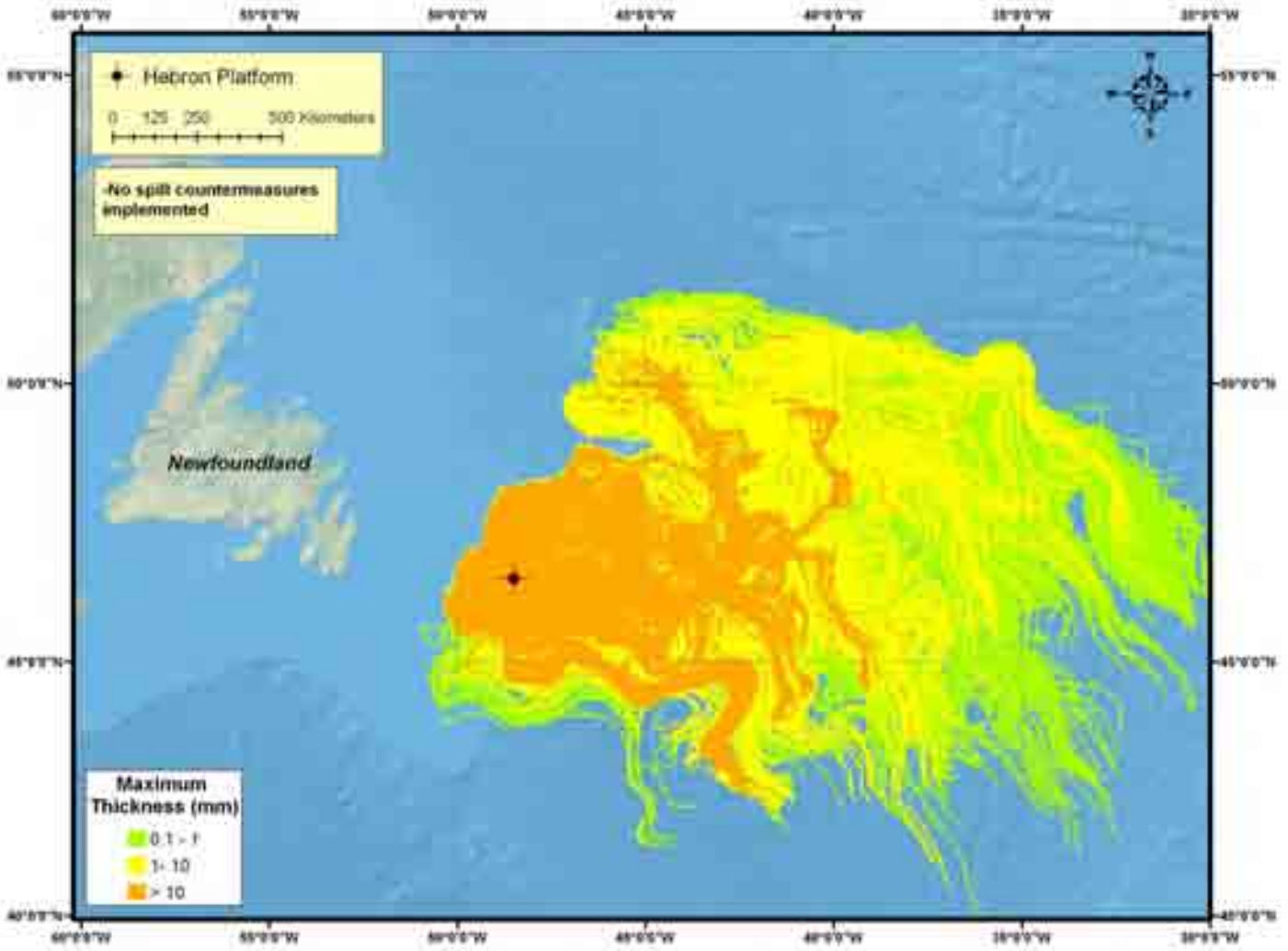


Figure 2. Maximum surface oil thickness for the 95th percentile surface oiling case based on the sea surface area oiled during a 30 day platform blow-out run for 60 days in the summer.

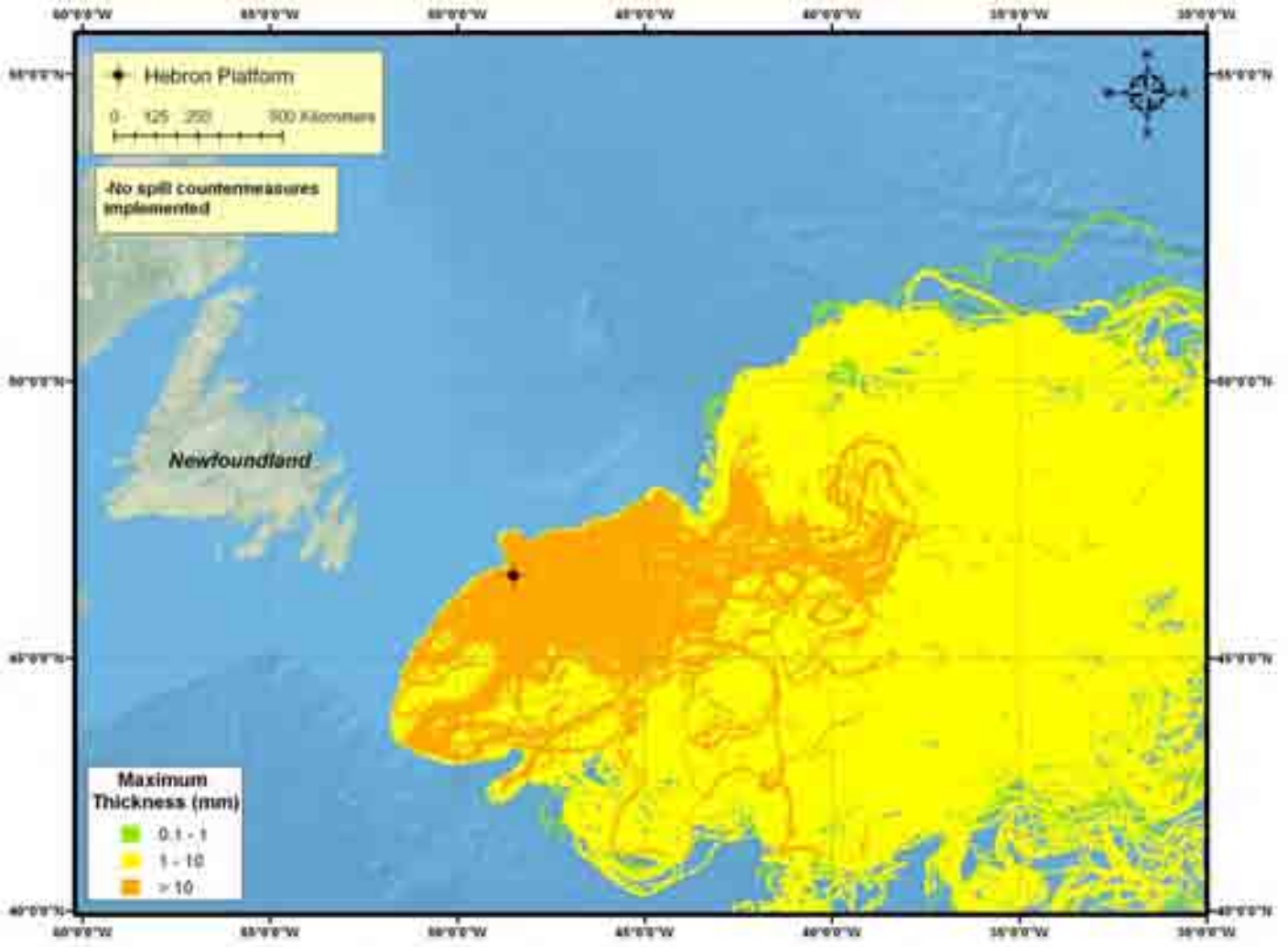


Figure 3. Maximum surface oil thickness for the 95th percentile surface oiling case based on the sea surface area oiled during a 100 day platform blow-out in the summer.

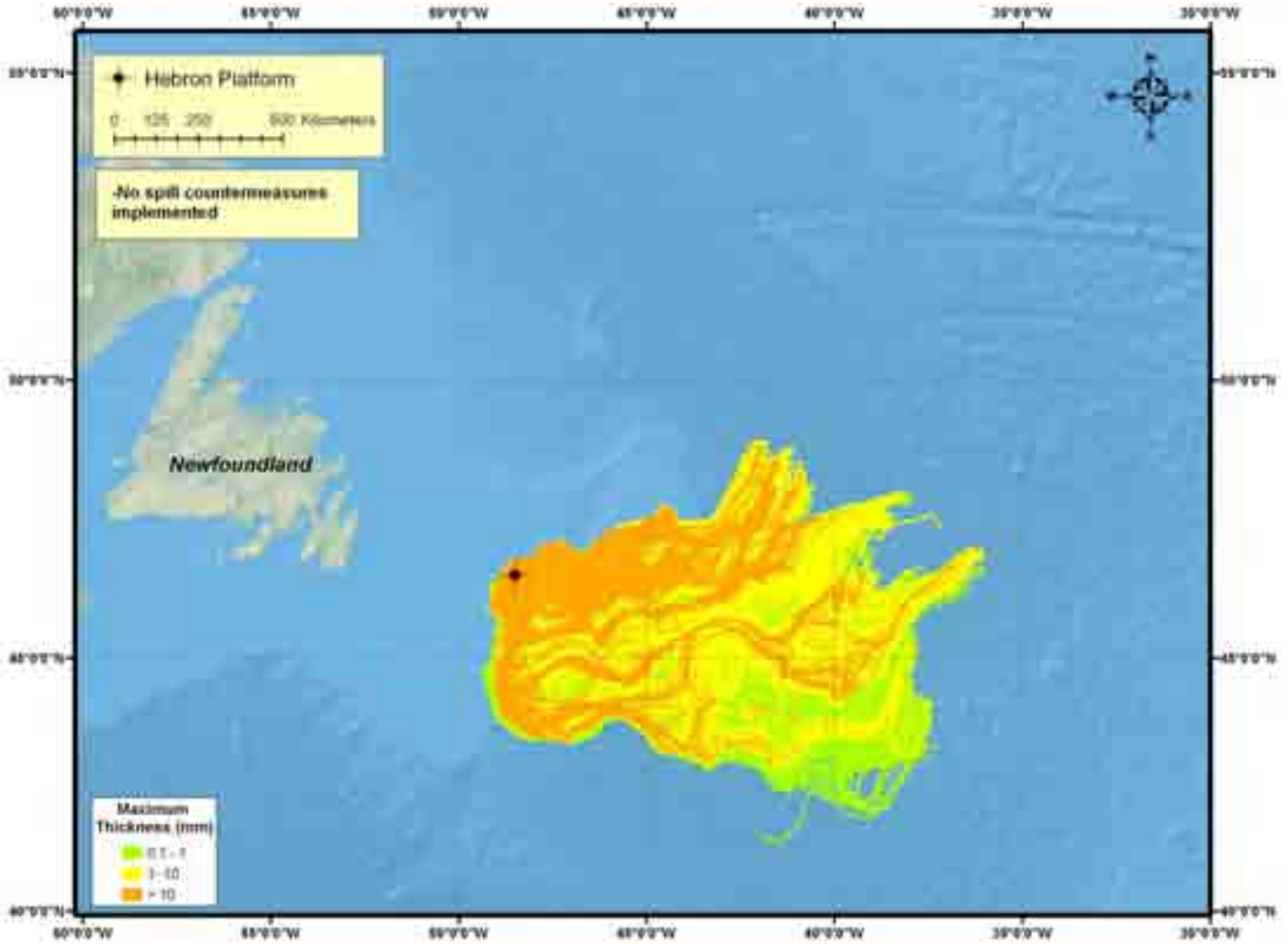


Figure 4. Maximum surface oil thickness for the 95th percentile surface oiling case based on the sea surface area oiled during a 30 day platform blow-out in the winter.

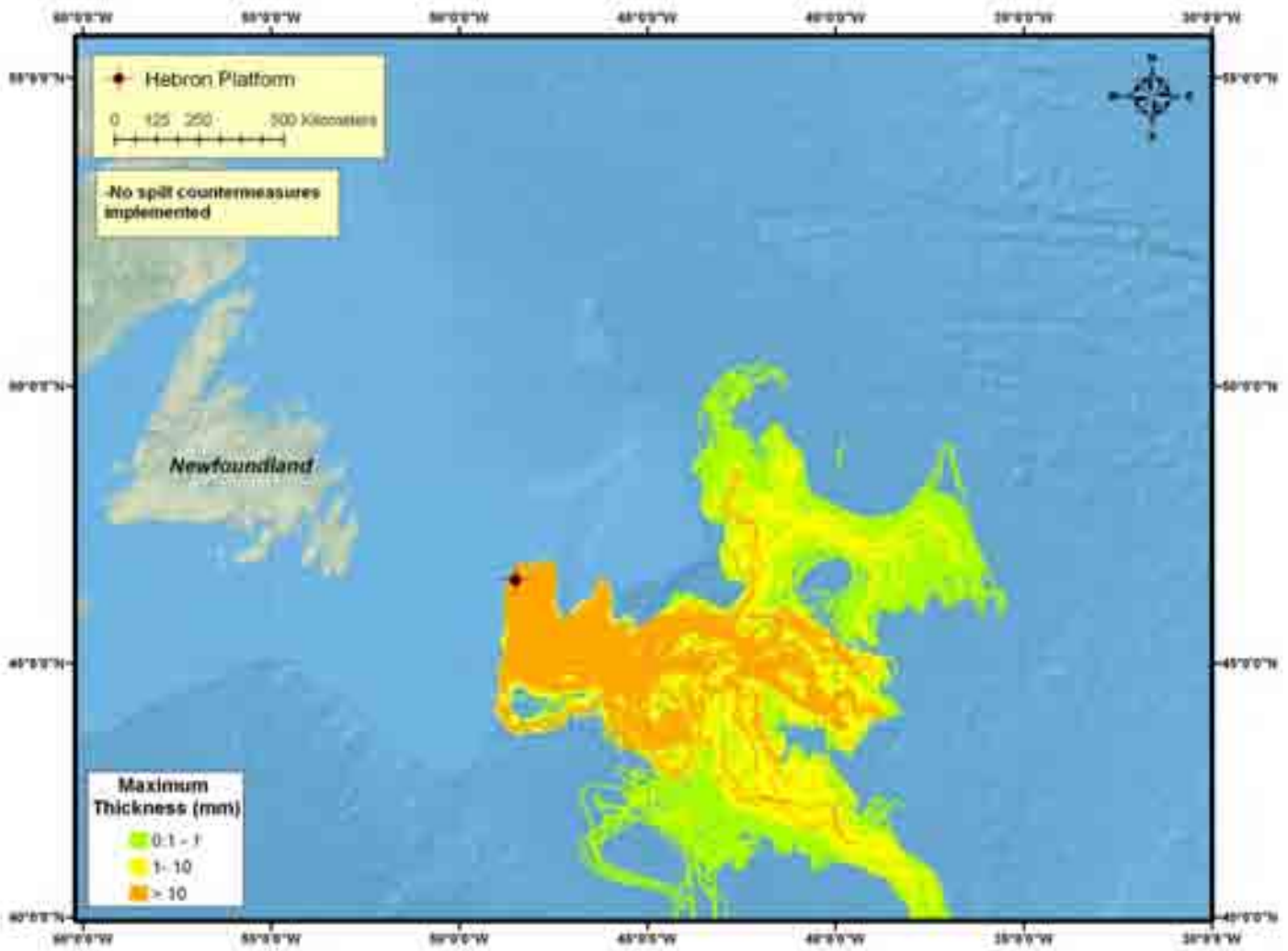


Figure 5. Maximum surface oil thickness for the 95th percentile surface oiling case based on the sea surface area oiled during a 30 day platform blow-out run in the winter with ice present.

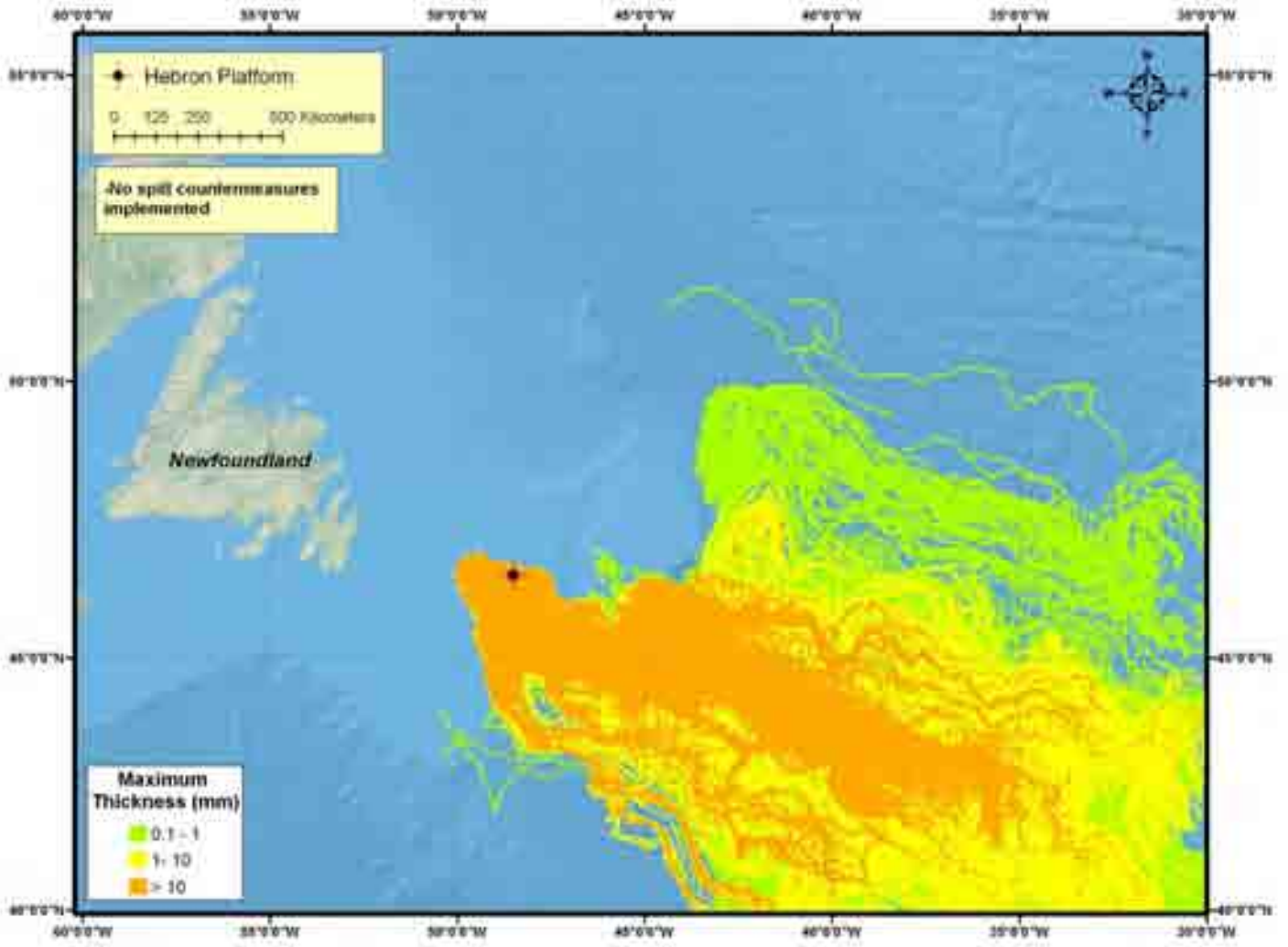


Figure 6. Maximum surface oil thickness for the 95th percentile surface oiling case based on the sea surface area oiled during a 30 day platform blow-out run for 60 days in the winter.

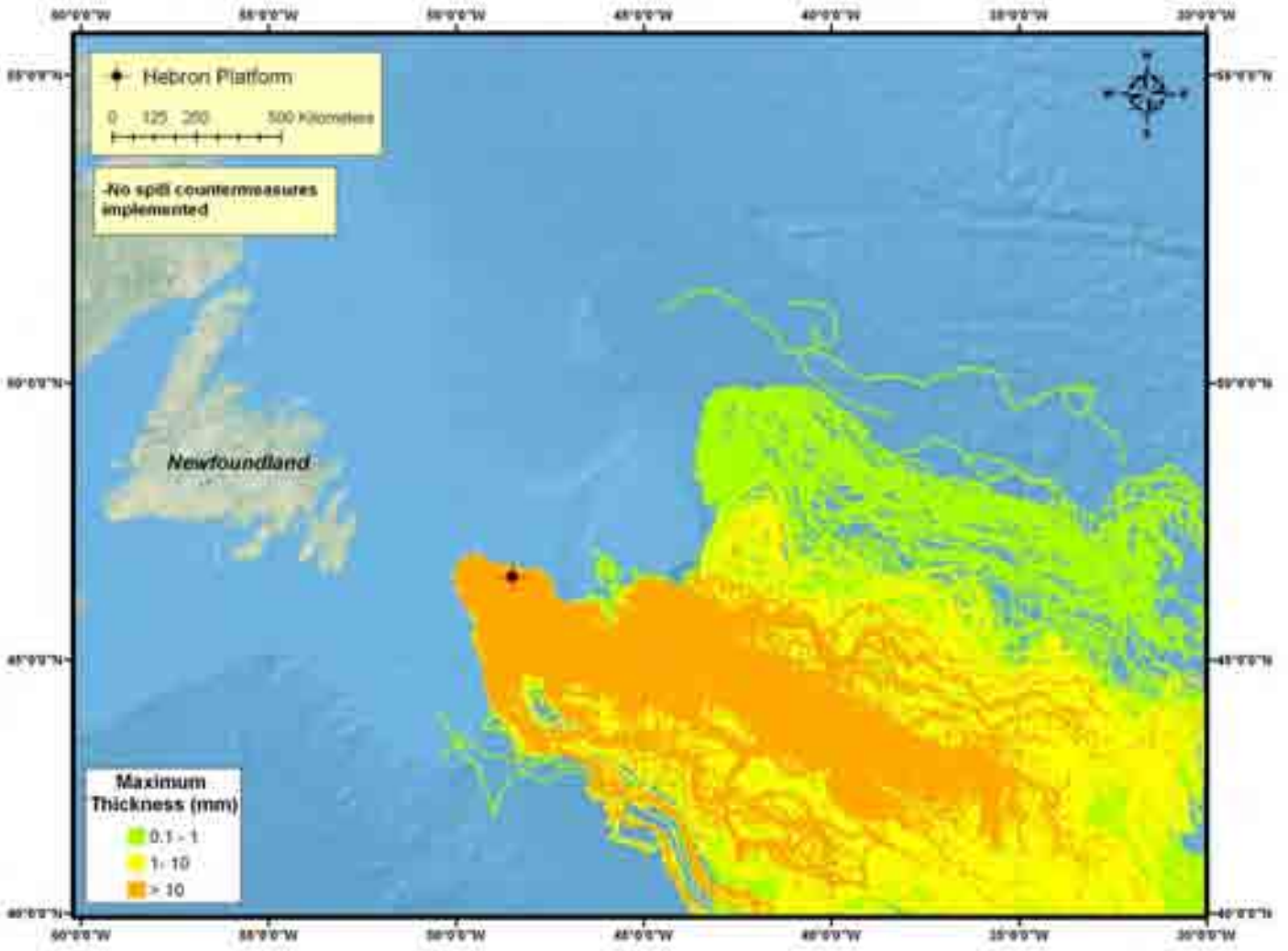


Figure 7. Maximum surface oil thickness for the 95th percentile surface oiling case based on the sea surface area oiled during a 30 day platform blow-out run for 60 days in the winter with ice present.

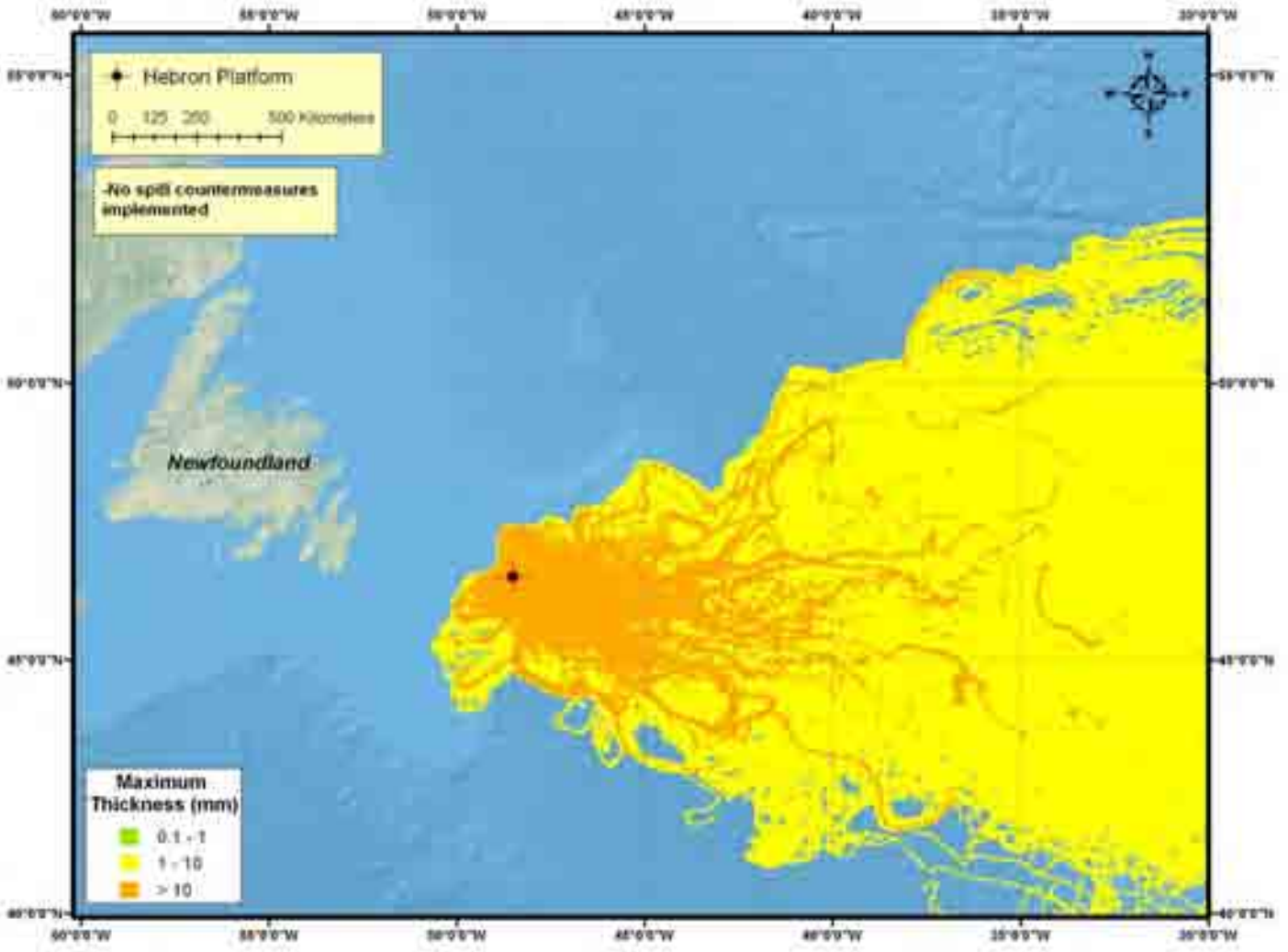


Figure 8. Maximum surface oil thickness for the 95th percentile surface oiling case based on the sea surface area oiled during a 120 day platform blow-out in the winter.

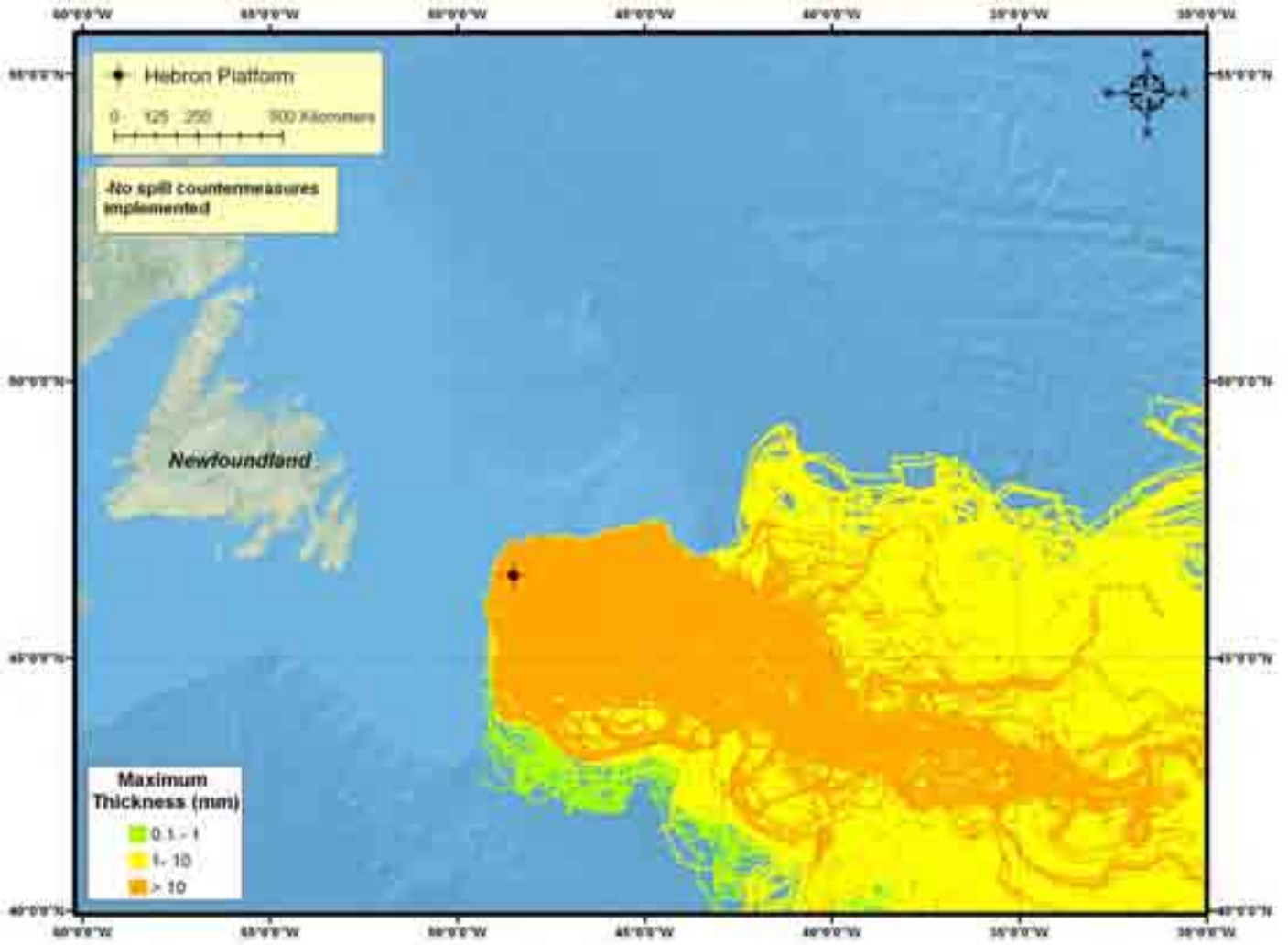


Figure 9. Maximum surface oil thickness for the 95th percentile surface oiling case based on the sea surface area oiled during a 120 day platform blow-out in the winter with ice present.

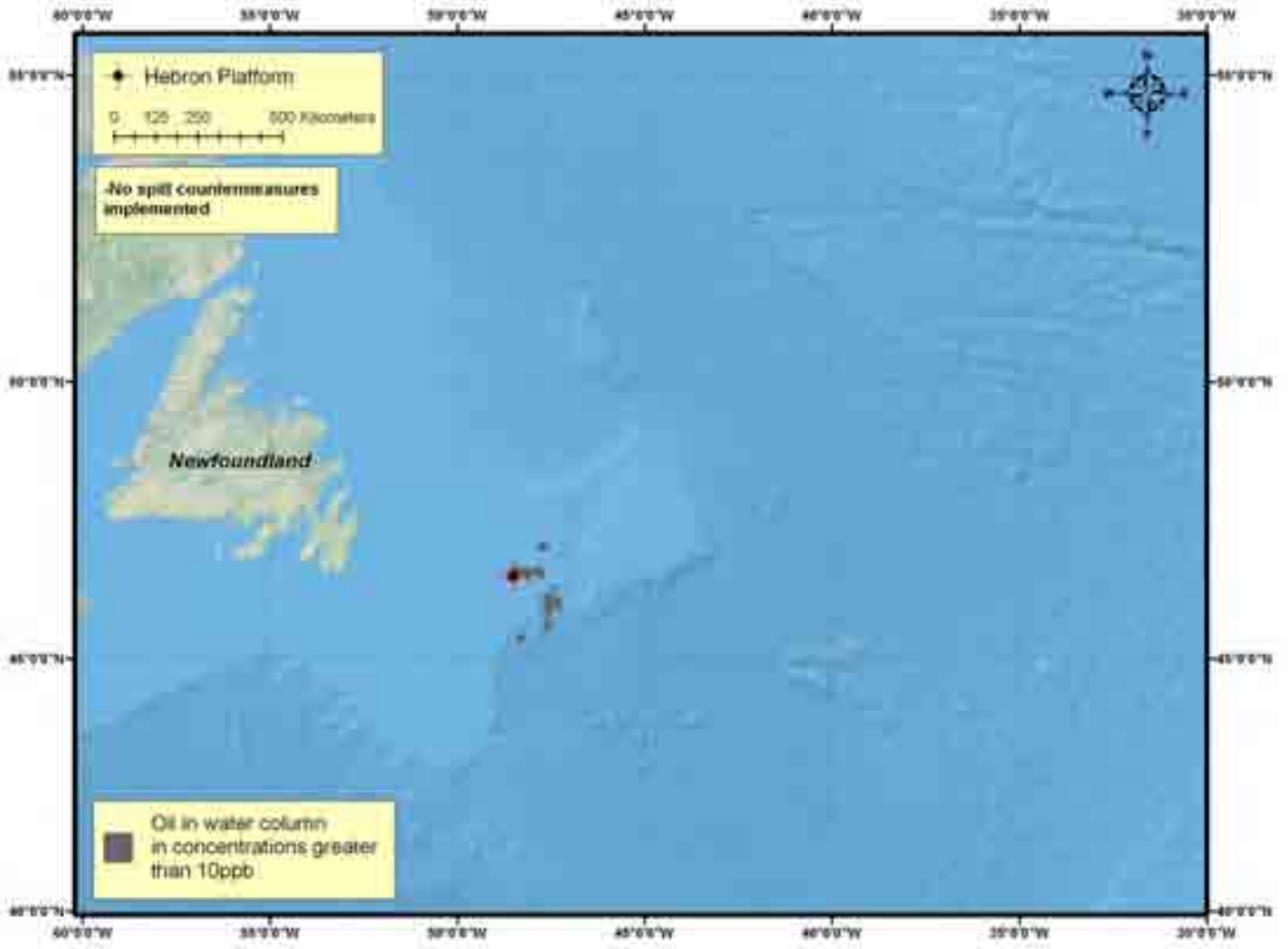


Figure 10. Area of entrained oil for the 95th percentile water column case based on the volume of oil entrained in the water column at the end of a 30 day platform blow-out during the summer.

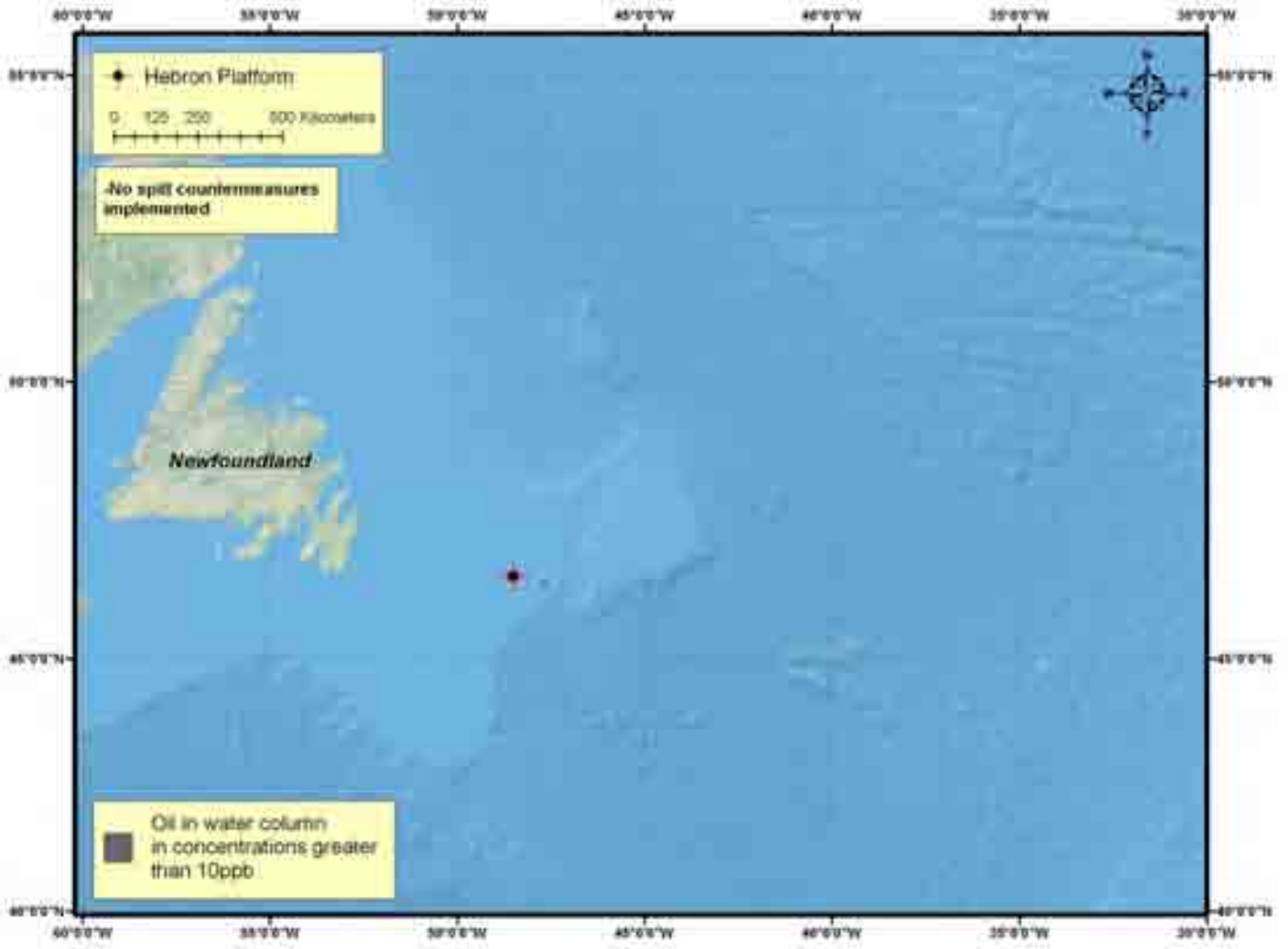


Figure 11. Area of entrained oil for the 95th percentile water column case based on the volume of oil entrained in the water column at the end of a 30 day platform blow-out run for 60 days during the summer.

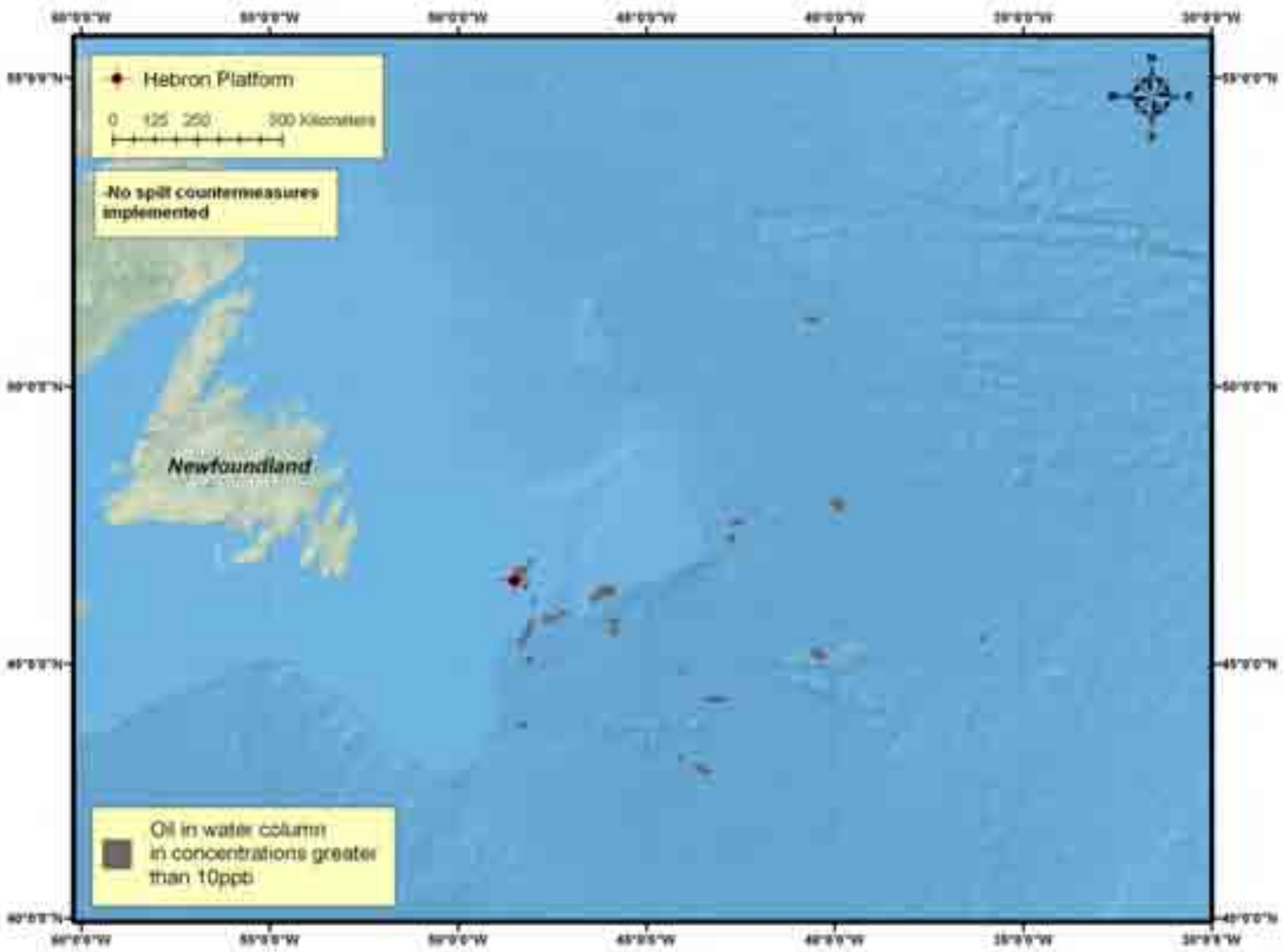


Figure 12. Area of entrained oil for the 95th percentile water column case based on the volume of oil entrained in the water column at the end of a 100 day platform blow-out during the summer.

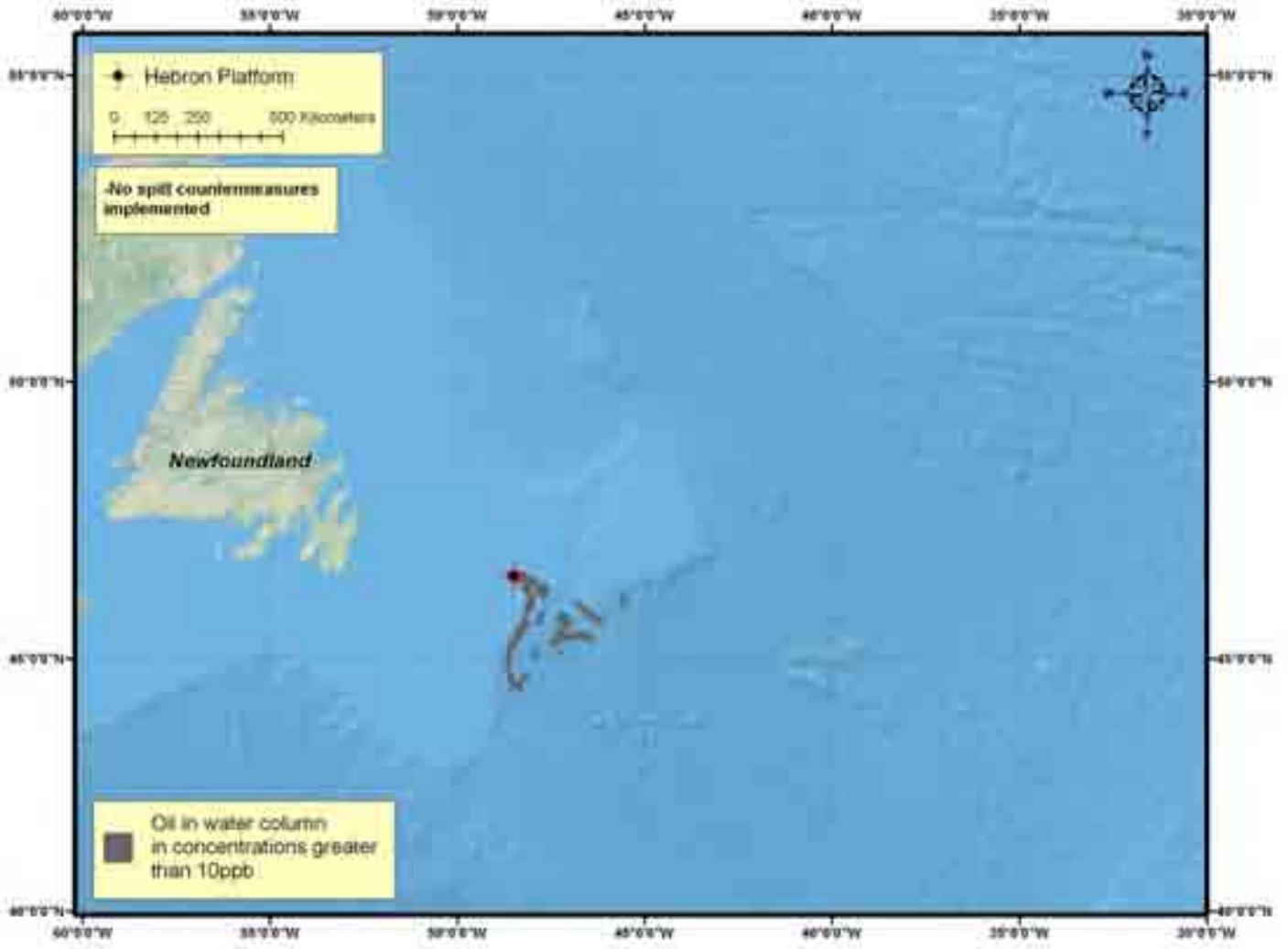


Figure 13. Area of entrained oil for the 95th percentile water column case based on the volume of oil entrained in the water column at the end of a 30 day platform blow-out during the winter.

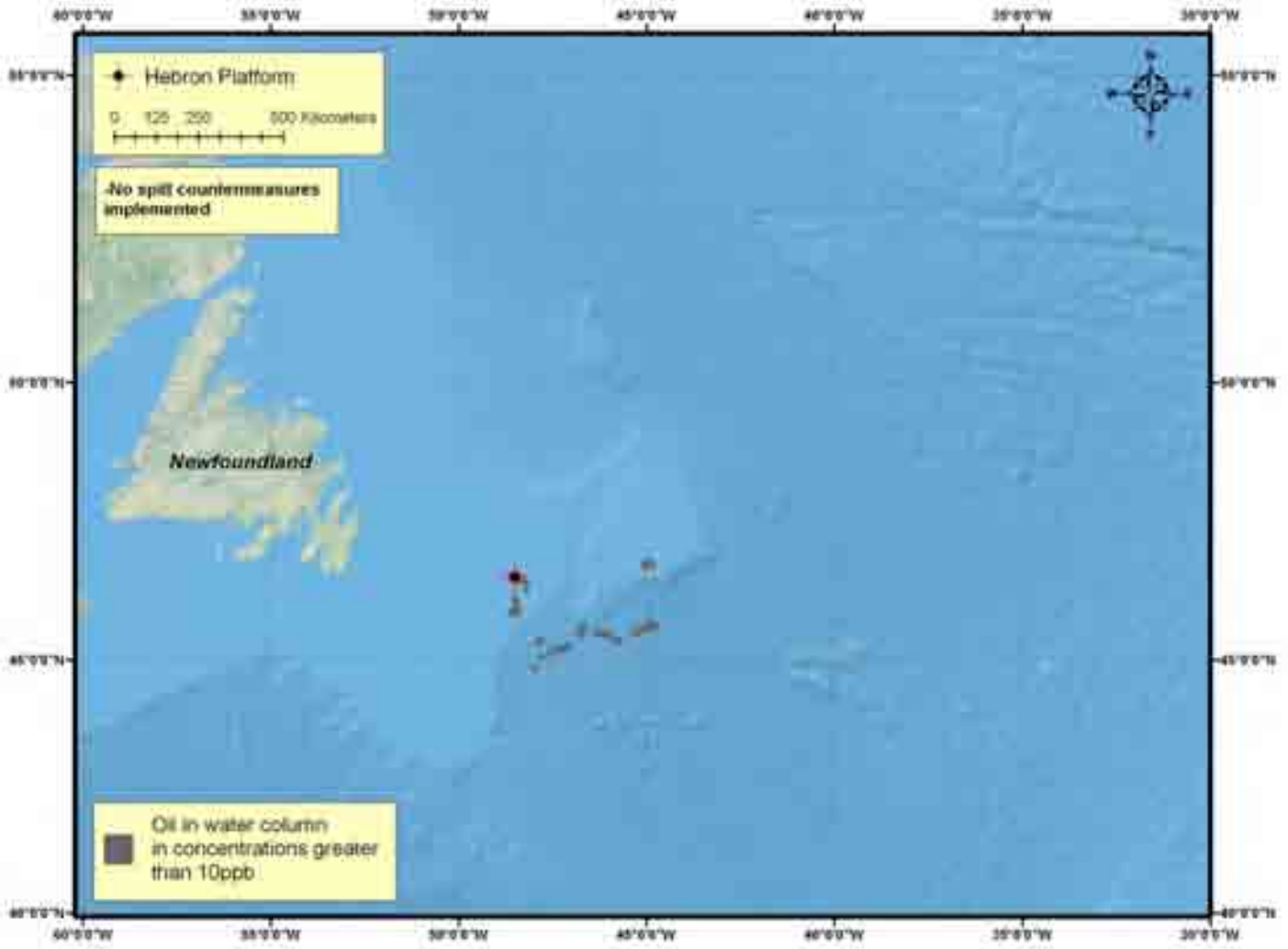


Figure 14. Area of entrained oil for the 95th percentile water column case based on the volume of oil entrained in the water column at the end of a 30 day platform blow-out during the winter with ice present.

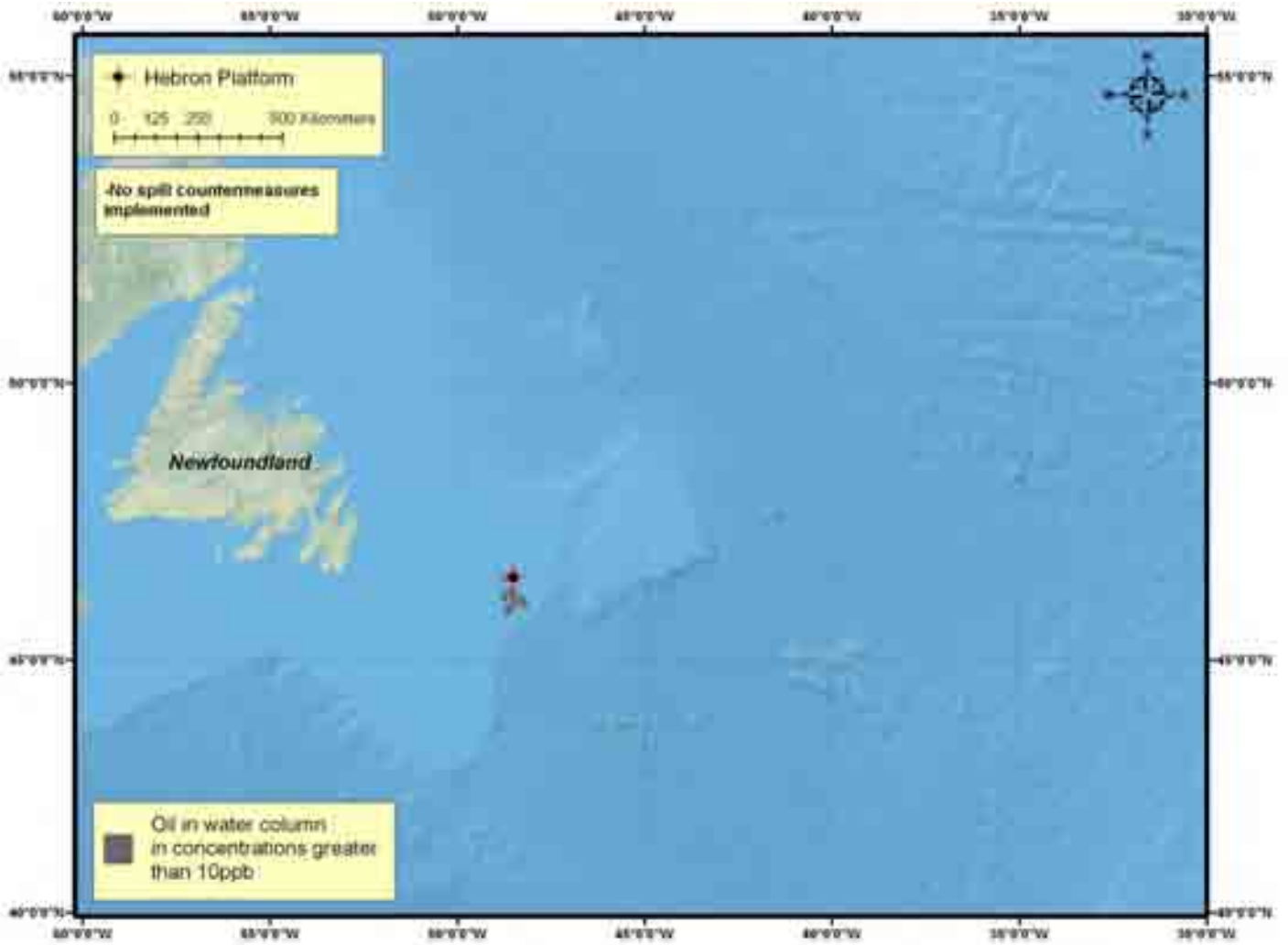


Figure 15. Area of entrained oil for the 95th percentile water column case based on the volume of oil entrained in the water column at the end of a 30 day platform blow-out run for 60 days during the winter.

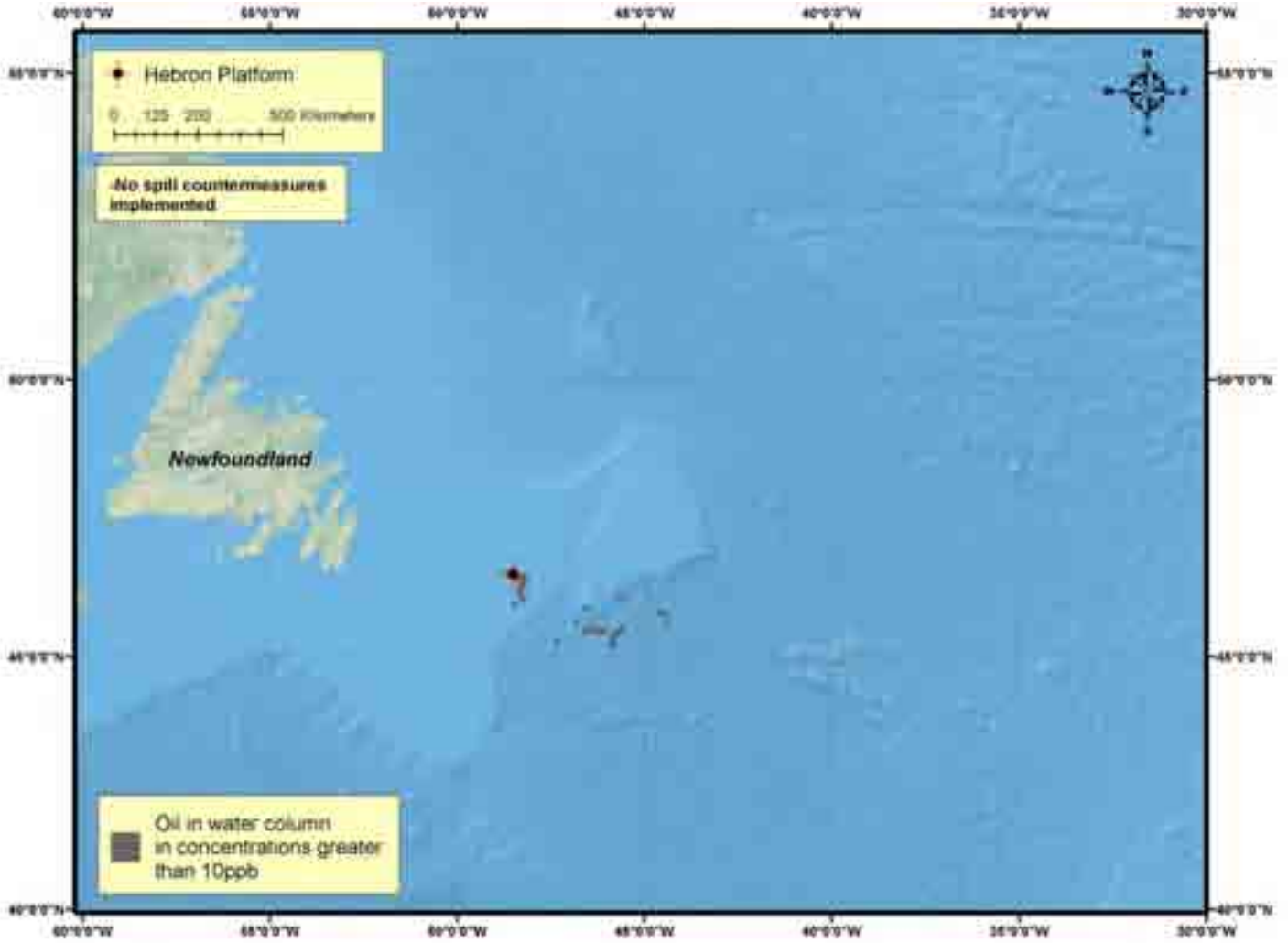


Figure 16. Area of entrained oil for the 95th percentile water column case based on the volume of oil entrained in the water column at the end of a 30 day platform blow-out run for 60 days during the winter with ice present.

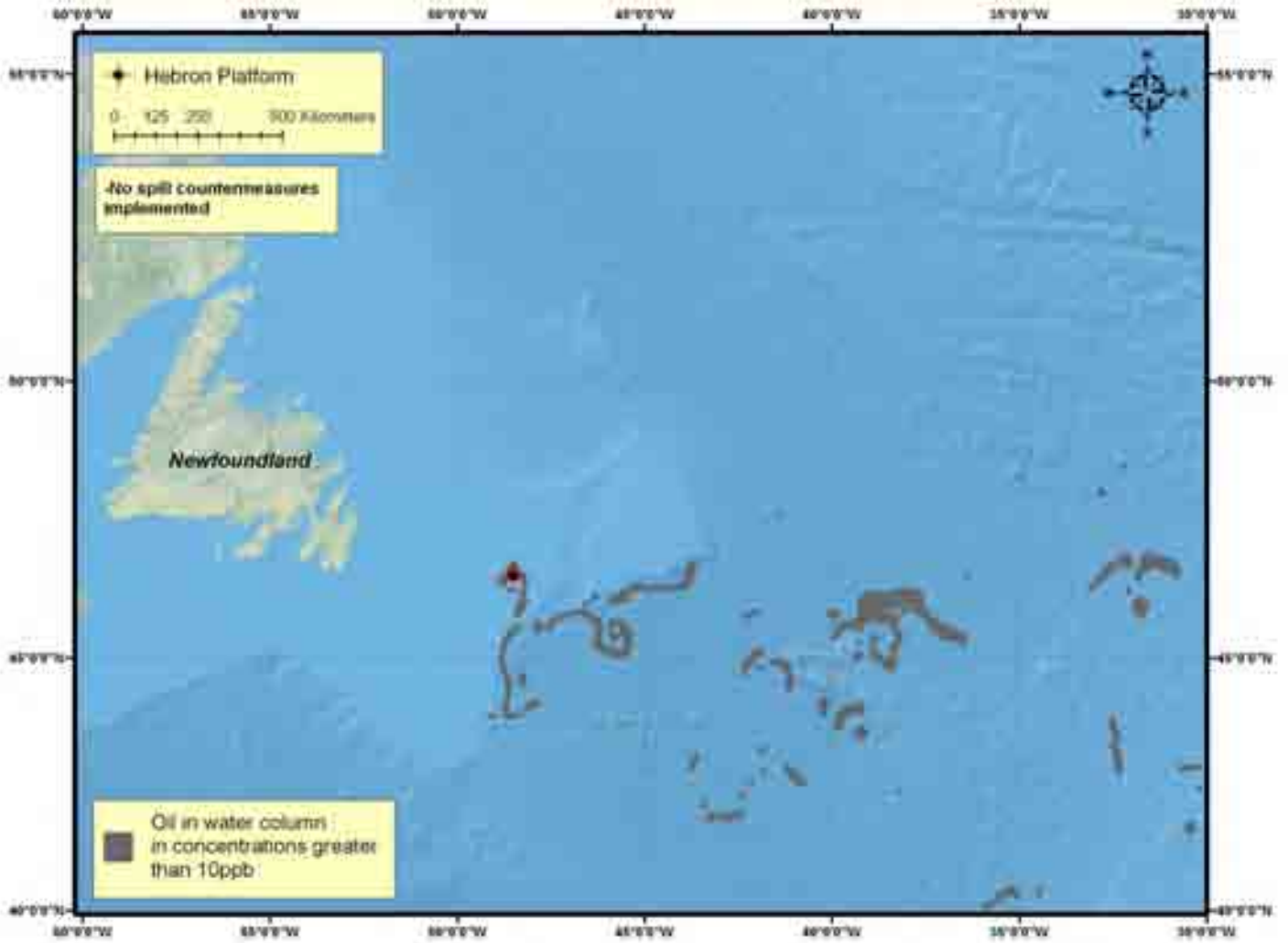


Figure 17. Area of entrained oil for the 95th percentile water column case based on the volume of oil entrained in the water column at the end of a 120 day platform blow-out during the winter.

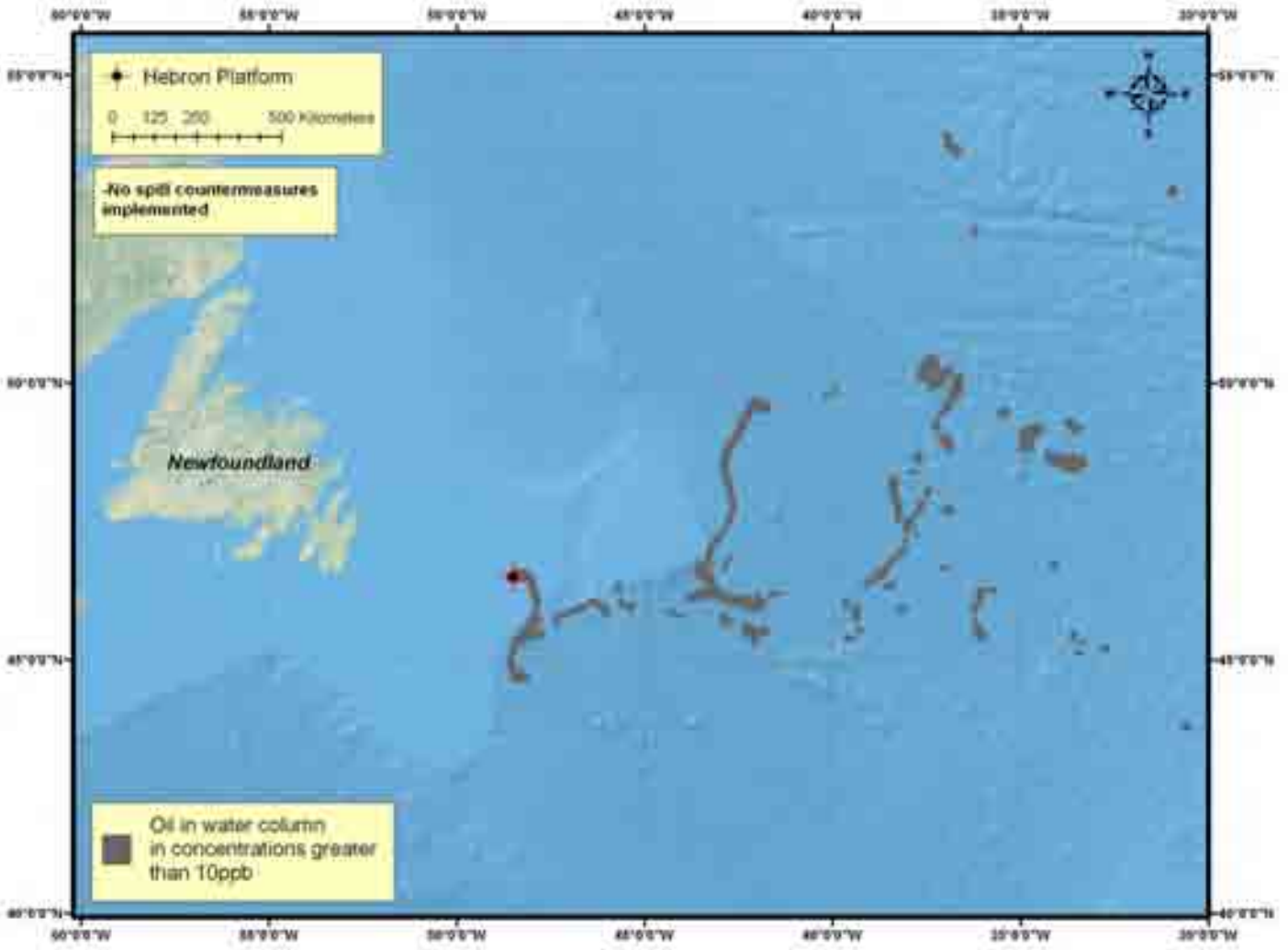


Figure 18. Area of entrained oil for the 95th percentile water column case based on the volume of oil entrained in the water column at the end of a 120 day platform blow-out during the winter with ice present.

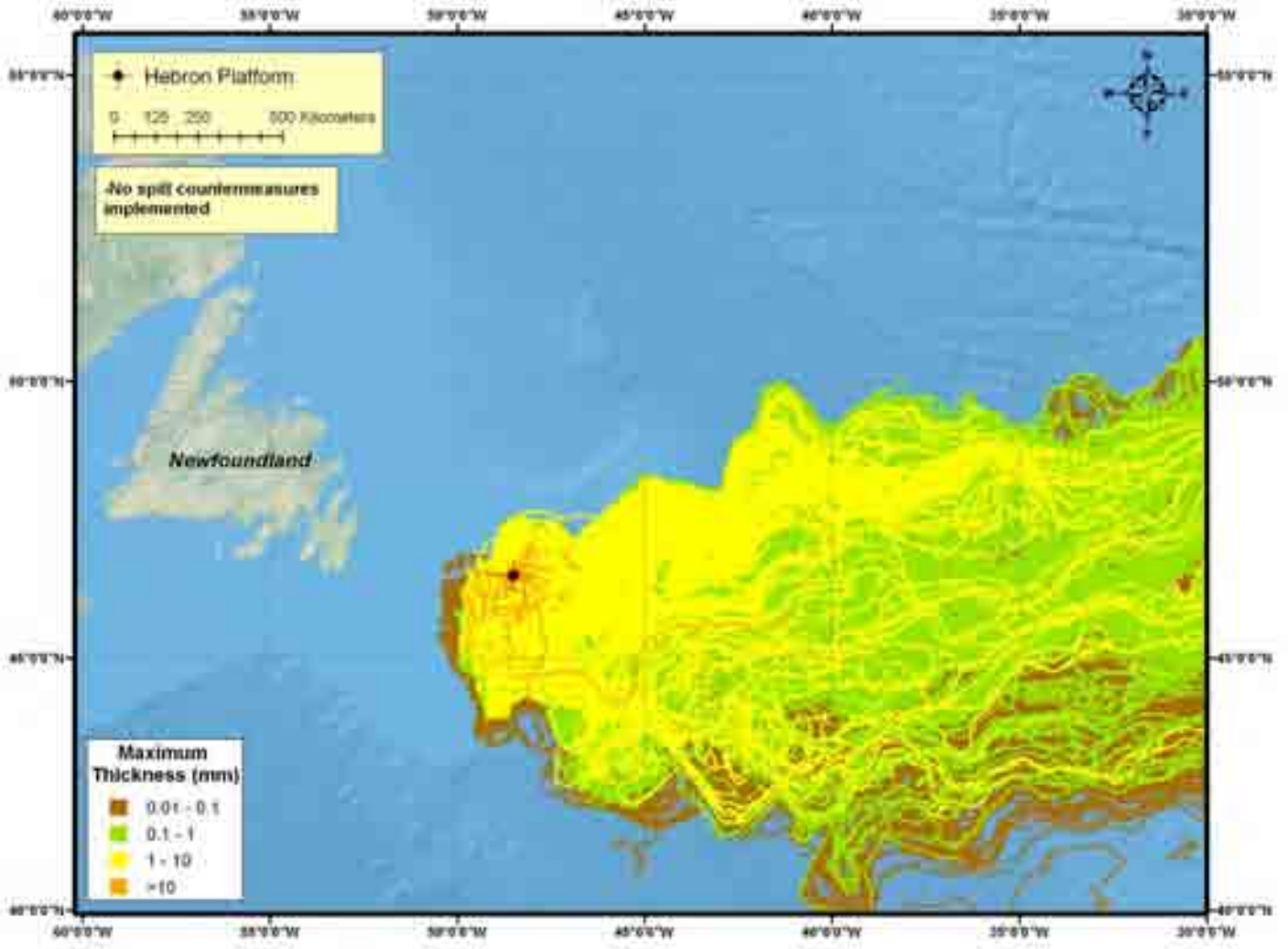


Figure 19. Maximum surface oil thickness for the 95th percentile surface oiling case based on the sea surface area oiled during a 100 day subsea blow-out in the summer.

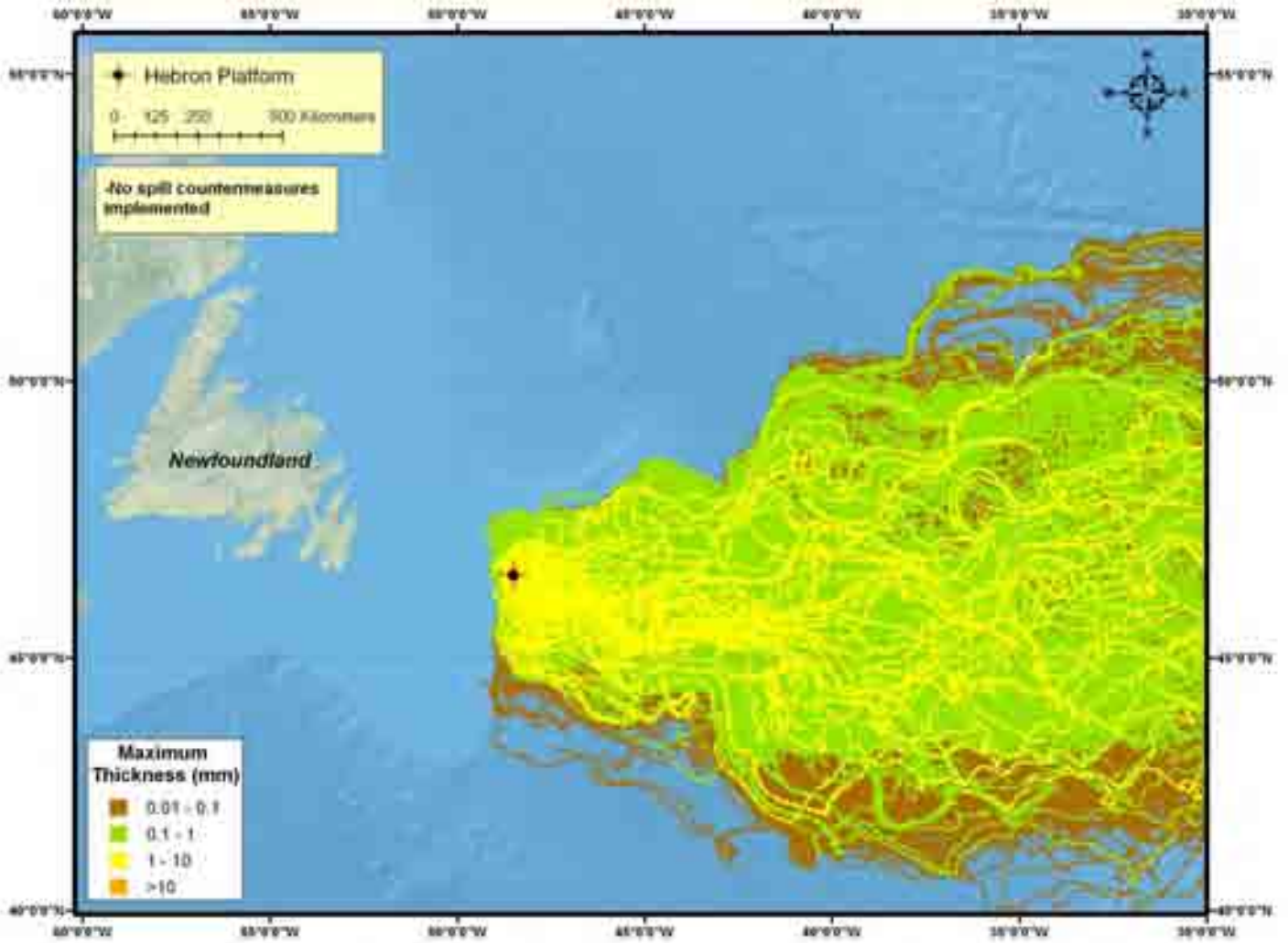


Figure 20. Maximum surface oil thickness for the 95th percentile surface oiling case based on the sea surface area oiled during a 120 day subsea blow-out in the winter.

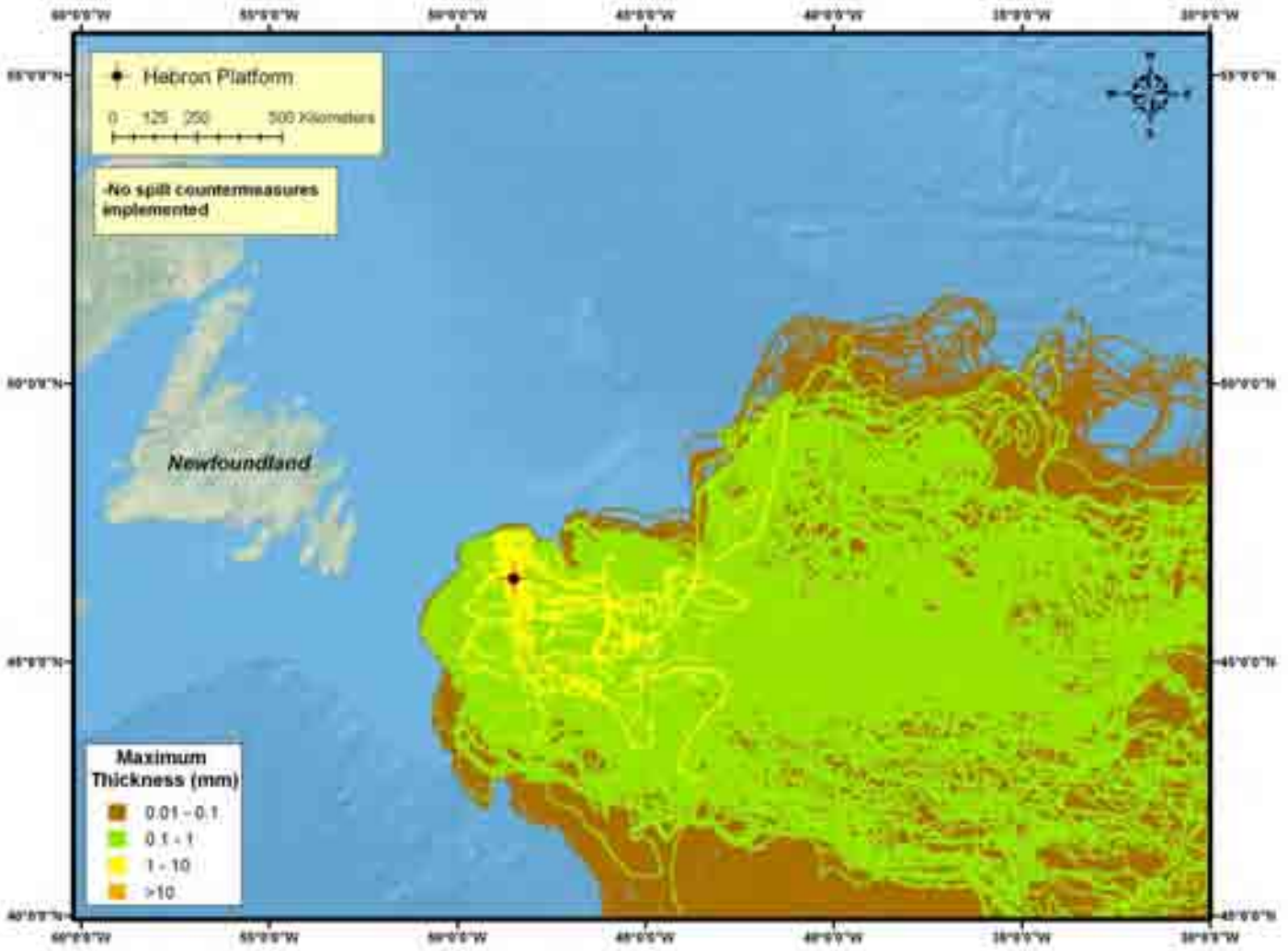


Figure 21. Maximum surface oil thickness for the 95th percentile surface oiling case based on the sea surface area oiled during a 120 day subsea blow-out in the winter with ice present.

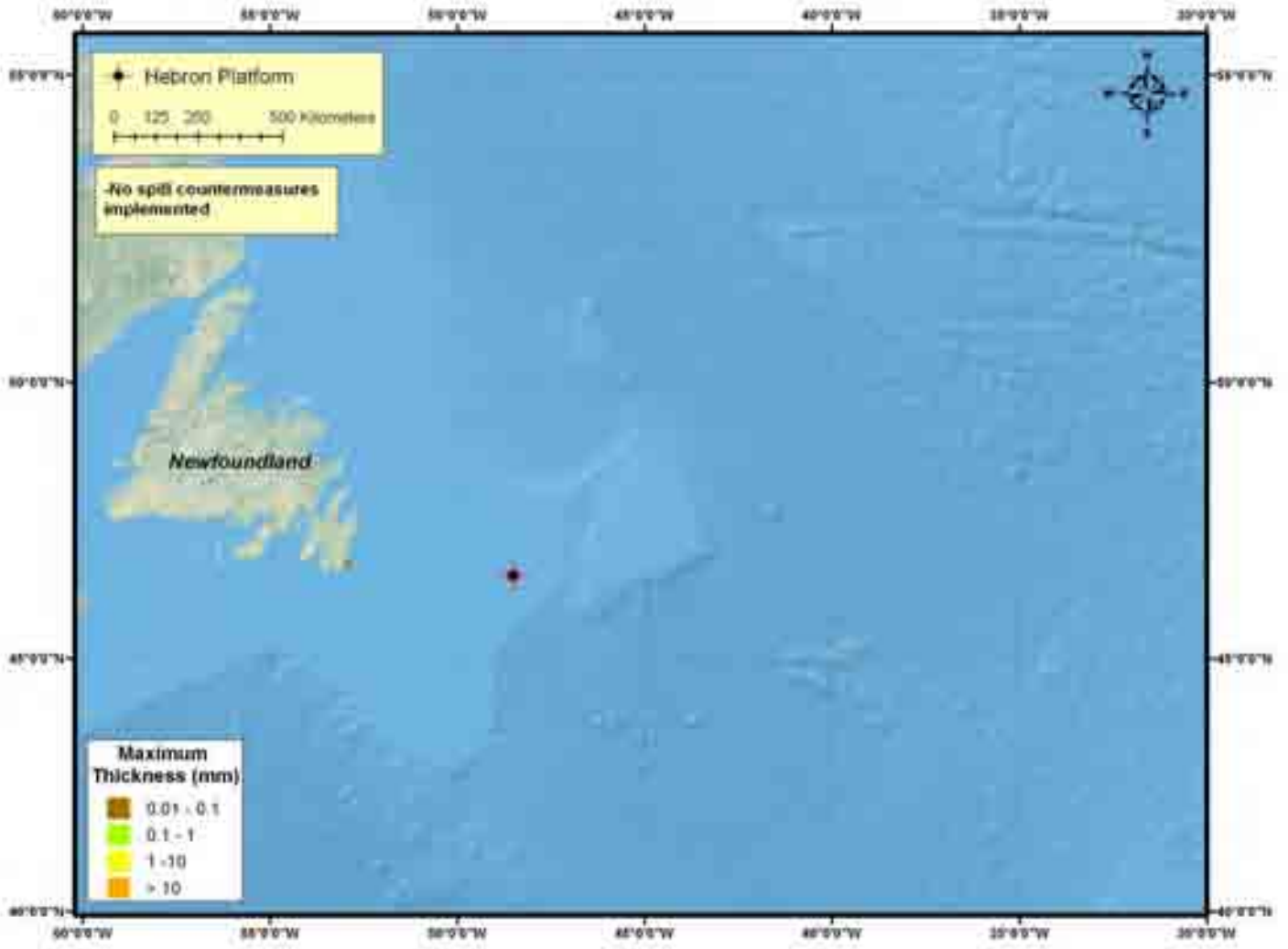


Figure 22. Maximum shoreline oil thickness for the 95th percentile shoreline oiling case based on the shoreline area oiled during a 100 day subsea blow-out in the summer.

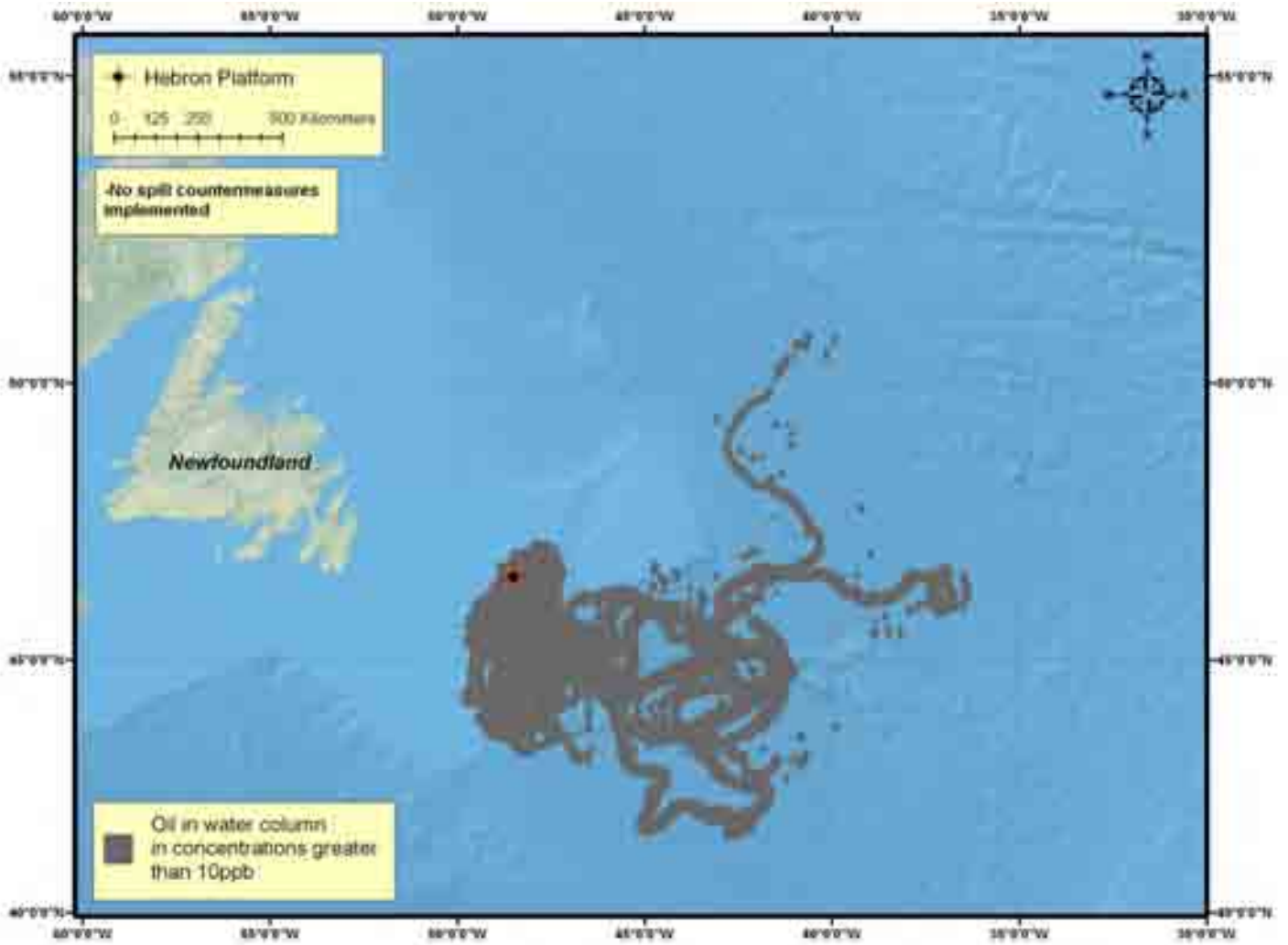


Figure 23. Area of entrained oil for the 95th percentile water column case based on the volume of oil entrained in the water column at the end of a 100 day platform blow-out during the summer.

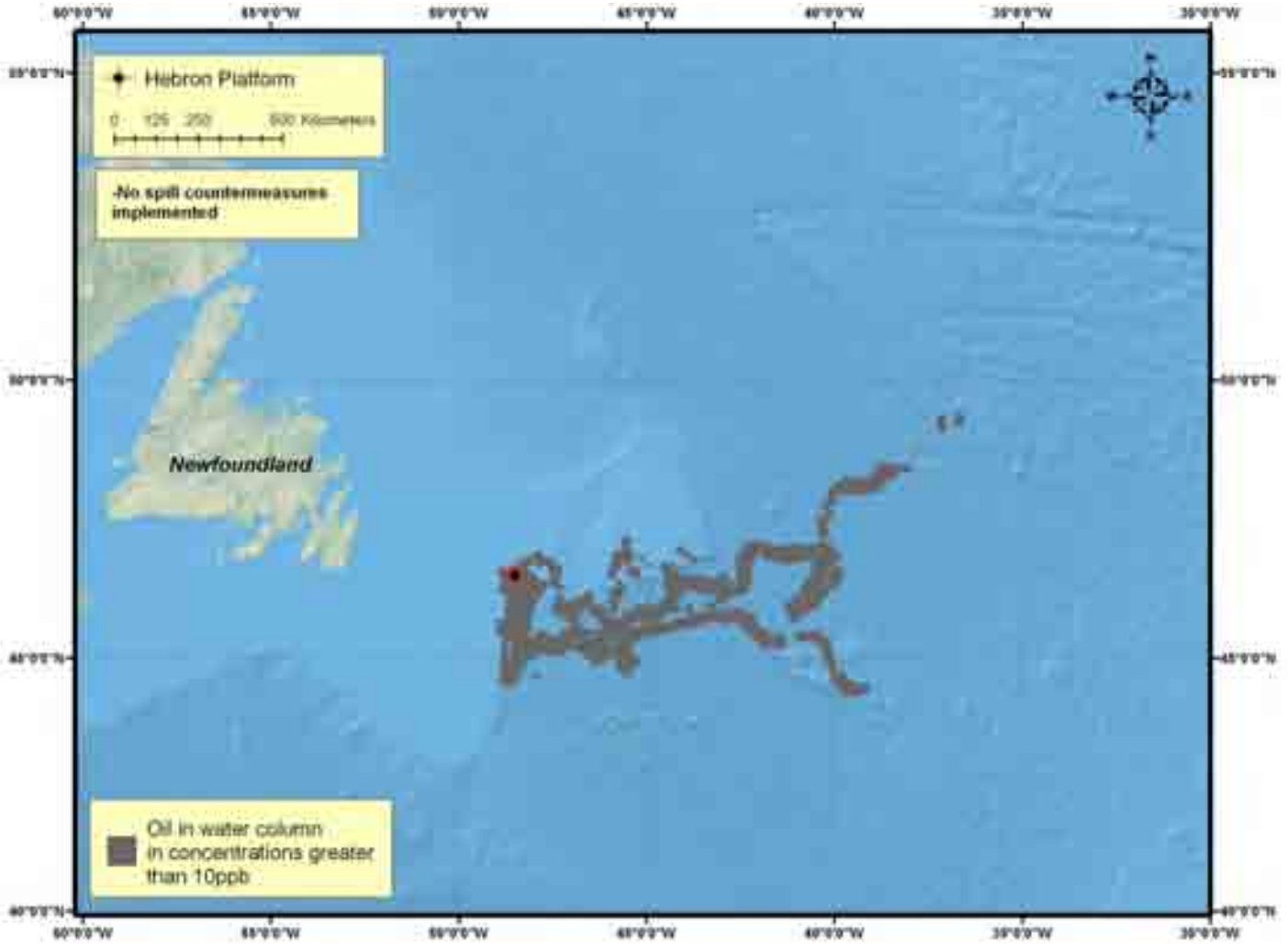


Figure 24. Area of entrained oil for the 95th percentile water column case based on the volume of oil entrained in the water column at the end of a 120 day subsea blow-out during the winter.

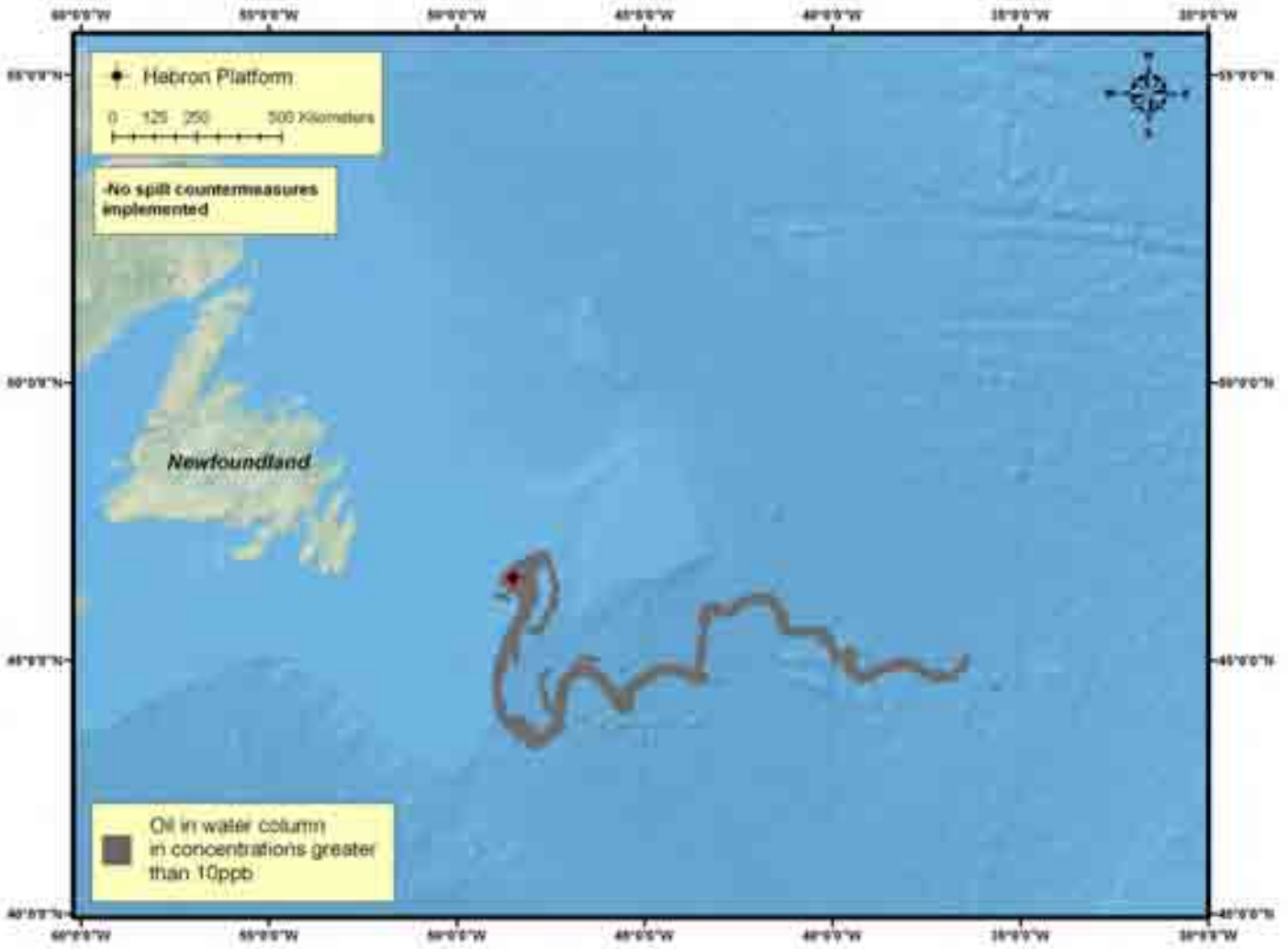


Figure 25. Area of entrained oil for the 95th percentile water column case based on the volume of oil entrained in the water column at the end of a 120 day subsea blow-out during the winter with ice present.

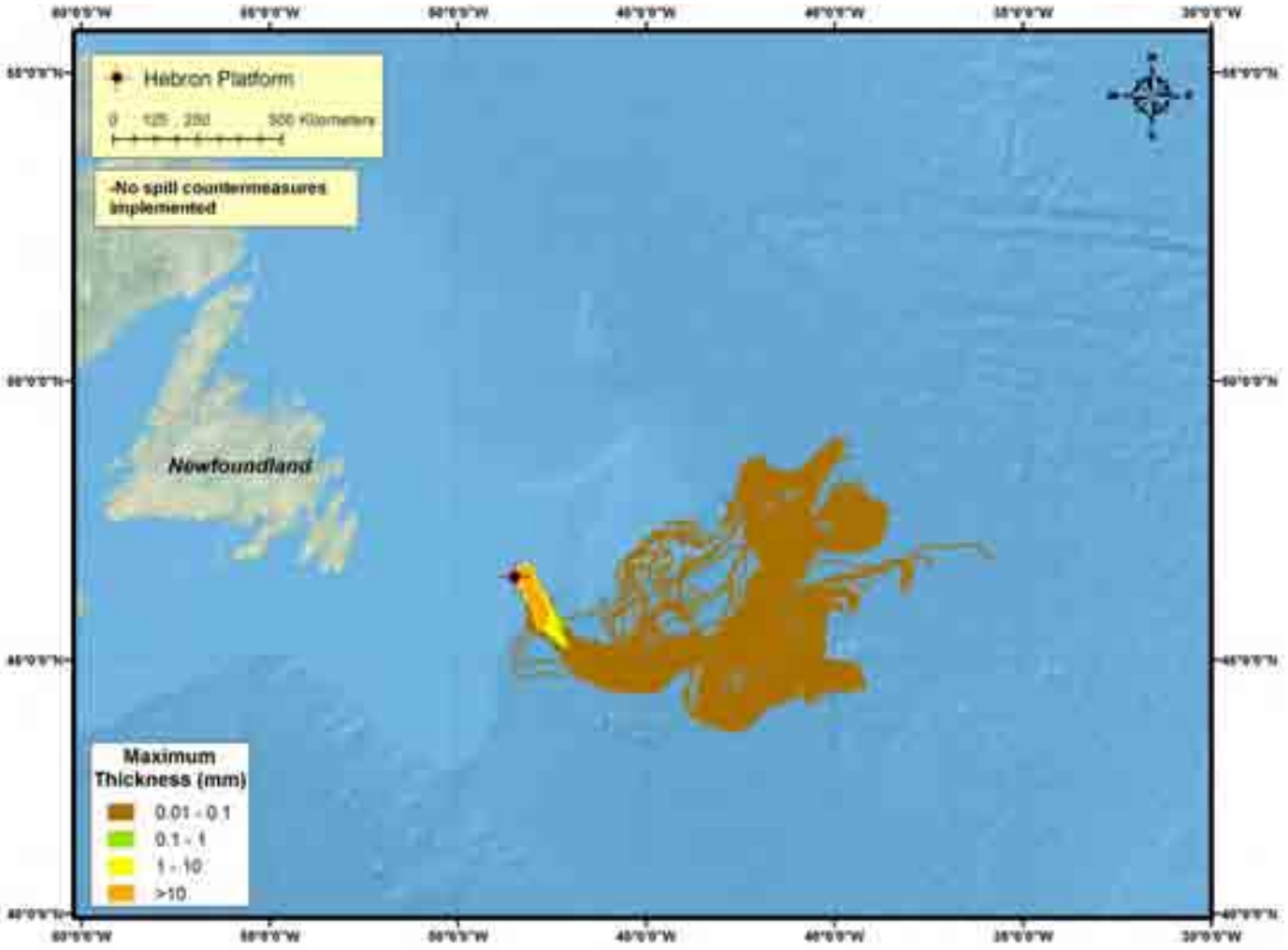


Figure 26. Maximum surface oil thickness for the 95th percentile surface oiling case based on the sea surface area oiled during an instantaneous release of marine diesel in the summer.

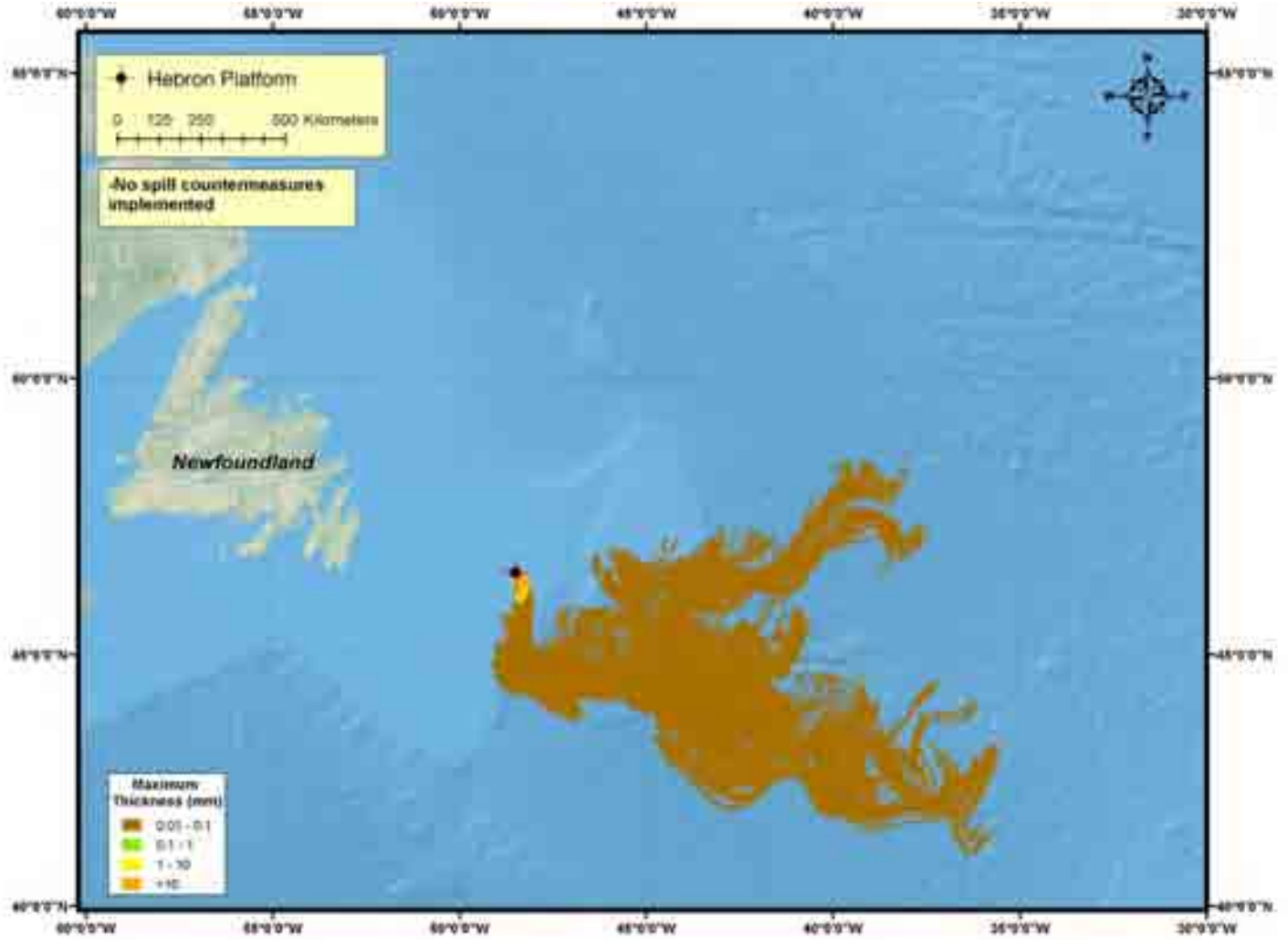


Figure 27. Maximum surface oil thickness for the 95th percentile surface oiling case based on the sea surface area oiled during an instantaneous release of marine diesel in the winter.

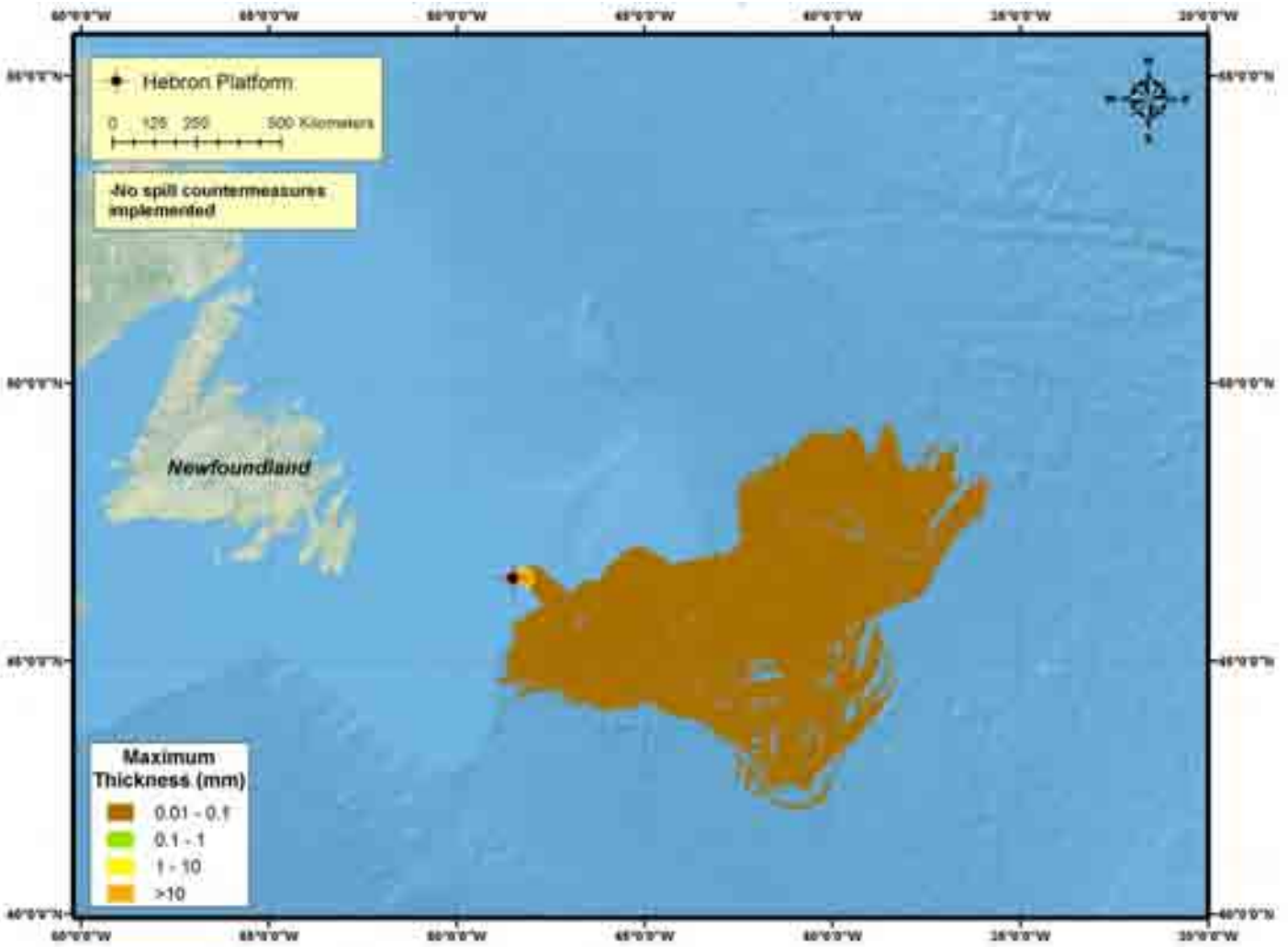


Figure 28. Maximum surface oil thickness for the 95th percentile surface oiling case based on the sea surface area oiled during an instantaneous release of marine diesel in the winter with ice present.

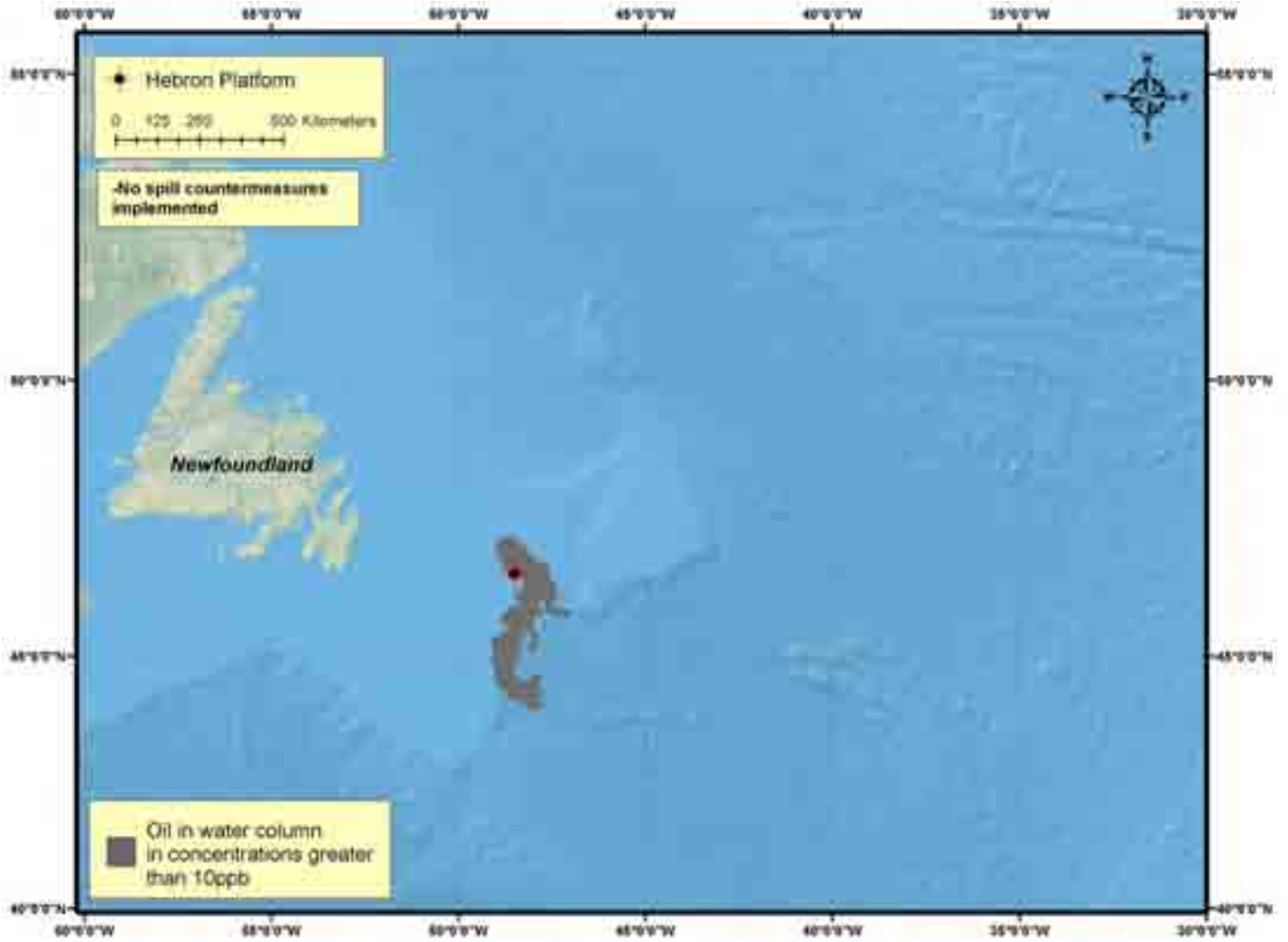


Figure 29. Area of entrained oil for the 95th percentile water column case based on the volume of marine diesel oil entrained in the water column at the end of a 30 day simulation during the summer.

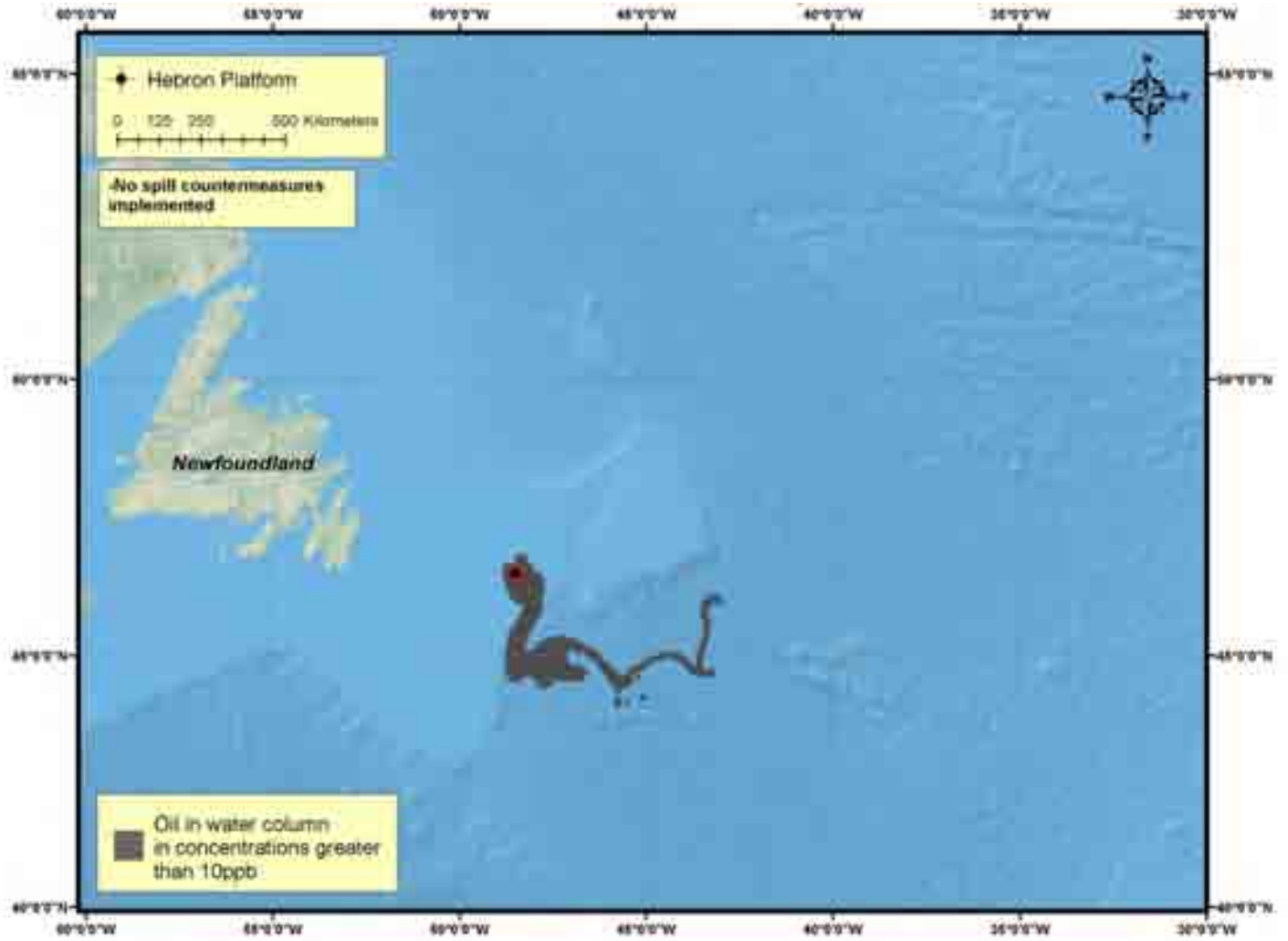


Figure 30. Area of entrained oil for the 95th percentile water column case based on the volume of marine diesel oil entrained in the water column at the end of a 30 day simulation during the winter.

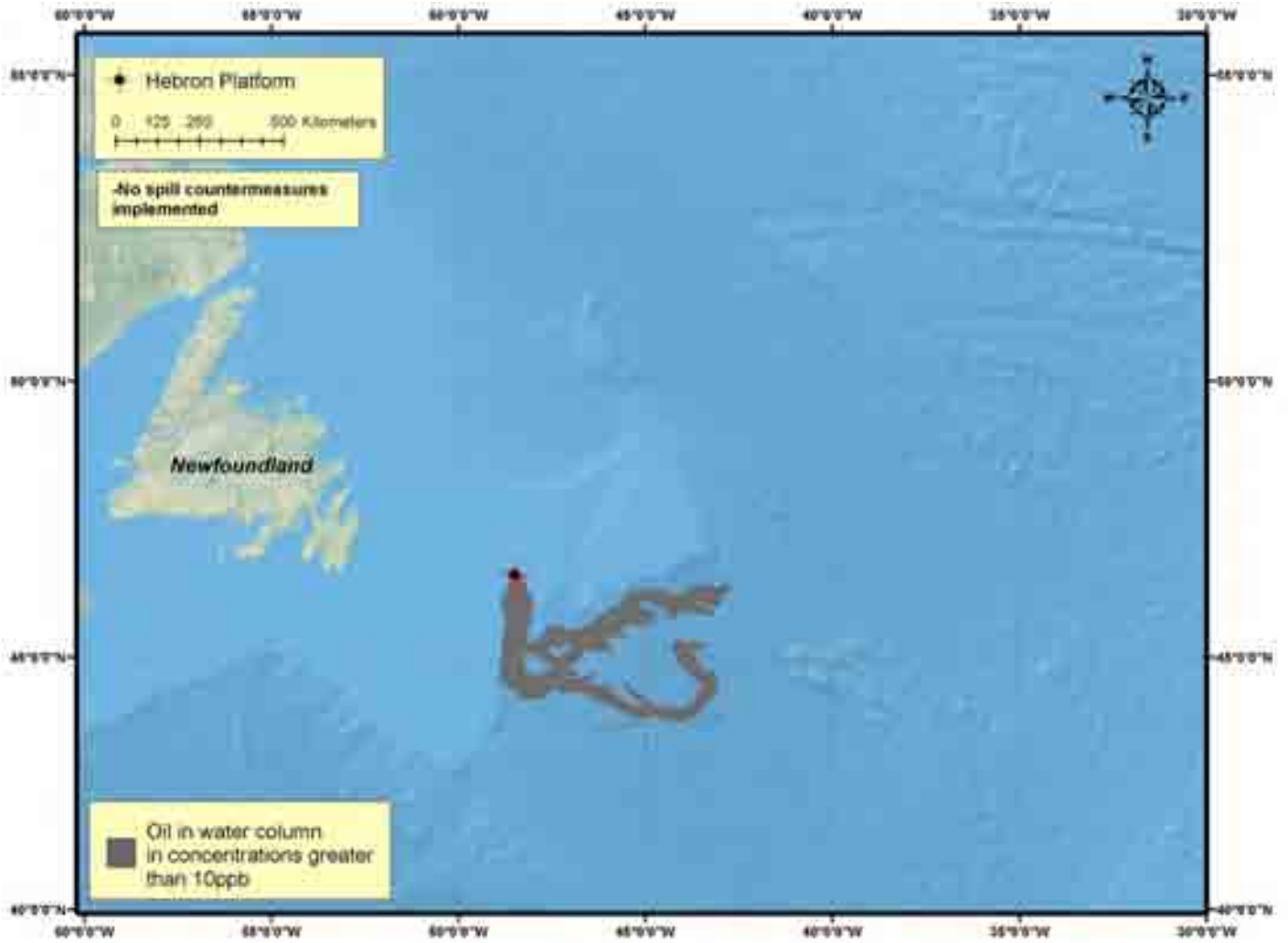


Figure 31. Area of entrained oil for the 95th percentile water column case based on the volume of marine diesel oil entrained in the water column at the end of a 30 day simulation during the winter with ice present.

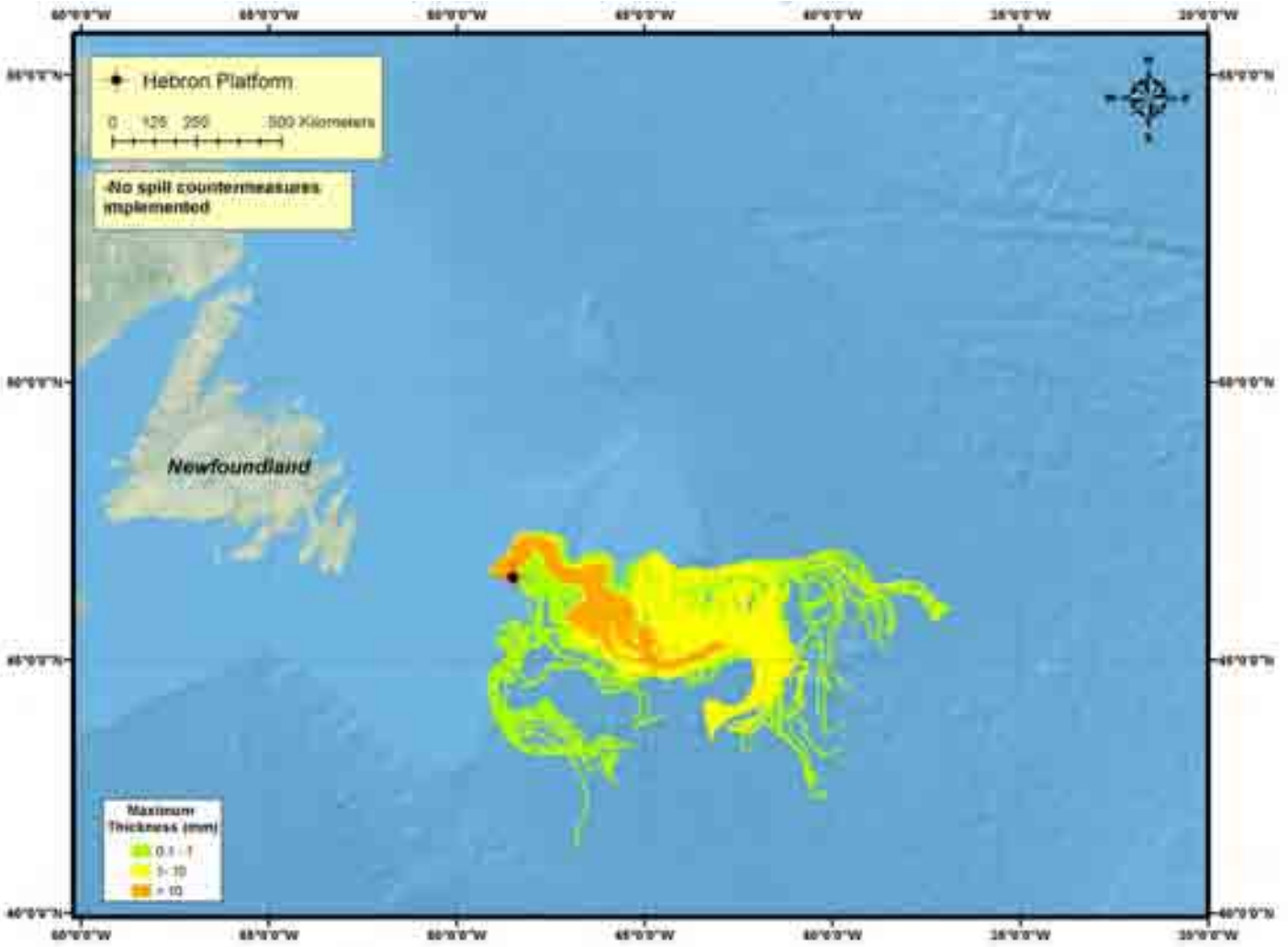


Figure 32. Maximum surface oil thickness for the 95th percentile surface oiling case based on the sea surface area oiled during a batch OLS transfer release of crude in the summer.

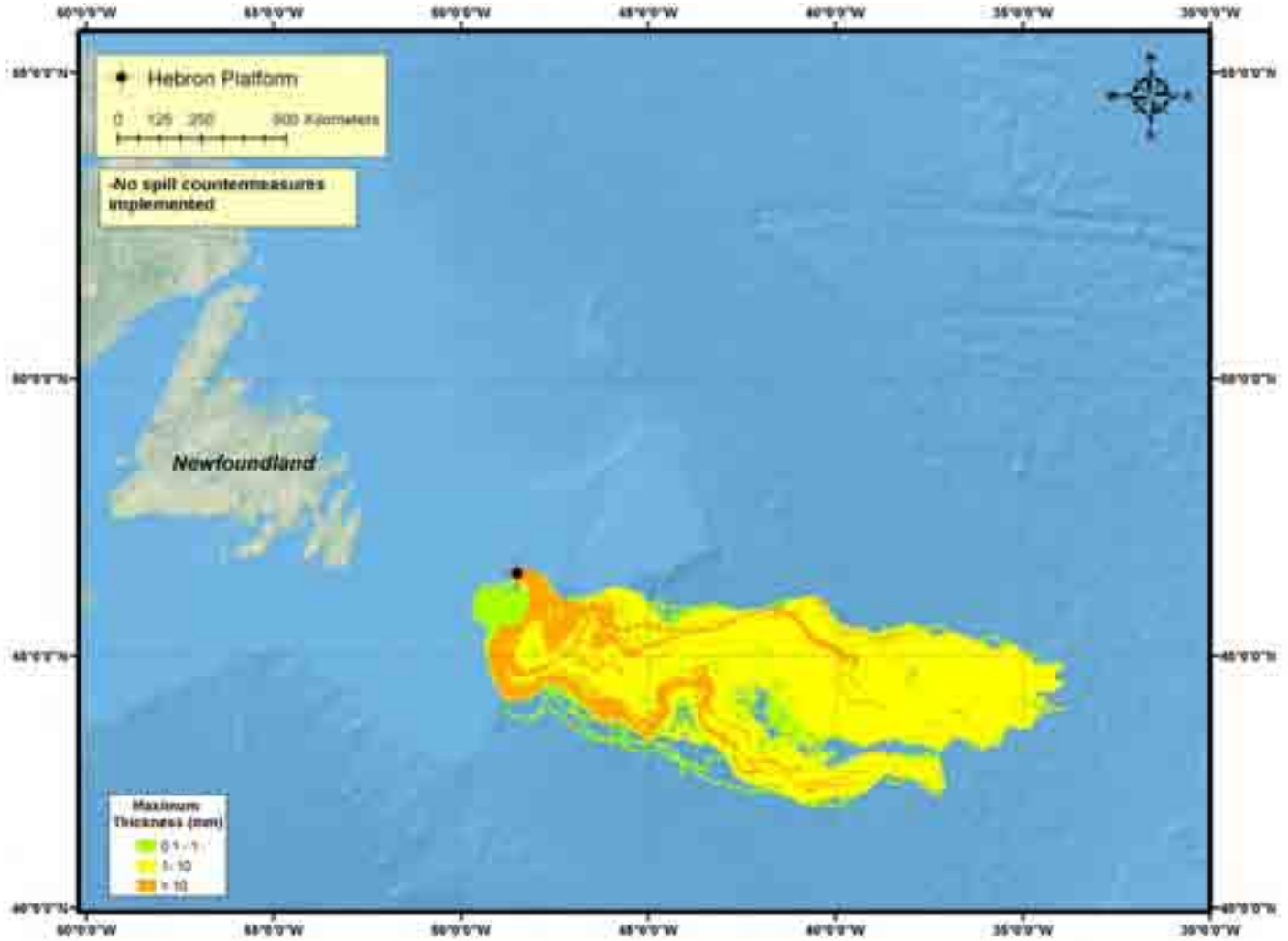


Figure 33. Maximum surface oil thickness for the 95th percentile surface oiling case based on the sea surface area oiled during a batch OLS transfer release of crude in the winter.

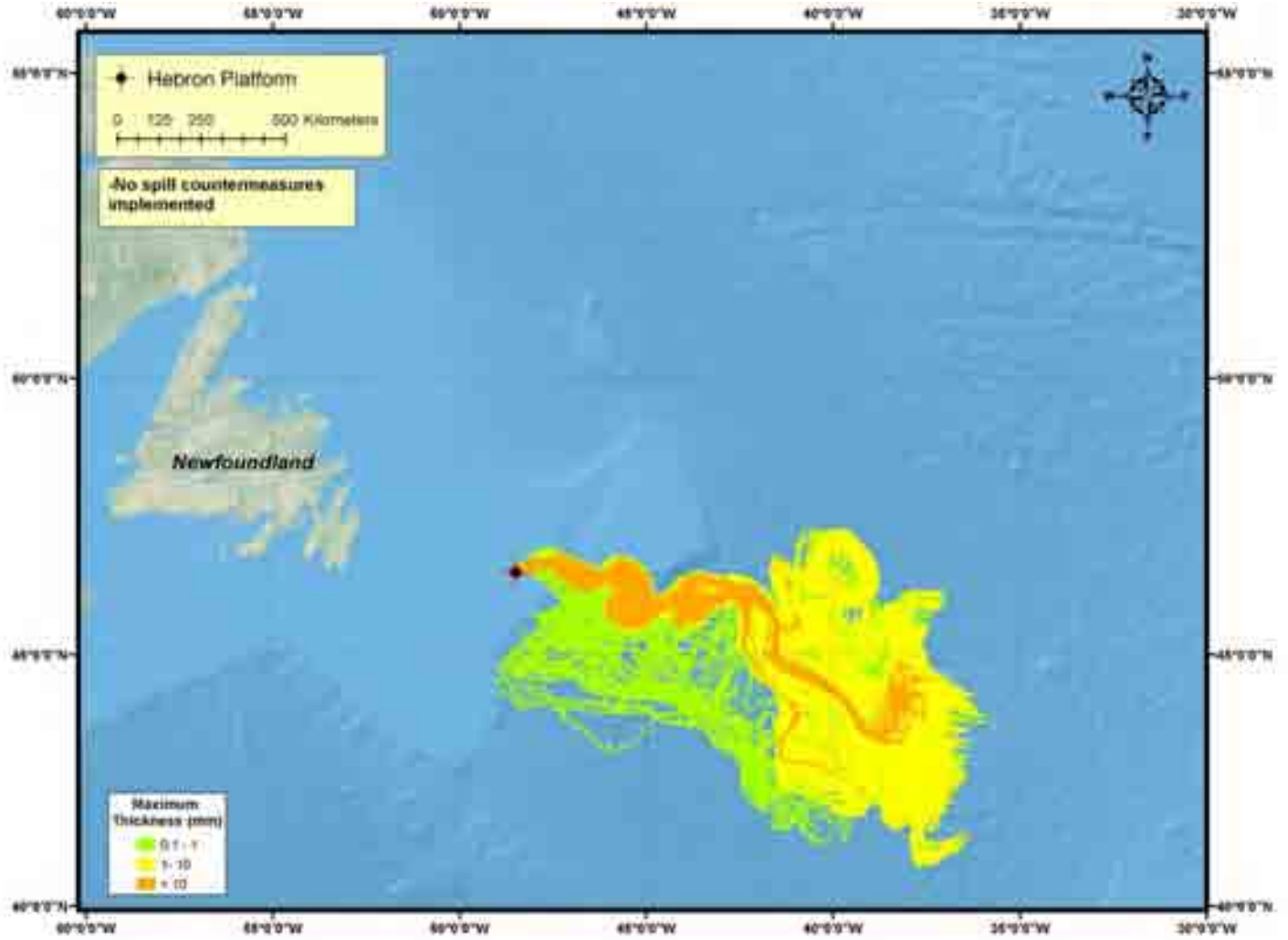


Figure 34. Maximum surface oil thickness for the 95th percentile surface oiling case based on the sea surface area oiled during a batch OLS transfer release of crude in the winter with ice present.

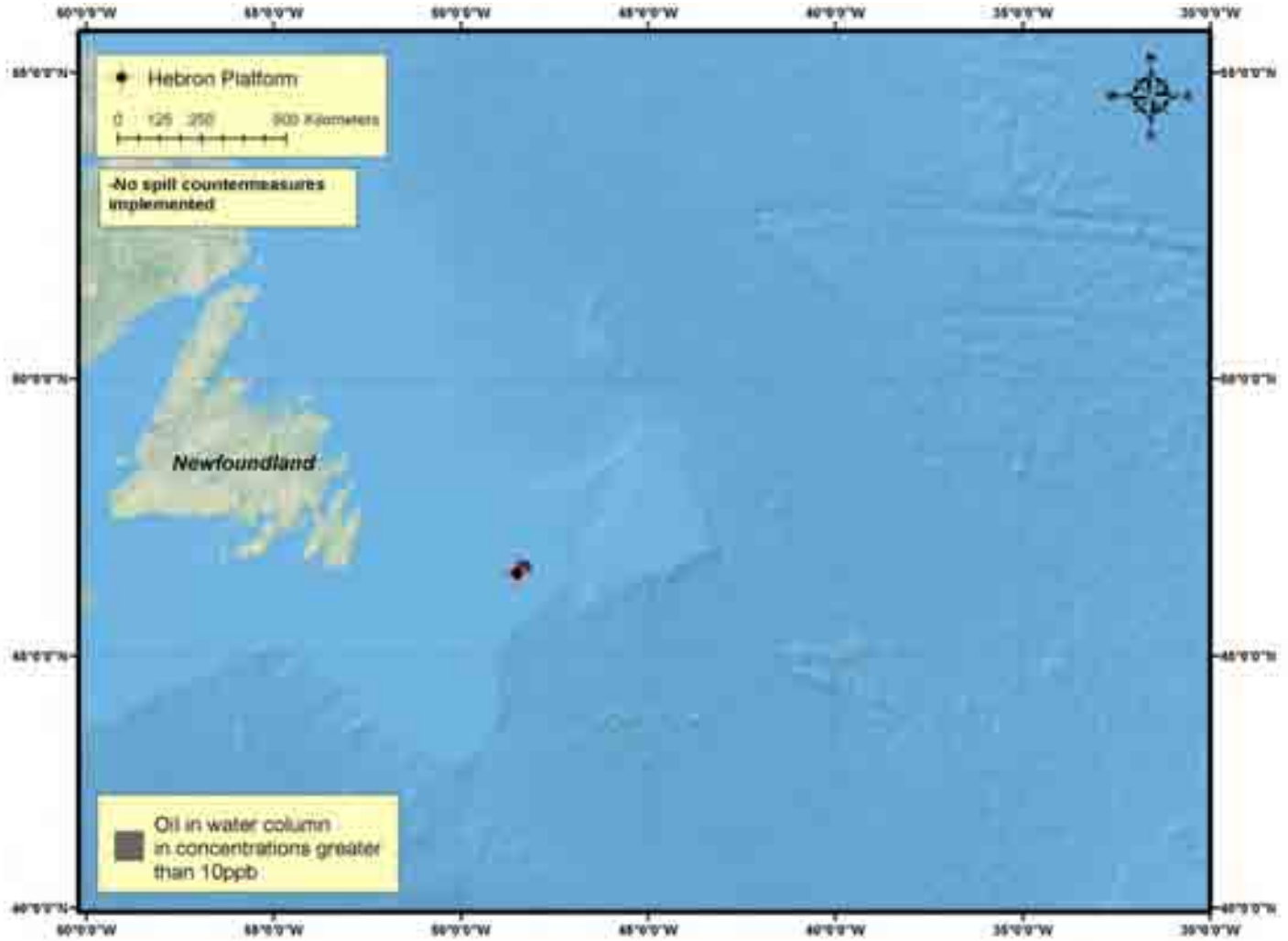


Figure 35. Area of entrained oil for the 95th percentile water column case based on the volume of crude oil entrained in the water column at the end of a 30 day simulation during the summer.

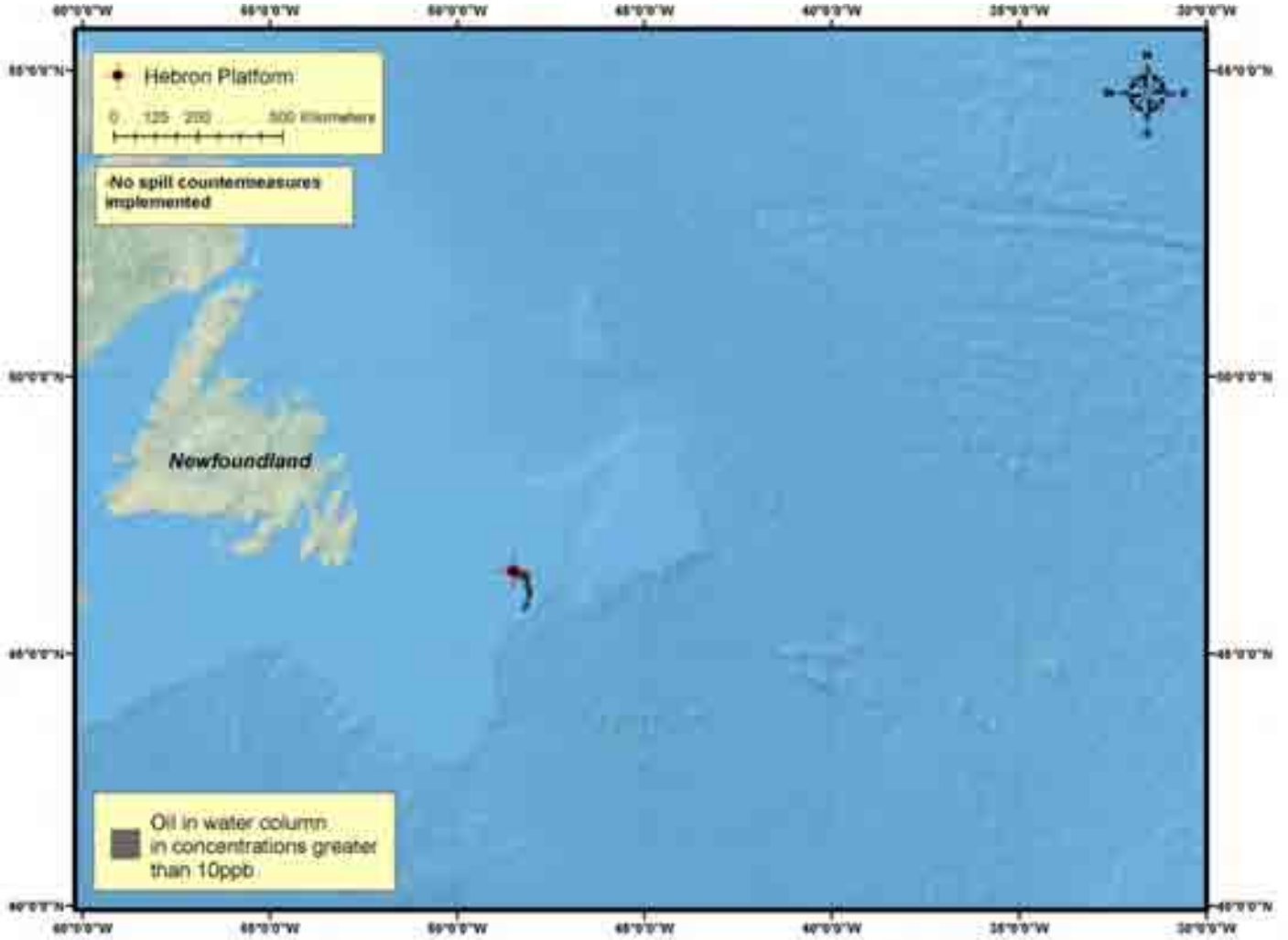


Figure 36. Area of entrained oil for the 95th percentile water column case based on the volume of crude oil entrained in the water column at the end of a 30 day simulation during the winter.

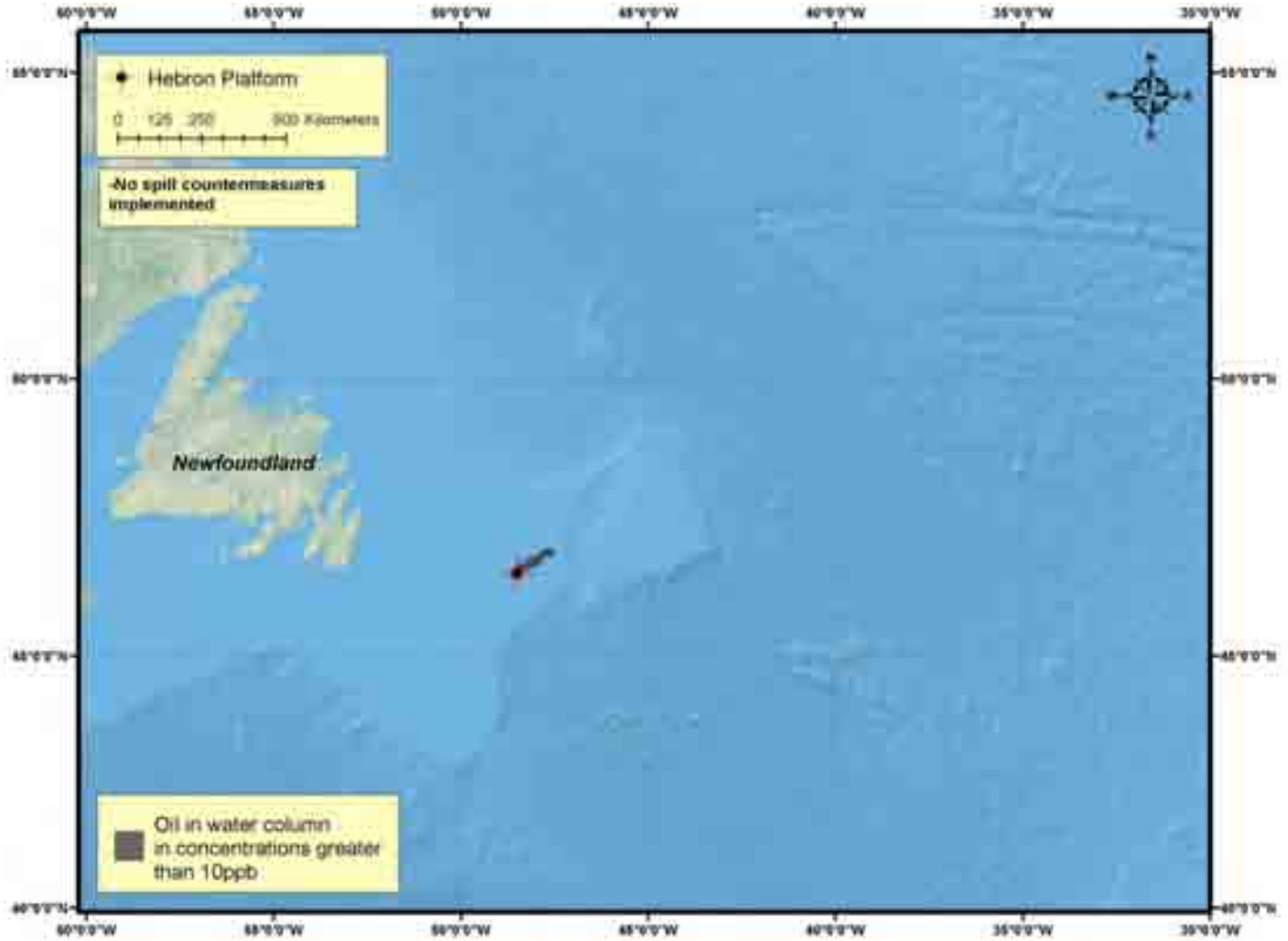


Figure 37. Area of entrained oil for the 95th percentile water column case based on the volume of crude oil entrained in the water column at the end of a 30 day simulation during the winter with ice present.